

Materials Characterization by Dynamic and Modulated Thermal Analytical Techniques

Alan T. Riga and
Lawrence Judovits, editors

ASTM STP 1402

STP 1402

Materials Characterization by Dynamic and Modulated Thermal Analytical Techniques

*Alan T. Riga
and Lawrence Judovits, editors*

ASTM Stock Number: STP1402



ASTM
100 Barr Harbor Drive
PO Box C700
West Conshohocken, PA 19428-2959

Printed in the U.S.A.

Library of Congress Cataloging-in-Publication Data

Materials characterization by dynamic and modulated thermal analytical techniques /

Alan T. Riga and Lawrence Judovits, editors.

p. cm.—(STP ; 1402)

"ASTM Stock Number: STP1402."

Includes bibliographical references.

ISBN 0-8031-2887-8

I. Riga, Alan T. II. Judovits, Lawrence, 1955– III. ASTM special technical publication ; 1402.

TA418.52.M375 2001

620.1' 1296—dc21

2001033491

Copyright © 2001 AMERICAN SOCIETY FOR TESTING AND MATERIALS, West Conshohocken, PA. All rights reserved. This material may not be reproduced or copied, in whole or in part, in any printed, mechanical, electronic, film, or other distribution and storage media, without the written consent of the publisher.

Photocopy Rights

Authorization to photocopy items for internal, personal, or educational classroom use, or the internal, personal, or educational classroom use of specific clients, is granted by the American Society for Testing and Materials (ASTM) provided that the appropriate fee is paid to the Copyright Clearance Center, 222 Rosewood Drive, Danvers, MA 01923; Tel: 978-750-8400; online: <http://www.copyright.com/>.

Peer Review Policy

Each paper published in this volume was evaluated by two peer reviewers and at least one editor. The authors addressed all of the reviewers' comments to the satisfaction of both the technical editor(s) and the ASTM Committee on Publications.

To make technical information available as quickly as possible, the peer-reviewed papers in this publication were prepared "camera-ready" as submitted by the authors.

The quality of the papers in this publication reflects not only the obvious efforts of the authors and the technical editor(s), but also the work of the peer reviewers. In keeping with long-standing publication practices, ASTM maintains the anonymity of the peer reviewers. The ASTM Committee on Publications acknowledges with appreciation their dedication and contribution of time and effort on behalf of ASTM.

Foreword

This publication, *Materials Characterization by Dynamic and Modulated Thermal Analytical Techniques*, contains papers presented at the symposium of the same name held in Toronto, Ontario, on May 25-26, 2000. The symposium was sponsored by ASTM Committee E-37 on Thermal Measurements. The symposium co-chairmen were Alan T. Riga, Cleveland State University, Cleveland, Ohio, and Lawrence Judovits, ATOFINA Chemicals, King of Prussia, Pennsylvania.

Contents

Overview

vii

FUNDAMENTALS OF MTDSC

- Temperature-Modulated Calorimetry of Polymers with Single and Multiple Frequencies to Determine Heat Capacities as Well as Reversible and Irreversible Transition Parameters—BERNHARD WUNDERLICH** 3

- Measurement of Crystallinity in Polymers Using Modulated Temperature Differential Scanning Calorimetry—MIKE READING, DUNCAN M. PRICE, AND HÉLÈNE ORLIAC** 17

- Crystallization of Polymers and the Rigid Amorphous Fraction Studied by the Temperature-Modulated Techniques TMDSC and TMDMA—CHRISTOPH SCHICK, ANDREAS WURM, AND MIKHAIL MERZLIAKOV** 32

THE USE OF MTDSC IN CURING AND CHEMICAL REACTIONS

- Evaluation of the Curing Process in a Fiber-Reinforced Epoxy Composite by Temperature-Modulated and Step Scan DSC and DMA—BRYAN BILYEU, WITOLD BROSTOW, AND KEVIN P. MENARD** 49

MEASUREMENT OF THE GLASS TRANSITION AND MELTING BY MODULATED AND COMPARATIVE TECHNIQUES

- Effects of TMDSC Variables on the Observed Glass Transitions of Elastomers—A Statistical Analysis—KRISTINE N. LUDWIG, KAREN E. BURKHOLDER, JOHN F. WILLEY, AND ALAN T. RIGA** 67

- Glass Transformation Studies of Vitreous As_2Se_3 by Temperature-Modulated DSC—S. O. KASAP AND D. TONCHEV** 81

GENERAL MODULATED TECHNIQUES

- Comparison Between Modulated Differential Scanning Calorimetry (MDSC) and Dynamic Differential Scanning Calorimetry (DDSC)—L. CHRISTINE FULLER AND LAWRENCE JUDOVITS** 89

OTHER MODULATED TECHNIQUES

Modulated-Temperature Thermomechanical Measurements—DUNCAN M. PRICE	103
Obtaining Kinetic Parameters Using Modulated Temperature—ROGER L. BLAINE	115

DYNAMIC TECHNIQUES—A

Analysis of Curing Using Simultaneous Dynamic Mechanical and Dielectric Measurements—JOHN H. SUWARDIE	131
Characterization of Electrorheological Processes By Dielectric Thermal Analysis—ALAN T. RIGA, JOHN M. CAHOON, AND JOSEPH W. PIALET	139
Characterization of Organic Surfactants and Dispersants by Frequency-Dependent Dielectric Thermal Analysis and Electrochemistry—VADIM LVOVICH, JOHN CAHOON, AND ALAN RIGA	157

DYNAMIC TECHNIQUES—B

Development of Bismaleimide/Cyanate Ester Copolymers—BRIAN C. SISK, KATHY CHUANG, AND WEI-PING PAN	177
Application of Theory to Prediction and Analysis of Dynamic Mechanical Properties of Polymer Composites—ANATOLIY YA. GOLDMAN	190
Glass Transition Temperature of Selected Polymers by TMDSC, DMTA and DETA Analyses—MARIA CRISTINA RIGHETTI, MARIA PIZZOLI, AND GIUSEPPINA CECCORULLI	200
Author Index	215
Subject Index	217

Overview

The dynamic and modulated thermal analysis technique symposium, May 2000, has now culminated in a timely presentation as an ASTM special technical publication (STP). The basis of many of the latest Differential Scanning Calorimetry (DSC) thermal methods is the modulation of temperature along with varying other parameters. The mode of modulation, a sinusoidal wave or a saw tooth curve, affords the thermal analyst an opportunity to study a physical or chemical change in greater detail.

The technical science presented is a timely event in the development of new thermal analytical techniques, interpretations, and applications. Major contributions to this science are the family of modulated temperature DSC (MTDSC) techniques, which are also known as temperature-modulated DSC (TMDSC) techniques. These innovative approaches to scanning calorimetry can distinguish a polymer glass transition temperature, T_g , from other overlapping thermal-physical properties and events. The window of measurement has been expanded for better sensitivity and higher resolution. A number of presenters/authors studied the factors effecting the T_g , such as the heating rate, modulation frequency or period, amplitude of the imposed wave, as well as the type of dynamic or modulated curve.

Professor Wunderlich found that MTDSC generated with a centrosymmetric saw-tooth oscillation could be considered a sinusoidal modulation with multiple frequency. Further, he observed that application of these methodologies can be used to calibrate heat capacity at very high precision. Reading et al. compared and developed programs for micro and macro thermal analysis based on MTDSC. He discovered that the modulated approach can be applied to analysis on the probe tip of an atomic force microscope (AMF), where a microanalysis can now be accomplished. Innovative applications of these methods include characterizing reacting polymer systems, relaxation behavior during chemical reactions, evaluating polymer melting and crystallization, kinetic parameters, and the factors effecting the T_g of elastomers in the temperature range of 160 to 270 K.

Price reported on the application of modulated temperature programs for TMA, with and without an underlying linear temperature change, affording methods for separating the reversible nature of thermal expansion from irreversible deformation. The latter arises from creep under the applied load or changes in dimensions due to relaxation orientation.

Riga, Cahoon, et al. used dielectric thermal analysis (DETA) to evaluate surfactants, dispersants, and electrorheological processes. Isothermal permittivity, conductivity, and tan delta curves (Debye plots) clearly differentiated various surface-active agents. The "real world" response time in an applied electric field is needed to rank Electrorheological (ER) fluids for semipassive shock absorbers. The ER response time is directly related to the readily determined DETA relaxation/polarization time.

As presented in this STP, frequency-varied dynamic and modulated methods included modulated thermogravimetric analysis (MTGA), modulated thermomechanical analysis (MTMA), DMA, and DETA, as well as MTDSC. The Thermal Measurements Committee E37 is actively working on developing and implementing Standard Test Methods for the frequency based methods, for example, specific heat capacity, diffusivity, and thermal conductivity by MTDSC. There are methods in place for calibrating and interpreting DMA and DETA. The committee will continue to serve the thermal

science community by establishing these standard methods, as well as their accompanying precision and bias characteristics.

We would like to acknowledge and extend our appreciation for those that helped with the organization of the symposium and publication of this STP. A very special thanks to our symposium committee, which consisted of R. Blaine, R. Seyler, B. Cassel, K. L. Lavanga, and J. A. Foreman and to the ASTM staff which includes D. Fitzpatrick, A. Adams, and T. O'Toole. Finally, many thanks to the lecturers, presenters, and reviewers who contributed to make this a high quality technical achievement.

Alan T. Riga

Cleveland State University,
Cleveland, Ohio; symposium
co-chairman and STP editor

Lawrence Judovits

ATOFINA Chemicals,
King of Prussia, Pennsylvania;
symposium co-chairman and STP editor

FUNDAMENTALS OF MTDSC

Bernhard Wunderlich¹

Temperature-Modulated Calorimetry of Polymers with Single and Multiple Frequencies to Determine Heat Capacities as Well as Reversible and Irreversible Transition Parameters *

REFERENCE: Wunderlich, B., "Temperature-Modulated Calorimetry of Polymers with Single and Multiple Frequencies to Determine Heat Capacities as Well as Reversible and Irreversible Transition Parameters," *Materials Characterization by Dynamic and Modulated Thermal Analytical Techniques, ASTM STP 1402*, A. T. Riga and L. Judovits, Eds., American Society for Testing and Materials, West Conshohocken, PA, 2001.

Abstract: Temperature-modulated differential scanning calorimetry (TMDSC) generated with a centrosymmetric saw-tooth oscillation can be considered to be a sinusoidal modulation with multiple frequencies. Different harmonics of the Fourier series of the heat-flow rate and heating rate of a single sawtooth-modulation can be deconvoluted to extract data pertaining to different frequencies. In order to give the higher harmonics similar amplitudes, a complex, but simple-to-program, sawtooth-modulation is generated for the harmonics 1, 3, 5, 7 and 9. In this fashion a single experiment can produce a frequency-dependent analysis under identical thermal history. Application of this method to TMDSC includes the calibration for heat capacity determination of high precision, even if steady state and a negligible temperature gradient are not achieved. The measurement of the frequency (ω) dependence of the heat-flow rate (A_{HF}) and sample temperature (A_{Ts}) allows to evaluate the expression:

$$C_p = A_{HF}/(A_{Ts} \nu \omega)[1 + (\tau \nu \omega)^2]^{0.5}$$

where the relaxation time τ is to be determined empirically from the multiple data generated by the single run. Typical values for the relaxation time for commercial calorimeters are between 3 and 9 s rad⁻¹. Frequency-dependent, apparent reversing heat capacities in the glass transition region and within first-order transition regions may also be analyzed to study local equilibria in globally metastable polymeric solids.

Keywords: temperature-modulated DSC, multifrequency modulation, metastable polymer, heat capacity, latent heat, phase transition, glass transition, first-order transition

¹ Department of Chemistry, The University of Tennessee, Knoxville, TN 37996-1600, and the Chemistry and Analytical Sciences Division at Oak Ridge National Laboratory, Oak Ridge, TN 37831-6197, USA.

* The submitted manuscript has been authored by a contractor of the U.S. Government under contract No. DE-AC05-96OR22464. Accordingly, the U.S. Government retains a non-exclusive, royalty-free license to publish, or reproduce the published form of this contribution, or allow others to do so, for U.S. Government purposes.

Introduction

Temperature-modulated differential scanning calorimetry (TMDSC) had its beginning in 1992 with the introduction of the first commercial calorimeter by TA Instruments, Inc. [1]. The special features of the TMDSC are the simultaneous evaluation of the thermal effect due to a slow, constant-rate temperature increase (typically 0.1 to 5 K min^{-1} , the “total differential heat-flow rate,” similar to the output of the standard, not-modulated DSC), and a faster effect, the response to the temperature modulation (called the “reversing differential heat-flow rate” with typical temperature modulation parameters of an amplitude of 0.05 to 3 K and a period from 10 to 500 s). Naturally the differences between these two quantities are then the “non-reversing differential heat-flow rates.” Since only the combined signal is generated, a deconvolution procedure is necessary, usually carried out in form of a discrete Fourier analysis of the sample temperature $T_s(t)$ and the heat-flow response $HF(t)$.

The root of measurements with modulation of power instead of temperature is the alternating current, or ac calorimeter [2]. Some attempts were also made at the development of twin ac calorimeters [3]. In all cases, however, the ac calorimeters were run quasi-isothermally, *i.e.*, the modulation occurred about a constant temperature, T_0 , yielding only the reversing response to the modulation. In this paper the special problems and advantages of TMDSC are traced as they became evident from work on multifrequency modulation in our laboratory [4]. Multifrequency modulation was already proposed in the TMDSC patent [1], but not studied.

Standard DSC with Negligible Temperature Gradient and at Steady State

The standard, not-modulated DSC can easily be described as long as one assumes a negligible temperature gradient within the sample and steady state during the period of measurement [5]. Under such idealized conditions, the heat flows of the sample calorimeter, consisting of pan and sample, and the reference calorimeter, usually only an empty pan, are

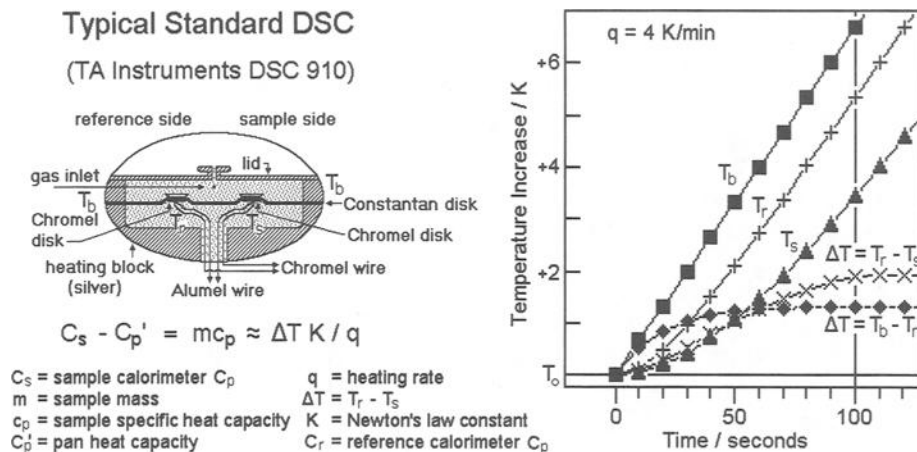


Figure 1 – Schematics and operation of a standard DSC.

governed solely by the heating rate, q , and their heat capacities, written as $C_s = (mc_p + C_p')$ and $C_r = C_p'$, respectively, as is shown in Figure 1. The heat flows generated by the different temperatures are proportional to the temperature differences ΔT . The experiment is started at time zero with a linear temperature increase of the heater, T_b . After about 120 s, the reference and sample temperatures reach steady state, *i.e.*, both increase with the same q as T_b , and ΔT becomes constant. The data in Figure 1 were calculated with values of K of $C_p'/20 \text{ J K}^{-1} \text{ s}^{-1}$, and the assumption that the Fourier equation of heat flow is valid [5].

A minor correction of the equation shown in Figure 1 is needed since the sample and reference calorimeters change their heat capacities with temperature, *i.e.*, T_r and T_s in Figure 1 are not strictly parallel to T_b . This correction needs no further measurement and could be derived some time ago [6] using equations given by Ozawa [7]:

$$mc_p = K \frac{\Delta T}{q} + C_s \left(\frac{d\Delta T}{dT_s} \right) \quad (1)$$

All of the equation symbols are explained in Figure 1. The correction is typically the order of magnitude of 1% as long as the mc_p is a substantial portion of C_s . Similarly, the negligible temperature gradient within the sample is not a stringent condition as long as steady state is kept. A temperature gradient of 2.0 K across crystalline polyethylene, for example, will cause an error in the measurement of the magnitude of dc_p/dT , or about 0.3% at 300 K [8].

Sinusoidal and Saw-tooth Modulation

The simplicity of the data analysis for a standard DSC is lost, as soon as temperature modulation is added. In particular, depending on the modulation method, different results are expected. In Figure 2, the curves on the left illustrate a sinusoidal modulation, and the ones on the right, a quasi-isothermal, sawtooth modulation. For simplicity, in both cases the heater temperatures, T_b , are modulated. In a quasi-isothermal experiment, the average rate of temperature change, $\langle q \rangle$, is zero. The input parameters for the calculation on the right are the same as used for Figure 1, just that at time $t_1 = 100 \text{ s}$ the heating rate is changed into

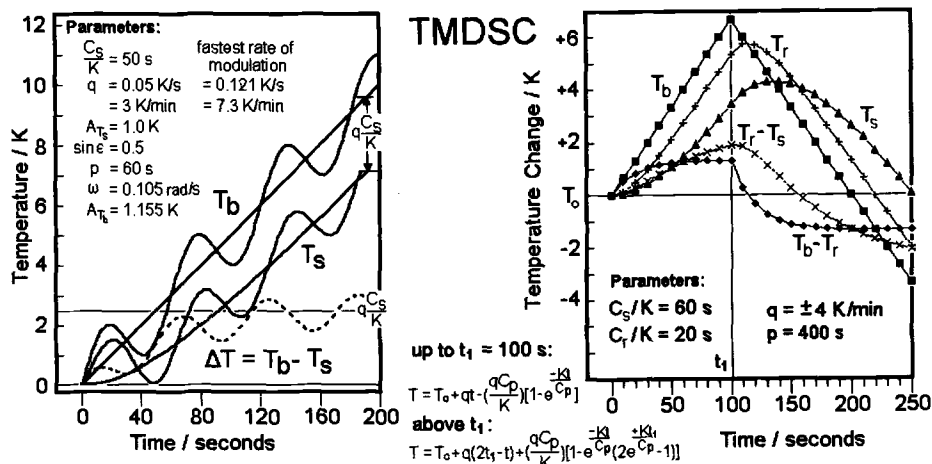


Figure 2 - Sinusoidal and sawtooth modulation.

cooling. The equations derived for the description of the curves on the right are listed in the figure. As long as the heat flows are described by the Fourier equation of heat flow, the solutions for different events are additive. Beyond time t_1 , for example, one can describe the temperature changes of T_s and T_r by assuming the heating is terminated at t_1 , resulting in an approach to an isotherm at +6.67 K, and simultaneously a new experiment of cooling is initiated [5]. The sum of these two events yields the bottom equation in Figure 2 and is plotted in the curves beyond t_1 . The top equation describes the temperatures T_s and T_r for times up to t_1 .

An immediate observation is that the sinusoidal modulation reaches after a few cycles a constant average level, and that the sliding averages over one modulation period $\langle T_b \rangle$, $\langle T_s \rangle$, and $\langle \Delta T \rangle$ yield the same curves as seen in Figure 1 for standard DSC. A simple subtraction of this average from the instantaneous values results in the contribution due to the modulation alone, the reversing signal. The signal applies pseudo-isothermally to $\langle T(t) \rangle$. The deconvolution of the two results of TMDSC is thus quite simple after about 200 s.

An extremely easy analysis of the reversing heat capacity is possible as long as $\langle T_b \rangle$, $\langle T_s \rangle$, and $\langle T \rangle$ change linearly with time. At every time or temperature, $\langle T_s(t) \rangle - T(t)$ is identical to that expected from a quasi-isothermal experiment under the same condition except that $\langle q \rangle \neq 0$. The quasi-isothermal analysis has been investigated in detail and yields for the heat capacity the following expression [9] which also holds for the pseudo-isothermal case:

$$(C_s - C_r) = \frac{A_\Delta K}{A_{T_s} \omega} \sqrt{1 + \left(\frac{C_r \omega}{K} \right)^2} \quad (2)$$

where A_Δ is the modulation amplitude of ΔT and A_{T_s} , that of T_s . The frequency ω is given in rad s^{-1} . The similarity of Equations (2) and (1) becomes obvious if one uses an empty reference calorimeter. Then, C_r is equal to C' and $C_s - C_r = mc_p$, and $A_{T_s} \omega$ represents the amplitude of the modulation of the heating rate $q(t) - \langle q \rangle = dT_s(t)/dt$. The square root accounts, as in Equation (1), for the difference between the modulation of reference and sample calorimeter. Only if there is an empty reference position (no pan, $C_r = \text{zero}$) does Equation (2) change into:

$$C_s = mc_p + C' = \frac{A_\Delta K}{A_{T_s} \omega} \quad (3)$$

an equation often erroneously also used with a reference calorimeter ($C_r \neq 0$). Note, however, that if calibration and measurement are done at the same frequency and the reference pans do not change between runs, all differences between Equations (2) and (3) can be eliminated by calibration; K of Equation (3) is then $K \times [\text{the square root of Equation (2)}]$.

The just discussed Equations (2) and (3) hold only if steady state is not lost during modulation and the temperature gradient within the calorimeters is negligible. This condition is more stringent than for the standard DSC, because if even a small temperature gradient is set up within the sample during the modulation, each modulation cycle has smaller positive and negative heat flows which depend on the unknown thermal conductivities. A negligible temperature gradient within the sample requires, thus, that the sample calorimeter oscillates in its entirety as shown in the left graph of Figure 2. It also requires a negligible thermal resistance between thermometer and pan, and the pan and sample calorimeter. The phase lag ϵ between heater and sample must in this case be entirely due to the thermal diffusivity of the

Constantan disk [$T_s(t) = A_{T_s} \sin(\omega t - \epsilon)$]. Typical conditions that have been used for measuring C_p of polymers with sinusoidal modulation are masses of about 10 mg, amplitudes of modulation of 1.0 K, and modulation periods of 60 s or longer.

Measurement Without Reaching Steady State and With Temperature Gradients

Turning to the sawtooth modulation displayed on the right-hand side of Figure 2, steady state is lost at the sharp change of q , at t_1 and any subsequent step. In the chosen condition, the heat-flow rate of the sawtooth is not in steady-state during about half the modulation period of 400 s, *i.e.*, one should not be able to compute the heat capacities using Equations (2) or (3). Attempts were made to use the maxima and minima of the modulation response which corresponds to a use of a standard DSC to test for the reversing nature of the sample and had been proposed some time ago using dynamic differential thermal analysis [10]. Naturally this simple measurement is only correct if steady state is reached in each half cycle.

An extensive analysis of the sawtooth modulation with the Perkin Elmer calorimeter brought a number of interesting results. Mathematically it could be shown that if there were no temperature gradient within the sample and if all lags and gradients could be assessed with the Fourier heat-flow equation, Equation (2) does allow the calculation of precise heat capacities [4]. Since, however, the temperature sensor of the power compensated calorimeter is much closer to the heater than the sample, temperature gradients cannot be avoided. The empirical solution to this problem was to modify Equation (3) as follows [11]:

$$(C_s - C_r) = \frac{A_{\Delta} K}{A_{T_s} \omega} \sqrt{1 + (\tau \omega)^2} \quad (4)$$

where τ , which has the dimension s rad^{-1} , is an adjustable constant to be determined by measurements at different frequencies. It depends not only on the heat capacity of the reference calorimeter and the Newton's-law constant, as one would expect from Equation (2), but also on the mass and thermal conductivity of the sample, as well as on all of the involved thermal contact resistances and possibly also on cross-flow between sample and reference calorimeters, depending on the calorimeter type. Modeling of such complicated situations has been attempted by Hatta [12], Höhne [13], and others, but it is difficult to evaluate the various constants such treatments generate. As a result, we decided to use Equation (4) as a tool to study τ empirically. As long as only sample mass and thermal conductivity are affecting τ (in addition to C_r and K), a plot of the inverse of the uncorrected square of the heat capacity of Equation (3) *versus* the square of the frequency should be linear, as it was indeed found for the Perkin Elmer DSC with modulation periods longer than 15 s (quasi-isothermal, $T_0 = 298$ K, with modulation amplitudes from one to four kelvins) [11]. Only with modulation periods beyond about 250 s did the frequency dependence become fully negligible. Before continuing this discussion, it is now necessary to briefly review the evaluation of the amplitudes of modulation and the heat-flow response and point out some interesting facts.

Evaluation of the Fourier Components of the Sawtooth Modulation

The sample temperature, $T_s(t)$ and the reversing heat-flow rate response, $HF(t)$ which is proportional to $\Delta T(t)$, are commonly represented by the amplitude of the first harmonic of

the Fourier representations. For the amplitude of the heat-flow rate, A_{HF} , one obtains:

$$HF(t) = \langle HF \rangle + \sum_{v=1}^{\infty} [A_v \sin(v\omega t) + B_v \cos(v\omega t)] \quad (5)$$

where A_v and B_v are coefficients that must be determined in the usual manner, and v is an integer. An analogous equation has to be used for the sample temperature. As long as the modulation starts at $t = 0$ and is symmetric about $\langle q \rangle t$, it is centrosymmetric and all B_v are zero, *i.e.*, the series contains only the sinusoidal harmonics. For a linear response of the sample to a sinusoidal modulation, no higher harmonics are generated in the heat-flow rate, *i.e.*, $A_{HF} = A_1$ of Equation (5). A centrosymmetric sawtooth modulation also simplifies the Fourier representation, it shows only odd, sinusoidal harmonics with $v = 1, 3, 5, \text{etc.}$

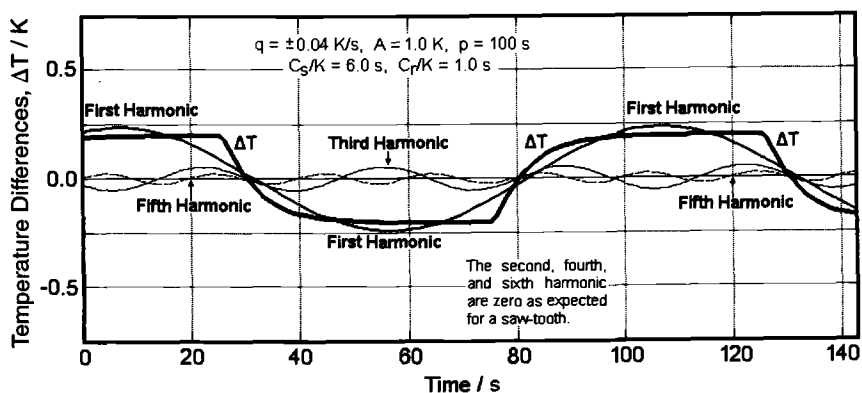


Figure 3 – Sawtooth model calculation for $\Delta T(t)$ and its harmonics.

Figure 3 illustrates the temperature difference, $\Delta T(t)$, for a centrosymmetric sawtooth modulation indicating the influence of the higher harmonics for the case of a modulation that reaches steady state after about half of every heating and cooling segment. If Equation (2) describes the TMDSC, each sinusoidal harmonic can separately be used to compute the heat capacity. Although the amplitudes of the higher harmonics decrease quickly, up to the 11th harmonics could be used to establish τ . Figure 4 shows the results for a typical copolymer and sapphire, analyzed with a Perkin-Elmer calorimeter [14]. Several runs with different modulation periods were used and the uncorrected heat capacities as calculated from Equation (3) are plotted on the left, and the corrected values from Equation 4 are plotted on the right for measurements that show a frequency-independent τ for higher harmonics with periods longer than 10–15 s ($\tau_{\text{polymer}} = 2.40 \text{ s rad}^{-1}$ and $\tau_{\text{sapphire}} = 2.24 \text{ s rad}^{-1}$). The dashed lines indicate the expected value of the heat capacity from the literature. Note that the calibration run with sapphire needs a different τ , and can thus only be used after evaluation of its separate τ value and extrapolation to zero frequency. It could also be shown that the common practice of subtracting a baseline of a run with two empty calorimeters to correct for the asymmetry of the calorimeter is not mathematically sound, but for highest precision must similarly be converted into a heat capacity contribution at zero frequency [15].

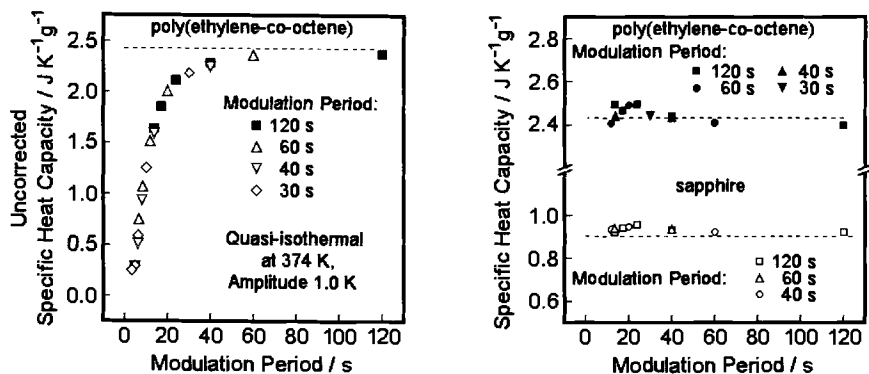


Figure 4 - Analysis with Equations (3) and (4).

Multiple Frequency Modulation

The final step in the analysis is to eliminate the problem that arises for the use of multiple frequencies from the quickly decreasing amplitudes of the higher harmonics in Equation (5). This was accomplished by replacing a simple sawtooth with one designed to have similar amplitudes for the 1st, 3rd, 5th, and 7th harmonics. Instead of the standard quasi-isothermal sawtooth given by the Fourier series:

$$T(t) - T_o = \frac{8 A_{Ts}}{\pi^2} \left[\sin \omega t - \frac{1}{9} \sin 3\omega t + \frac{1}{25} \sin 5\omega t - \frac{1}{49} \sin 7\omega t + \frac{1}{81} \sin 9\omega t - \dots \right] \quad (6)$$

the following complex sawtooth was created [15]:

$$T(t) - T_o = A [0.378 \sin \omega t + 0.251 \sin 3\omega t + 0.217 \sin 5\omega t + 0.348 \sin 7\omega t - 0.067 \sin 9\omega t \dots] \quad (7)$$

Its harmonics are presented in Figure 5 for the sample temperature, T_s . A single cycle of the complex sawtooth contains 14 segments and can easily be programmed, even for a standard DSC of high quality. It produces simultaneously four modulations with different frequencies and similar amplitudes. If using also the 9th harmonic, which is only increased by a factor of nine, five harmonics can be used to establish τ with a single measurement and produce high quality data for the heat capacity at zero modulation frequency. All heat losses due to drifts and losses of other frequencies are rejected.

The complex sawtooth was chosen because of the missing even harmonics and the rapid decrease in amplitude of the higher harmonics. The missing harmonics space the measured frequencies more widely, and by summation of the different harmonics, the initial detriment of decreasing amplitudes turns to an advantage since leaving out higher harmonics does not remove much of the measurement after adjusting the first four harmonics. The total temperature variation in Figure 5, shown by the heavy line, is closely fitted by the sum of the first five harmonics (thin line), *i.e.*, adding any higher harmonics cannot yield significant additional information, and all used harmonics have similar contributions (except the smaller 9th harmonic). In actual measurements, typical calorimeters do not have a sufficiently fast response to respond to high harmonics, improving the precision of this method even further.

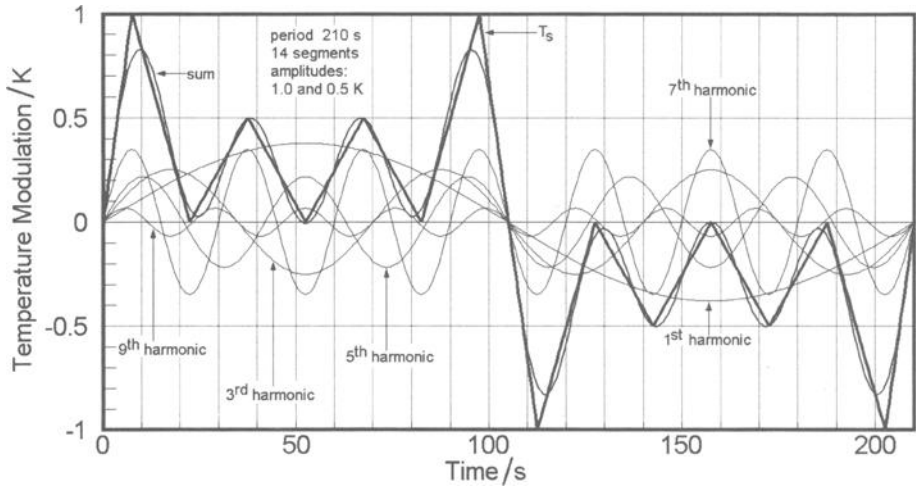


Figure 5 – Complex sawtooth modulation showing similar amplitudes of the harmonics.

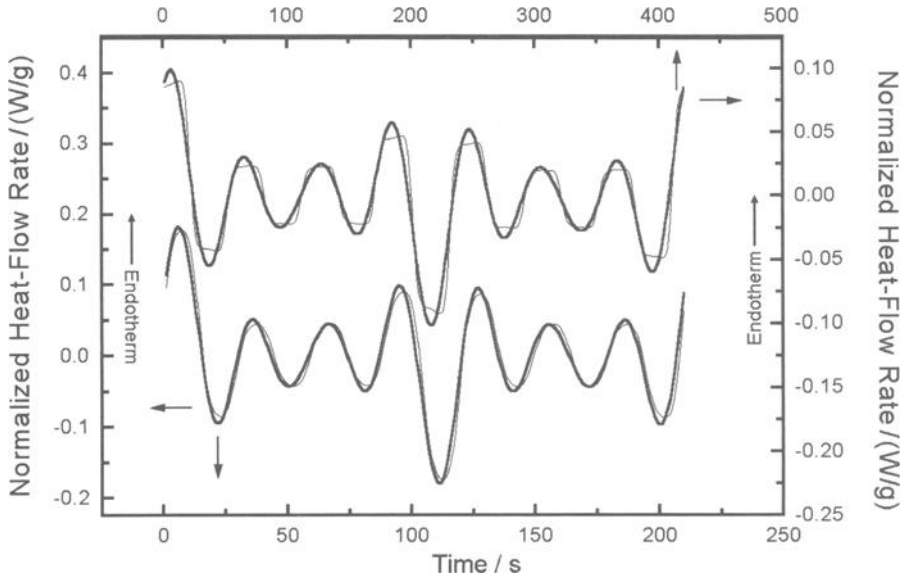


Figure 6 – Complex sawtooth TMDSC (thin: measurement, thick: sum of the harmonics).

Applications

An application of the complex sawtooth in the measurement of the heat capacity of polystyrene is shown in Figure 6 using the Perkin-Elmer Pyris-1 DSC in a quasi-isothermal mode at 333.6 K [16]. Two overall modulation periods of 210 and 420 s were applied. The heat-flow rates shown in Figure 6 illustrate that during the 15 s sections of the 210 s

modulation steady state was not reached, while for 420 s modulation steady state was reached for part of each section (thin curves). The sum of the five Fourier components is shown by the thick curves. The sample temperatures were only slightly rounded relative to Figure 5.

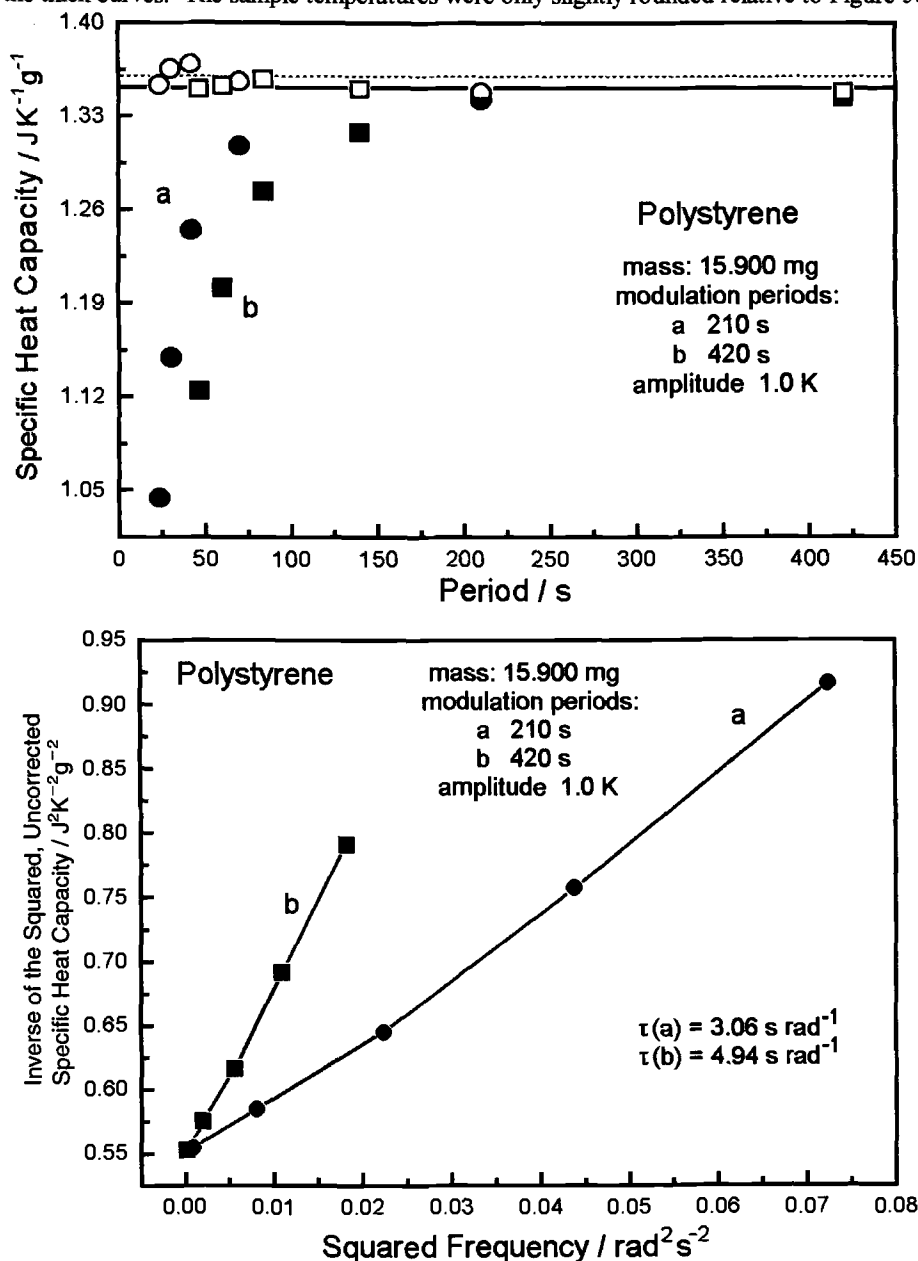


Figure 7 - Analysis of Figure 6 (dashed line literature value, heavy line, average).

Analyzing the data of each harmonic with Equation (3) yields the filled symbols in the top graph of Figure 7. Only the harmonics with periods of more than 250 s give satisfactory data. The dashed line marks the literature value of the polystyrene specific heat capacity. The corrections to Equation (4) are documented in the bottom graph of Figure 7. With the indicated values for τ , the open symbol data result, with the heavy line representing the average value ($\pm 0.5\%$).

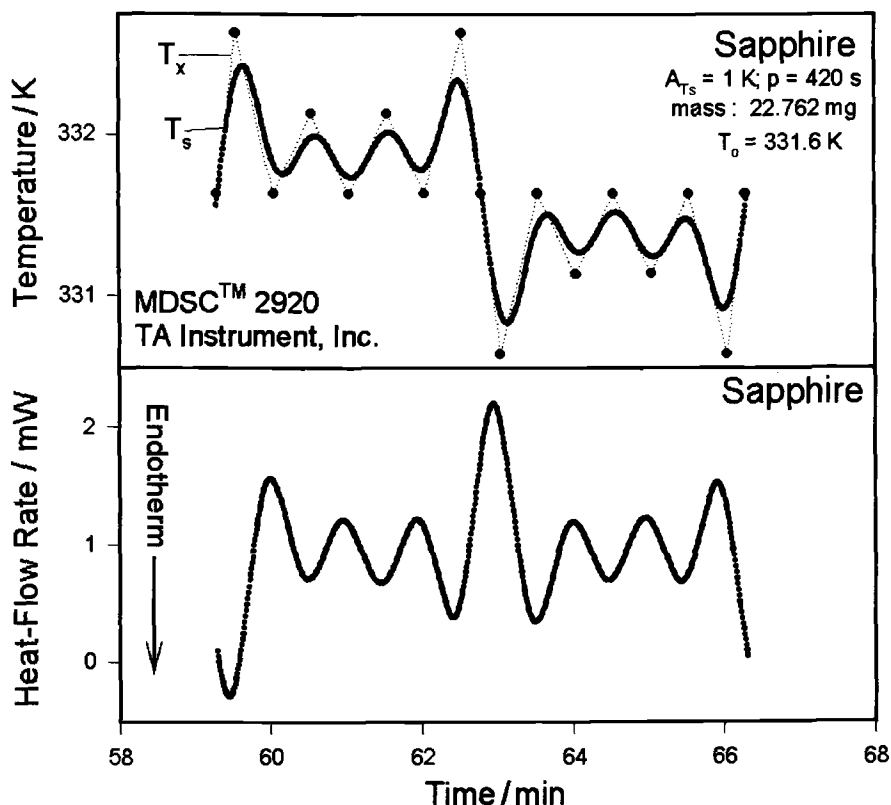


Figure 8 – Temperature-modulation with a complex sawtooth for a heat-flux-type DSC.

Next, data were gathered on sapphire with a heat-flux TMDSC of the TA Instruments type (see Figure 1), programmed with a 420 s complex sawtooth [17]. Figure 8 shows the sample temperature and heat-flow rate data. Since the temperature sensing occurs far from the heater, the programmed temperature (\bullet) was not reached, but the *HF*-response remained linear. The heat-flow response does not show any even harmonics, and the 1st, 3rd, 5th, 7th, and 9th harmonic represent practically the whole curve of Figure 8, with amplitudes as expected. The analysis of the data is shown in Figure 9 with an almost constant τ for all harmonics.

Another heat-flux DSC is the Mettler-Toledo 820. In this calorimeter, temperature is measured close to the heater and used to control the modulation and establish the reference

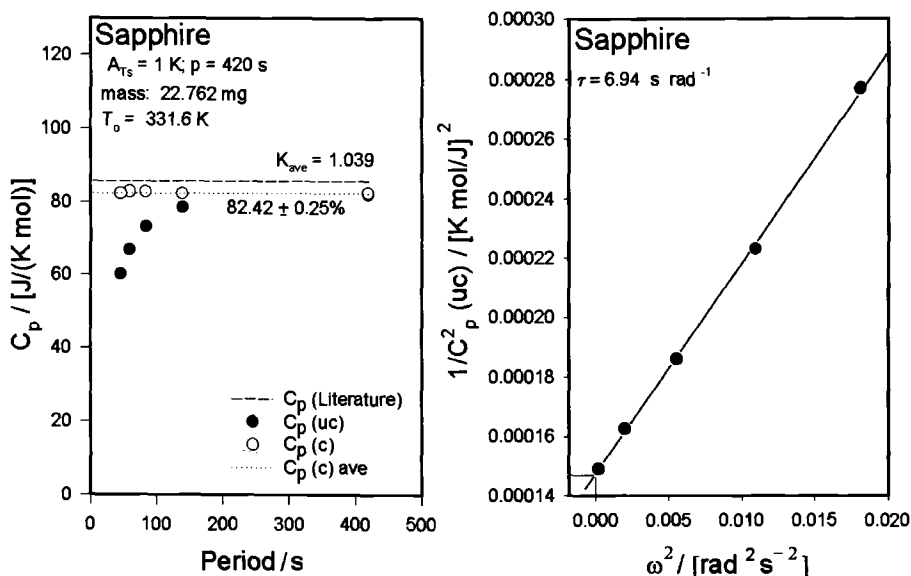


Figure 9 – Analysis of the data of Figure 8 (dashed line, literature value for Al_2O_3).

temperature. The temperature difference, however, is established separately with higher resolution, using a heat-flux sensor (FRS-5). Heat capacities were measured quasi-isothermally for poly(methyl methacrylate) (PMMA) at 300 K [18]. Figure 10 illustrates on the left the uncorrected data for the complex sawtooth (○) and also the standard DSC data taken from the different heating (Δ) and cooling rates (∇). The corrected data with a τ established in the right graph are marked (●). The literature data are given by the solid horizontal. They are closely matched by the experimental data and have a standard deviation of $\pm 0.04\%$. The average is marked by the dotted line. The literature value is 0.76% lower than the experimental average, but it must be remembered that the data bank is usually accurate only to within 3%. The graph on the right shows that there is practically no region

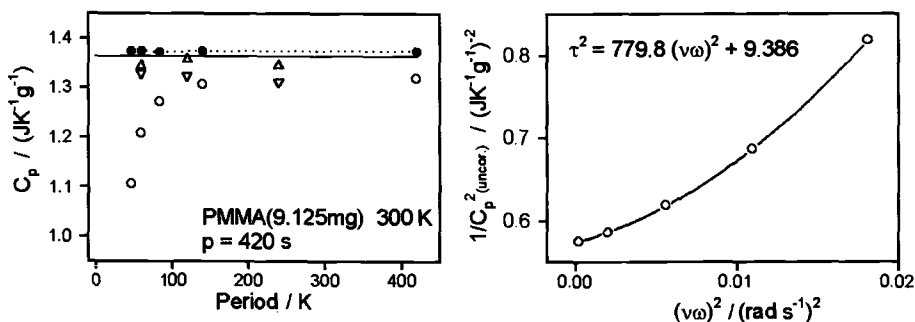


Figure 10 – Analysis of PMMA with a Mettler-Toledo DSC 820.

of constant τ and a quadratic fit was made with good success, as shown by the drawn-out curve. The heat capacity data were corrected with the frequency-dependent τ .

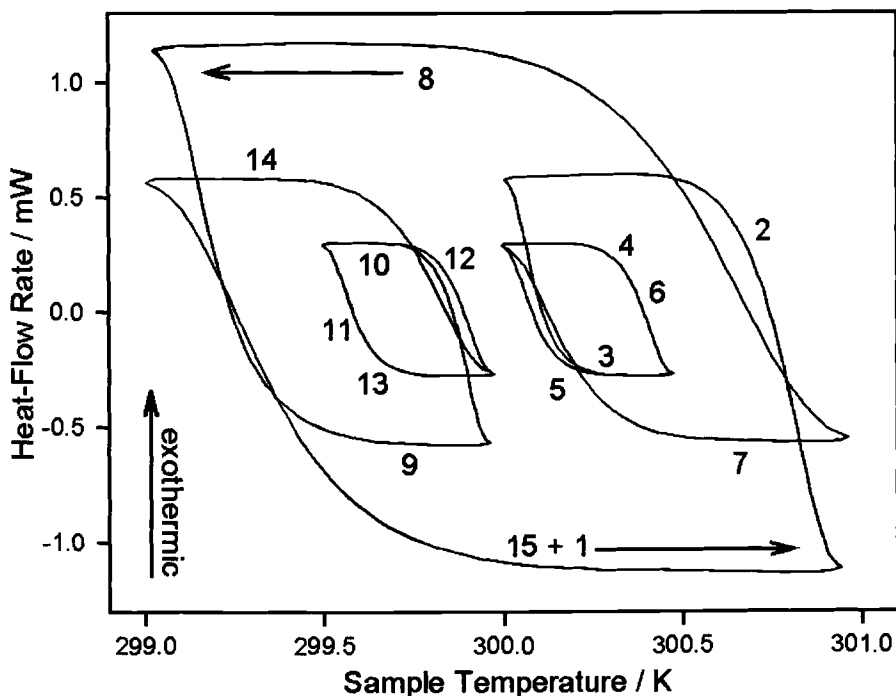


Figure 11 – Lissajous figure of an analysis as Figure 10, but using 22.6 mg of sapphire.

Also of interest is the Lissajous figure of the complex sawtooth. Figure 11 displays the third to the sixth complex cycle on 22.6 mg sapphire, taken with a modulation period of 420 s at 300 K. The numerals indicate the sequence of the section of the complex modulation, starting with “1” and matching the first half-segment with the last, 15, which completes the cycle. The width of the lines covers the repeatability.

Besides improving the measurement of heat capacity, which outside of the transition regions react practically instantaneously to a change in temperature, it is of interest to study the slow response of samples in the glass and melting transition regions. The slow response of the sample adds then to the lags due to the thermal resistances just discussed. The method of analysis for the additional slow sample response has not been fully developed yet; it must be found as a deviation of τ from the value set by the heat capacity outside the transition region. Using the displayed method, it should then be possible to gain kinetic information on the same sample configuration using a single measurement. A single measurement is of particular importance so that one can analyze an identical sample with all frequencies.

For the glass transition, it was found when using a single sinusoidal frequency that the sample adds the following effects: (1) higher harmonics due to the cooperative freezing or

unfreezing of large-amplitude motion, (2) frequency shifts due to coupling of the linear and modulated time scales if the analysis is not done quasi-isothermally, and (3) asymmetry in the reversing response due to an exponential temperature dependence of relaxation times [19]. For quantitative analysis it was necessary to work quasi-isothermally to eliminate (2), to extrapolate the data to zero modulation amplitude to eliminate (3), and to separate the first harmonic and second harmonic (1).

The largest differences in the description of the modulated parameter can show up, however, in first-order transitions. The observed effects may be as follows: (1) The transitions may be only partially reversible or even irreversible. (2) Large exotherms or endotherms may cause time periods of constant temperature within the sample and disturb the modulation. (3) Instrument lags due to melting and crystallization may cover more than one modulation period. (4) Irreversible processes may contain accidental Fourier components of the modulation frequency. (5) The transition kinetics may cause lags in the sample response. For recent publications with single-frequency modulation see [20]. In all of these cases it is necessary to inspect the heat-flow rate in the time domain before accepting "apparent heat capacities" computed from a first-harmonic Fourier fit of the reversing parameters.

Conclusions

Temperature-modulated calorimetry has recently experienced a strong increase in interest, and new methods of modulation and analysis have been developed. The advantage of the multifrequency modulation for the measurement of heat capacity is the possibility to increase the precision by a factor 10 or more over the common $\pm 3\%$ seen for the standard DSC. This is possible by deriving data for different frequencies through a calibration of the various thermal conductivity effects inside and outside the calorimeters during the actual run.

It is proposed that the same method may be able to analyze the frequency-dependence of transition effects by comparison of the calibration factors outside and inside the transition region. This method would for the first time permit a study of the frequency dependence on a sample of identical thermal history for all frequencies.

Since temperature modulation has recently also been applied to the analysis of mechanical properties and thermogravimetry, as well as to DSC coupled with atomic force microscopy (microcalorimetry), the here-proposed multi-frequency modulation may also be applied to these techniques.

Acknowledgments

Supported by the Division of Materials Research, National Science Foundation, Polymers Program, Grant # DMR-9703692 and the Division of Materials Sciences and Engineering, Office of Basic Energy Sciences, U.S. Department of Energy at Oak Ridge National Laboratory, managed and operated by UT-Batelle, LLC, for the U.S. Department of Energy, under contract number DOE-AC05-00OR22725.

References

- [1] Reading, M., Hahn, B. K., and Crowe, B. S. U.S. Patent 5,224,775, 6 July 1993.
- [2] Sullivan, P. F., and Seidel, *Physical Review*, Vol. 173, 1969, p. 679; see also the review by Gmelin, E., *Thermochimica Acta*, Vol. 304/305, 1997, p. 1.

- [3] Gobrecht, H., Hamann, K., and Willers, G., *Journal of Physics, E: Scientific Instruments*, Vol. 4, 1971, p. 21; Dixon, G. S., Black, S. G., Butler, C. T., and Jain, A. K., *Analytical Biochemistry*, Vol. 121, 1982, p. 55.
- [4] Wunderlich, B., Boller, A., Okazaki, I., Ishikiriya, K., Chen, W., Pyda, M., Pak, J., Moon, I., and Androsch, R. *Thermochim. Acta*, Vol. 330, 1999, pg. 21-38.
- [5] B. Wunderlich, *Thermal Analysis*, Academic Press, New York, 1990; updated and expanded to a computer-course *Thermal Analysis of Materials*, with over 2879 screens, downloadable from: web.utk.edu/~athas/courses/tham99.html.
- [6] Wunderlich, B., "Differential Thermal Analysis," in *Physical Methods of Chemistry*, A. Weissberger and B. W. Rossiter, eds. Vol. 1, Part V, Chapter 8. J. Wiley & Sons, New York, 1971.
- [7] Ozawa, T., *Bulletin of the Chemical Society of Japan*, Vol. 39, 1966, p. 2071.
- [8] Gaur, U. and Wunderlich, B., *Journal of Physical and Chemical Reference Data*, Vol. 10, 1981, p. 119.
- [9] Boller, A. Jin, Y., and Wunderlich, B., *Journal of Thermal Analysis*, Vol. 42, 1994, p. 307.
- [10] Wunderlich, B., Bodily, D. M., and Kaplan, M. H., *Journal of Applied Physics*, Vol. 35, 1964, 95.
- [11] Androsch, R., Moon, I., Kreitmeier, S., and Wunderlich, B., *Thermochimica Acta*, in press, 2000.
- [12] Hatta, I. and Maramatsu, S., *Japanese Journal of Applied Physics*, Vol. 35, 1996, p. L858; Hatta, I. and Katayama, N., *Journal of Thermal Analysis*, Vol. 54, 1998, p. 557.
- [13] Höhne, G. W. H., *Thermochimica Acta*, Vol. 330, 1999, p. 45.
- [14] Androsch, R. and Wunderlich, B., *Thermochimica Acta*, Vol. 333, 1999, p. 27.
- [15] Wunderlich, B., Androsch, R., Pyda, M., and Kwon, Y. K., *Thermochimica Acta*, Vol. 348, 2000, p. 181.
- [16] Kwon, Y. K., Androsch, R., Pyda, M., and Wunderlich, B., *Thermochimica Acta*, accepted for publication, 2001.
- [17] Pyda, M., Kwon, Y. K., and Wunderlich, B., *Thermochimica Acta*, accepted for publication, 2001; *Proceedings 27th NATAS Conference*, K. R. Williams and K. Kociba, eds., Vol. 27, 1999, p. 345.
- [18] Pak, J. and B. Wunderlich, B., *Thermochimica Acta*, accepted for publication, 2001; *Proceedings 27th NATAS Conference*, K. R. Williams and K. Kociba, eds., Vol. 27, 1999, p. 339.
- [19] Wunderlich, B. and Okazaki, I., *Journal of Thermal Analysis*, Vol. 49, 1997, p. 57; Thomas, L. C., Boller, A., Okazaki, I., and Wunderlich, B., *Thermochimica Acta*, Vol. 291, 1997, p. 85; Okazaki, I. and Wunderlich, B., *Journal of Polymer Science, Part B: Polymer Physics*, Vol. 34, 1966, p. 2941; Wunderlich, B., Boller, A., Okazaki, I., and Kreitmeier, S., *Journal of Thermal Analysis*, Vol. 47, 1996, p. 1013; Boller, A., Okazaki, I. and Wunderlich, B., *Thermochimica Acta*, Vol. 284, 1996, p. 1; Boller, A. Schick, C., and Wunderlich, B., *Thermochimica Acta*, Vol. 266, 1995, p. 97.
- [20] Androsch, R. and Wunderlich, B., *Macromolecules*, Vol. 32, 1999, p. 7238; and to be published; see also: Boller, A., Ribeiro, M., and Wunderlich, B., *Journal of Thermal Analysis and Calorimetry*, Vol. 54, 1998, p. 545; Ishikiriya, K. and Wunderlich, B., *Macromolecules*, Vol. 30, 1997, p. 4126; and *Journal of Polymer Science, Part B, Polymer Physics*, Vol. 35, 1997, p. 1877; Okazaki, I. and Wunderlich, B., *Macromolecular Chemistry and Physics, Rapid Communications*, Vol. 18, 1997, p. 313; and *Macromolecules*, Vol. 30, 1997, 1758.

Mike Reading¹, Duncan M. Price¹ and Hélène Orliac¹

Measurement of Crystallinity in Polymers Using Modulated Temperature Differential Scanning Calorimetry

REFERENCE: Reading M., Price D. M. and Orliac H., “Measurement of Crystallinity in Polymers Using Modulated Temperature Differential Scanning Calorimetry” *Materials Characterization by Dynamic and Modulated Thermal Analytical Techniques, ASTM STP 1402*, A. T. Riga and L. Judovits, Eds., American Society for Testing and Materials, West Conshohocken, PA, 2001.

Abstract: Some time ago a proposal was made [1] for an approach to calculating the initial crystallinity for polymers using MTDSC, i.e., the crystallinity of the sample before the start of the experiment. The essence of the technique is that it attempts to estimate the contribution from the vibrational heat capacity to the total enthalpy absorbed by the sample over the temperature range where crystallization, rearrangement and melting occur. This estimate is made from the reversing signal by using interpolation to subtract any contributions to this signal from crystallisation rearrangement or melting processes. The difference between the total enthalpy and the estimate of the vibrational heat capacity contribution must then be a measure of the enthalpy of melting of any initial crystallinity. The thermodynamic basis of this approach is presented in this article together with examples of its application to both simple and complex systems. There are alternatives to this procedure and the advantages and disadvantages of the various possible approaches are discussed.

Keywords: modulated differential scanning calorimetry, crystallinity, ATHAS database

Introduction

In the following discussion we will consider only the case where we assume that a sample is made up of only two phases, crystalline and amorphous.

The thermodynamic basis for measuring crystallinity has been well known for many years. The relevant enthalpy diagram is given in Figure 1. At any temperature the vertical distance between the enthalpy line for a completely amorphous polymer and the enthalpy line for a 100% crystalline polymer gives the enthalpy evolved when transforming from a perfectly amorphous sample to a perfectly crystalline one (supercooling means that this might occur over a range of temperature on cooling from the melt). It can be seen that this enthalpy changes with temperature, thus the enthalpy associated with a given degree of crystallinity, changes as a function of temperature. This is one of the factors that must be taken into account when calculating initial crystallinity.

¹ Senior Research Fellow, Research Fellow and Visiting Research Associate respectively, IPTME, Loughborough University, Loughborough, Leicestershire LE11 3TU, UK.

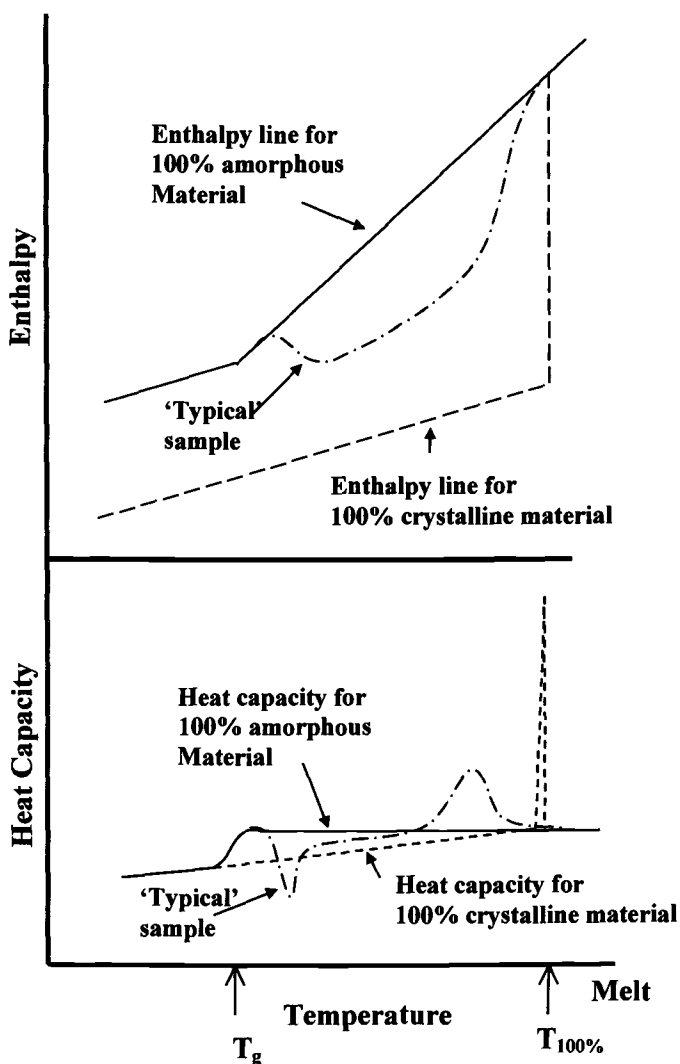


Figure 1- Schematic of idealized enthalpy diagram for a semicrystalline polymer.

Any degree of crystallinity can be represented by an enthalpy line similar to the one given in Figure 2 for a 50% crystalline sample. These types of lines correspond to samples made up of a given fraction of amorphous material with the remaining fraction being perfectly crystalline. In reality, the crystalline material will always be less than perfect and thus melt at a lower temperature than the equilibrium melting temperature.

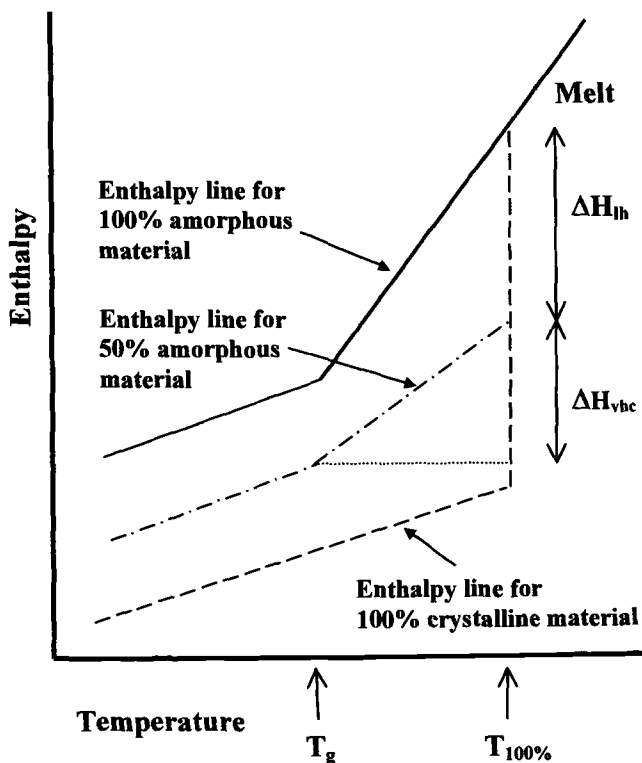


Figure 2 – Schematic of idealized enthalpy plot for 50% crystallinity.

However, when a single figure is used to express crystallinity, it can be said that the sample with the less than perfect crystals is held to be equivalent, in terms of enthalpy, to a sample made of some combination of perfectly amorphous and perfectly crystalline polymer. For each of the lines given in Figure 2 the total enthalpy from just above the glass transition to just after the melt can be divided into a contribution from the vibrational heat capacity ΔH_{vhc} and that from the latent heat of melting, ΔH_{lh} . Now let us consider the case represented by the “typical” sample in Figure 1. In this example, as the sample is heated, it partially crystallizes then increase its crystallinity as it is heated up before, finally, all the crystalline material melts. This kind of behavior is often encountered in practice. The initial crystallinity of this sample can be found by determining the total enthalpy change in moving between the glass transition and the equilibrium melting temperature then subtracting from this figure the enthalpy change for the perfectly amorphous case over the same temperature region. The answer, in this case, can be seen to be zero.

We now turn to real samples, all experiments were carried out using a TA Instruments 2920 heated at 2 °C/min., 60 second period, 1°C amplitude. The total signal from a MTDSC trace for quenched poly(ethylene terephthalate) (PET) is given in Figure 3 (equivalent of conventional DSC). We can see that, after the glass transition,

crystallization occurs then a melting endotherm is clearly seen at higher temperatures. We know from other evidence, to be described later, that in between these two events, rearrangement is occurring although this is not apparent from the DSC alone. The first step in applying the procedure outlined above for determining the initial crystallinity is to express the heat flow in terms of apparent heat capacity.

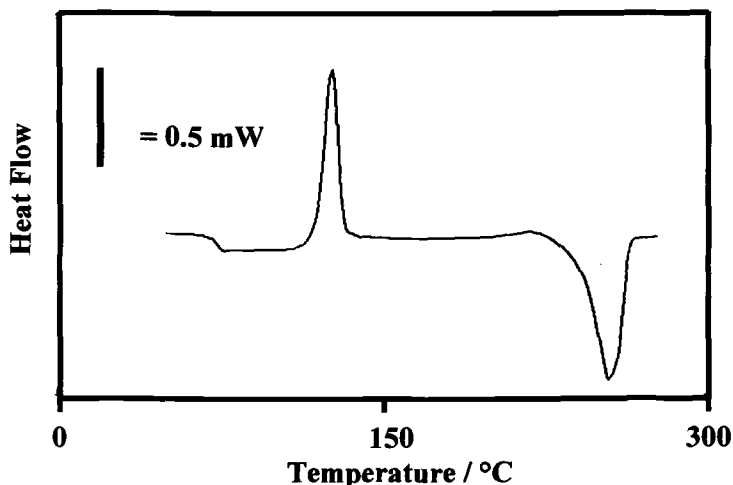


Figure 3 – *Quenched PET*.

The simplest method of doing this is: 1) make a baseline correction by subtracting the heat flow from an experiment carried out under the same conditions using an empty pan of equivalent weight and 2) divide the resulting heat flow by the heating rate and sample mass. The results of doing this are shown in Figure 4. Also given in Figure 4 are the theoretical values for the vibrational heat capacity of PET from the ATHAS database compiled by Wunderlich and available over the internet (<http://web.utk.edu/~athas/>). There are some discrepancies below the glass transition and above the melt that can only be ascribed to experimental error. Here we have applied a simple linear baseline correction to the experimental results to bring them into agreement as shown in Figure 5 (see [2]). From this we have constructed the complete enthalpy diagram given in Figure 6. To do this we have measured the area under the heat capacity curves from the equilibrium melting temperature (also obtained from the ATHAS database) downwards. To the crystalline heat capacity we add the enthalpy of melting of the 100% crystalline sample (taken as 140 J/g again from the ATHAS database). The result is that, to within experimental error, the initial crystallinity is zero (there is always scope for altering the values obtained by changing the integration limits, errors of a few % are typical).

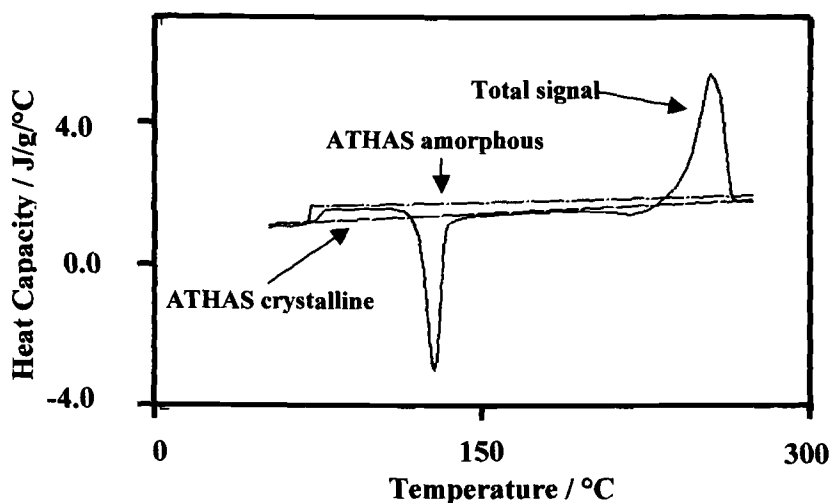


Figure 4 – Quenched PET with ATHAS values for vibrational heat capacity.

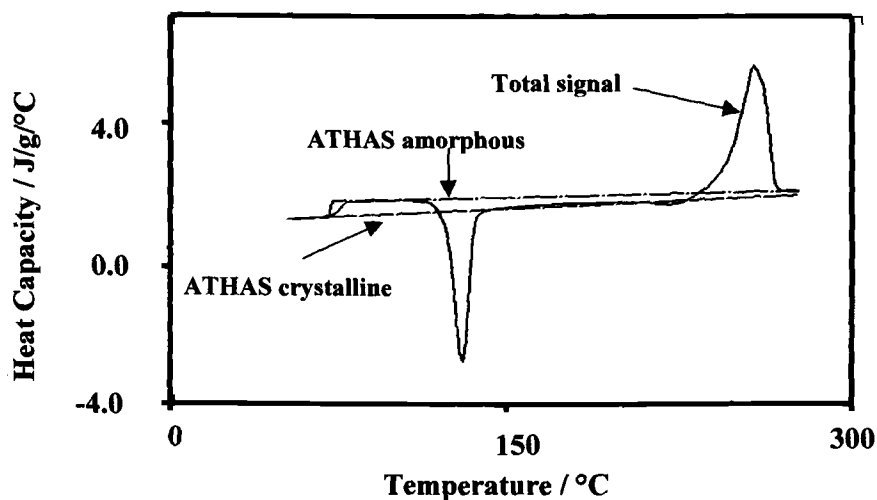


Figure 5—Same as Figure 4 with linear baseline shift to force agreement with the ATHAS values below the glass transition and above the melt.

Alternative Methods for Determining Initial Crystallinity for Simple Systems

An alternative is based on the empirical observation that the heat capacities of amorphous polymers are approximately linear. This being the case, we can extrapolate

from the melt region toward the glass transition as shown in Figure 7. This then gives us the same result for the amorphous vibrational heat capacity as the ATHAS database. If we imagine that we do not have the information contained in the ATHAS system or that this sample is unknown, we can still attempt to investigate its crystallinity using this approach.

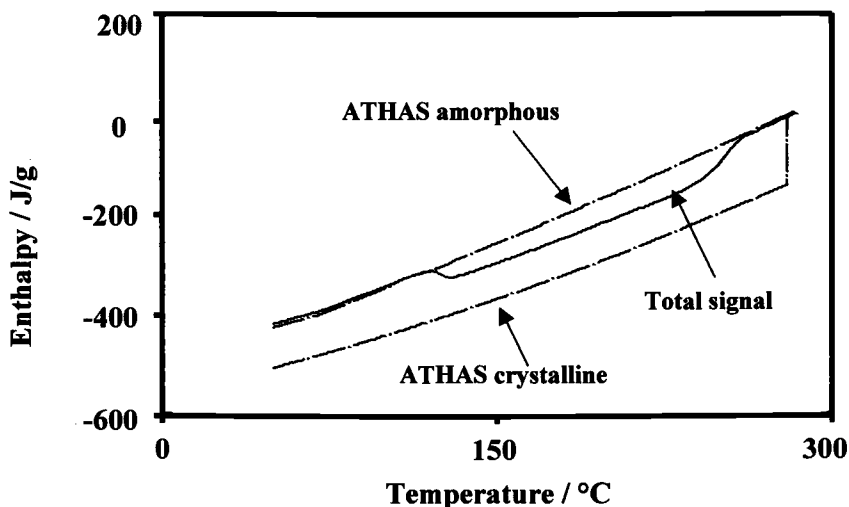


Figure 6 - Full enthalpy diagram for PET using data from Figure 5.

Using the extrapolation we could construct part of the enthalpy diagram shown in Figure 6, i.e. the crystalline enthalpy would be omitted. An equivalent approach is to use it as a baseline so that the difference between the extrapolation and the total heat capacity is integrated. The result is, necessarily, again zero.

In Figure 8 the results of an MTDSC experiment on the same sample are shown. We shall omit any use of the phase angle because, as shall be seen, it is not relevant to the analysis that will be demonstrated.

We can consider the complex heat capacity in isolation as shown in Figure 9. A large peak is seen that starts immediately after the cold crystallisation and ends when melting is complete. This is caused by the rearrangement process outlined above. One of the advantages of MTDSC is that the occurrence of this process can be clearly seen whereas conventional DSC gives little or no indication it is happening. Knowing that this peak is not due to vibrational heat capacity, we can attempt to approximate the values of the vibrational heat capacity by interpolation between the beginning and ending of this peak to obtain an approximation to the vibrational heat capacity. This baseline must also be used to eliminate changes due to the cold crystallization. This is because we are attempting to approximate the contribution to the total enthalpy from the vibrational heat capacity as if the sample were composed from a completely amorphous component and a completely crystalline one that does not melt until reaching the equilibrium melting

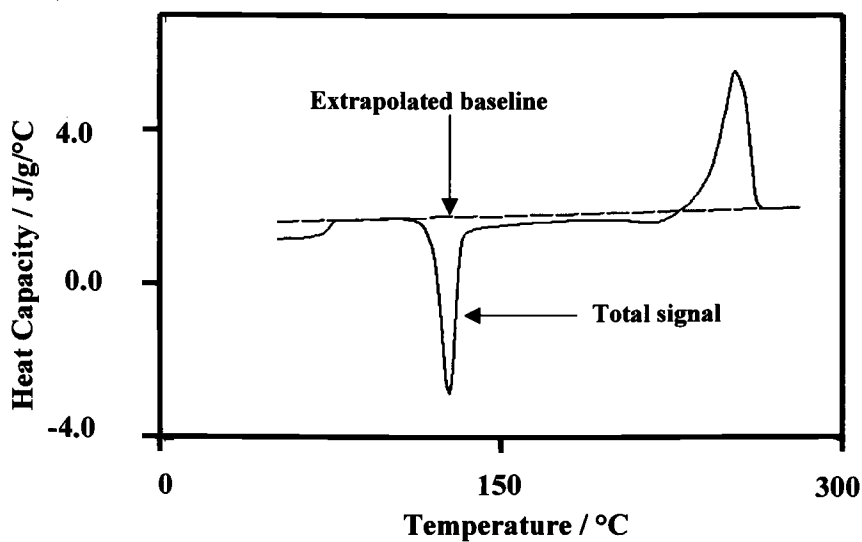


Figure 7 – Quenched PET with baseline extrapolated from the melt.

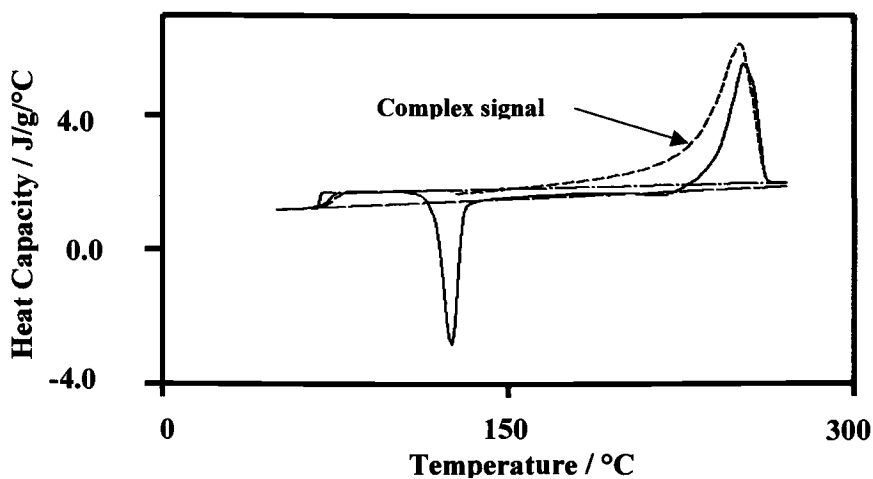


Figure 8 – MTDSC experiment on PET, same as Figure 5 with complex signal added.

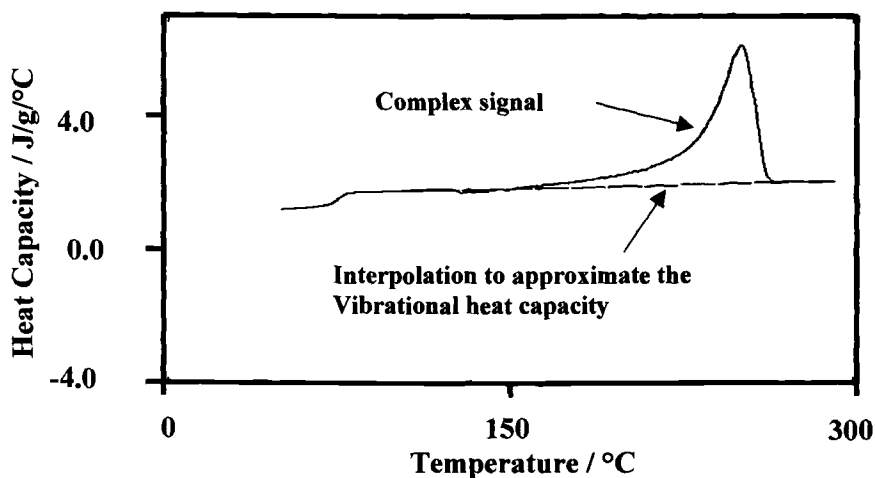


Figure 9 – Complex heat capacity shown with interpolation.

temperature. This being the case, we need to eliminate changes that occur as a consequence of crystallization as well as rearrangement and melting.

This is shown in Figure 10 together with the original total apparent heat capacity. This approximation to vibrational heat capacity can then be subtracted from the total to obtain the difference signal which then should contain that part of enthalpy that is due to the crystallisation, rearrangement and melting. The integral of this is then, once again, zero to within experimental error. Note that the peak in the complex heat capacity is subtracted so any change in its height resulting from the use of the phase lag correction would make no difference to the end result. Similarly, changing the frequency of the modulation would change the height of this peak. Again this does not alter the calculation.

The only difference between the method illustrated in Figure 7 and that shown in Figure 10 is that, in the first case, the baseline that is used for the integration is extrapolated from the melt, in the second case, it is derived by interpolating within the complex heat capacity to eliminate effects due to the heats of crystallization, rearrangement and melting. In the case of pure amorphous PET, the extrapolation and interpolation methods are equivalent. However, in other cases they will give quite different answers.

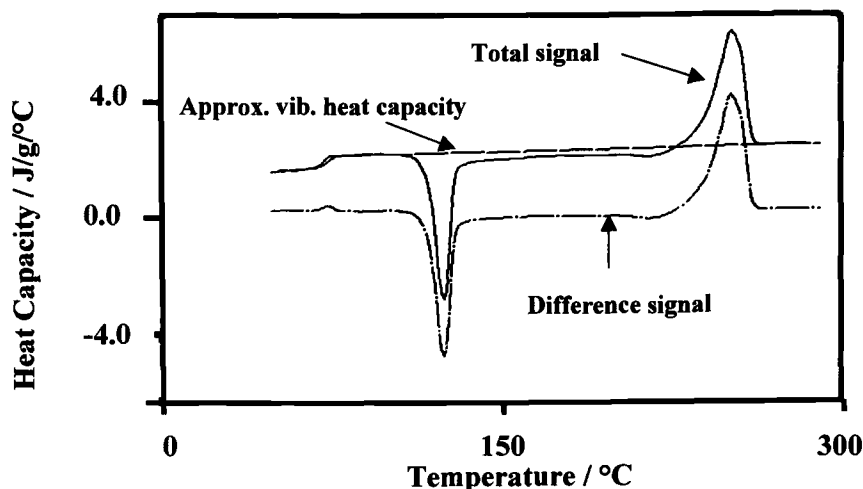


Figure 10 – MTDSC results for PET after “correcting” the complex signal.

Determining the Crystallinity of Complex Systems

In Figure 11 the results for an MTDSC experiment on a PET-PC 50-50 mixture (PC = polycarbonate) are given. A baseline correction has been applied and the total and complex heat capacities have been forced to be the same as each other and the ATHAS vibrational heat capacity values just below the first glass transition and just after the melt by use of a linear baseline adjustment. This is a model sample prepared by simply placing some PC in the same sample pan as PET before the combined sample is heated above 280°C then quenched. The glass transition of the PC is obscured by the cold crystallization of the PET in the total signal (which is equivalent to a conventional DSC experiment) but it is clearly visible in the complex heat capacity. Following the procedure outlined above, the peak that can be seen in the complex C_p that is due to the rearrangement process is removed by interpolation to provide the “corrected” heat capacity signal (intended to approximate the vibrational heat capacity). This is shown in Figure 12 together with the difference or “corrected” non-reversing curve. The integration of this signal gives an enthalpy for the crystallinity of 1.8 J/g (= 2.5% calculated using the known fraction of PET), close to the real value of zero. Figure 10 also shows the extrapolated baseline following the method illustrated in Figure 7. The extrapolation method, which fails to take account of the presence of the amorphous PC, gives an apparent enthalpy associated with crystallinity of 116 J/g.

One source of error in the interpolation method in this case is the contribution from the difference between the total and complex heat capacities at the glass transition of the PC due to their different effective frequencies and any possible annealing [3]. This can be estimated by looking at pure PC as shown in Figure 13. This suggests that, in the mixture, an error of 1.2 J/g could be expected. If this is taken into account, then the figure for the mixture becomes 0.6 J/g which is 1% crystallinity.

An extreme example of a PET-PC blend is presented in Figure 14. This sample contains only 15% PET. Using the “corrected” complex signal as the baseline, a value of 4.5 J/g is obtained for the enthalpy due to crystallinity. Applying the correction for frequency difference at the PC glass transition gives a value of 2.5 J/g. This does, in this sample, correspond to an apparent crystallinity of 12%. However, given that this is a very challenging system, we consider this to be a reasonable result that encourages confidence in the interpolation method.

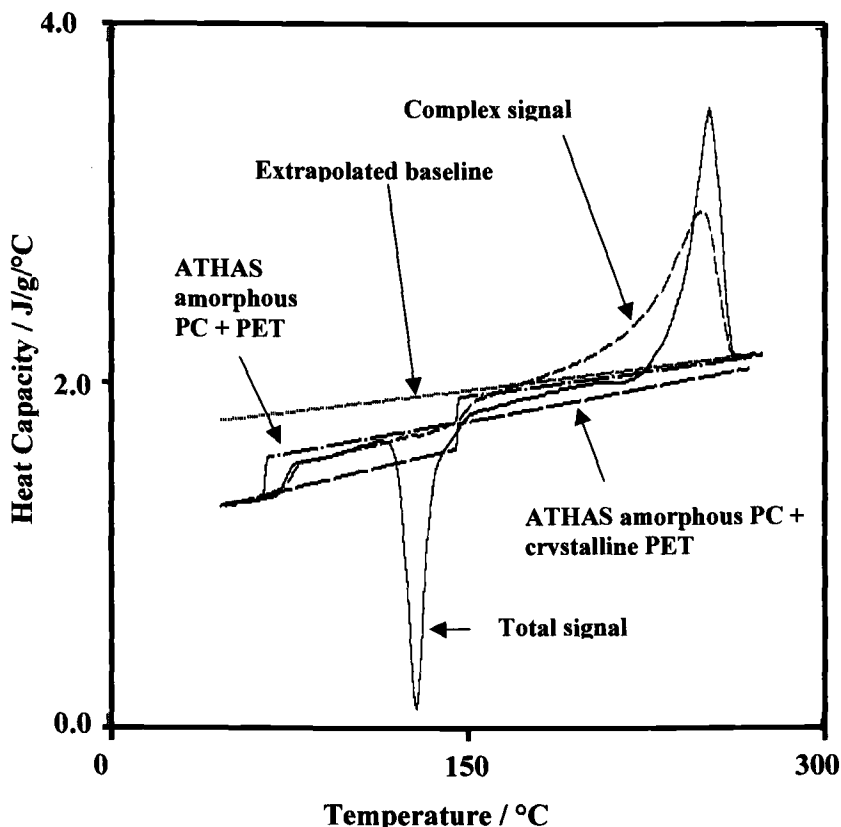


Figure 11 – MTDSC results for a quenched PC-PET mixture.

Sources of Error in the Interpolation Method

In addition to the error discussed above that can arise if a glass transition is present in the temperature interval between the onset of crystallization/rearrangement and the end of melting, there are two main sources of error in the interpolation method.

- 1) In samples that are not almost completely amorphous the linear interpolation may not be accurate because the crystalline vibrational heat capacity is generally not linear with temperature.
- 2) The higher temperature point selected for the interpolation always has a heat capacity value that is, in effect, taken to be equal to that of the 100% amorphous sample. This will clearly not be correct for crystalline samples.

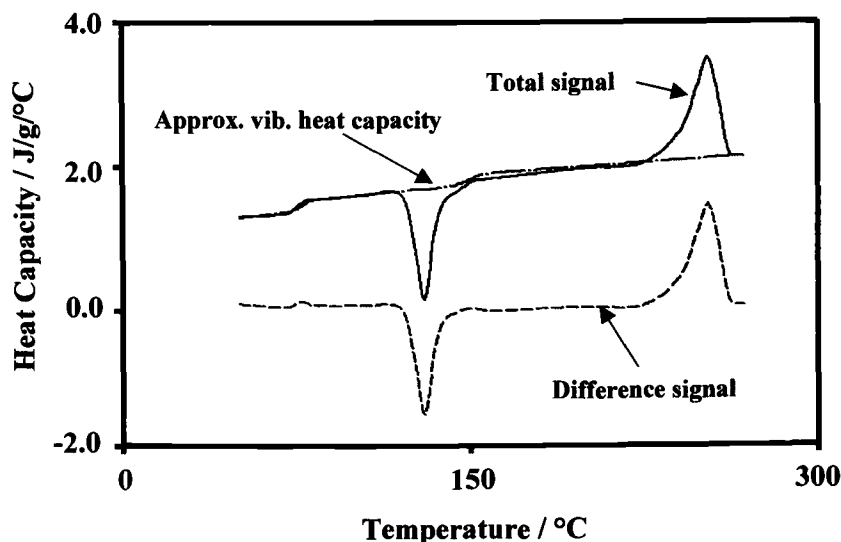


Figure 12 – *Quenched PET-PC mixture after “correcting” the complex signal.*

At first sight these may seem to be significant problems but in many cases these errors are very small. There are two reasons for this:

- 1) The first error has a self-compensating feature. It is zero for a fully amorphous sample and then increase as the sample crystallinity increases. As this happens, the temperature interval over which it becomes necessary to make the interpolation becomes smaller consequently the error become smaller.
- 2) With regard to the second error, it is small when the sample is close to amorphous. As the crystallinity of the sample increases, the potential error increases. However, in many cases the heat capacities for the amorphous and crystalline phases converge as the temperature increases toward the equilibrium melting temperature. This can be seen in the case of PET in Figure 8 and for the blend in Figure 11. The convergence means the error of assuming that the upper heat capacity used for the interpolation is the amorphous heat capacity, which is often very small.

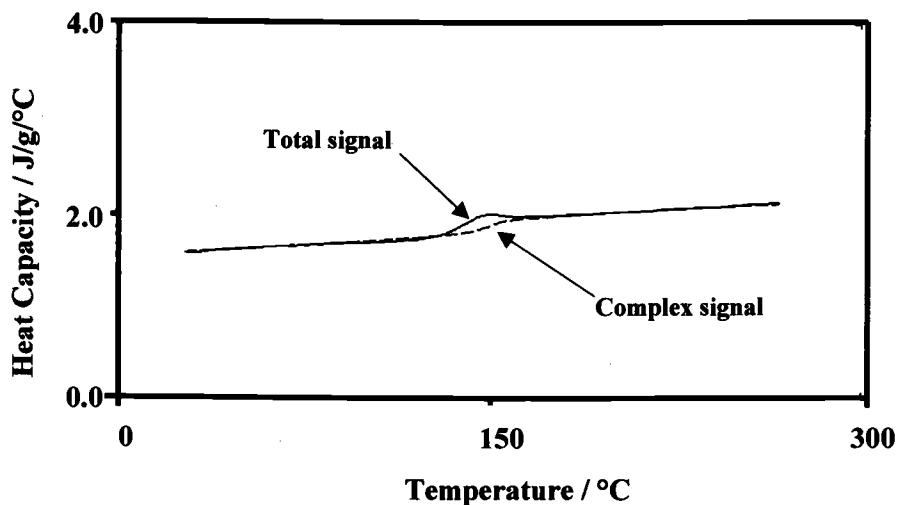


Figure 13 – MTDSC of quenched PC.

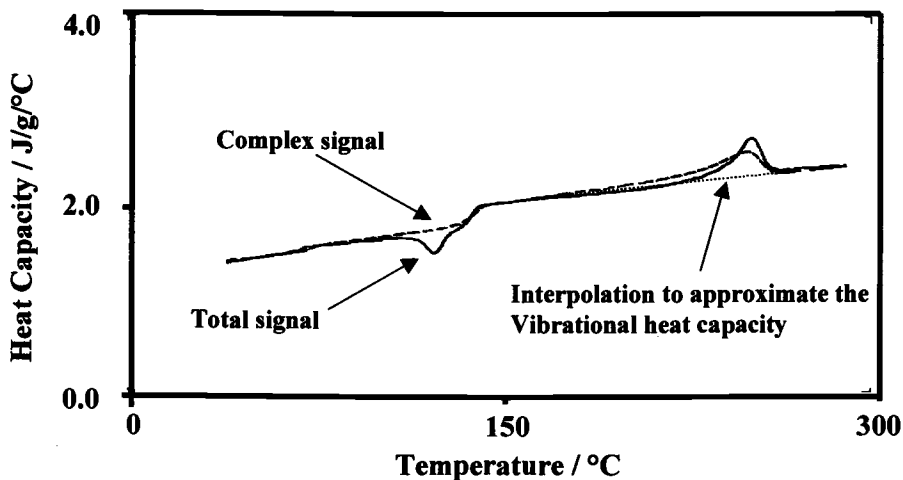


Figure 14 – MTDSC of PET-PC blend.

It is also worth noting that, while both of the above errors increase in terms of enthalpy as the crystallinity increases, as a percentage error they would generally decrease. The second of the above points is illustrated in Figure 15 which gives the MTDSC results for a relatively crystalline sample of PET. The interpolation method gives a crystallinity of 43%. When the theoretical vibrational heat capacity for a 43% crystalline sample is calculated, this and the interpolation are barely distinguishable, as

can be seen in Figure 15. The enthalpy difference between the two methods is less than 1.5%. This then gives us an estimate of a typical error for more crystalline samples from second cause given above. Errors from this source will decrease as the crystallinity decreases.

When considering the question of measuring crystallinity by any of the methods discussed in this article, it should be remembered that in the case of PET, and many other polymers, a rigid amorphous phase is formed which will compromise any calculation of crystallinity based on a simple two phase model. It is important not to push any of the methods outlined here beyond any realistic expectation of their true accuracy.

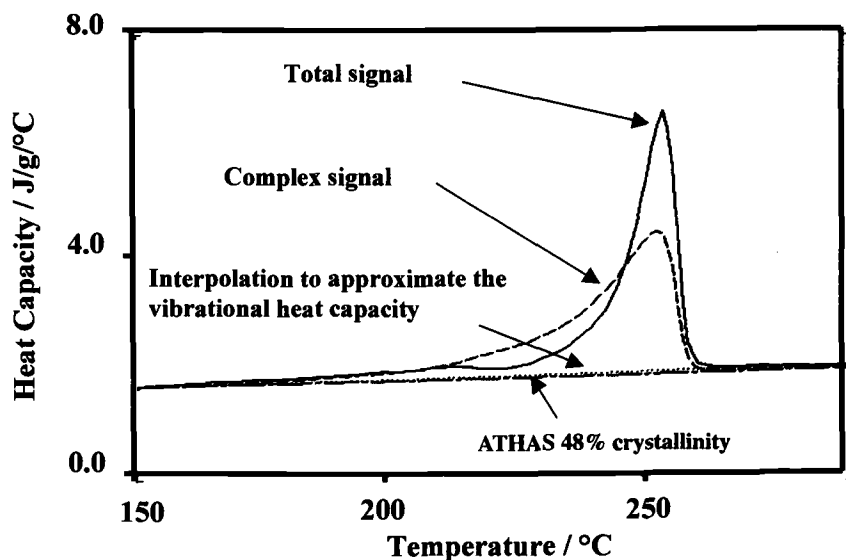


Figure 15 – MTDSC of crystalline PET.

Another source of error in the interpolation method arises from the fact that the enthalpy calculated from the difference signal is a measure of the enthalpy associated with crystallinity at the temperature at the end of the melting peak and not the equilibrium melting temperature. However, in this and most other cases, this error will be small enough to be neglected.

Conclusions

In general, for a pure polymer the best method of measuring crystallinity is to construct the complete enthalpy diagram and compare it with reliable theoretical values such as can be obtained from the ATHAS database. However, most real world samples are not pure polymers. They will be plasticised, or blended or contain fillers and other additives. This makes the enthalpy diagram approach unrealistic in many cases.

The extrapolation method has the advantages that it can deal with samples without reference to a database and it does not require that heat capacities be calculated (although heat capacity has been used here, it is just as applicable to the heat flow curve). However it has the disadvantage that the heat capacity or heat flow values beyond the melt have to be known with very high precision in order for the extrapolation be reliable. Any decomposition, loss of volatiles or chemical reactions will make this impossible. Furthermore, the linear extrapolation is only valid when the sample is a pure or nearly pure polymer. Fillers, a second amorphous polymer (as illustrated above) or other additives might not have a linear relationship between heat capacity and temperature. Given the large temperature interval over which the extrapolation must be made, this could lead to large errors.

The interpolation method based on MTDSC does have possible sources of error. However, in practice these errors will often be small and it has the advantage that it can cope with the kinds of problems outlined above with regard to real world samples. It also has the advantage that it does not require that full heat capacities are calculated or that a database is used. It simply requires that, using the linear baseline shift method, the total complex heat capacities (or total and reversing heat flows) are set to be the same below the glass transition and above the melt. The examples of the application of this method to the mixture and blend given above are, admittedly, somewhat extreme. However, the basic point is that, if this method is robust enough to give reasonable values even when dealing with such difficult samples, it should be able to give reliable results on simpler samples. Probably the main source of error is the second one given above. Inspection of the ATHAS database suggests that there are many polymers that follow PET in having closely converging heat capacities for the amorphous and crystalline phases. However, there will undoubtedly be cases where the difference in heat capacity between the crystalline and amorphous phases close to the melt temperature are sufficient to make the use of the interpolation method inadvisable. Whether to apply this method or one of the alternatives must, in the end, be a decision made by the experimenter in the light of the possible sources of error when set against the advantages.

Finally, it should be noted that the interpolation method described above is exactly equivalent to adding the reversing and non-reversing signals in MTDSC. In this paper we remove the peak in the “reversing” signal (equivalent to the complex signal here) then calculate the “non-reversing” signal (equivalent to the “corrected” difference signal here) before integrating it. This is equivalent to calculating the ‘non-reversing signal’ integrating it then adding (subtracting due to the opposite sign) the integral of the peak in the “reversing” signal.

Acknowledgements

The authors would like to thank N. A. Bailey, Birmingham University UK for providing the samples of the blends.

References

- [1] Reading M., Wilson R. and Pollock H. M., "Modulated Differential Scanning Calorimetry: Theory, Practice and Applications" *Proceedings 23rd NATAS*, Toronto, 1994, pp. 2-11.
- [2] Reading M., Luget A. and Wilson R., "Modulated Differential Scanning Calorimetry", *Thermochimica Acta*, 1994, Vol. 238, pp. 295-307.
- [3] Jones K. J., Kinshott I., Reading M., Lacey A. A., Nikolopoulos C. and Pollock H. M., "The Origin and Interpretation of the Signals of MTDSC", *Thermochimica Acta*, 1997, Vol. 305, pp. 187-199.

Christoph Schick,¹ Andreas Wurm,² and Mikhail Merzliakov³

Crystallization of Polymers and the Rigid Amorphous Fraction Studied by the Temperature-Modulated Techniques TMDSC and TMDMA

REFERENCE: Schick, C., Wurm, A., and Merzliakov, M., “Crystallization of Polymers and the Rigid Amorphous Fraction Studied by the Temperature Modulated Techniques TMDSC and TMDMA,” *Materials Characterization by Dynamic and Modulated Thermal Analytical Techniques*, ASTM STP 1402, A. T. Riga and L. Judovits, Eds., American Society for Testing and Materials, West Conshohocken, PA, 2001.

Abstract: Quasi-isothermal temperature-modulated DSC and DMA measurements (TMDSC and TMDMA, respectively) were performed to determine heat capacity and shear modulus as a function of time during crystallization. Non-reversible and reversible phenomena in the crystallization region of polymers can be observed. The combination of TMDSC and TMDMA yields new information about local processes at the surface of polymer crystals, like reversible melting. Until now we have found only one semicrystalline polymer showing no excess heat capacity during crystallization, namely Bisphenol-A Polycarbonate (PC). This allows study of vitrification and devitrification of the rigid amorphous fraction in PC. For other polymers the fraction of material involved in reversible melting, which is established during main crystallization, keeps constant during secondary crystallization. Simply speaking, polymer crystals are “living crystals.”

Keywords: crystallization, calorimetry, temperature modulation, TMDSC, TMDMA, polymer

Introduction

Calorimetry, mainly differential scanning calorimetry (DSC), is widely used to study isothermal crystallization of polymers. The measured heat flow rate is determined by the large effects due to latent heat. Small changes in baseline heat capacity (fast degrees of freedom) can not be obtained from isothermal DSC measurements. There was the hope to be able to measure baseline heat capacity during quasi-isothermal crystallization by temperature modulated DSC (TMDSC) [1]. Unfortunately, reversing or

¹ Professor, Physics Department, University of Rostock, Universitaetsplatz 3, D-18051 Rostock, Germany, e-mail: christoph.schick@physik.uni-rostock.de.

² Ph.D. student, Physics Department, University of Rostock, Universitaetsplatz 3, D-18051 Rostock, Germany.

³ Research scientist, Physics Department, University of Rostock, Universitaetsplatz 3, D-18051 Rostock, Germany.

complex heat capacity⁴ obtained from TMDSC measurements during crystallization of polymers is often not a measure of baseline heat capacity [2]. It is a complicated superposition of baseline heat capacity, latent heat, kinetics and last but not least effects related to heat transfer in the sample-calorimeter system [3].

In TMDSC a small periodic temperature (correctly speaking heating rate) perturbation in the order of some tenth of a Kelvin is superimposed to a temperature program as normally used in DSC:

$$T(t) = T_o + q_o t + A_T \sin(\omega t) \quad q(t) = q_o + \omega A_T \cos(\omega t) = q_o + A_q \cos(\omega t) \quad (1)$$

where T_o is starting temperature, q_o is underlying heating or cooling rate, A_T is amplitude of temperature and A_q amplitude of heating rate perturbation, ω is angular frequency with $\omega = 2\pi/t_p$, t_p is period. Quasi-isothermal measurements ($q_o = 0$) allow for determination of heat capacity as a function of time [1, 4, 5]. For example, isothermal (quasi-isothermal) crystallization experiments can be performed. Like in isothermal DSC experiments the exothermic effect can be observed. Averaging the measured heat flow rate over one period of the temperature perturbation yields the so called "total" heat flow rate, $\langle HF \rangle$. In response to the periodic temperature perturbation a periodic heat flow rate occurs. From the amplitudes of measured heat flow rate A_{HF} and of heating rate perturbation A_q the modulus of complex heat capacity can be obtained, for details see e.g. [4, 6, 7].

$$\left| C_p^* \right| = \frac{A_{HF}}{A_q} \quad (2)$$

Because of time-dependent processes a phase angle between perturbation and response can be observed in TMDSC too. In the case of isothermal polymer crystallization information about crystal growth rate is available from the measured phase angle as discussed by Toda et al. [8]. But again, the measured heat capacity during quasi-isothermal crystallization of polymers is, in general, not a measure of baseline heat capacity. Often an increase of measured complex heat capacity instead of the expected decrease is observed [9, 10]. Wunderlich [2] introduced the term "reversible melting" to explain the occurrence of some latent heat effects during quasi-isothermal TMDSC measurements. This reversible melting contributes to the periodic part of the observed heat flow rate. Reversible melting and crystallization can even be observed during quasi-isothermal measurements when temperature amplitude is as small as 0.005 K [11]. Consequently, no super-cooling seems to be necessary for reversible melting and crystallization. It is still an open question what is the microscopic origin of this reversible melting. Possible explanations are given by Wunderlich [12] and Strobl [13]. In this paper we will show that reversible melting does not only contribute to the modulus of complex heat capacity but even to the amplitude of shear modulus oscillations in temperature-modulated DMA measurements. On the example of PC it is shown that

⁴ Because reversing heat capacity and modulus of complex heat capacity are two different terms for the same quantity we only use the term modulus of complex heat capacity, $\left| C_p^* \right|$.

baseline heat capacity can be measured at sufficiently high frequencies. This allows study of vitrification and devitrification of the rigid amorphous fraction (RAF) in PC.

Experimental

TMDSC is a technique described for the first time in 1971 by Gobrecht et al. [1], and the necessary data treatments are described elsewhere [1, 4, 6, 7]. Similar to TMDSC in TMDMA the temperature profile as normally used is superimposed with a small periodical temperature perturbation. For the TMDMA measurements an Advanced Rheometric Expansion System (ARES) from Rheometric Scientific was used. The Rheotest software includes a comfortable programming language. With that it is possible to synthesize any periodic temperature-time-program with or without underlying heating or cooling rate.

As shown in [14-16] a data treatment algorithm like in TMDSC can be applied to TMDMA measurements. Nevertheless, there is at least one fundamental difference. Whereas in DSC only temperature or time derivatives of changes in structure can be observed, in DMA a quantity is measured which is directly related to structure. Unfortunately, in heterogeneous materials the relation between shear modulus and crystallinity is complicated and not well understood [17, 18]. Nevertheless, shear modulus measurements allow for the investigation of small changes in crystallinity especially if they occur over very long times. This gives the opportunity to study very slow processes during quasi-isothermal measurements in the crystallization region of polymers as discussed below.

There are two different perturbations of the sample in TMDMA, the first is the periodic shear strain and the second is the periodic temperature profile. In order to get enough (>50) data points for data evaluation during one period of the temperature modulation the mechanical perturbation has to be much faster than the temperature modulation.

The period length of the temperature modulation was limited to lower periods by the time constant of the equipment, for details see [15]. Periods of 1200 s for the temperature modulation, periods of 1 - 10 s for the mechanical perturbation and shear strain between 0.1 % and 0.5 % have been used for the TMDMA measurements. For the TMDMA measurements these long periods are easy to realize and reasonable results can be obtained. If one wants to compare the results from TMDMA measurements with that from TMDSC using the same temperature-time profile or to measure heat capacity in a broad frequency range high sensitive DSC apparatuses like Perkin Elmer Pyris 1 DSC or Setaram DSC 121 must be used, for details see [15]. Additional measurements were made at a fixed frequency of 0.01 Hz using a TA Instruments DSC 2920CE and at 1 Hz using an AC calorimeter (for details see reference 32). For the comparison careful temperature calibration of all instruments is necessary. The calorimeters are calibrated according to the GEFTA recommendation [19]. The calibration was checked in TMDSC mode with the smectic A to nematic transition of 8OCB [20, 21]. The DMA apparatus was temperature calibrated with melting of water, indium, tin, and lead. A small solid sample of the calibrant was placed between the two parallel plates and the rapid change of its thickness during melting caused by a small compression was measured.

Samples

The polycaprolactone (PCL) is a commercial sample synthesized by Aldrich Chemie with a molecular weight average $M_w = 55700$ g/mol. More details about the sample are reported in [22]. The Bisphenol-A Polycarbonate (PC) was obtained from General Electric (tradename LEXAN™) and was purified by dissolution in chloroform, filtering and precipitation in methanol [23, 24]. The weight average molar mass and polydispersity index for the polycarbonate were obtained by Gel Permeation Chromatography in chloroform ($M_w = 28,400$ g/mol and $M_w/M_n = 2.04$). The heat capacity data for these polymers in the liquid and the solid state are available from ATHAS data bank [25].

For the calorimetric measurements the sample size of the melt-pressed samples ($T = T_m + 10$ K) was adapted according to the frequency applied to avoid large temperature gradients inside the samples. Sample mass was about 1 mg at 1 Hz, 15 mg in the range 0.1 Hz and 0.001 Hz, and 100 mg in the range 0.01 Hz and 0.0001 Hz. For the TMDMA measurements a similar melt pressed cylinder of about 5 mm diameter and 4 mm height was used in a parallel plate geometry.

Baseline heat capacity

In a first approximation, using a simple two-phase model, the expected baseline heat capacity c_{pb} for the semicrystalline sample can be calculated according to

$$c_{pb}(T, t) = \chi_c(T, t) c_{p\ crystal}(T) + (1 - \chi_c(T, t)) c_{p\ melt}(T) \quad (3)$$

with $c_{p\ crystal}$ specific heat capacity for the crystal, $c_{p\ melt}$ that for the melt and χ_c degree of crystallinity. For most polymers deviations from such a simple two-phase model are observed [26, 27]. Introducing a rigid amorphous fraction the baseline heat capacity can be obtained from

$$c_{pb}(T, t) = \chi_r(T, t) c_{p\ rigid}(T) + (1 - \chi_r(T, t)) c_{p\ melt}(T) \quad (4)$$

with $c_{p\ rigid}$ specific heat capacity of the rigid fraction that contains crystalline and rigid (immobilized, vitrified) amorphous material (RAF). For most polymers $c_{p\ rigid}$ equals $c_{p\ crystal}$ and is available from [25]. $\chi_r(T, t)$ is the rigid fraction. At the glass transition temperature $\chi_r(T_g)$ can be obtained from the step of heat capacity

$$\chi_r = 1 - \frac{\Delta c_p}{\Delta c_{pa}} \quad (5)$$

where Δc_p is the heat capacity step of the semicrystalline sample while Δc_{pa} is that of the totally amorphous sample. To obtain the exact baseline heat capacity in the temperature range between glass transition and melt for a three phase model iterative procedures are necessary [28, 29].

Results

Figure 1 shows the heat flow rate during quasi-isothermal crystallization at average temperature 328 K for PCL. The sample was melted at 343 K for 20 minutes and cooled at 1 K/min to the crystallization temperature. Temperature perturbation has an amplitude of 0.5 K and a period of 1200 s. The crystallization process has been followed for 3 days.

After crystallization the sample was heated with $q_0 = 10$ K/min to the melt at 343 K. From this DSC scan the heat of fusion Δh was determined to be 82 J/g. The ratio between the measured and the heat of fusion for an infinite crystal ($\Delta h^\circ = 156.8$ J/g [25]) yields crystallinity $\chi \approx 0.5$.

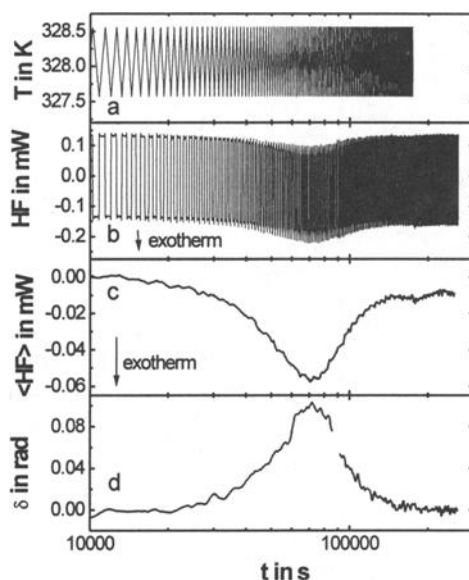


Figure 1 - Quasi-isothermal crystallization of PCL at $T_0 = 328$ K, $t_p = 1200$ s, $A_T = 0.5$ K. curve a- quasi-isothermal temperature profile, curve b- measured heat flow rate, c- total heat flow rate $\langle HF \rangle$, d- phase angle between heat flow rate and heating rate.

In Figure 2 modulus of complex heat capacity, eq.(2), for measurements at different frequencies is shown together with the values for baseline heat capacity for the melt [25] and the semicrystalline sample, eq.(3), for $\chi = 0.5$, dotted line. Complex heat capacity calculated from the heat flow rate amplitude is always larger than the value from eq. (3). From the difference an excess heat capacity of about 0.1 J/gK at 0.05 Hz can be obtained.

To determine the excess heat capacity during crystallization as a function of time the curve for the baseline heat capacity must be obtained. This was done with the time dependence of crystallinity and eq. (3). Crystallinity was estimated from the enthalpy

change during crystallization. The result for crystallinity is shown in Figure 3, curve a, and that for expected baseline heat capacity, $c_{pb}(t)$ in Figure 2, dashed line.

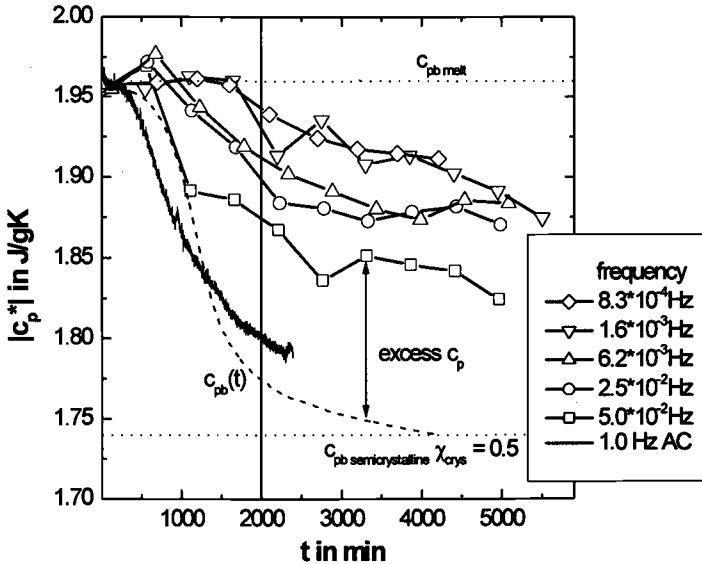


Figure 2 - Modulus of complex heat capacity during crystallization of PCL at 328 K (327.5 K for AC-calorimetric measurement) as a function of crystallization time. Parameter is frequency of temperature modulation. Temperature amplitude 0.5 K for TMDSC and 0.02 K for AC-calorimeter. $c_{pb}(t)$ denotes baseline heat capacity according to eq. (3).

Complex heat capacity is always larger than baseline heat capacity, except the very beginning when both equal heat capacity of the melt. The difference between complex and baseline heat capacity can be considered as excess heat capacity because of some latent heat occurring due to reversible melting. Reversible melting of PCL is studied in more detail in [11, 30]. No RAF is taken into account in eq. (3). Doing so would additionally lower the expected baseline heat capacity and increase the excess heat capacity. In case of PCL this would not change the picture discussed below because of the small amount of RAF in PCL. The time courses of excess heat capacity and degree of crystallinity are shown in Figure 3.

As can be seen (Figure 3) excess heat capacity and degree of crystallinity behave differently. While degree of crystallinity is still increasing during secondary crystallization excess heat capacity stays more or less constant from the end of main crystallization. This indicates that some additional information is available from the excess heat capacity [11].

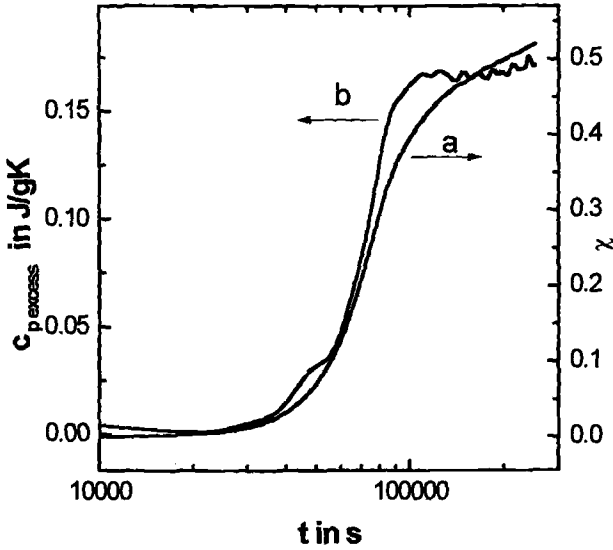


Figure 3 - Time evolution of crystallinity (curve a) and excess heat capacity (curve b), see text, during quasi-isothermal crystallization of PCL (Figure 1) at frequency $8.3 \cdot 10^{-4}$ Hz ($t_p = 1200$ s).

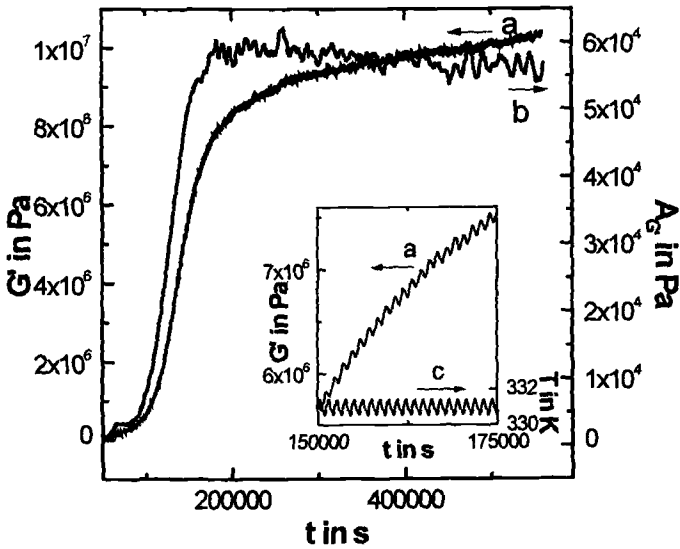


Figure 4 - Time evolution of storage shear modulus (curve a) and amplitude of storage modulus oscillations (curve b) during quasi-isothermal crystallization of PCL at $T_0 = 331$ K, $t_p = 1200$ s, $A_T = 0.5$ K (curve c).

Next, we checked if reversible melting can be probed with other techniques than calorimetry. Because shear modulus is very sensitive to changes in crystallinity temperature modulated DMA measurements (TMDMA) were performed [14-16]. First the influence of shear stress, applied during shear modulus measurements, on crystallization kinetics was checked. An isothermal crystallization experiment with continuous shearing was compared to one with only partial shearing of the sample [15]. No difference between both curves could be seen for shear stress frequency 0.5 Hz and amplitude 1 % which is larger than that used for the other measurements. Therefore it seems to be possible to use DMA under these measuring conditions to study crystallization of PCL.

The sample was melted at 343 K for 20 minutes and cooled with 1 K/min to the crystallization temperature. Figure 4, curve *a* shows the data of the storage modulus for a quasi-isothermal TMDMA crystallization experiment at 331 K with temperature amplitude 0.5 K and period 1200 s. The relatively high crystallization temperature (slow crystallization) was chosen to be able to follow the whole crystallization process in one measurement. The total time for this experiment was more than 6 days.

Crystallization starts after an induction time due to nucleation. With increasing crystallinity the storage modulus increases for 2.5 orders of magnitude, curve *a*. The relation between the storage modulus and crystallinity is very complicated. A lot of (for the most polymers unknown) sample properties are needed to describe this relation with theories taking into account combinations of amorphous and crystalline parts in the sample. So it is difficult to estimate changes in crystallinity from shear modulus measurements quantitatively. From the shape of the modulus curve two different crystallization regimes can be distinguished – until about 200,000 s main and up to the end secondary crystallization.

The insert (Figure 4) shows a magnified part of the modulus curve at the end of main crystallization. It is remarkable and unexpected that at the heating segments of temperature modulation there is always a decrease of storage modulus. This may indicate that parts of the sample melt or undergo a glass transition in the time scale of the modulation.

Using Fourier analysis, as for the periodic part of the heat flow rate, an amplitude of the shear modulus oscillations can be obtained, curve *b*. One can see an increase during main crystallization with a relatively abrupt change to a constant or slowly decreasing value during secondary crystallization. This is contrary to the behavior of the storage modulus itself which is related to crystallinity, and increases up to the end of the measurement.

Similar experiments for Poly(ethylene terephthalate) (PET), Poly(ethylene-2,6-naphthalene dicarboxylate) (PEN) and Poly(ether ether ketone) (PEEK) yield the same results as shown in [31].

In order to obtain information about the characteristic time scale of the molecular processes related to excess heat capacity we have studied the frequency dependence of complex heat capacity during quasi-isothermal crystallization, see Figure 2. To extend the frequency range available with TMDSC (10^{-5} Hz - 10^{-1} Hz) AC calorimetric measurements were performed at a frequency of 1 Hz.

A mean relaxation time in the order of seconds can be estimated from Figure 5 for the process at 328 K for PCL.

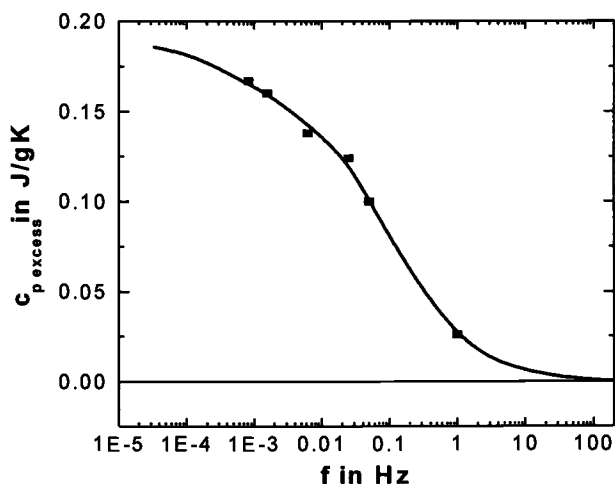


Figure 5 - Excess-heat capacity of PCL after 2000 minutes crystallization at 328 K as a function of modulation frequency, data from Figure 2.
PerkinElmer Pyris 1 DSC and AC calorimeter [32]

As can be seen from Figure 5 the frequency range available is still not broad enough for a detailed discussion of the curve shape. From this curve one expects for frequencies higher than about 100 Hz to measure baseline heat capacity without contributions due to reversible melting. Base-line heat capacity corresponds to the heat necessary to increase the temperature of the sample without changing crystallinity. In other words it is the heat capacity without any contribution from latent heat. Next we will focus on baseline heat capacity which can be measured at the high frequency limit, see Figure 5. In this case vitrification and devitrification of the rigid amorphous fraction of semicrystalline polymers can be studied. There are two possible paths to reach this goal: To extend the frequency range of heat capacity measurements or to study polymers with very slow dynamics of the reversible melting so that the high frequency limit is reached at standard frequencies of temperature modulated DSC. For PCL, as an example, frequencies above 100 Hz are necessary to measure baseline heat capacity. This is far above the TMDSC high frequency limit of 0.1 Hz. A chance to reach such high frequencies for heat capacity measurements is given with recent developments of AC calorimetry [32] rather than by the 3ω -method [33] where it seems to be difficult to distinguish between heat capacity and thermal conductivity contributions. In this paper we followed the second approach and have studied Bisphenol-A Polycarbonate. PC was chosen for this study because of its very slow crystallization behavior [34] and because there is no reversible melting outside the main melting peak [35].

The time evolution of heat capacity during isothermal crystallization of PC at 456.8 K is shown in Figure 6. Measured heat capacity becomes smaller than baseline heat capacity obtained from eq. (3), curve *d*, – indicating the occurrence of a significant RAF during the crystallization process. After 10^6 s (ca. 11 days) the heat capacity equals baseline heat capacity according to eq. (4), curve *e*, using the data for the RAF from the step of heat capacity at the glass transition at 420 K. From this observation we can conclude that the total RAF of PC is established (vitrified) during the isothermal crystallization and no additional vitrification occurs during cooling to the glass transition temperature. We also checked the frequency dependence of the measured heat capacity by using the high performance DSC's from PerkinElmer Instruments and Setaram. In the frequency range 0.03 Hz to 8×10^{-5} Hz no frequency dependence can be detected, see points (f) in Figure 6. This indicates that there is no excess heat capacity for PC at 456.8 K and that base line heat capacity is measured.

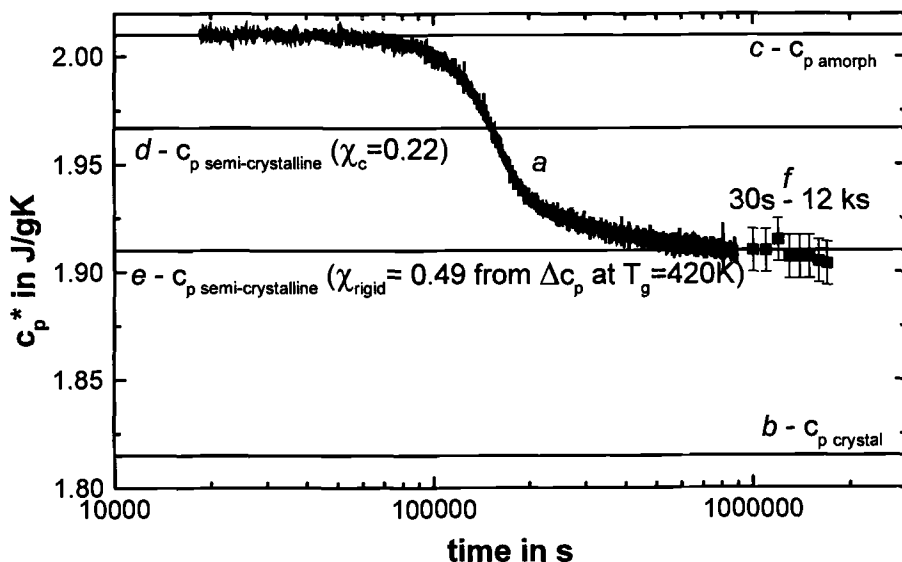


Figure 6 - Time evolution of heat capacity during quasi-isothermal crystallization of PC at 456.8 K, $A_T = 0.5$ s, $t_p = 100$ s, curve *a* (TAI DSC2920). Curve *b* and *c* correspond to crystalline and liquid heat capacities, respectively. Curve *d* was estimated from a two phase model, eq. (1) and curve *e* from a three phase model, eq. (2). The points *f* are measured in the frequency range as indicated (PE Pyris 1 DSC, Setaram DSC 121).

The question arises at what temperature the RAF devitrifies on heating – before the crystals melt or is devitrification of the RAF part of the main melting. The heat capacity measured at scanning through the melting region of PC shows some excess heat capacity in the temperature range 460 K – 510 K due to reorganization on slow heating (0.5 K/min) (Figure 2, curve *a*). To measure heat capacity without contributions from reorganization quasi-isothermal TMDSC measurements at stepwise increasing

temperatures were performed. The results in the temperature range above glass transition are shown in Figure 7.

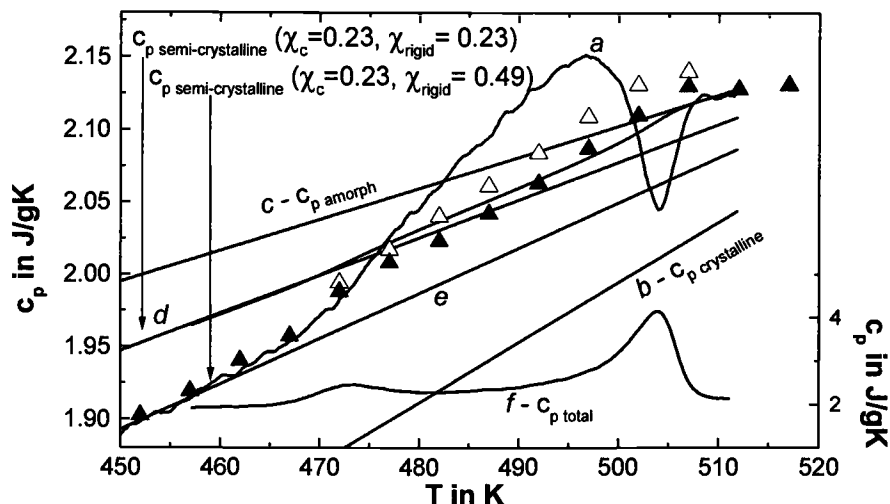


Figure 7 - Curve *a*: TMDSC scan measurement of semicrystalline PC at underlying heating rate 0.5 K/min, temperature amplitude 0.5 K and period 100 s in the temperature range above glass transition. Curve *b* and *c* correspond to heat capacities for crystalline and liquid PC, respectively. Curve *d* was estimated from a two phase model, eq. (3) taking into account the change in crystallinity in the main melting region and curve *e* from a three phase model, eq. (4) using data from T_g . Curve *f* shows the total heat capacity in the melting region. The triangles show the heat capacities from quasi-isothermal TMDSC measurements on stepwise increasing temperatures. The data were taken after 15 minutes, open triangles, and after 3 hours, solid triangles. TA Instruments DSC 2920

From about 470 K changes in heat capacity during the quasi-isothermal measurements can be seen. The difference between open and solid triangles corresponds to 3 hours. After 3 hours, solid triangles, the sample has stabilized, except in the temperature range 490 K – 505 K where re-crystallization occurs. Let us focus on the region of the pre-melting peak between 460 K - 485 K. An increase of heat capacity can be observed. The heat capacity starts to deviate from the baseline heat capacity obtained from a three-phase model including RAF, eq. (4) curve *e*, and around 480 K it is close to the baseline heat capacity obtained from a two phase model, eq. (3) curve *d*. In eq. (3) only crystalline and mobile amorphous material are taken into account. At higher temperatures, during main melting, heat capacity approximately follows increasing baseline heat capacity as estimated from the temperature dependent crystallinity and eq. (3), curve *d*, and finally reaches the liquid heat capacity, curve *c*. This stepwise increase of heat capacity between 465 K and 475 K towards the value expected from a two phase model can be interpreted as the devitrification of the RAF.

Discussion

Temperature-modulated DSC and DMA allow for the investigation of reversible and non-reversible phenomena in the crystallization region of polymers. The combination of TMDMA and TMDSC yields new information about local processes at the surface of polymer crystals, like reversible melting. Reversible melting can be observed in complex heat capacity and in the amplitude of sheer modulus in response to temperature perturbation. The fraction of material involved in reversible melting, which is established during main crystallization, keeps constant during secondary crystallization. This shows that also after long crystallization times the surfaces of the individual crystallites are in equilibrium with the surrounding melt. Simply speaking, polymer crystals are "living crystals." For reversible melting a strong frequency dependence of heat capacity can be seen. From this the characteristic time for the corresponding molecular processes can be estimated. For PCL at 328 K it is in the order of several seconds. In the high frequency limit excess heat capacity tends to zero. Consequently, baseline heat capacity can be measured at high frequencies. Because the time scale of the molecular processes depends on the polymer also the high frequency limit depends on the polymer under investigation. No frequency dependence of heat capacity was observed for PC outside the main melting peak in the frequency range 0.03 Hz to $8 \cdot 10^{-5}$ Hz indicating the absence of reversible melting in this frequency range. Therefore we are able to measure baseline heat capacity at frequency 0.01 Hz and to study vitrification and devitrification of the RAF. For PC the RAF is established during isothermal crystallization as can be seen from Figure 6. Devitrification of the RAF seems to be related to the pre-melting peak or lowest endotherm, see Figure 7. For PC the melting of small crystals between the lamellae yield the pre-melting peak [23, 24, 34, 36]. The immobilization of the amorphous material around these small crystals, which are formed during isothermal crystallization [36], results in the vitrification of the RAF during crystallization and in its devitrification during melting. A remaining RAF of about 10% can be estimated from the small difference between measured and baseline heat capacity (Figure 7). This RAF may be at the fold surface of the lamellae.

Conclusions

As shown herein, TMDSC and TMDMA provide us with new information regarding crystallization of polymers that is unavailable from other measurements. It should be noted that especially the frequency dependence of excess heat capacity yields additional information. The study of the RAF is not possible unless the frequency-independent heat capacity (baseline heat capacity) is measured. Therefore, we need high performance calorimeters (DSC's) which allow measurement of the heat capacity in a wide frequency range. To achieve this goal measured heat capacity must be carefully corrected for instrumental effects, mainly heat transfer problems between temperature sensor and sample as well as heat transfer inside the sample [3,37,38], and care must be taken not to violate linearity and stationarity which are prerequisites of the method [39,40].

Acknowledgement

We are thankful to Prof. H. Marand, Blacksburg, VA, for supplying the PC sample and for stimulating discussions. This research was supported by the European Commission (grant IC15CT96-0821), the German Science Foundation (grant DFG Schi-331/5-1) and the government of Mecklenburg-Vorpommern. Support by PerkinElmer Instruments and TA Instruments is acknowledged.

References

- [1] Gobrecht, H., Hamann, K., and Willers, G., "Complex plane analysis of heat capacity of polymers in the glass transition region" *Journal of Physics E: Scientific Instruments* 4, 1971, 21, pp. 21-23.
- [2] Okazaki, I., and Wunderlich, B., "Reversible local melting in polymer crystals" *Macromolecular Chemistry Rapid Communications* 18, 1997, pp. 313-318.
- [3] Merzlyakov, M., and Schick, C., "Complex heat capacity measurements by TMDSC Part 2: Algorithm for Amplitude and Phase Angle Correction" *Thermochimica Acta* 330, 1999, pp. 65-73.
- [4] Wunderlich, B., Jin, Y.M., and Boller, A., "Mathematical description of differential scanning calorimetry based on periodic temperature modulation" *Thermochimica Acta* 238, 1994, pp. 277-293.
- [5] Wunderlich, B., Boller, A., Okazaki, I., and Kreitmeier, S., "Linearity, steady state, and complex heat capacity in modulated differential scanning calorimetry" *Thermochimica Acta* 282/283, 1996, pp. 143-155.
- [6] Reading, M., "Modulated differential scanning calorimetry - A new way forward in materials characterization" *Trends in Polymer Science* 8, 1993, pp. 248-253.
- [7] Schawe, J. E. K., "A comparison of different evaluation methods in modulated temperature DSC" *Thermochimica Acta* 260, 1995, pp. 1-16.
- [8] Toda, A., Oda, T., Hikosaka, M., and Saruyama, Y., "A new analyzing method of temperature modulated DSC of exo- or endo-thermic process - application to polyethylene crystallization" *Thermochimica Acta* 293, 1997, pp. 47-63.
- [9] Toda, A., Oda, T., Hikosaka, M., and Saruyama, Y., "A new method of analysing transformation kinetics with temperature modulated differential scanning calorimetry - application to polymer crystal growth" *Polymer* 38, 1997, pp. 231-233.
- [10] Scherrenberg, R.L., Mathot, V.B.F., and van Hemelrijck, A., "The practical applicability of TMDSC to polymeric systems" *Thermochimica Acta* 330, 1999, pp. 3-19.
- [11] Merzlyakov, M., Wurm, A., Zorzut, M., and Schick, C., "Frequency and temperature amplitude dependence of complex heat capacity in the melting region of polymers" *Journal of Macromolecular Science-Physics* 38, 1999, pp. 1045-1054.
- [12] Wunderlich, B., "Macromolecular Physics," Vol. 2, Academic Press, New York, 1976.

- [13] Strobl, G., "A new approach to polymer crystallization used in an analysis of data of syndiotactic polypropylene" *Acta Polymerica* 48, 1997, pp. 562-570.
- [14] Wurm, A., Merzlyakov, M., and Schick, C., "Reversible melting probed by temperature modulated dynamic mechanical and calorimetric measurements" *Colloid and Polymer Science* 276, 1998, pp. 289-296.
- [15] Wurm, A., Merzlyakov, M., and Schick, C., "Temperature modulated dynamic mechanical analysis" *Thermochimica Acta* 330, 1999, pp. 121-130.
- [16] Wurm, A., Merzlyakov, M., and Schick, C., "Crystallization of polymers studied by temperature-modulated techniques (TMDSC, TMDMA)" *Journal of Macromolecular Science-Physics* 38, 1999, pp. 693-708.
- [17] Alig, I., Lellinger, D., and Tadjbakhsh, S., "Ultrasonic methods for characterization of polymeric materials" *Polymeric Material Science & Engineering* 79, 1998, pp. 31-32.
- [18] Floudas, G., and Tsitsilianis, C., "Crystallization kinetics of poly(ethylene oxide) in poly(ethylenen oxide) polystyrene poly(ethylene oxide) triblock copolymers" *Macromolecules* 30, 1997, pp. 4381-4390.
- [19] Sarge, S.M., Hemminger, W. Gmelin, E. Höhne, G.W.H., Cammenga, H.K., and Eysel, W., "Metrologically based procedures for the temperature, heat and heat flow rate calibration of DSC" *Journal of Thermal Analysis and Calorimetry* 49, 1997, pp. 1125-1134.
- [20] Hensel, A., and Schick, C., "Temperature calibration of temperature-modulated differential scanning calorimeters" *Thermochimica Acta* 304/305, 1997, pp. 229-237.
- [21] Schick, C., Jonsson, U., Vassiliev, T., Minakov, A., Schawe, J., Scherrenberg, R., and Lőrinczy, D., "Applicability of 8OCB for temperature calibration of temperature modulated calorimeters" *Thermochimica Acta* 347, 2000, pp. 53-61.
- [22] Skoglund, P. and Fransson, A., "Continuous cooling and isothermal crystallization of polycaprolactone," *Journal of Applied Polymer Science* 61, 1996, pp. 2455-2465.
- [23] Sohn, S., Alizadeh, A., and Marand, H., "On the multiple melting behavior of bisphenol-A polycarbonate" *Polymer* 41, 2000, pp. 8879-8886.
- [24] Alizadeh, A., Sohn, S., Quinn, J., Marand, H., Shank, L., and Iler, H.D., *Macromolecules*, submitted (May 2000).
- [25] Wunderlich, B., "The ATHAS database on heat capacities of polymers" *Pure & Applied Chemistry*, 67, 1995, pp. 1019-1026; see on WWW URL: <http://web.utk.edu/~athas/databank/intro.html>
- [26] Ishida, Y., Yamafuji, K., Ito, H., und Takayanagi, M., "Effects of Degree of Crystallinity upon Dielectric Behaviors in some Aromatic Polyesters" *Kolloid-Zeitschrift & Zeitschrift für Polymere* 184, 1962, pp. 97-108.
- [27] Suzuki, H., Grebowicz, J., and Wunderlich, B., "Heat capacity of semicrystalline, linear poly(oxyethylene) and poly(oxyethylene)" *Makromolekulare Chemie* 186, 1985, pp. 1109-1119.
- [28] Mathot, V.B.F., Ch. 5: "Thermal Characterization of States of Matter" in "Calorimetry and Thermal Analysis of Polymers", V.B.F. Mathot (Ed.); Hanser Publishers, München 1994.

- [29] Alsleben, M., and Schick, C., "The melting of polymers-a three-phase approach" *Thermochimica Acta* 238, 1994, pp. 203-227.
- [30] Schick, C., Merzlyakov, M., Minakov, A.A., and Wurm, A., "Crystallization of polymers studied by temperature modulated calorimetric measurements at different frequencies" *Journal of Thermal Analysis and Calorimetry* 38, 1999, pp. 279-288.
- [31] Wurm, A., Merzlyakov, M., and Schick, C., "Reversible melting during crystallization of polymers studied by temperature modulated techniques (TMDSC, TMDMA)" *Journal of Thermal Analysis and Calorimetry* 60, 2000, pp. 807-820.
- [32] Minakov, A.A., Bugoslavsky, Yu., and Schick, C., "Improvement of AC calorimetry for simultaneous measurements of heat capacity and thermal conductivity of polymers" *Thermochimica Acta* 317, 1998, pp. 117-131.
- [33] Birge, N.O., and Nagel, S.R., "Specific-heat spectroscopy of the glass transition" *Physical Review Letters* 54; 1985, pp. 2674-2677.
- [34] Sohn, S., "Crystallization Behavior of Bisphenol A Polycarbonate: Effect of Time, Temperature and Molar Mass", Ph.D. Thesis, Virginia Polytechnic and State University, April 2000
- [35] Schick, C., Wurm, A., Merzlyakov, M., Minakov, A.A., and Marand, H., "Molecular dynamics revealed from frequency dependent heat capacity" *Macromolecular Symposia*, submitted (May 2000).
- [36] Marand, H., Alizadeh, A., Farmer, R., Desai, R., and Velikov, V., "Influence of structural and topological constraints on the crystallization and melting behavior of polymers. 2. poly(arylene ether ether ketone)" *Macromolecules* 33; 2000, pp. 3392-3403.
- [37] Schenker, B., and Stäger, F., "Influence of the Thermal-Conductivity on the Cp-Determination by Dynamic Methods" *Thermochimica Acta* 304/305, 1997, pp. 219-228.
- [38] Lacey, A.A., Nikolopoulos, C., and Reading, M., "A mathematical model for modulated differential scanning calorimetry" *Journal of Thermal Analysis and Calorimetry* 50, 1997, pp. 279-333.
- [39] Merzlyakov, M., and Schick, C., "Complex heat capacity measurements by TMDSC Part 1. Influence of nonlinear thermal response" *Thermochimica Acta* 330, 1999, pp. 55-64.
- [40] Schick, C., Merzlyakov, M., and Hensel, A., "Nonlinear thermal response at the glass transition" *Journal of Chemical Physics* 111, 1999, pp. 2695-2700.

THE USE OF MTDSC IN CURING AND CHEMICAL REACTIONS.

Bryan Bilyeu,¹ Witold Brostow,¹ and Kevin P. Menard²

Evaluation of the Curing Process in a Fiber-Reinforced Epoxy Composite by Temperature-Modulated and Step Scan DSC and DMA

REFERENCE: Bilyeu, B., Brostow, W., and Menard, K. P., "Evaluation of the Curing Process in a Fiber-Reinforced Epoxy Composite by Temperature-Modulated and Step Scan DSC and DMA," *Materials Characterization by Dynamic and Modulated Thermal Analytical Techniques, ASTM STP 1402*, A. T. Riga and L. Judovits, Eds., American Society for Testing and Materials, West Conshohocken, PA, 2001.

Abstract: Fiber-reinforced epoxy preregs are commonly processed using isothermal curing. Although processing appears simple, the development of properties during curing is a complex multistep process. In addition, the relationship between the curing temperature and time to a specific conversion value is not linear. Industrial processing control can be simplified using a time-temperature-transformation (TTT) diagram. However, construction of a TTT diagram requires knowledge of the rate and degree of conversion as well as the time to reach gelation and vitrification at each isotherm. The rate and degree of conversion are determined either with a series of DSC isotherms which show the change of enthalpy in time or with the change in glass transition temperature (T_g) during the isothermal cure. Since gelation appears as a change in physical properties, it is conveniently determined by DMA. Vitrification is a rubber-to-glass transition and appears in both DMA and DSC. Although vitrification is commonly determined by DMA, DSC offers increased temperature accuracy and control. However, since vitrification occurs before complete conversion, the T_g is usually masked by the curing exotherm in traditional DSC. Since vitrification and curing are thermodynamically different effects, the two signals can be separated using either Temperature Modulated DSC (TMDSC) or Step Scan DSC.

Keywords: temperature, modulated, dynamic, differential, scanning, calorimetry, DSC, DMA, vitrification

Introduction

Epoxy resins represent a class of polymers that are commercially important due primarily to their versatility. A high degree of crosslinking and the nature of the interchain bonds give cured epoxies many desirable characteristics, including excellent adhesion to many substrates, high strength, chemical resistance, fatigue resistance,

¹Laboratory of Polymers and Composites, Department of Materials Science, University of North Texas, Denton, TX 76203-5310.

²Perkin Elmer Instruments, 761 Main Ave. F71, Norwalk, CT 06987.

corrosion resistance and electrical resistance[1]. In addition, processing is simplified by the low shrinkage and lack of volatile by-products. The properties which result in successful applications for the resins also made epoxies the obvious choice for matrices in fiber-reinforced composites[2]. A complete review of epoxies and applications is available[3].

Since epoxy resins must be mixed with various curing agents, catalysts, modifiers and additives, as well as reinforcements, many epoxy suppliers provide premixed molding compounds (MCs) and preimpregnated fibers (prepregs). MCs and prepregs have many advantages to manufacturers since all of the careful mixing is done and ensured by the supplier in large batches[4]. The manufacturer is thus only concerned with the actual processing of the compound. MCs are very popular in high volume industries like automotive and consumer products whereas prepregs are very common in hand and machine layup of high fiber content laminates in aerospace and specialty markets[5].

Epoxy curing involves two phenomena, polymerization and crosslinking. Although each phenomenon is complicated and the two are in competition during the overall curing process, several generalizations can be made. During the initial stage of curing, polymerization is favored [6] because in the case of catalyzed homopolymerization terminal epoxides are the most reactive, and in the case of coreactive agents primary reactions are more reactive than secondary ones, as well as the terminal epoxide reactivity playing a role. The molecular weight of the growing polymer increases until gelation occurs. Originally defined as the point where the polymer gel forms an insoluble gel, the molecular weight is said to approach infinity. At this point the polymer possesses high molecular weight and few crosslinks, and thus behaves much like a very high molecular weight thermoplastic[7]. From the gel point, crosslinking becomes the dominant phenomenon. Crosslinking involves interchain bonding of intrachain reactive sites, either intrachain epoxides or secondary sites on coreactive agents.

Although crosslinking is a different phenomenon, the rate of chemical conversion of the epoxide groups is unaffected in most epoxy systems. The crosslinking reactions produce a growing network [8] and reduce the mobility of the chain segments. The growth of the network results in mechanical and thermal stabilization of the structure, resulting in increasing viscosity, modulus, glass transition and degradation temperatures. At a high degree of crosslinking, the material transforms into a glass, a process called vitrification[9]. In the high viscosity glassy state, the mobility of reactants is severely restricted, which reduces the rate of the reaction to a diffusion-controlled reaction[10].

Fiber-reinforced epoxy processing typically involves isothermal curing after molding or laying up a prepreg or premixture (molding compound). Due to the multi-step nature of epoxy curing, optimization of industrial processing requires knowledge of how each step is affected by time and temperature. This is usually facilitated by the construction of a time-temperature-transformation (TTT) diagram[11].

Epoxy Cure Characterization

Characterization of the epoxy curing reaction and generation of a TTT diagram requires knowledge of the rate and degree of cure as a function of time and temperature

as well as the conditions which produce gelation, vitrification, full cure and degradation. The rate and degree of cure is typically tracked by a change in a cure-dependent property, such as glass transition temperature (T_g). Gelation can be determined by examining the molecular weight-dependent properties or chain mobility. Vitrification is a rubber to glass transition, which results in a thermodynamic as well as a physical change. A complete review of thermal analysis techniques applicable to epoxy characterization is available [12] as well as an extensive study using a variety of techniques to fully characterize an epoxy system[13].

Due to the high potential energy of the ring-strained epoxide groups in the uncured resin, there is a large Gibbs function difference associated with the ring-opening reaction. Since the opening of the epoxide rings results in the evolution of thermal energy or heat, the amount and the rate will correspond to the number of epoxide groups reacting and the rate of the reaction. The current standard technique for quantitative evaluation is the measurement of this change using Differential Scanning Calorimetry (DSC).

Two types of DSCs are available, a heat-flux DSC and a power-compensation DSC. The heat-flux DSC [14] measures the difference in temperature between a sample and reference heated at a programmed rate in a common oven using thermocouples attached to the bottom of the sample holders. The power-compensation DSC [15] employs separate heating elements and thermocouples for sample and reference applying separate currents to the heaters to maintain a null difference in the temperature. Both types of DSC instruments generate plots of heat flow as a function of the programmed temperature. However, due to the difference in measurement techniques, the heat flow value is calculated differently. Since the heat-flux DSC measures the temperature difference between the sample and reference cells, calculation of the heat flow requires an accurate temperature and sample dependent thermal resistance value of the system as a proportionality factor[16]. The power-compensation DSC also requires a thermal resistance value; however, that value represents the heating elements, not the entire system, and is constant [17] over a wide operating temperature range[18]. The power-compensation DSC maintains the programmed temperature ramp in both sample and reference, ensuring greater temperature control in the sample[19]. This is extremely important in temperature sensitive reactions such as thermoset curing. The sensitivity and limits of detection[20], as well as the linearity of the signals [21] of both types of DSC have been evaluated.

To determine the extent of a curing reaction or the degree of cure, α , the change in enthalpy is compared to the total change in enthalpy of the complete reaction. The reaction rate, $d\alpha/dt$, is related to the heat flow, dH/dt . The rate of the curing reaction can be determined from the isothermal data used to determine the degree of cure. Since the enthalpy change is plotted as a function of time, the rate of change in time, dH/dt will represent the rate of the reaction[22].

Epoxy curing involves an increase in both linear molecular weight and crosslink density, both of which result in reduced chain segment mobility. Increasing the linear molecular weight or crosslink density of a polymer chain increases the position of the glass transition temperature, T_g . Many thermosetting polymer systems exhibit a relationship between the T_g and the degree of chemical conversion[23]. Most epoxy-amine systems exhibit a linear relationship, which implies that the change in molecular structure with conversion is independent of the cure temperature[24]. Such a T_g shift

often gives better resolution than exothermic enthalpy changes[25]. A review of models and equations relating the degree of cure to physical properties is available[26].

The most convenient and generally most accurate method for determining the T_g of polymers is Differential Scanning Calorimetry (DSC)[27]. The T_g is taken as the temperature at the inflection point (peak of derivative curve) [28] of the baseline shift in heat flow or as the temperature at the half height shift in baseline heat flow. In situations where the T_g is distorted or masked by other events, like curing exotherms or enthalpic relaxations, the T_g may be determined by the onset, but results should be noted as onset values to avoid confusion. For consistency in reporting, the ASTM Test Method for Assignment of the Glass Transition (E1356-98) describes the methods of T_g calculation.

A limitation of DSC is that when measuring an uncured or a partially cured thermoset, a residual exotherm often overlaps the T_g . One solution to this difficulty is Temperature-Modulated DSC (TMDSC). TMDSC utilizes a modulated temperature ramp, much like dynamic mechanical analysis uses a dynamic force and dielectric relaxation analysis uses an alternating current. TMDSC is a derivative of an earlier technique, Alternating Current (AC) Calorimetry. AC Calorimetry utilizes an oscillating heating ramp, accomplished by the use of an auxiliary pulsed heat source (usually a chopped laser) over the linear programmed heating ramp, to measure the C_p during the single experiment[29]. TMDSC mathematically deconvolutes the response into two types of signals, an in-phase and an out-of-phase response to the modulations, as well as producing an average heat flow, which is analogous to the DSC signal using a linear heating ramp. There are two available methods of performing TMDSC, sinusoidal and square wave modulation.

The first method, introduced by Reading [30-34] utilizes a sinusoidal modulation superimposed over the traditional linear heating ramp or isotherm. The other method, introduced by Schawe [35-37] utilizes square wave modulations. The two methods can be described by the single temperature function

$$T(t) = T_0 + \beta_0 t + (4/\pi)T_a [(\sin(\omega_0 t)/1^2) - (\sin(3\omega_0 t)/3^2) + (\sin(5\omega_0 t)/5^2) - \dots] \quad (1)$$

where T_0 is the initial temperature, β_0 is the underlying heating rate, T_a is the amplitude of the temperature modulation and ω_0 is the angular frequency[38]. In the special case of sinusoidal modulation, the first harmonic would dominate the series.

Although the modulations are related and can be described by a single function (Equation 1), the methods of evaluation of the signal developed by Reading and Schawe are quite different. Reading's technique [39] produces three values. The total heat flow ($H_T = h_{av}/q_{av}$) is usually expressed as the total heat capacity (C_p^T) representing the response to the overall average heating ramp, which is similar to what would be observed in linear DSC heat capacity measurements. The "reversing" component ($C_p^{rev} = A_h/A_q$) represents the ratio of the amplitude of the heat flow to the amplitude of the heating rate. These two signals are subtracted to yield the "non-reversing" component ($C_p^{nr} = C_p^T - C_p^{rev}$). The reversing component represents thermally reversible events, such as T_g s and meltings, whereas the non-reversing component will represent thermally irreversible events, including relaxations, crystallizations and curing exotherms.

Schawe's technique [40-42] uses a linear response approach, which includes a dependence on the phase lag between the signal and response. His approach also begins

with the total heat capacity ($C_p^T = h_{av}/q_{av}$) and includes a C_p value calculated as the ratio of the heat flow amplitude to the heating rate amplitude, however his value is called the complex heat capacity ($C_p^* = A_h/A_q$). The reason for the difference is that from this value, he proposes a separation of the complex heat capacity (C_p^*) into two components, real and imaginary

$$C_p^* = C_p' + iC_p'' \quad (2)$$

with C_p' representing the real, in-phase component, termed storage heat capacity, and C_p'' representing the imaginary, out-of-phase component, termed loss heat capacity. The two values are calculated using the phase angle, ϕ , between the signal and response

$$C_p' = C_p^* \cos\phi \quad (3)$$

$$C_p'' = C_p^* \sin\phi \quad (4)$$

Practically, Reading's technique produces two signals (total and reversing heat capacities), while Schawe's technique produces three (total, storage and loss heat capacities). As described above, Reading's technique calculates the third signal (non-reversing) by subtracting the two primary signals. As explained by Sichina[43], Reading's non-reversing component contains errors and artifacts from the two signals used to calculate it. However, the Schawe's heat capacity doesn't suffer this problem since it is calculated directly from the complex heat capacity and the phase lag. Hutchinson [44] has evaluated the various types of modulations based on sine and square waves and the methods of evaluation and constructed a single parameter model to explain and predict the signals generated in TMDSC.

As in DMA measurements, the storage signal will include the elastic or in-phase response of the material, which in this case will be the molecular level responses, including glass transitions. The loss signal represents viscous or out-of-phase events, which are the kinetic effects, such as stress relaxations and curing. The total heat capacity is the non-separated average signal, which is equivalent to the heat capacity signal produced by traditional DSC. In epoxy T_g shifts, this allows separation of the T_g from the exotherm.

Epoxies undergo changes in mechanical behavior as a function of cure[45]. In addition to the shift in T_g , there are changes in the viscoelastic behavior due to both polymerization and crosslinking[46]. Dynamic Mechanical Analysis (DMA) instruments [47] allow the application of a dynamic force in addition to the static force of TMA, just as TMDSC allows a modulated temperature signal over the linear temperature ramp of DSC. The phase lag between the applied dynamic force and the response yields a complex modulus, which can be mathematically separated into storage or in-phase, elastic response and loss or out-of-phase, viscous response, as shown in Equation (5).

$$E^* = E' + iE'' = \sigma^* / \epsilon^* \quad (5)$$

$$\tan \delta = E''/E' \quad (6)$$

The T_g can be measured accurately using dynamic mechanical analysis (DMA). DMA measures dimensional changes and force responses using a variety of fixtures, each

with specific applications and benefits[48]. Specialized techniques for shear measurements include torsional pendulum[49], torsional braid analysis (TBA)[50] and torsional impregnated cloth analysis (TICA)[51]. Reviews of techniques [52] and applications [53] are available. In the case of highly filled [54] or highly crosslinked polymers [55] DMA gives better resolution and more information than DSC [56, 57] and better reproducibility [58] than techniques, such as Vicat softening temperature (ASTM D1525-96) and deflection temperature (ASTM D648-97)[59]. The T_g in a DMA measurement is generally taken as the peak in tangent delta (Figure 1)[60]. However, there is no consensus on a single method and six methods are currently used[52].

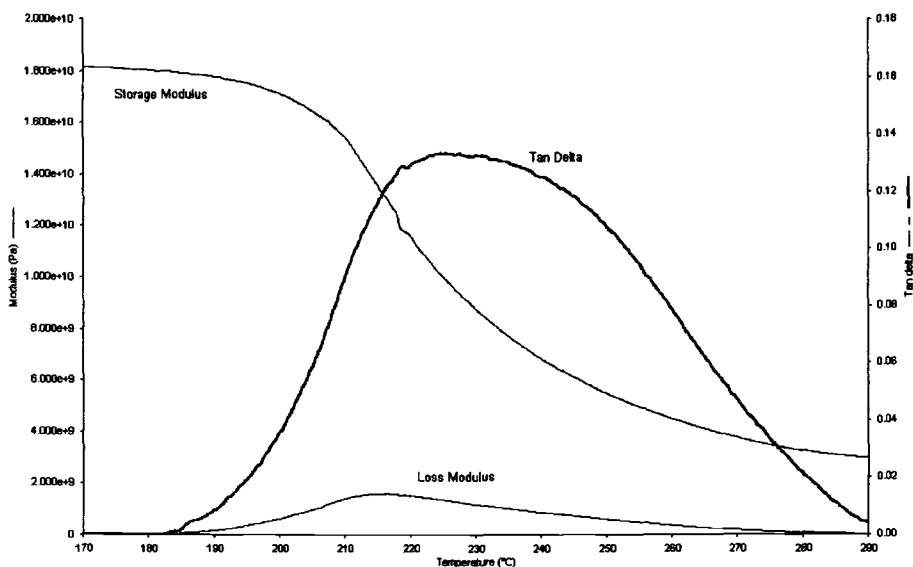


Figure 1 – Changes in DMA signals through the glass transition showing decrease in storage modulus, increase in loss modulus and peak in tangent Delta.

Experimental

The materials chosen to study were Hercules (Hexcel) 8552 neat and glass fiber-reinforced prepreps, which are an amine-rich mixture of the tetrafunctional epoxy tetraglycidyl 4,4'-diaminodiphenyl methane (TGDDM) and the tetrafunctional amine 4,4'-diaminodiphenylsulfone (DDS), along with an ionic initiator/accelerator and a thermoplastic modifier[61, 62]. The fiber-reinforced prepreps contain 66 weight percent unidirectional glass fiber.

DSC, DDSC™ and Step Scan™ DSC experiments were performed on a PerkinElmer Pyris-1™ DSC equipped with liquid nitrogen cooling, operating on a Windows NT platform. For comparison, DSC experiments were also performed on a PerkinElmer DSC-7 with ice coolant, operating on a UNIX platform. Both DSCs were calibrated for temperature and heat of fusion following the ASTM Practice for Calibration of DSC and DTA (E967-97). Baseline subtraction was used on all runs.

DDSC scans were performed in two modes – Heat/Cool and IsoScan™. Heat/Cool runs are a 10 °C heating at 20 °C/min. followed by a 5 °C cooling at 10 °C/min, for an average heating rate of 5 °C/min. IsoScan runs were a 30 second isotherm followed by a 5 °C heating at 10 °C/min, which also yields an average rate of 5 °C/min. T_g values were calculated as the half height shift in baseline storage C_p . Exothermal changes in enthalpy in the loss C_p were determined by comparing the area under the curve to the total. As in all TMDSC techniques, isothermal operation is not really possible as this reduces to classical DSC. A pseudo-isothermal approach was used where the temperature was varied around the temperature of interest. For the pseudo-isothermal TMDSC determination of vitrification point, experiments were performed in Heat/Cool mode, heating to 5 °C above the isothermal temperature at 10 °C/min. and cooling to 5 °C below at 10 °C/min. The vitrification point was calculated as the half height shift in baseline storage C_p just as traditional glass transitions are done.

StepScan DSC scans involve two steps : heating and isothermal. The scans were a 5 °C increase at 10 °C/min. followed by a 30 second isotherm, repeated cyclically. Pseudo-isothermal runs here involved a very small ramp from 5 °C below the temperature of interest to 5 °C above in steps of 0.2 degrees with one minute holds. From this, a Thermodynamic C_p curve was generated. T_g and vitrification could be separated from the curing exotherm.

DMA experiments in both 3-point bending and parallel plate compression were carried out on a PerkinElmer DMA-7e using liquid nitrogen cooling for scans and ice for isotherms, operating on a Windows NT platform. The DMA-7e was calibrated for temperature following ASTM Test Method for Temperature Calibration of DMA (E1867-97) and for height using a quartz standard. The 3-point bending apparatus used on the 0.55 mm thick prepreg tapes was a 5 mm wide probe with 5 mm separation between supports. The bending program used 10 μ m amplitude in position control. The parallel plate compression measurements were performed on 0.55 mm thick prepreg tapes using a 5 mm diameter circular plate in a 10 μ m amplitude in position control. DMA temperature scans were performed in both modes to determine the gelation temperature, as well as the initial and final T_g s.

Results and Discussion

Gelation refers to the point during the curing reaction where polymer becomes an insoluble gel and the molecular weight approaches infinity. While gelation is a microscopic effect, it produces macroscopic effects and occurs at a specific degree of conversion[63].

Microscopic gelation is difficult to measure since the measurable properties would be solubility and molecular weight. However, macroscopic gelation is much easier to measure. Beyond gelation, there is no increase in molecular weight, only an increase in crosslink density and a decrease in free chain segment length[64].

Gelation does not significantly affect the chemical conversion or curing reaction, so it does not appear in DSC measurements[65]. It does have a large influence on the mechanical properties of the polymer and affects the stiffness (modulus), adhesion and general processability of material, so it is important from an industrial processing standpoint[66]. Gelation appears in the complex modulus of DMA measurements;

however, as with many thermal events, there is no unequivocal definition at which point the gelation occurs. Gillham[67] and Enns[68], define it as the a peak in the tangent delta of a DMA isotherm, which is also ASTM Practice for Measuring Cure Behavior of Thermosetting Resins using DMA (D4473-90). The problem in this method lies primarily in the application for which the data is being used, i.e. someone concerned with laminate adhesion would identify a different point than someone concerned with ensuring dimensional stability or a researcher interested in characterizing the physical state of the material. The DMA isothermal plot below (Figure 2) identifies the gel point using Gillham's terminology, i.e. the peak in tangent delta. Another commonly used method [52] is the use of the crossover point of the storage and loss moduli. However, as seen in Figure 2, some materials don't have a crossover point.

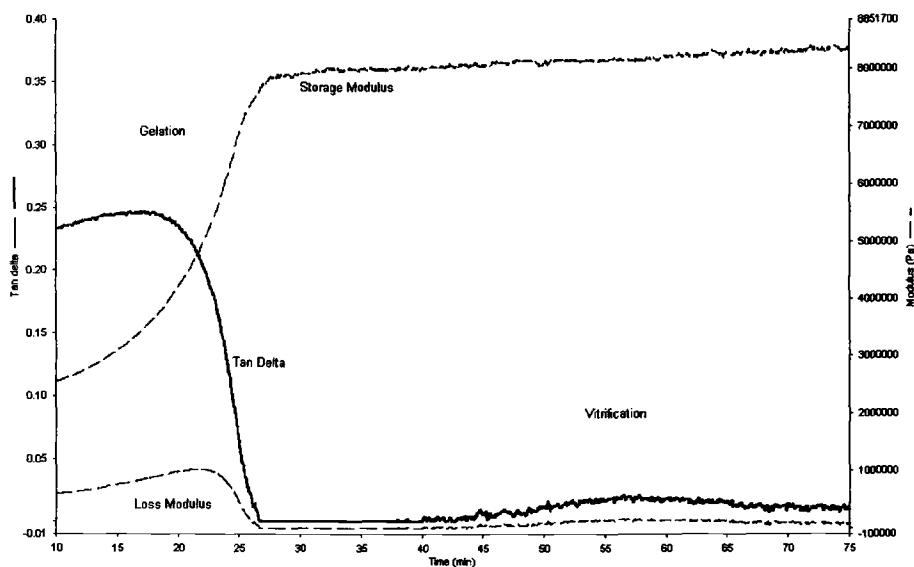


Figure 2 – Changes in parallel plate DMA signals during isothermal curing at 160 °C with gelation identified by first peak in tangent Delta.

Vitrification is defined as the point at which the molecular weight or cross-link density of the curing polymer exceeds that which is thermodynamically stable as a rubber, and the material undergoes a transition from a rubber to a glass at which point the reaction dramatically slows due to the reduced mobility of the reactants. The vitrification point was determined using DSC, TMDSC and DMA.

The vitrification point usually occurs around the end of the curing (since it is a decrease in the reaction rate) and as such is usually masked by the curing reaction exotherm in classical DSC. This is one of the clearest applications of TMDSC since the curing exotherm appears in the loss C_p and the vitrification appears in the storage C_p [69-72]. A series of pseudo-isothermal TMDSC plots identifies the vitrification points (Figure 3).

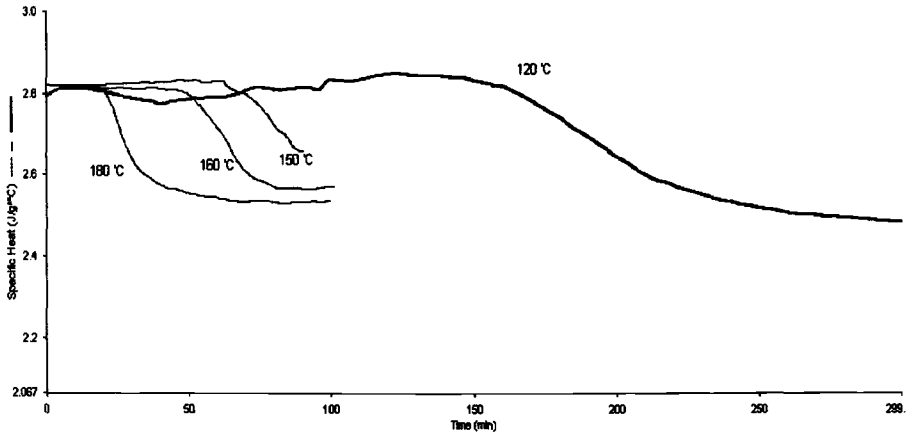


Figure 3 – *Vitrification points for samples during four different pseudo-isothermal cures as shown in the storage heat capacities of TMDSC.*

Step Scan DSC, a technique which gives similar information to TMDSC without the temperature modulation, was also found to allow detection of the vitrification point in the thermodynamic heat capacity curve. This data shows general agreement with that of TMDSC and DMA. A Step Scan curve is shown in Figure 4.

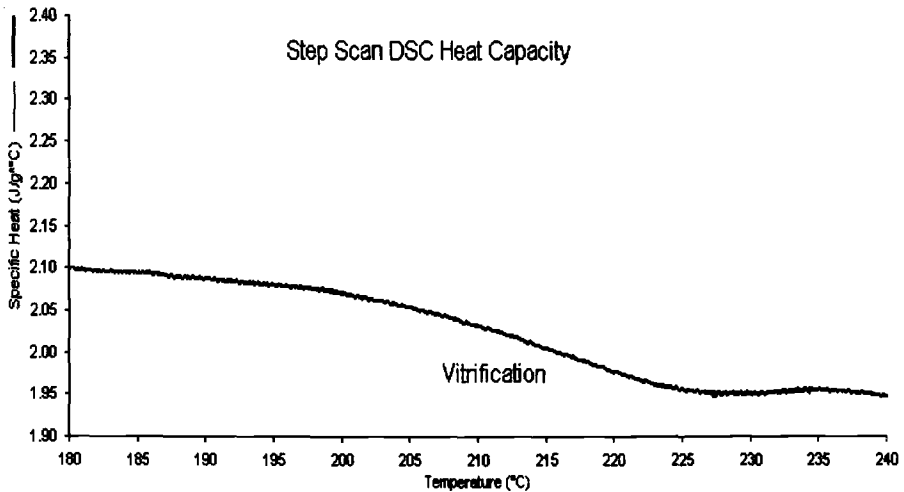


Figure 4 – *Step Scan DSC measurement of the glass transition temperature as seen in the thermodynamic component of the heat capacity*

As noted earlier, the glass transition is also often obscured by the curing exotherm. TMDSC allows separation of the glass transition from the curing exotherm. In addition to the TMDSC series of glass transitions shown in Figure 5, Step Scan DSC also allowed separation of the signals.

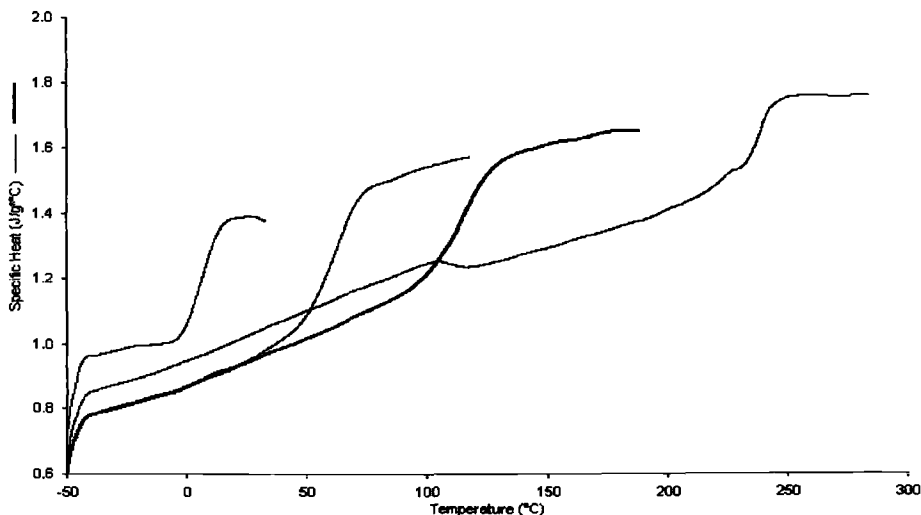


Figure 5 – Changes in glass transition as a function of degree of cure, as shown in the storage heat capacities of separated TMDSC scans of four samples.

DMA has been used extensively to investigate the vitrification point, and continues to be the most common method. The first epoxy TTT diagram, proposed by Gillham and Enns[73], was constructed from torsional braid analysis (TBA)[74], a torsional DMA measurement. Gillham defines the vitrification in DMA measurements as the highest tangent Delta peak below the melt, which usually corresponds to the maximum value of the storage modulus during an isothermal experiment. Vitrification points can be obtained from parallel plate and 3-point bending modes (Figures 2 and 6), with a series of 3-point bending isotherms showing the shift (Figure 7). Vitrification generally occurs when the increasing T_g equals the cure temperature[75].

A comparison of results from the various methods used is given in Table 1. This data was used to construct the time-temperature-transformation (TTT) diagram shown in Figure 8. The initial T_g was determined by both TMDSC and DMA three-point bending, with TMDSC more reliable. The final T_g was measured by TMDSC, TMA and DMA three-point bending with DMA being the best resolved. The increase in T_g with time at various temperatures was measured by DSC, gelation was measured by DMA parallel plate and vitrification was measured by TMDSC and DMA three-point bending. The regions and transitions identified follow conventions proposed by Gillham[73]. Notable curing temperature effects can be seen in the TTT diagram. At temperatures below the T_{g0} (6 °C) there is no reaction, so this is the safe storage temperature. Between T_{g0} and

T_{g-gel} (6 to 86 °C) the material will react, albeit very slowly, and will eventually vitrify before it gels. Between T_{g-gel} and T_{g-vit} (86 to 248 °C) the material will first gel, then vitrify. Above T_{g-vit} (248 °C) the material will gel, but will not vitrify. This diagram provides an easy to read description of the transformations taking place in processing of composite preregs, and allows manipulation of processing conditions to modify physical properties.

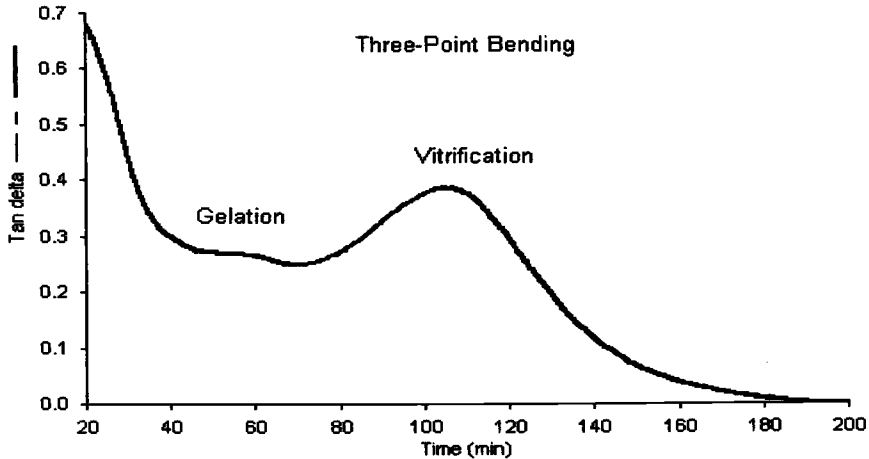


Figure 6 – A DMA three-point bending isotherm at 120 °C showing both gelation and vitrification

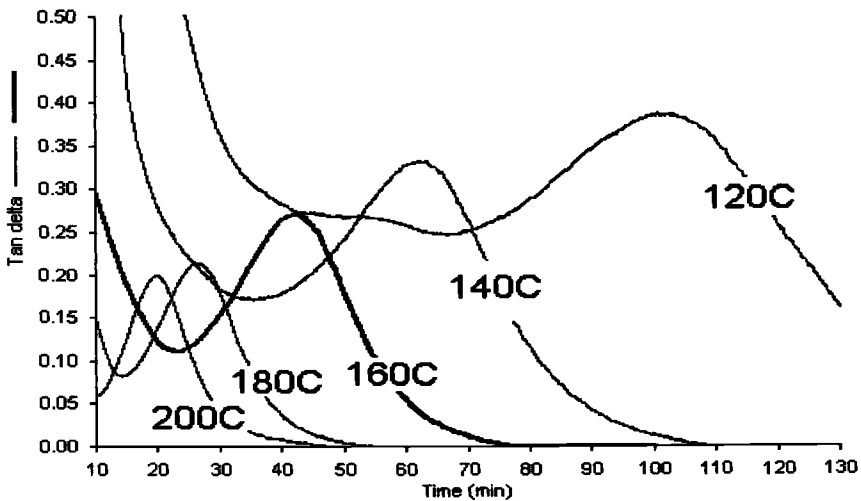


Figure 7 – A series of DMA three-point bending isotherms showing the vitrification peaks in tangent Delta at increasing times for higher cure temperatures

Table 1 – Comparison of Results from DDSC, Step Scan DSC and DMA.

Cure Temperature	DDSC Vitrification	Step Scan Vitrification	DMA Vitrification
160 °C	50 minutes	51 minutes	46 minutes
180 °C	31 minutes	29 minutes	27 minutes
200 °C	19 minutes	18 minutes	22 minutes
5 °C/min.	221 °C	216 °C	235 °C

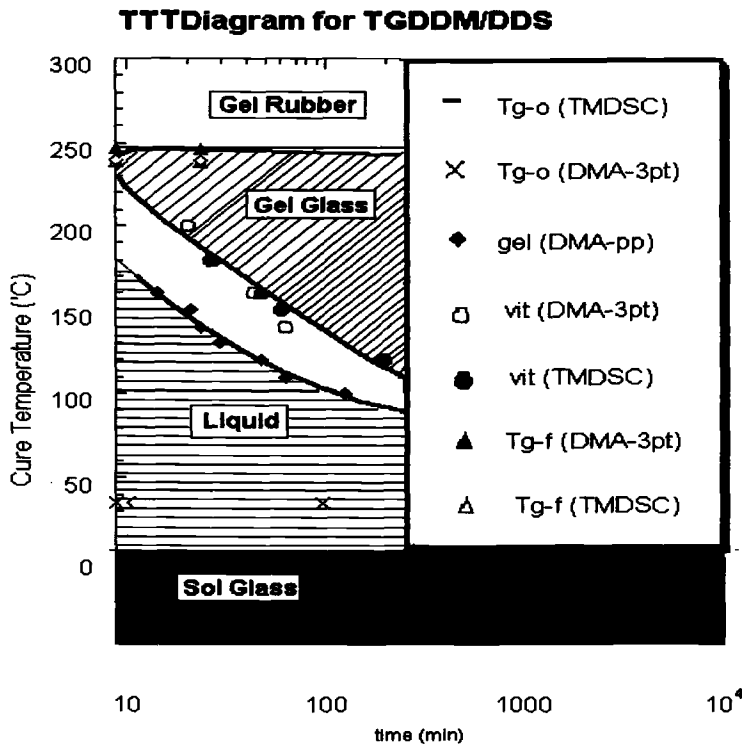


Figure 8 - Time temperature transformation diagram for the TGDDM/ DDS system in this study with gelation and vitrification curves identified. The initial T_g used for the curve was determined by DSC; however, the value from DMA three-point bending is included as points for comparison. The gelation points were determined by DMA parallel plate measurements. The points used to construct the vitrification curve were determined by TMDSC; however, values from DMA three-point bending were included as experimental points for comparison. The final T_g values were determined by DMA three-point bending, TMDSC and TMA, with DMA three-point bending values used to construct the curve since it was the highest, ensuring that this is the maximum.

Conclusions

DDSC™ and StepScan™ DSC temperature scans allow separation of the curing exotherm from the baseline shift of the glass transition, so both can be accurately calculated. Likewise, pseudo-isotherms allow separation of the exothermic change in enthalpy from the baseline shift in heat capacity due to vitrification, so both can be calculated separately.

The DDSC T_g , degree of conversion, and vitrification results, combined with the gelation data generated from DMA, allows construction of a TTT diagram which provides information necessary for optimization of industrial processing of the epoxy prepreg, including the effects of storage, preprocessing, and post processing on the overall curing process.

References

- [1] Dorman, E.N., *Handbook of Fiberglass and Advanced Plastics Composites*, G. Lubin, Ed., Van Nostrand Reinhold, New York, 1969, p. 46.
- [2] Jaffe, M., Menczel, J.D. and Bessey, W.E., *Thermal Characterization of Polymeric Materials*, E. Turi, Ed., Academic Press, San Diego, 1997, p. 1767.
- [3] Bilyeu, B., Brostow, W. and Menard, K. P., *Journal Materials Education*, in press, 2001.
- [4] Reffe, H.R., *Handbook of Fiberglass and Advanced Plastics Composites*, G. Lubin, Ed., Van Nostrand Reinhold, New York, 1969, p. 421.
- [5] Schott, N.R. and Malloy, R., *Applied Polymer Science*, R. Tess and G. Poehlein, Eds., American Chemical Society, Washington D.C., 1985, p. 581.
- [6] Zhu, S. and Hamielec, A.E., *Macromolecules*, Vol. 25, 1992, p. 5457.
- [7] Carraher, C.E., Jr. and Seymour, R.B., *Applied Polymer Science*, R. Tess and G. Poehlein, Eds., American Chemical Society, Washington D.C., 1985, p. 13.
- [8] Stepto, R.F.T., *Cross-Linked Polymers*, R.A. Dickie, S.S. Labana and R.S. Bauer, Eds., American Chemical Society, Washington D.C., 1988, p. 28.
- [9] LeMay, J.D. and Kelley, F.N., *Advances in Polymer Science* 78, K. Dušek, Ed., Springer Verlag, Berlin, 1986, p. 115.
- [10] Gillham, J.K. and Glandt, C.A., *Chemistry and Properties of Crosslinked Polymers*, S.S. Labana, Ed., Academic Press, New York, 1977.
- [11] Gillham, J.K., *Developments in Polymer Characterization 3*, Applied Science Publishers, Barking, Essex, 1982.
- [12] Bilyeu, B., Brostow, W. and Menard, K. P., *Journal Materials Education*, in press, 2001.
- [13] Bilyeu, B., M.S. Thesis, University of North Texas, Denton, 1999.
- [14] David, D.J., *Journal of Thermal Analysis*, Vol. 3, 1971, p. 1.
- [15] Watson, E.S., O'Neill, M.J., Justin, J. and Brenner, N., *Analytical Chemistry*, Vol. 36, 1964, p. 1233.
- [16] Speyer, R.F., *Thermal Analysis of Materials*, Marcel Dekker, New York, 1994.
- [17] Quinn, T.J., *Temperature*, Academic Press, San Diego, 1990.
- [18] Flynn, J.H., *Analytical Calorimetry*, Vol. 3, R.S. Porter and J.F. Johnson, Eds., Plenum Press, New York, 1970, p. 17.
- [19] Hemminger, W., *Calorimetry and Thermal Analysis of Polymers*, V.B.F. Mathot,

- Ed., Hanser, Munich, 1994, p. 17.
- [20] Wies, S., Geyer, A. and Eysel, W., *Journal of Thermal Analysis*, Vol. 38, 1992, p. 277.
- [21] Ozawa, T. and Kanari, K., *Thermochimica Acta*, Vol. 253, 1995, p. 183.
- [22] Khanna, U. and Chanda, M., *Journal of Applied Polymer Science*, Vol. 50, 1993, p. 1635.
- [23] May, C.A., *Applied Polymer Science*, R. Tess and G. Poehlein, Eds., American Chemical Society, Washington D.C., 1985, p. 557.
- [24] Wisanrakkit, G. and Gillham, J.K., *Polymer Characterization*, C. Craver and T. Provder, Eds., American Chemical Society, Washington D.C., 1990, p. 143.
- [25] Richardson, M.J., *Pure & Applied Chemistry*, Vol. 64, 1992, p. 1789.
- [26] Bilyeu, B., Brostow, W. and Menard, K. P., *Journal Materials Education*, in press, 2001.
- [27] Sperling, L.H., *Introduction to Physical Polymer Science*, Wiley, New York, 1986.
- [28] Bershtein, V.A. and Egorov, V.M., *Differential Scanning Calorimetry of Polymers*, Ellis Horwood, New York, 1994.
- [29] Viswenathan, R., *Analytical Calorimetry*, Vol. 3, Eds. R.S. Porter, J.F. Johnson, Plenum Press, New York, 1970, p. 81.
- [30] Reading, M., Elliot, D. and Hill, V., *Proceedings of N.A.T.A.S. Conference*, Vol. 21, 1992, p. 145.
- [31] Reading, M., Hahn, B.K and Crowe, B.S., U.S. Patent 5346306, 1994.
- [32] Reading, M., U.S. Patent 5439291, 1995.
- [33] Reading, M., Hahn, B.K. and Crowe, B.S., U.S. Patent 5224775, 1993.
- [34] Reading, M., U.S. Patent 5248199, 1993.
- [35] Schawe, J. and Marguilies, M., U.S. Patent 5549387, 1996.
- [36] Schawe, J.E.K. and Bergmann, E., *Thermochimica Acta*, Vol. 304/305, 1997, p. 179.
- [37] Schawe, J.E.K. and Höhne, G.W.H., *Journal of Thermal Analysis*, Vol. 46, 1996, p. 893.
- [38] Gopalanarayanan, B., Ph.D. Dissertation, University of North Texas, Denton, 1998.
- [39] Jones, K.J., Kinshott, I., Reading, M., Lacey, A.A., Nikolopoulos, C. and Pollock, H.M., *Thermochimica Acta*, Vol. 304/305, 1997, p. 187.
- [40] Schawe, J.E.K., *Thermochimica Acta*, Vol. 270, 1995, p. 1.
- [41] Schawe, J.E.K., *Thermochimica Acta*, Vol. 261, 1995, p. 183.
- [42] Schawe, J.E.K., *Thermochimica Acta*, Vol. 260, 1995, p. 1.
- [43] Sichina, W., *Proceedings of N.A.T.A.S. Conference*, Vol. 24, 1995, p. 123.
- [44] Hutchinson, J.M. and Montserrat, S., *Thermochimica Acta*, Vol. 286, 1996, p. 263.
- [45] Wingard, D., Williams, W., Wolking, K. and Beatty, C.L., *Cross-Linked Polymers*, R.A. Dickie, S.S. Labana, R.S. Bauer, Eds., American Chemical Society, Washington D.C., 1988, p. 199.
- [46] Ferry, J.D., *Viscoelastic Properties of Polymers*, Wiley, New York, 1980.
- [47] Provder, T., Holsworth, R.M. and Grentzer, T.H., *Polymer Characterization*, C. Craver, Ed., American Chemical Society, Washington D.C., 1983, p. 77.
- [48] Boyer, R.F., *Polymer Characterization*, C. Craver, Ed., American Chemical Society, Washington D.C., 1983, p. 3.
- [49] Boyer, R.F., *Polymer Engineering & Science*, Vol. 19, 1979, p. 661.

- [50] Lewis, A.F. and Gillham, J.K., *Journal of Applied Polymer Science*, Vol. 6, 1962, p. 422.
- [51] Lee, C.Y.-C. and Goldfarb, I.J., *Polymer Characterization*, C. Craver, Ed., American Chemical Society, Washington D.C., 1983, p. 65.
- [52] Menard, K.P., *Dynamic Mechanical Analysis*, CRC Press, Boca Raton, 1999.
- [53] Menard, K.P., *Performance of Plastics*, W. Brostow, Ed., Hanser, Berlin, 2001.
- [54] Schneider, N.S. and Gillham, J.K., *Polymer Composites*, Vol. 2, 1980, p. 97.
- [55] Hurwitz, F.I., *Polymer Composites*, Vol. 4, 1983, p. 89.
- [56] O'Neal, H.R., Welch, S., Rogers, J., Guilford, S., Curran, G. and Menard, K.P., *Journal of Advanced Materials*, Vol. 26, 1995, p. 49.
- [57] Lee, C.Y.-C. and Goldfarb, I.J., *Polymer Engineering & Science*, Vol. 21, 1981, p. 787.
- [58] Scobbe, J.J. and Cometti, P.L., *Proceedings of the Annual Technical Conference of the Society of Plastics Engineers*, Vol. 40, 1994, p. 3326.
- [59] Akay, M., Cracknell, J.G. and Farnham, H.A., *Polymers & Polymer Composites*, Vol. 2, 1994, p. 317.
- [60] Wilson, T.W., Fornes, R.E., Gilbert, R.D. and Memory, J.D., *Cross-Linked Polymers*, R.A. Dickie, S.S. Labana, R.S. Bauer, Eds., American Chemical Society, Washington D.C., 1988.
- [61] Opalicki, M., Kenny, J.M. and Nicolais, L., *Journal of Applied Polymer Science*, Vol. 61, 1996, p. 1025.
- [62] Arnold, F.E. and Thoman, S., *International SAMPE Technical Conference*, Vol. 28, 1996, p. 222.
- [63] Flory, P.J., *Principles of Polymer Chemistry*, Cornell University Press, Ithica, 1953.
- [64] Dušek, K. and MacKnight, W.J., *Cross-Linked Polymers*, R.A. Dickie, S.S. Labana, R.S. Bauer, Eds., American Chemical Society, Washington D.C., 1988, p. 2.
- [65] Prime, R.B., *Thermal Characterization of Polymeric Materials*, E. Turi, Ed., Academic Press, San Diego, 1997, p. 1380.
- [66] Schott, N.R. and Malloy, R., *Applied Polymer Science*, R. Tess and G. Poehlein, Eds., American Chemical Society, Washington D.C., 1985, p. 581.
- [67] Gillham, J.K., *Polymer Engineering & Science*, Vol. 19, 1979, p. 319.
- [68] Enns, J.B. and Gillham, J.K., *Polymer Characterization*, C. Craver, Ed., American Chemical Society, Washington D.C., 1983, p. 27.
- [69] Bilyeu, B., Brostow, W. and Menard, K.P., *Proceedings of A.C.S. (P.M.S.E.) Conference*, Vol. 78, 1998, p. 232.
- [70] Bilyeu, B., Brostow, W. and Menard, K.P., *Proceedings of the Annual Technical Conference of the Society of Plastics Engineers*, Vol. 45, 1999, p. 2724.
- [71] Schick, C., Dobberty, J., Potter, M., Dehne, H., Hensel, A., Wurm, A., Ghoneim, A.M. and Weyer, S., *Journal of Thermal Analysis*, Vol. 49, 1997, p. 499.
- [72] Van Assche, G., Van Hemelrijck, A., Rahier, H. and Van Mele, B., *Thermochimica Acta*, Vol. 304/305, 1997, p. 317.
- [73] Gillham, J.K., *AIChE Journal*, Vol. 20, 1974, p. 1066.
- [74] Lewis, A.F. and Gillham, J.K., *Journal of Applied Polymer Science*, Vol. 6, 1962, p. 422.
- [75] Gillham, J.K., *Polymer Engineering & Science*, Vol. 26, 1986, p. 1429.

**MEASUREMENT OF THE GLASS TRANSITION
AND MELTING BY MODULATED
AND COMPARATIVE TECHNIQUES**

Kristine N. Ludwig,¹ Karen E. Burkholder,¹ John F. Willey,¹ and Alan T. Riga²

Effects of TMDSC Variables on the Observed Glass Transitions of Elastomers- a Statistical Analysis

REFERENCE: Ludwig, K. N., Burkholder, K. E., Willey, J. F., and Riga, A. T., "Effects of TMDSC Variables on the Observed Glass Transitions of Elastomers- a Statistical Analysis," *Materials Characterization by Dynamic and Modulated Thermal Analytical Techniques*, ASTM STP 1402, A. T. Riga and L. Judovits, Eds., American Society for Testing and Materials, West Conshohocken, PA, 2001.

Abstract: A two-level, three-variable full factorial experimental design was employed to probe the effects of temperature-modulated differential scanning calorimetry variables (heating rate, modulation frequency, and modulation amplitude) on the observed glass transitions of polybutadiene, poly(styrene-co-butadiene) and polystyrene. The statistical significance of individual variables was ascertained by Student's *t*-tests. Standard least-squares fitting of the model was employed to determine interaction effects between the variables. Frequency was determined to have a statistically significant effect on extrapolated onset glass transition temperature, half-height glass transition temperature, and the change in heat capacity across the glass transition for all three polymers. Within the confines of these experiments, changes in heating rate and amplitude did not have a statistically significant effect on glass transition measurement. No synergistic interaction effects were observed between the variables.

Keywords: TMDSC, polystyrene, poly(styrene-co-butadiene), polybutadiene, frequency, glass transition, statistical analysis

Introduction

Knowledge of the temperature regime at which an elastomer undergoes the transition from a rubbery to a glassy state is important in determining structure/property relationships as well as for assessing potential end-use applications [1]. Glass transition temperatures of elastomers have been correlated to abrasion resistance [2], resilience [3], and have even been highlighted as crucial factors in understanding the catastrophic

¹Senior Research Scientist, Research Engineer, and Section Head, respectively, Research Division, The Goodyear Tire and Rubber Company, 142 Goodyear Boulevard, Akron, OH 44305.

²Senior Scientist, TechCon, Inc., 6325 Aldenham Drive, Cleveland, OH 44143.

failure of products used outside of specifications [4].

With the advent of temperature-modulated differential scanning calorimetry (TMDSC) in the 1990s, it became possible to separate reversing and non-reversing thermal events [5]. Among the many benefits this technique offers is the ability to separate non-reversing enthalpic relaxation from a reversing glass transition (Figure 1).

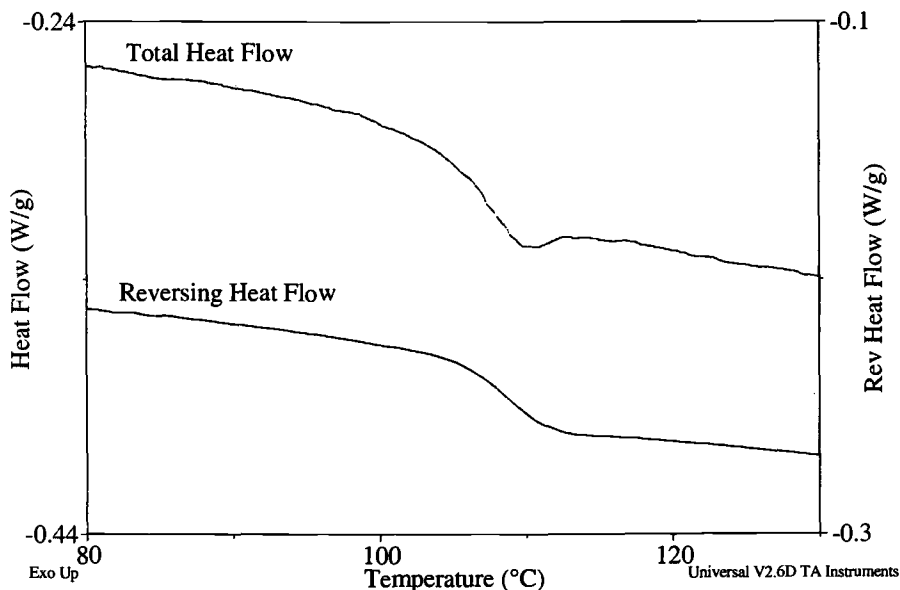


Figure 1 - Typical DSC (top) and TMDSC (bottom) heat flow traces of PS; heating rate: 5°C/min.

This facilitates discernment of the glass transition, enabling the analyst to make a more accurate measurement.

Three operator-defined variables are used in TMDSC: underlying heating rate, frequency of modulation, and temperature amplitude of modulation. The effect that changing these variables has on glass transition measurement has been the subject of numerous studies [6-13]. It was reported that transitions detected in the reversing mode of TMDSC shifted to higher temperatures as frequency was increased [6, 11-13], similar to temperature shifts observed in dynamic mechanical analysis (DMA). It was also noted that total heat flow traces did not show any frequency dependence [6].

The aim of the present study is to determine the statistical significance of the effects of heating rate, modulation frequency and amplitude on observed glass transition temperatures of several elastomeric and plastic materials.

Experimental

An atactic polystyrene (PS) NIST standard, uncrosslinked poly(styrene-co-

butadiene) (50-55% styrene) (SBR), and uncrosslinked 97% *cis*-polybutadiene (BR) were used in this study.

All samples were examined with a TA Instruments 2920 MDSC equipped with a liquid nitrogen cooling apparatus (LNCA). Sample mass ranged from five to ten milligrams.

A two-level, three-variable (2^3) full factorial experimental design was utilized with the coded and experimental variables as shown in Table 1.

Table 1 - Coded and Experimental Variable Matrix

Coded Values			Experimental Values		
Heating Rate	Amplitude	Frequency	Heating Rate ($^{\circ}\text{C}/\text{min}$)	Amplitude ($\pm^{\circ}\text{C}$)	Frequency (Hz)
-1	-1	-1	2	0.318	0.105
-1	-1	1	2	0.318	0.251
-1	1	-1	2	0.796	0.105
-1	1	1	2	0.796	0.251
1	-1	-1	5	0.318	0.105
1	-1	1	5	0.318	0.251
1	1	-1	5	0.796	0.105
1	1	1	5	0.796	0.251

The experimental order of runs was randomized and conditions were as follows:

1. Helium flow rate: 25 mL/min,
2. Equilibrate at starting temperature (T_0) (Table 2),
3. Isothermal at T_0 for 5 minutes,
4. Ramp/heat at heating rate (β) with a modulation (A_T) at a frequency (ω), where $\omega = 2\pi/\text{period}$, up to end temperature (T_e). See Table 1 for heating rate, modulation, and frequency values used.

Table 2 - Start and End TMDSC Program Temperatures for Polymer Series

Polymer	T_0 ($^{\circ}\text{C}$)	T_e ($^{\circ}\text{C}$)
PS	70.0	140.0
SBR	-60.0	20.0
BR	-125.0	-75.0

The minimum number of temperature cycles across the glass transition was four, as was seen in the case of PS, $\beta = 5^{\circ}\text{C}/\text{min}$, $\omega = 0.105$ Hz, and $A_T = 0.796^{\circ}\text{C}$.

The responses observed were: extrapolated onset glass transition temperature ($T_g(e)$), half-height glass transition temperature ($T_g(h)$), extrapolated end glass transition temperature ($T_g(f)$), and change in heat capacity across the glass transition (ΔC_p). The breadth of the glass transition (ΔT) was calculated as $|T_g(e) - T_g(f)|$.

Three additional experiments were performed using the same instrumentation *sans*

modulation. Polystyrene was analyzed by heating at 5, 10, and 20°C/min from 70 to 140°C.

Statistical analysis of the data was performed using SAS JMP® 3.2, Professional Edition software (SAS Institute Inc., Cary, NC, 1997).

Results and Discussion

Reversing Heat Flow

The observed responses to changes in experimental variables are recorded in Tables 3-5. Representative TMDSC reversing heat flow traces of BR, SBR and PS are shown in Figure 2.

Table 3 - TMDSC Glass Transition Data from Reversing Heat Flow Trace of PS

Run Order	β (°C/min)	ω (Hz)	A_T (°C)	$T_g(e)$ (°C)	$T_g(h)$ (°C)	$T_g(f)$ (°C)	ΔT (°C)	ΔC_p (J/(g °C))
3	2	0.105	0.318	103.7	106.9	109.8	6.1	0.25
5	5	0.105	0.318	104.0	107.0	110.1	6.1	0.33
2	2	0.251	0.318	106.4	109.1	112.1	5.7	0.20
1	5	0.251	0.318	108.3	109.9	111.4	3.1	0.14
				107.0	110.0	113.1	6.1	0.24
8	2	0.105	0.796	105.4	108.1	110.6	5.2	0.29
				105.4	108.0	110.6	5.2	0.28
6	5	0.105	0.796	105.4	108.7	112.1	6.7	0.34
				104.6	108.1	111.5	6.9	0.35
4	2	0.251	0.796	106.6	109.7	112.7	6.1	0.23
7	5	0.251	0.796	106.7	109.9	113.0	6.3	0.23
				107.3	110.3	113.4	6.1	0.24

Table 4 - TMDSC Glass Transition Data from Reversing Heat Flow Trace of SBR

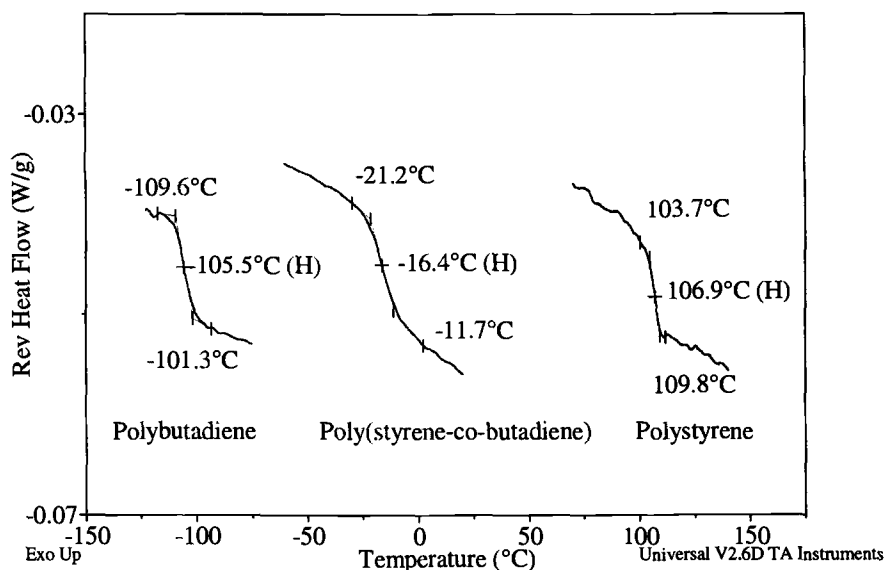
Run Order	β (°C/min)	ω (Hz)	A_T (°C)	$T_g(e)$ (°C)	$T_g(h)$ (°C)	$T_g(f)$ (°C)	ΔT (°C)	ΔC_p (J/(g °C))
3	2	0.105	0.318	-20.3	-15.4	-10.5	9.8	0.27
				-21.2	-16.4	-11.7	9.5	0.22
5	5	0.105	0.318	-20.4	-15.1	-9.8	10.6	0.29
2	2	0.251	0.318	-19.8	-14.2	-8.6	11.2	0.17
1	5	0.251	0.318	-20.2	-14.6	-9.2	11.0	0.17
8	2	0.105	0.796	-20.0	-14.4	-9.8	10.2	0.28
				-20.8	-15.6	-10.7	10.1	0.28
6	5	0.105	0.796	-20.1	-13.9	-7.5	12.6	0.31
				-21.1	-15.4	-9.7	11.4	0.30
4	2	0.251	0.796	-19.9	-14.0	-8.3	11.6	0.19
7	5	0.251	0.796	-18.9	-12.9	-7.3	11.6	0.20

Table 5 - TMDSC Glass Transition Data from Reversing Heat Flow Trace of BR

Run Order	β (°C/min)	ω (Hz)	A_T (°C)	$T_g(e)$ (°C)	$T_g(h)$ (°C)	$T_g(f)$ (°C)	ΔT (°C)	ΔC_p (J/(g °C))
3	2	0.105	0.318	-109.3	-105.9	-102.5	6.8	0.17
				-109.6	-105.5	-101.3	8.3	0.26
5	5	0.105	0.318	-109.0	-104.7	-100.6	8.4	0.29
2	2	0.251	0.318	-107.4	-104.5	-101.6	5.8	0.11
1	5	0.251	0.318	-106.3	-103.9	-101.4	4.9	0.10
				-107.2	-104.0	-100.8	6.4	0.12
8	2	0.105	0.796	-108.9	-105.5	-102.2	6.7	0.28
6	5	0.105	0.796	-109.8	-106.0	-102.0	7.8	0.17
4	2	0.251	0.796	-107.9	-104.5	-100.9	7.0	0.13
7	5	0.251	0.796	ND	ND	ND	NA	ND

ND = None Detected

NA = Not Applicable

Figure 2 - TMDSC reversing heat flow traces of BR (left), SBR (center), and PS (right); β : 2°C/min, ω : 0.105 Hz, A_T : $\pm 0.318^\circ\text{C}$.

To determine statistical significance of changing a single variable for a single response, group means analysis of variance (ANOVA) and Student's t -tests, using $\alpha = 0.05$, were performed on each set of data. Visual comparisons of group means were then performed. Graphical representation of group means ANOVA t -test results indicate the sample number and values (individual points), 95% confidence interval (height of diamond), group sample size (width of diamond), group means (center line in diamond), total response sample mean (black line in center of box), mean with error

bars (error bars extending above and below group means lines), and standard deviation (horizontal dashes in each group).

The Student's t -test for each pair of group levels and comparisons is depicted geometrically in the right-hand portion of Figures 3-6.

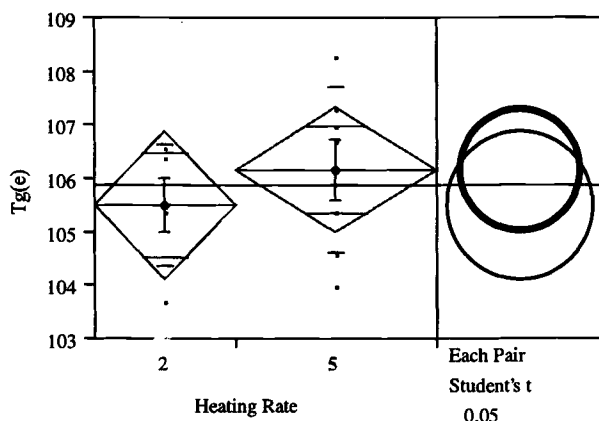


Figure 3 - Means ANOVA (left) and comparison circles (right) for the $T_g(e)$ of PS as a function of β .

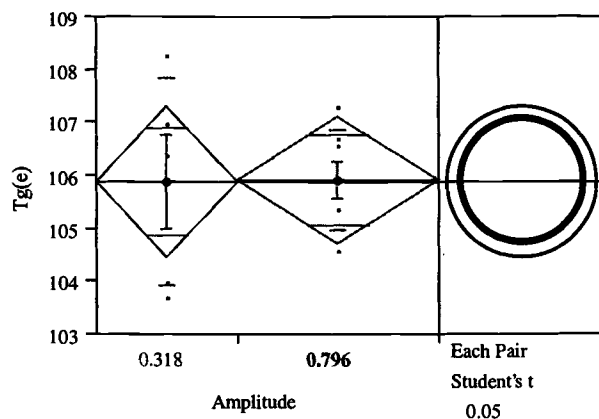


Figure 4 - Means ANOVA (left) and comparison circles (right) for the $T_g(e)$ of PS as a function of A_T .

The distance between the center of each circle represents the actual difference between the group means. The least significant difference is what the distance would be if the circles intersected at right angles. For the Student's t -test/Compare Each Pair analysis, only individual comparisons are tested. Group means can be inspected visually by examining how the comparison circles intersect (i.e. comparing the angle between the tangents of the two circles). An intersection angle of greater than 90° (Figure 3), or if they are concentric (Figure 4), indicates the means are not significantly different. If the

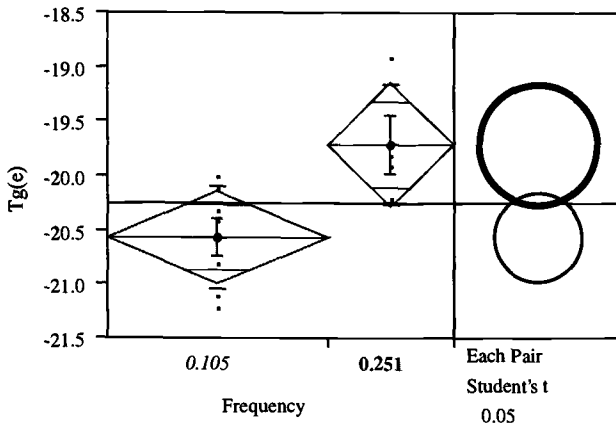


Figure 5 - Means ANOVA (left) and comparison circles (right) for the $T_g(e)$ of SBR as a function of ω

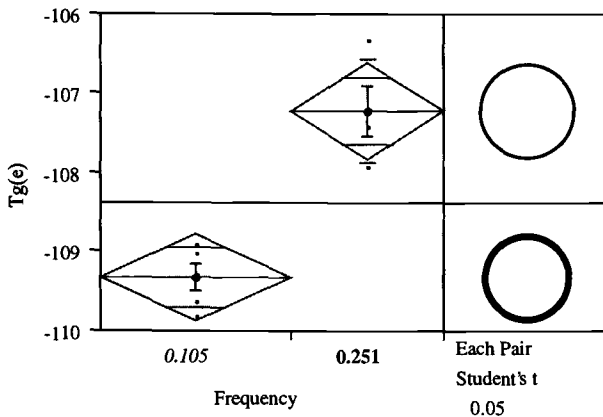


Figure 6 - Means ANOVA (left) and comparison circles (right) for the $T_g(e)$ of BR as a function of ω

intersection angle is equal to 90° , the groups are borderline significantly different. If the intersection angle is less than 90° (intersect only slightly, Figure 5), or if the circles do not intersect (Figure 6), the means are significantly different. Group means are recorded in Table 6. The results of the group means comparisons are summarized in Table 7.

Heating rate- Heating and cooling rate effects on the glass transition are well-known and have been studied extensively [14, 15]. When the heating rate is increased, the observed temperature range of the glass transition should also be increased. Two underlying heating rates were examined in this study.

As β was increased from 2 to $5^\circ\text{C}/\text{min}$, PS response means increased 0.7°C for $T_g(e)$, 0.7°C for $T_g(h)$, 0.9°C for $T_g(f)$, 0.2°C for ΔT , and $0.02 \text{ J}/(\text{g } ^\circ\text{C})$ for ΔC_p . Response

Table 6 - Group Means and Standard Deviations across Variables

Sample	Experimental Variable	Value	T _g (e) (°C)	Std Dev	T _g (h) (°C)	Std Dev	T _g (f) (°C)	Std Dev	ΔT (°C)	Std Dev	ΔC _p (J/(g °C))	Std Dev
PS	β	2	105.5	1.15	108.4	1.08	111.2	1.20	5.7	0.45	0.25	0.04
		5	106.2	1.56	109.1	1.23	112.1	1.18	5.9	1.28	0.27	0.08
	ω	0.105	104.8	0.77	107.8	0.70	110.8	0.87	6.0	0.72	0.31	0.04
		0.251	107.1	0.69	109.8	0.40	112.6	0.74	5.6	1.22	0.21	0.04
	A _T	0.318	105.9	1.98	108.6	1.53	111.3	1.38	5.4	1.31	0.23	0.07
SBR	β	0.796	105.9	0.96	109.0	0.97	112.0	1.13	6.1	0.67	0.28	0.05
		2	-20.3	0.56	-15.0	0.95	-9.9	1.30	10.4	0.82	0.24	0.05
	ω	5	-20.1	0.80	-14.4	1.00	-8.7	1.21	11.4	0.75	0.25	0.06
		0.105	-20.6	0.48	-15.2	0.82	-10.0	1.29	10.6	1.07	0.28	0.03
	A _T	0.251	-19.7	0.56	-13.9	0.73	-8.4	0.79	11.4	0.30	0.18	0.02
BR	β	0.318	-20.4	0.51	-15.1	0.84	-10.0	1.20	10.4	0.74	0.22	0.06
		0.796	-20.1	0.77	-14.4	1.01	-8.9	1.38	11.3	0.95	0.26	0.05
	ω	2	-108.6	0.94	-105.2	0.64	-101.7	0.65	6.9	0.90	0.19	0.08
		5	-108.1	1.61	-104.7	0.97	-101.2	0.63	6.9	1.56	0.17	0.09
	A _T	0.105	-109.3	0.38	-105.5	0.51	-101.7	0.77	7.6	0.81	0.23	0.06
	ω	0.251	-107.2	0.67	-104.2	0.32	-101.2	0.39	6.0	0.90	0.12	0.01
		0.318	-108.1	1.34	-104.8	0.80	-101.4	0.67	6.8	1.38	0.18	0.08
	A _T	0.796	-108.9	0.95	-105.3	0.76	-101.7	0.70	7.2	0.57	0.19	0.08

Table 7 - Statistical Significance of Variables on Measured Values

Sample	Experimental Variable	$T_g(e)$	$T_g(h)$	$T_g(f)$	ΔT	ΔC_p
PS	β	N	N	N	N	N
	ω	YD	YD	YD	N	YD
	A_T	N	N	N	N	N
SBR	β	N	N	N	N	N
	ω	YS	YS	N	N	YD
	A_T	N	N	N	N	N
BR	β	N*	N*	N*	N*	N*
	ω	YD	YD	N	YS	YD
	A_T	N	N	N	N	N

YS = Statistically significant, slightly overlapping

YD = Statistically significant, distinct/non-overlapping

N = Not statistically significant

* Unstable signal at 5°C/min, 0.251 Hz, $\pm 0.796^\circ\text{C}$; Could not determine T_g

means of SBR increased 0.2°C for $T_g(e)$, 0.6°C for $T_g(h)$, 1.2°C for $T_g(f)$, 1.0°C for ΔT , and $0.01 \text{ J/(g } ^\circ\text{C)}$ for ΔC_p . Polybutadiene response means increased 0.5°C for $T_g(e)$, 0.5°C for $T_g(h)$, 0.5°C for $T_g(f)$, remained constant for ΔT , and decreased $0.02 \text{ J/(g } ^\circ\text{C)}$ for ΔC_p .

Although $T_g(e)$, $T_g(h)$, and $T_g(f)$ were all increased with increasing β , the values were raised 1.2°C or less. None of the changes observed were statistically significant. However, it should be noted that a T_g could not be determined for BR using a β of 5°C/min , ω of 0.251 Hz and A_T of $\pm 0.796^\circ\text{C}$. Under these conditions, there appeared to be insufficient time for the baseline to equilibrate prior to the glass transition event. Selection of a lower starting temperature may be advised for the BR samples, to allow adequate time for the system to equilibrate.

Frequency- The time scale of an oscillating experiment affects the temperature range at which a glass transition is observed. This is observed with techniques such as DMA, where ω may be varied over several decades, typically from 0.01 to 100 Hz [16]. Temperature-modulated differential scanning calorimetry employs frequencies between 0.05 and 1 Hz. Two frequencies were utilized in this study.

As ω was increased from 0.105 to 0.251 Hz, PS response means increased 2.3°C for $T_g(e)$, 2.0°C for $T_g(h)$, and 1.8°C for $T_g(f)$, decreased 0.4°C for ΔT , and decreased $0.10 \text{ J/(g } ^\circ\text{C)}$ for ΔC_p . Response means for SBR increased by 0.9°C for $T_g(e)$, 1.3°C for $T_g(h)$, 1.6°C for $T_g(f)$, and 0.8°C for ΔT , and decreased $0.10 \text{ J/(g } ^\circ\text{C)}$ for ΔC_p . Polybutadiene response means increased 2.1°C for $T_g(e)$, 1.3°C for $T_g(h)$, and 0.5°C for $T_g(f)$, and decreased 0.4°C for ΔT and $0.11 \text{ J/(g } ^\circ\text{C)}$ for ΔC_p .

Increases in ω had a statistically significant effect on the $T_g(e)$ (increased), $T_g(h)$ (increased) and ΔC_p (decreased) of all three polymers. Frequency also significantly affected the $T_g(f)$ of PS (increased) and the ΔT of BR (decreased).

Amplitude- As A_T was increased from 0.318 to 0.796, response means for PS

remained constant for $T_g(e)$, and increased 0.4°C for $T_g(h)$, 0.7°C for $T_g(f)$, 0.7°C for ΔT , and $0.05 \text{ J/(g } ^\circ\text{C)}$ for ΔC_p . Poly(styrene-co-butadiene) response means increased 0.3°C for $T_g(e)$, 0.7°C for $T_g(h)$, 1.1°C for $T_g(f)$, 0.9°C for ΔT , and $0.04 \text{ J/(g } ^\circ\text{C)}$ for ΔC_p . Response means of BR decreased 0.8°C for $T_g(e)$, 0.5°C for $T_g(h)$, and 0.3°C for $T_g(f)$, and increased 0.4°C for ΔT and $0.01 \text{ J/(g } ^\circ\text{C)}$ for ΔC_p .

With increasing A_T , ΔT and ΔC_p for all three polymers increased. Polystyrene and SBR displayed increases in $T_g(e)$, $T_g(h)$, and $T_g(f)$, while the same values for BR appeared to decrease. One caveat is that a T_g could not be discerned for BR using a β of 5°C/min , ω of 0.251 Hz and A_T of $\pm 0.796^\circ\text{C}$ (see Heating Rate section) and, therefore, calculations did not include that combination of conditions.

Interaction effects- Data were fitted to a standard least squares full factorial model (Equation 1). The fitting results and interaction parameter estimates for PS and SBR are recorded in Tables 8 and 9, respectively. Due to the inability to measure T_g at one of the design conditions, model fitting could not be applied to BR.

$$y = \text{Int} + \beta + \omega + A_T + \beta * \omega + \beta * A_T + \omega * A_T + \beta * \omega * A_T \quad (1)$$

where:

Int = intercept,
 β = heating rate,
 ω = frequency, and
 A_T = amplitude.

Interaction effects were also inspected graphically. Model fitting r^2 values ranged from 0.577 (model inadequate to explain data) for ΔT of PS to 0.982 (model adequate to explain data) for the $T_g(h)$ of PS. No interaction terms were determined to be statistically significant for any of the responses of PS or SBR.

Total Heat Flow

In the course of this study, total heat flow traces acquired via conventional DSC and modulated DSC were examined for PS. Data appears in Table 10. It was noted that the glass transition temperature as determined by conventional DSC was higher than that determined by modulated DSC (Figure 7). A greater discrepancy was observed when comparing $T_g(e)$ values (2.5°C) than when comparing $T_g(h)$ values (1.4°C) for traces acquired at 5°C/min . This data supports the interpretation that $T_g(h)$ is a more reliable glass transition value.

Conclusions

The effect of varying heating rate, frequency, and temperature amplitude on

Table 8 - Interaction Parameter Estimates for Polystyrene

Response	Model r^2	Calculated Value	Intercept	β	ω	$\beta * \omega$	A_T	$\beta * A_T$	$\omega * A_T$	$\beta * \omega * A_T$
$T_g(e)$	0.937	Estimate	103.7	0.3	2.7	0.95	1.7	-0.7	-1.5	-0.15
		Std Error	0.580	0.820	0.820	1.085	0.710	1.004	1.085	1.420
		t Ratio	178.83	0.37	3.29	0.88	2.39	-0.70	-1.38	-0.11
		Prob> t	<0.0001	0.7330	0.0301	0.4306	0.0749	0.5242	0.2389	0.9210
$T_g(h)$	0.982	Estimate	106.9	0.1	2.2	0.75	1.15	0.25	-0.55	-0.7
		Std Error	0.260	0.367	0.367	0.486	0.318	0.450	0.486	0.636
		t Ratio	411.46	0.27	5.99	1.54	3.61	0.56	-1.13	-1.10
		Prob> t	<0.0001	0.7990	0.0039	0.1977	0.0225	0.6081	0.3211	0.3331
$T_g(f)$	0.897	Estimate	109.8	0.3	2.3	-0.15	0.8	0.9	-0.2	-0.55
		Std Error	0.653	0.923	0.923	1.221	0.800	1.131	1.221	1.599
		t Ratio	168.18	0.32	2.49	-0.12	1.00	0.80	-0.16	-0.34
		Prob> t	<0.0001	0.7615	0.0674	0.9082	0.3737	0.4707	0.8779	0.7482
ΔT	0.577	Estimate	6.1	-3.02e-14	-0.4	-1.1	-0.9	1.6	1.3	-0.4
		Std Error	1.065	1.507	1.507	1.993	1.304	1.845	1.993	2.610
		t Ratio	5.73	0.00	-0.27	-0.55	-0.69	0.87	0.65	-0.15
		Prob> t	0.0046	1.000	0.8038	0.6104	0.5283	0.4348	0.5498	0.8856
ΔC_p	0.876	Estimate	0.25	0.08	-0.05	-0.09	0.035	-0.02	-0.005	0.035
		Std Error	0.036	0.051	0.051	0.067	0.044	0.062	0.067	0.088
		t Ratio	6.97	1.58	-0.99	-1.34	0.80	-0.32	-0.07	0.40
		Prob> t	0.0022	0.1900	0.3802	0.2511	0.4704	0.7637	0.9442	0.7108

Table 9 - Interaction Parameter Estimates for Poly(styrene-co-butadiene)

Response	Model r^2	Calculated Value	Intercept	β	ω	$\beta^*\omega$	A_T	β^*A_T	ω^*A_T	$\beta^*\omega^*A_T$
$T_g(e)$	0.707	Estimate	-20.75	0.35	0.95	-0.75	0.35	-0.55	-0.45	1.95
		Std Error	0.452	0.783	0.783	1.195	0.639	1.010	1.107	1.629
		t Ratio	-45.92	0.45	1.21	-0.63	0.55	-0.54	-0.41	1.20
		Prob> t	<0.0001	0.6850	0.3116	0.5749	0.6220	0.6240	0.7116	0.3173
$T_g(h)$	0.755	Estimate	-15.9	0.8	1.7	-1.2	0.9	-0.45	-0.7	1.95
		Std Error	0.625	1.083	1.083	1.654	0.884	1.398	1.531	2.254
		t Ratio	-25.43	0.74	1.57	-0.73	1.02	-0.32	-0.46	0.87
		Prob> t	0.0001	0.5136	0.2144	0.5206	0.3836	0.7686	0.6787	0.4506
$T_g(f)$	0.808	Estimate	-11.10	1.30	2.50	-1.90	0.85	0.35	-0.55	1.25
		Std Error	0.769	1.331	1.331	2.034	1.087	1.719	1.883	2.771
		t Ratio	-14.44	0.98	1.88	-0.93	0.78	0.20	-0.29	0.45
		Prob> t	0.0007	0.4009	0.1570	0.4191	0.4913	0.8517	0.7892	0.6826
ΔT	0.910	Estimate	9.65	0.95	1.55	-1.15	0.50	0.90	-0.10	-0.70
		Std Error	0.358	0.620	0.620	0.948	0.507	0.801	0.877	1.291
		t Ratio	26.94	1.53	2.50	-1.21	0.99	1.12	-0.11	-0.54
		Prob> t	0.0001	0.2233	0.0879	0.3118	0.3964	0.3430	0.9165	0.6255
ΔC_p	0.956	Estimate	0.245	0.045	-0.075	-0.045	0.035	-0.02	-0.015	0.03
		Std Error	0.0147	0.0255	0.0255	0.0389	0.0208	0.0329	0.0361	0.0531
		t Ratio	16.64	1.77	-2.94	-1.16	1.68	-0.61	-0.42	0.57
		Prob> t	0.0005	0.1757	0.0604	0.3316	0.1913	0.5863	0.7054	0.6114

Table 10 - Glass Transition Temperatures of PS Determined from Total Heat Flow Trace

Method	β (°C/min)	ω (Hz)	A_T (±°C)	$T_g(e)$ (°C)	$T_g(h)$ (°C)
TMDSC	2	0.105	0.318	103.2	105.1
TMDSC	5	0.105	0.796	103.6	106.0
DSC	5	NA	NA	106.1	107.4
DSC	10	NA	NA	107.5	108.8
DSC	20	NA	NA	109.3	110.7

NA = Not Applicable

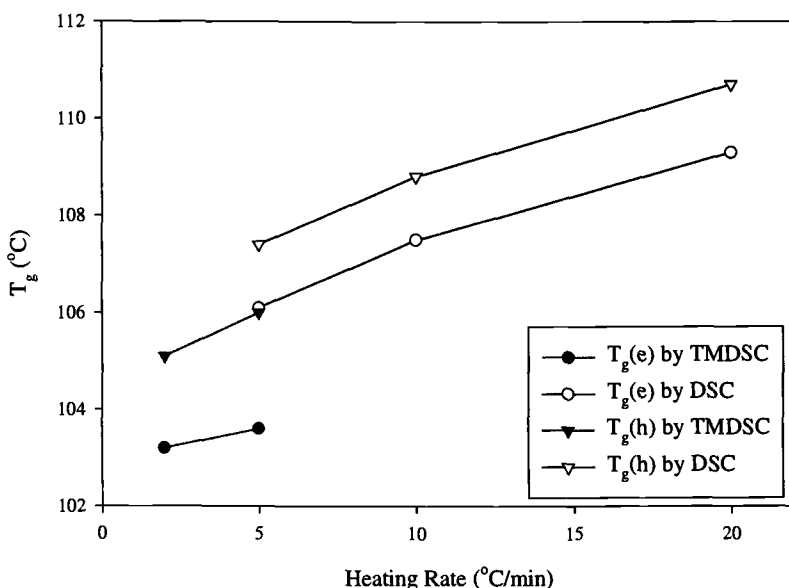


Figure 7 - Glass transition temperatures of PS determined from TMDSC and DSC total heat flow traces as a function of heating rate.

reversing heat flow glass transition measurement of PS, SBR, and BR was statistically evaluated. A $\times 2.5$ increase in β resulted in an increase in $T_g(e)$, $T_g(h)$, and $T_g(f)$ for all three polymers, but was not statistically significant. A $\times 2.4$ increase in ω resulted in a statistically significant increase in the $T_g(e)$ and $T_g(h)$ and a significant decrease in the ΔC_p of all three polymers. A $\times 2.5$ increase in A_T resulted in an increase in the ΔT and ΔC_p of all three polymers, but was not statistically significant. Standard least-squares full factorial model fitting for PS and SBR did not reveal any significant variable interaction effects. A full factorial design is an effective means to evaluate experimental parameters. These statistical methods are highly recommended for other thermal analytical techniques.

Glass transition measurements taken from total heat flow traces acquired by TMDSC

and DSC were compared. Extrapolated onset and half-height glass transitions acquired by TMDSC at 5°C/min were lower than those determined by conventional DSC.

References

- [1] Sircar, A. K., Galaska, M. L., Rodrigues, S., and Chartoff, R. P., "Glass Transition of Elastomers Using Thermal Analysis Techniques," *Rubber Chemistry and Technology* 1999, 72, p. 513.
- [2] Blümel, H., "Molecular Structure and Properties of Polybutadiene Rubbers," *Rubber Chemistry and Technology* 1964, 37, p. 408.
- [3] Lal, J. and Scott, K. W., "Properties and Structure of Elastomers," *Journal of Polymer Science: Part C- Polymer Symposia* 1965, No. 9, p. 113.
- [4] Rogers, W. P., Armstrong, N. A., Archeson, D. A., Covert, E. E., and Feynman, R. P. *Presidential Commission on the Space Shuttle Challenger Accident*, Washington, D.C., N86-24726/XAD, 6 June 1986.
- [5] Reading, M., "Modulated Differential Scanning Calorimetry- A New Way Forward in Materials Characterization," *Trends in Polymer Science* 1993, 1, p. 248.
- [6] Aubuchon, S., "Use of MDSC to Study Physical Aging in Amorphous Sucrose," *TA Instruments 2nd Annual Post-NATAS Seminar*, Cleveland, 1998, p. 1.
- [7] Cser, F., Rasoul, F., and Kosior, E., "Modulated Differential Scanning Calorimetry. The Effect of Experimental Variables," *Journal of Thermal Analysis* 1997, 50, p. 727.
- [8] Flikkema, E., van Ekenstein, G. A., and ten Brinke, G., "Temperature Modulated Calorimetry of Glassy Polymers and Polymer Blends," *Macromolecules* 1998, 31, p. 892.
- [9] Hutchinson, J. M., "Characterising the Glass Transition and Relaxation Kinetics by Conventional and Temperature-Modulated Differential Scanning Calorimetry," *Thermochimica Acta* 1998, 324, p. 165.
- [10] Sauerbrunn, S. R. and Blaine, R. L., "Modulated DSC: The Effect of Amplitude," *23rd NATAS Conference Proceedings*, Toronto, 1994, p. 57.
- [11] Sauerbrunn, S. R., Gill, P. S., and Foreman, J. A., "Modulated DSC: The Effect of Period," *23rd NATAS Conference Proceedings*, Toronto, 1994, p. 51.
- [12] Schawe, J. E., "Modulated Temperature DSC Measurements: The Influence of the Experimental Conditions," *Thermochimica Acta* 1996, 271, p. 127.
- [13] Tomasi, C., Mustarelli, P., Hawkins, N.A., and Hill, V., "Characterisation of Amorphous Materials by Modulated Differential Scanning Calorimetry," *Thermochimica Acta* 1996, 278, p. 9.
- [14] Tool, A. Q. and Eichlin, C. G., "Variations Caused in Heating Curves of Glass by Heat Treatment," *Journal of Research, National Bureau of Standards* 1930, 6, p. 523.
- [15] Wunderlich, B., Bodily, D. M., and Kaplan, M. H., "Theory and Measurements of the Glass-Transformation Interval of Polystyrene," *Journal of Applied Physics* 1964, 35, p. 95.
- [16] Ferry, J. D. *Viscoelastic Properties of Polymers*, John Wiley and Sons, Inc., New York, 1980.

Glass Transformation Studies of Vitreous As₂Se₃ by Temperature-Modulated DSC

REFERENCE: Kasap, S.O., and Tonchev, D., "Glass Transformation Studies of Vitreous As₂Se₃ by Temperature-Modulated DSC," *Materials Characterization by Dynamic and Modulated Thermal Analytical Techniques, ASTM STP 1402*, A. T. Riga and L. Judovits, Eds., American Society for Testing and Materials, West Conshohocken, PA, 2001.

Abstract: We have carried out temperature-modulated differential scanning calorimetry (TMDSC) measurements on a typical chalcogenide glass system, As₂Se₃, which has been well-characterized previously in the literature by conventional DSC. We have studied the behavior of the total and reversing heat flows as the glass is cooled from a temperature above the glass transition temperature, that is, from a liquid-like state. The glass transition temperature T_g was operationally defined as the temperature where the reversing heat flow evinces an inflection point in changing from liquid-like to solid-like behavior. We have studied (a) the dependence of T_g on the cooling rate q under conventional DSC conditions and (b) the dependence of T_g on the modulation period P under TMDSC conditions. These two studies were carried out towards characterizing the glass relaxation kinetics. We have also examined whether T_g shows any dependence on the modulation amplitude A at a given cooling rate.

Keywords: temperature-modulated differential scanning calorimetry (TMDSC), glass transformation, chalcogenide glass, As₂Se₃.

1. Introduction

At present there is considerable scientific interest in applying temperature-modulated differential scanning calorimeter (TMDSC) measurements to the study of glass transformation in glasses and polymers. Glass transformation phenomena in glasses and polymers have been, of course, studied extensively by conventional DSC. Although TMDSC measurements have been recently also used to study the glass transition in glasses, for example, vitreous chalcogenides, the exact interpretation of the results has been subject to various controversies, in particular, the interpretation of the nonreversing heat flow.

Hutchinson and Montserrat [1] considered the interpretation of TMDSC experiments in the glass transition region of glasses by using a single relaxation time approach in which the relaxation time τ followed the Narayanaswamy form; τ depends not only on the temperature but also on the deviation of the structure from the equilibrium state. To obtain further insight into the interpretation of TMDSC measurements in the glass transformation region we decided to study structural relaxation kinetics in vitreous As₂Se₃, which is a typical chalcogenide glass. We carried out both conventional and temperature-modulated DSC experiments by using cooling scans starting from a state above the glass transition temperature, that is from a liquid-like state. The following experiments and analyses were carried out:

¹ Department of Electrical Engineering, University of Saskatchewan, Saskatoon, S7N 5A9, Canada.

- (a) TMDSC measurements for the dependence of the glass transition temperature T_g on the modulation period P and the apparent activation energy from $\ln(P)$ vs. $1/T_g$ plots.
- (b) Conventional DSC experiments for the dependence of T_g on the cooling rate q and the apparent activation energy from $\ln(q)$ vs. $1/T_g$ plots as in references [2] and [3].
- (c) TMDSC experiments for the dependence of T_g on the modulation amplitude A .

2. Experimental Procedure

Vitreous As_2Se_3 samples were prepared by conventional glass quenching techniques. Stoichiometric high purity As_2Se_3 bulk samples were obtained from AlfaAesar. About 10 g of As_2Se_3 was placed in precleaned and outgassed (by heating under vacuum to 900 °C) quartz ampoules. The ampoules were evacuated to a pressure of 10^{-3} Pa for 30 mins. and then sealed. The synthesis was performed in a rocking furnace with the ampoules exposed to a temperature of 800 °C for 24 h. Following heating, the ampoules were immediately immersed into ice-water for quenching down to a temperature of 0 °C. The samples were then aged at room temperature for about three months prior to thermal analysis measurements. The bulk samples were crushed into small pieces, weighted into aluminum crimped pans, and then sealed. A typical sample weight was about 20 mg. An empty crimped pan was used as a reference sample and matched the sample pans by ± 0.15 mg.

The differential scanning calorimetry experiments were performed on a temperature-modulated DSC (MDSCTM, TA Instrument Inc., USA) using a liquid nitrogen cooling accessory and a nitrogen gas DSC cell purge. The DSC 2910 system allows both heating and cooling scans in the modulated or non-modulated (DSC) regime. The instrument was calibrated for enthalpy and temperature readings using a standard of high purity elemental indium. The instrument was also calibrated for specific heat capacity (C_p) with a standard sample of sapphire using the same heating rate, oscillation period and amplitude in the temperature range of interest as those used in the subsequent experiments. The reference value for C_p of sapphire was obtained from the manufacturer (TA Instruments).

Each TMDSC or DSC scan was carried out on a "new" As_2Se_3 sample that was not used previously to avoid thermal history effects. The sample was heated at a rate of 50 °C/min in conventional DSC mode to a temperature of 300 °C, above the glass transition temperature for that heating rate, and then equilibrated at this temperature for several minutes (corresponding to 5 cycles). Immediately following the equilibration, the cooling TMDSC or DSC scan was initiated down to room temperature. TMDSC and DSC measurements are therefore carried out on samples that have identical thermal history and all starting from a liquid-like state at 300 °C. It is generally accepted that representable and meaningful TMDSC measurements must correspond to at least four full T - t cycles over the half-width of the transition of interest. Although a slower cooling rate than 1 °C/min would be preferable, the present rate was practical and, over the T_g transition region, gave at least 10 cycles when the period was 100 seconds (the worst case). The repeatability of T_g measurements was better than 1%.

3. Results and Discussions

Figure 1 shows a typical conventional DSC cooling scan through the glass transition region at a cooling rate q of 30 °C/min. The glass transition temperature T_g was operationally defined as the temperature of the inflection point as indicated in Figure 1. We have investigated how T_g changes with the cooling rate from $q = 30$ °C/min down to 1 °C/min towards characterizing the glass transition kinetics as discussed below. Figure 2 shows a typical TMDSC cooling result in terms of the sample heat capacity (from the

reversing heat flow) vs. temperature behavior through the glass transition region. The modulation period P was 80 s and the modulation amplitude was $\pm 1^\circ\text{C}$. The inflection point was taken as the operational definition of T_g as determined from the heat capacity vs. temperature curve in TMDSC measurements.

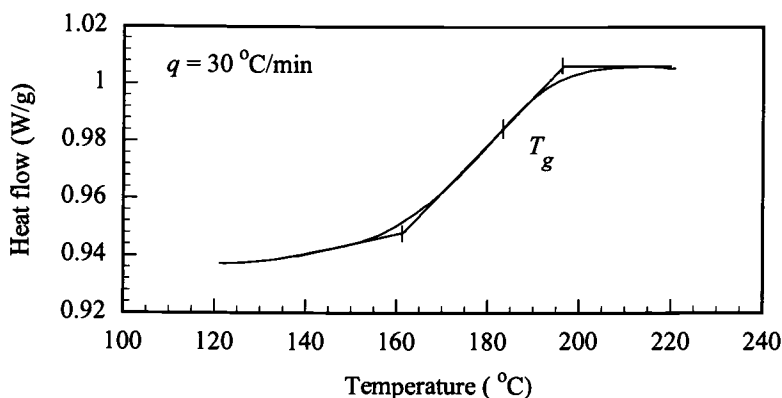


Figure 1 - Typical example of a conventional DSC cooling scan through the T_g region and the definition of T_g at the inflection point.

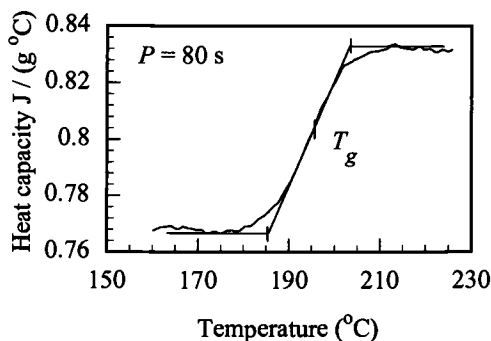


Figure 2 - Typical example of a TMDSC cooling scan through the T_g region and the definition of T_g at the inflection point. Average cooling rate was 1°C/min and the modulation period P was 80 s.

The changes in the T_g with the cooling rate in conventional DSC and changes in T_g with the period P in TMDSC can be used to characterize the structural relaxation kinetics of the glass structure. It is generally accepted that the activation energy Δh obtained from a $\ln(q)$ vs. $1/T_g$ plot is reproducible, independent of the sample thermal history and, over the same temperature range, corresponds to the activation energy of the glass viscosity, that is the structural relaxation time is inversely proportional to the viscosity [2, 3].

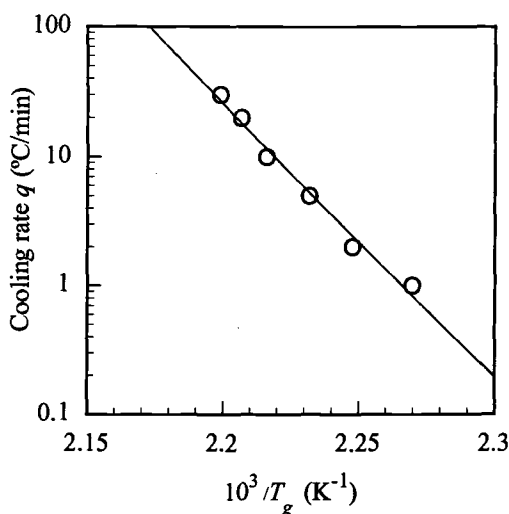


Figure 3 - Semilogarithmic plot of the cooling rate vs. reciprocal glass transition temperature from conventional DSC cooling scans.

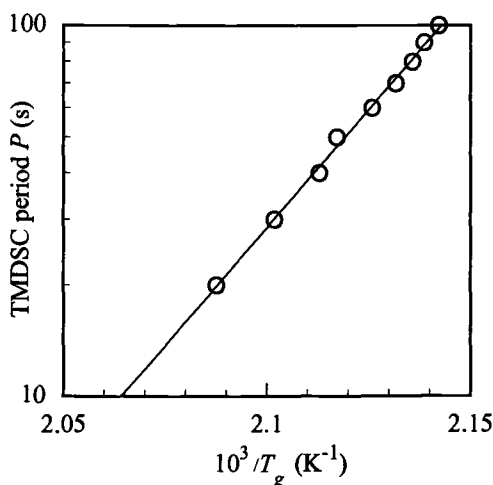


Figure 4 - Semilogarithmic plot of the modulation period vs. reciprocal glass transition temperature from TMDSC cooling scans.

Figure 3 shows a semilogarithmic plot of the cooling rate against the reciprocal glass transition temperature where the slope of the straight line indicates an activation energy of 407 kJ mol^{-1} . This value is very close to the viscosity activation energy of 380 kJ mol^{-1} in the same temperature range as available from the viscosity data of Henderson and Ast [4]. The viscosity of As_2Se_3 does not exhibit an Arrhenius temperature dependence but rather a Vogel type of temperature dependence. The activation energy therefore depends on the temperature but, over a small temperature interval as in Figure 3, it can be approximated

by an Arrhenius dependence. The viscosity activation energy of 380 kJ mol^{-1} is that value at the mean temperature of the T_g interval in Figure 3.

In the case of TMDSC measurements, the relaxation kinetics are characterized by examining the dependence of T_g on the modulation frequency or the period P . Figure 4 is a semilogarithmic plot of P vs. $1/T_g$ and the slope of the line indicates an activation energy of 243 kJ mol^{-1} , substantially smaller than that from $\ln(q)$ vs. $1/T_g$ behavior. However, the temperature regions are not identical; T_g values in TMDSC are higher than those in conventional DSC for reasons apparent in reference [5]. An interesting observation is the fact that, in the same temperature interval, the viscosity activation energy is 290 kJ mol^{-1} . Given the experimental difficulties in carrying out P - T_g measurements, we believe that the agreement between the activation energies from $\ln(P)$ vs. $1/T_g$ and viscosity data are close. Experimental settings (heating and cooling rates, amplitude, period etc.) have been specially chosen to ensure full separation of the DSC and TMDSC response and to obtain clear dynamical experiment from the TMDSC measurements. The activation data from Figures 3 and 4 and from the viscosity data are summarized in Table 1. The determination of the kinetic parameters from variable period scans is currently under further study.

Table 1 - Activation energy (Δh) from DSC cooling rate (q) scans; Δh from TMDSC period (P) scans; Δh calculated from Henderson and Ast viscosity data [4] using an average T_g value that represents T_g range of interest.

Δh	$\ln(P)$ vs. $1/T_g$	$\ln(q)$ vs. $1/T_g$
	243 kJ mol^{-1}	407 kJ mol^{-1}
Δh from viscosity (kJ mol^{-1})	290 kJ mol^{-1}	380 kJ mol^{-1}
T_g average	471.9 K	448.8 K
	198.9°C	175.8°C

As summarized in Table 2 we find that A did not affect the T_g measurement, what is expectable regarding previously published results in the connected literature.

Table 2 - Effect of TMDSC amplitude (A) on glass transition temperature T_g data taken from the heat capacity curve during a cooling scan of 1°C min^{-1} . The modulation period was 70 s .

Amplitude A ($^\circ\text{C}$)	T_g onset ($^\circ\text{C}$)	T_g inflection ($^\circ\text{C}$)	T_g end ($^\circ\text{C}$)
± 0.2	206.7	196.8	187.0
± 1	205.2	196.9	187.7
± 5	205.0	196.8	187.4

4. Conclusions

We carried out both conventional and temperature-modulated DSC cooling experiments on stoichiometric vitreous As_2Se_3 glass starting from a liquid-like state above the glass transition temperature to room temperature. Variable cooling rate conventional DSC scans, i.e. q - T_g data, were analyzed as $\ln(q)$ vs. $1/T_g$ plots and indicated an activation energy for the structural relaxation that was 407 kJ mol^{-1} and close to the activation energy of 380 kJ mol^{-1} for the viscosity in the same temperature range.

TMDSC experiments in which the period P was varied were analyzed as $\ln(P)$ vs. $1/T_g$ plots and indicated an activation energy of 243 kJ mol^{-1} , substantially less than q - T_g experiments but not far out from the activation energy of 290 kJ mol^{-1} for the viscosity in

the same temperature range. T_g measurements show no dependence on the modulation amplitude from 0.2 to 5 °C.

References

- [1] Hutchinson, J.M. and Montserrat, S., "A theoretical model of temperature-modulated differential scanning calorimetry in the glass transition region," *Thermochimica Acta*, Vol. 304-305, 1997, pp. 257-265 and references therein.
- [2] Kasap, S.O. and Yannacopoulos, S., "Apparent activation energy of the glass transformation in vitreous As₂Se₃ via heating and cooling DSC scans," *Physics and Chemistry of Glasses*, Vol. 31, 1990, pp. 71-74.
- [3] Avramov, I., Grantscharova, E., and Gutzow, I., "Structural relaxation in two metaphosphate glasses," *Journal of Non-Crystalline Solids*, Vol. 91, 1987, pp. 386-390.
- [4] Henderson, D.W., and Ast, D. G., "Viscosity and crystallization kinetics of As₂Se₃," *Journal of Non-Crystalline Solids*, Vol. 64, 1984, pp. 43-70.
- [5] Wunderlich, B., Boller, A., Okazaki, I., and Kreitmeier, S., "Modulated differential scanning calorimetry in the glass transition region II," *Journal of Thermal Analysis*, Vol. 64, 1996, pp. 1013-1026.

GENERAL MODULATED TECHNIQUES

L. Christine Fuller¹ and Lawrence Judovits¹

Comparison Between Modulated Differential Scanning Calorimetry (MDSC) and Dynamic Differential Scanning Calorimetry (DDSC)

REFERENCE: Fuller, L. C. and Judovits, L., “Comparison Between Modulated Differential Scanning Calorimetry (MDSC) and Dynamic Differential Scanning Calorimetry (DDSC),” *Materials Characterization by Dynamic and Modulated Thermal Analytical Techniques, ASTM STP 1402*, A. T. Riga and L. Judovits, Eds., American Society for Testing and Materials, West Conshohocken, PA, 2001.

Abstract: Both modulated differential scanning calorimetry (MDSC) and dynamic differential scanning calorimetry (DDSC) are registered tradenames for instrumental techniques which are part of the temperature-modulated differential scanning calorimetry (TMDSC) family. Both oscillate their input ramps differently in that the MDSC uses a sine wave while DDSC generates a sawtooth wave. Although we have found similarities between both techniques we do note some differences. These differences primarily occur in the melting reversing signal for the same conditions and as one changes period and amplitude. These differences may be ascribed to the different time response as noted between a heat flux and power compensation DSC.

Keywords: differential scanning calorimetry, modulated differential scanning calorimetry, dynamic differential scanning calorimetry, temperature-modulated differential scanning calorimetry, polyvinylidene fluoride, polystyrene

Introduction

During the 1990s, differential scanning calorimetry (DSC) performance was enhanced by the invention of modulated DSC (MDSC) [1]. MDSC has spawned a number of related temperature-modulated DSC (TMDSC) techniques such as dynamic DSC (DDSC). MDSC and DDSC are manufactured by TA Instruments (TAI) and Perkin-Elmer (PE), respectively [2]. A pictorial representation of the signals seen by each technique is given in Figures 1 and 2. More has been published on the specifics of the mathematics of MDSC than DDSC which is reflected in the MDSC diagram [3,4,5]. Corresponding signals can be noted between the figures for both techniques in that similar TMDSC quantities are determined such as:

- Complex heat capacity
- Reversing (phase corrected) or storage heat capacity
- Kinetic or loss heat capacity

¹ ATOFINA Chemicals, Inc., 900 First Avenue, King of Prussia, PA 19406.

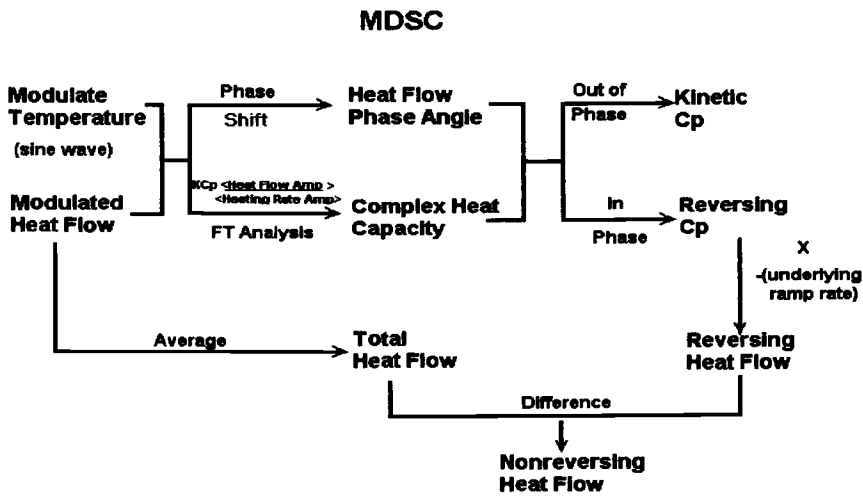


Figure 1, MDSC 2920 schematic based on reference 4, phase correction applied.

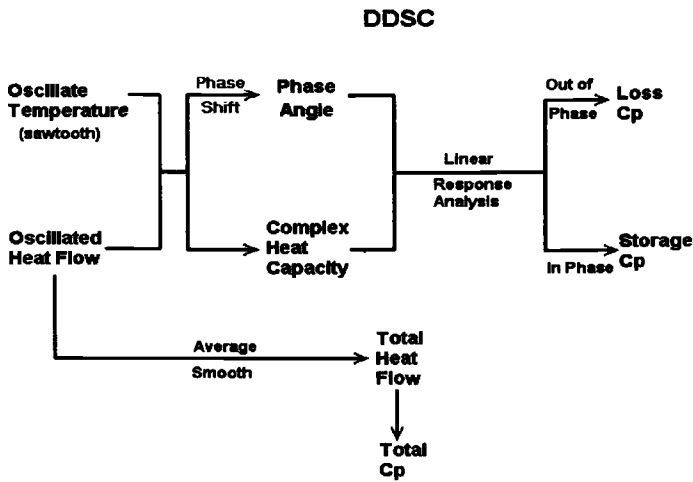


Figure 2, DDSC 7 schematic based on reference 5, a corresponding MDSC nonreversing C_p can be calculated by manual curve subtraction.

The principle of MDSC consists of superimposing a sinusoidal signal over an underlying DSC ramp. Advantages of this technique include the separation of reversing and nonreversing effects from the heat flow signal as well as improved heat capacity determinations [6,7]. For DDSC a sawtooth wave is used. The reversing heat flow and the reversing or storage heat capacity are related to the heat capacity component of the heat flow while the nonreversing heat flow or heat capacity arises when the heat flow does not follow the temperature oscillation. For the TAI unit, the nonreversing element is easily calculated from the difference between the total heat flow and the reversing heat flow. A corresponding heat capacity can be determined for the PE unit by manual subtraction of the appropriate curves. The explanation of the kinetic or loss heat capacity is not as easy. This quantity arises from the phase angle between the in-phase and out-of-phase signals, and is often compared to the loss modulus seen for dielectric analysis (DEA) or dynamic mechanical analysis (DMA) [8]. A direct analogy, of course, would be imprecise since no heat is lost during a TMDSC experiment. As to its physical meaning there seems to be a number of interpretations in the literature as summarized in reference 9.

Problems with correspondence between Figures 1 and 2 arise with both terminology and variations in the calculation of each signal. The MDSC 2920 flow diagram used depicts the use of the phase correction for MDSC data. Without the phase correction, the nonreversing heat flow would now be determined by subtracting from the total heat flow a "complex heat flow signal". In current TAI terminology the "complex heat flow" would also be referred to as reversing heat flow (but not phase corrected). However, care should be taken in the calculation of the nonreversing heat flow as to not simply interchange scalar and vector quantities. Still, both nonreversing signals provide information on kinetic processes occurring in a DSC run. Additionally other nomenclature exists in the literature for these signals [3]. As to which nomenclature to use, this study has taken the position to use the particular vendors terminology, when discussing their software, with the exception of the nonreversing signal which is not described by PE.

In this study, we have tried to subject for analysis under similar conditions the glass transition of polystyrene (PS) and the melting of polyvinylidene fluoride (PVDF) by both MDSC and DDSC. Our study is the investigation and comparison of commercial software only using conditions as similar as possible considering manufacturer differences. Other studies have been performed comparing the units under other experimental conditions using proprietary software [10]. A heat/cool program was used and the effect of changing both period and amplitude was investigated since this is the only ramp program recommended in the Perkin-Elmer operating software. For this study the TMDSC signals investigated with changing period and amplitude were the complex, reversing/storage and kinetic/loss heat capacities.

Experimental

The MDSC measurements were made on a TA Instruments 2920 equipped with a liquid nitrogen accessory (LNCA II) or a refrigerated accessory (RCS) while the DDSC

measurements were made on a Perkin-Elmer DDSC 7 equipped with a refrigerated accessory (intracooler II). A sample mass between 5 to 6 mg was utilized and the cells were purged with nitrogen gas. A heat/cool program was employed as recommended for DDSC use [5] and an underlying heating rate of 1 °C/min was used. Both the MDSC and the DDSC were calibrated at 1 °C/min using indium and lead. For the TAI instrument a heat capacity adjustment as described in their manual [11] was also performed while a baseline subtraction was performed for the PE system. TAI universal analysis software (v2.6) was used for the MDSC analysis while Pyris software (v3.5A) was used for DDSC analysis. The Pyris software has a help option which was followed in setting the DDSC experimental parameters. Both the PS and PVDF samples were preconditioned using a cooling rate of 10 °C/min from the melt. The PS was purchased from Aldrich Chemical Company and has a molecular weight of 212,400 Dalton. The PVDF obtained from ATOFINA Chemicals, Inc. has a Mw of 178,000 and a Mn of 84,000 Dalton relative to PMMA.

Results

Since the PE unit favors the use of a heat/cool method, an oscillation resulting in a TMDSC mode having an underlying heating rate with a cooling component was selected. For comparison purposes no baseline subtraction at first was selected for the DDSC analysis, however, later we found it necessary to run a baseline subtraction. Specimens were first run on the DDSC and a period with an estimated amplitude was determined from the sample temperature. This amplitude and period were then used as parameters in the MDSC experiment as noted here for the 1 °C/min heats.

Period/seconds	Amplitude/ \pm °C		Measured Amplitude/°C
for 1 °C/min heats	Melting	Glass Transition	Melting
30	0.34	0.34	0.31
60	0.72	0.73	0.69
90	1.08	1.08	1.06

Checks of the estimated and actual amplitude for the TAI system gave good agreement as noted previously for the 1 °C/min heating rate. The amplitudes obtained for the modulation period appear to be typical for a PE unit using its software [12,13] although other authors have pursued measurements at lower amplitudes apparently using their own software [10]. It should be noted that PE recommends the iso-scan mode for melting studies [5].

Melting

For the PVDF sample the complex heat capacity at 60 seconds for the 1 °C/min heating rates for the MDSC and DDSC are very similar. Doublet peak temperatures are seen at 165-166 and 171 °C with heats of fusion from 41 to 48 J/g. The TAI nonadjusted results gave close results of 44 J/g with doublet peaks at 166 and 170 °C. The heat flow

signal from the MDSC and total heat capacity signal from the DDSC are also similar with peak temperatures at 165 and 171°C and having a slightly higher heats of fusion than the melting in the complex signal of between 58 to 69 J/g. The storage and the reversing heat capacity are vastly different with the reversing heat capacity showing a predominate peak at 165°C in the reversing heat capacity while the storage heat capacity shows what appears to be an exothermic doublet at 166 and 171°C superimposed on a broad endothermic peak. Since the storage and reversing signals are different than as one would expect differences exist for the kinetic and loss heat capacity meltings, and the PE unit is found to have a much higher heat of fusion. Surprisingly, no differences were noted for the nonreversing meltings nor did the TAI heat capacity adjustment change the shape of the melting peaks in any of the signals.

Glass Transition

As noted for the melting analysis the glass transition also shows similarity between the two techniques independent of any adjustments. As seen in Table 1, one notes agreement between the complimentary signals between the two units as one can see between the data obtained from the total heat flow and heat capacity, both complex heat capacities, and reversing and storage heat capacities, respectively. For the glass transition even the loss and kinetic capacity and the nonreversing signals show agreement between the two techniques. However, the nonreversing heat capacity for the PE unit is sensitive to the smoothing procedure in the determination of the total heat capacity. Also of interest is that the glass transition determined from the total signal is less than the reversing or complex signals which appear identical. As has been noted in the literature, the heat flow in the glass transition region on heating contains a time or frequency dependence and an enthalpy relaxation [14]. The enthalpy relaxation has been noted to separate into the nonreversing signal but the reversing and complex heat capacity signals retain the frequency dependence and the transition therefore appears at a higher T_g due to the modulation effect [15]. Use of the heat capacity adjustment for the TAI data had little or no effect on the T_g or ΔC_p measurements performed for this study.

Period and Amplitude Effects

Unlike the TAI system, we were unable to separately alter the period and amplitude effects for the PE unit using their software. So both were altered together for this study. Similar changes can be noted between the two techniques for the complex, storage or reversing and loss or kinetic heat capacities. This is true for both the melting and the glass transition. In general as the amplitude and period increases, the melting endotherm and the glass transition change in heat capacity (ΔC_p) increases for the complex and reversing or storage heat capacity. The peak temperature for the glass transition in the loss or kinetic heat capacity decreases with increasing period. The melting results for the loss and kinetic heat capacities also correlate when the PE data is baseline subtracted, however, a trend was not noted. The TAI also shows spikes indicating a poor run since

Table 1-glass transition analysis, period and amplitude study for 1 °C/min heating ramps

TMDSC Type	Period (s)	Amplitude (± °C)	Total Heat Flow or Total C_p T_g (°C)	Total Heat Flow or Total C_p ΔC_p (J/g°C)	Complex C_p T_g (°C)	Complex C_p ΔC_p (J/g°C)	Reversing/Storage C_p T_g (°C)	Reversing/Storage C_p ΔC_p (J/g°C)
MDSC	30	0.34	102	0.26	107	0.21	107	0.23
MDSC	60	0.73	101	0.24	106	0.22	105	0.23
MDSC	90	1.08	100	0.43	104	0.22	104	0.24
DDSC	30	0.34	102	0.33	106	0.20	106	0.20
DDSC	60	0.73	102	0.29	106	0.24	106	0.25
DDSC	90	1.08	102	0.22	106	0.26	106	0.26
MDSC, not corrected	30	0.34	100	0.34	106	0.19	106	0.20
MDSC, not corrected	60	0.73	102	0.25	106	0.24	106	0.24
MDSC, not corrected	90	1.08	101	0.24	104	0.26	105	0.25
DDSC, not subtracted	30	0.34	104	0.30	108	0.19	107	0.19
DDSC, not subtracted	60	0.73	102	0.34	106	0.20	106	0.22
DDSC, not subtracted	90	1.08	102	0.22	103	0.26	104	0.23

the parameters chosen were not optimized for proper run conditions but to match the PE results. The melting results can be noted in the following figures for the different signals. Figures 3 and 4 show the melting results for the complex heat capacities, Figures 5 and 6 show the results for the reversing and storage heat capacities while Figures 7 and 8 show the kinetic and loss heat capacities.

Baseline Subtraction

Since the purpose of this study was to compare MDSC to DDSC under similar conditions, no baseline subtraction was utilized initially. Usually MDSC experiments are not run using a baseline subtraction whereas the subtraction is suggested for DDSC and appears necessary for the proper calculation of the total heat capacity. One would assume that not performing the subtraction should not effect the calculation of the complex, storage and loss heat capacities. However, the negative heat capacities were noted during the melting for the PE unit for the storage and loss heat capacities. No negative heat capacities were noted after subtraction. Recently, instrument problems have been associated with spiking in a saw-tooth modulation which could result in instrumental problems with baseline subtracting sometimes resolving the problem [10].

Discussion

For the runs performed at 60 seconds, both units appear similar, however, as one departs from this period, differences are to be noted. Large differences can be noted between the two techniques for the melting in the reversing/storage heat capacity. Since the glass transition trends with changing frequency appear similar between the instrumental techniques as noted in Table 1, one would suppose that the differences noted between the meltings are in part due to instrumental response as one loses steady state. This would be especially true for large modulations resulting in a heat/cool program. The dual furnace design of the PE cell should allow a quicker response. However, one can not still rule out a software analysis effect which was not corrected by baseline subtraction.

For short periods, The TAI unit has problems modulating a large amplitude within the time constraints of a short period. The cause of these differences appears to be instrumental in that the unit can not maintain a full oscillation

Since we had to change both amplitude and period to match effects between the instruments, we also performed a separate study on the TAI system keeping each parameter constant while changing the other. In general for the melting the complex and the reversing heat capacities become more endothermic with increasing period or amplitude with the period having the more profound effect within the parameters we investigated. The increase in ΔC_p noted above appears to be more related to a period effect.

Conclusions

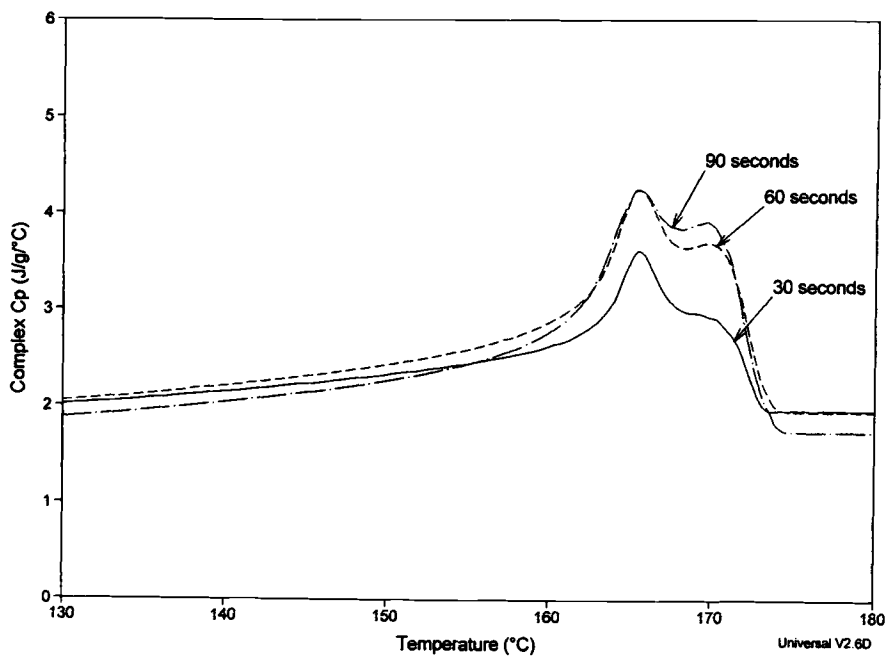


Figure 3, MDSC 2920 Complex Heat Capacity Signals for PVDF

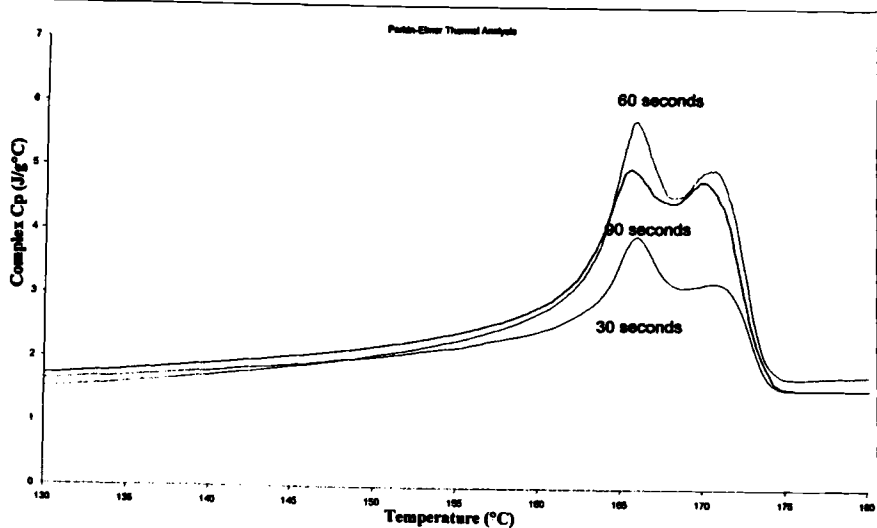


Figure 4, DDSC 7 Complex Heat Capacity Signals for PVDF

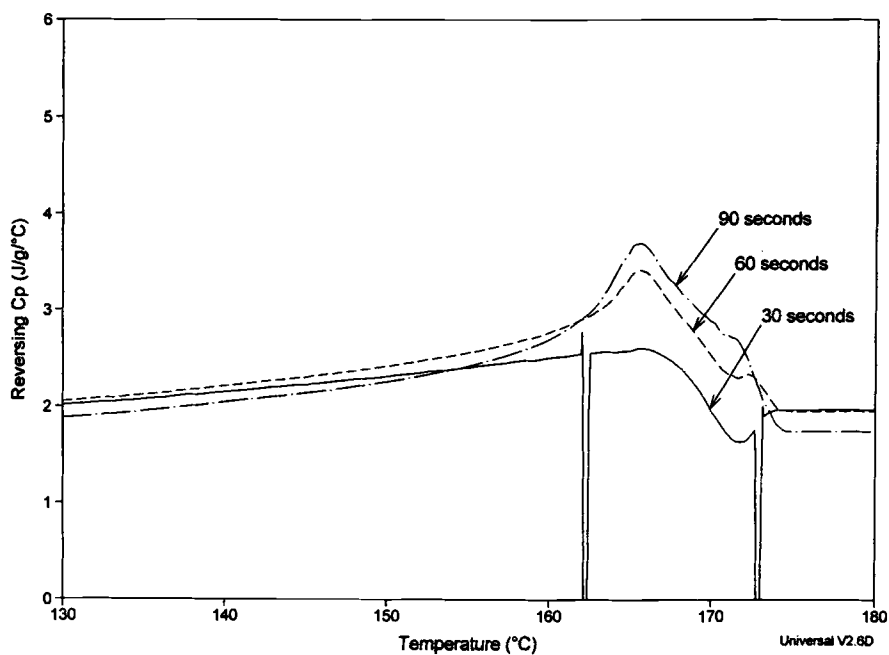


Figure 5, MDSC 2920 Reversing Heat Capacity Signals for PVDF

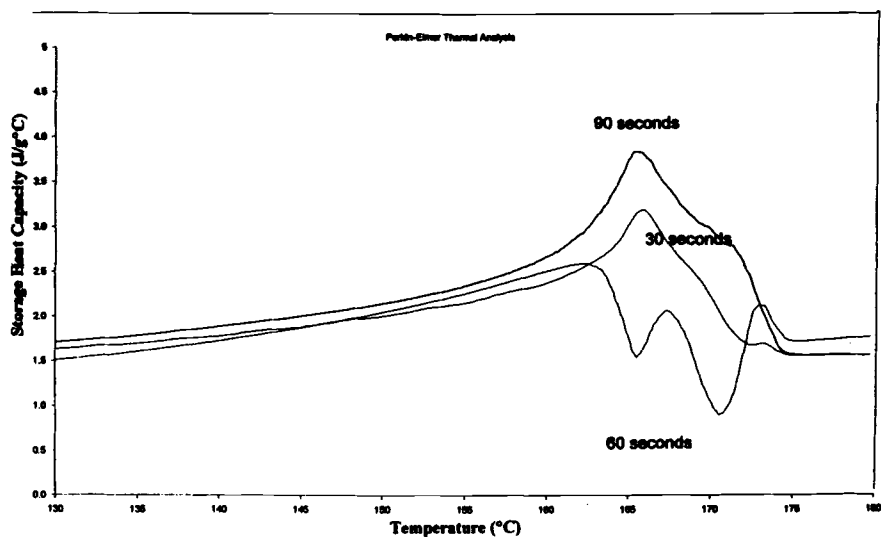


Figure 6, DDSC 7 Storage Heat Capacity Signals for PVDF

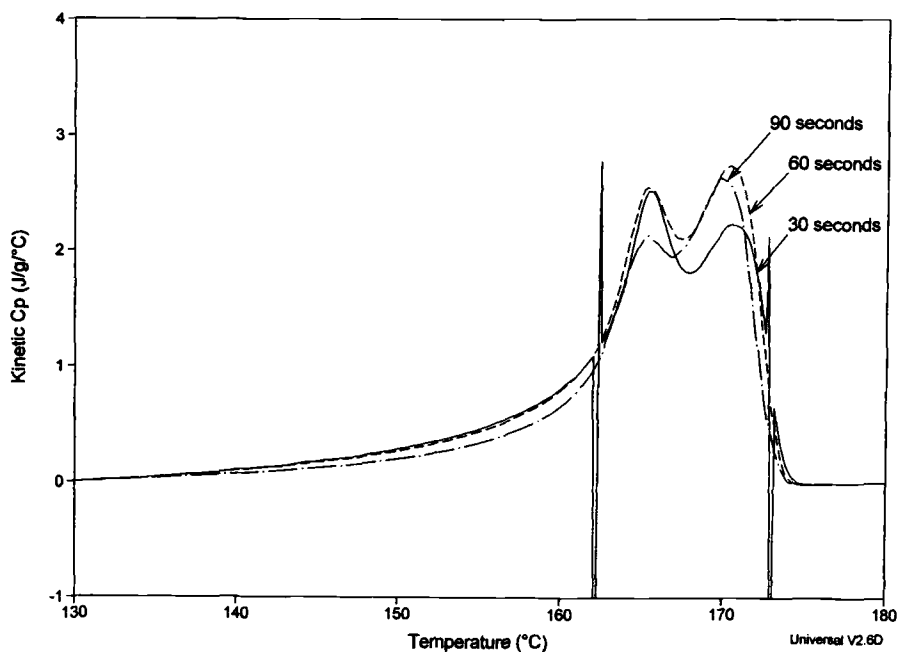


Figure 7, MDSC 2920 Kinetic Heat Capacity Signals for PVDF

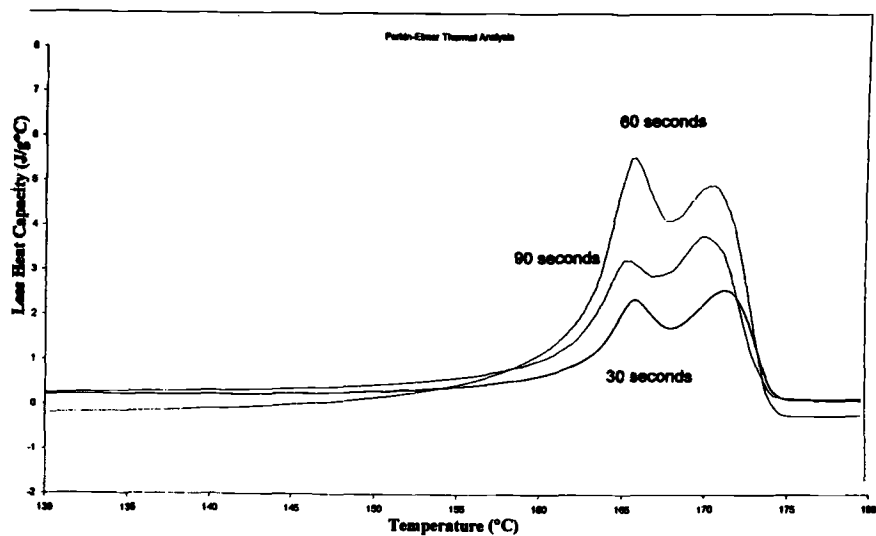


Figure 8, DDSC 7 Loss Heat Capacity Signals for PVDF

Both the MDSC and DDSC, although based on different approaches, show many similarities. The main difference between the two techniques for this study occurs for the melting between the reversing and storage heat capacities for the same conditions and the differences in the trend noted in the loss and kinetic heat capacities as the period increases. This appears due to instrumental response resulting from the use of large modulation amplitudes rather than a significant difference in the mathematics. The use of the large amplitudes selected was determined from standard experimental parameters from the DDSC heat/cool mode.

References

- [1] Reading, M., Hahn B. K., and Crow B. S., U.S. Patent 5,224,775, 6 July 1993.
- [2] Judovits, L., Introduction to MDSC, Theory and Application, NATAS Notes, 1997, 29, 31.
- [3] Wunderlich, B., Jin, Y. and Boller, A., Mathematical description of differential scanning calorimetry based on periodic temperature modulation, *Thermochimica Acta*, 1994, 238, 277.
- [4] Modulated DSC Training Workshop, McLean, VA, September 11, 1997
- [5] DiVito, M. P., Cassel, R. B., Margulies, M., and Goodkowsky, S., Dynamic differential scanning calorimetry, American Laboratory, 1995, 28, 26.
- [6] Reading, M., Wilson, R., Pollock, H. M., Modified Differential Scanning Calorimetry: Theory Practice, and Application, *Proceedings of the 23rd NATAS Conference*, Toronto, 1994, 2.
- [7] Varma-Nair, M. and Wunderlich, B., Non Isothermal Heat Capacities and Chemical Reactions Using a Modulated DSC, *J. Thermal Analysis*, 1996, 46, 879.
- [8] Schawe, J. E. K., A comparison of different evaluation methods in modulated temperature DSC, *Thermochimica Acta*, 1995, 260, 1.
- [9] Buehler, F. U. and Seferis, J. C., Effect of sample thickness in TMDSC measurements, *Thermochimica Acta*, 2000, 348, 161.
- [10] Wunderlich, B., Androsch, R., Pyda, M., Kwon, Y. K., Heat capacity by multi-frequencies sawtooth modulation, *Thermochimica Acta*, 2000, 348, 181.
- [11] TAI Instruments DSC 2920 CE Operator's Manual Appendix C: Modulated DSC™ Option, 1998.

[12] Bilyeu, B. W., Brostow, W. K., and Menard, K. P., Evaluation of the Curing Process in a Fiber-Reinforced Epoxy Composite by Temperature-Modulated and Step Scan DSC and DMA, *Materials Characterization by Dynamic and Modulated Thermal Analytical Techniques*, ASTM STP 1402, Riga, A. T. and Judovits, L., Eds., this publication.

[13] Righetti, M. C., Pizzoli, M., Ceccorulli, G., Glass Transition of Polymers by TMDSC, DMTA and DETA Analyses, *Materials Characterization by Dynamic and Modulated Thermal Analytical Techniques*, ASTM STP 1402, Riga, A. T. and Judovits, L., Eds., this publication.

[14] Wunderlich, B., Bodily, D. M., and Kaplan, M. H., Theory and Measurement of the Glass-Transformation Interval of Polystyrene, *J. Appl. Phys.*, 1964, 35, 95.

[15] Wunderlich, B. and Okazaki, I., Modulated Differential Scanning Calorimetry in the Glass Transition Region VI. Model calculations based on poly(ethylene terephthalate), *J. Thermal Analysis*, 1997, 49, 57.

OTHER MODULATED TECHNIQUES

Duncan M. Price¹

Modulated-Temperature Thermomechanical Measurements

REFERENCE: Price, D. M., “**Modulated-Temperature Thermomechanical Measurements,**” *Materials Characterization by Dynamic and Modulated Thermal Analytical Techniques*, ASTM STP 1402, A. T. Riga and L. Judovits, Eds., American Society for Testing and Materials, West Conshohocken, PA, 2001.

ABSTRACT: There are close analogies between DSC (which measures enthalpy changes) and thermomechanical analysis (TMA) (which measures volume or length changes). This naturally leads to the application of modulated temperature programs to TMA as a means to separate the reversible nature of thermal expansion from irreversible deformation arising from creep under the applied load or changes in dimensions due to relaxation of orientation. The effect of experimental variables and calibration are described and the application of the technique to study the glass-rubber transition and melting of polymers is discussed.

KEYWORDS: calibration, glass transition, melting, modulated temperature, thermomechanical analysis, thermal expansion, shrinkage, creep

Introduction

The earliest use of modulated-temperature programming in thermal analysis to separate thermally reversible from irreversible processes appears to be the work of Garn and Sharp published in 1982 [1,2]. By employing a small sinusoidal temperature wave superimposed on a constant heating rate they were able to distinguish between rapidly reversible pyroelectric currents and the irreversible discharge which occurs over a longer timescale due to the decay of oriented dipoles in thin dielectric polymer films. Ten years later similar principles were described by Reading to deconvolute heat capacity from heat flow arising from time dependant chemical and physical transformations (e.g., polymerization, crystallization and melting) in differential scanning calorimetry (DSC) [3]. Furthermore, modulated-temperature DSC (MTDSC) offers the advantage of increasing the temperature resolution of thermal events without sacrificing sensitivity by a combination of slow underlying scanning rates and rapid temperature modulation [4].

Thermomechanical analysis (TMA) involves measurement of the response of a material to a constant load or deformation as a function of temperature [5]. Although the technique was first applied to polymers in 1948 there is often difficulty in interpreting the results due to the superposition of creep and stress relaxation upon linear thermal

¹ Research Fellow, Institute of Polymer Technology and Materials Engineering, Loughborough University, Loughborough, Leicestershire LE11 3TU UK.

expansion [6]. Hedvig has described the use of a differential thermomechanical technique to overcome these effects [7]. Since thermal expansion is due to reversible changes in molecular vibrational modes which occur with temperature (c.f., changes in enthalpy due to the absorption or dissipation of heat in DSC) a simpler approach might be to employ modulated-temperature programs in TMA.

Theory

The theory of modulated-temperature TMA (MTTMA) can be developed by direct analogy to the equations used to describe MTDSC by simply substituting the specimen's length or thermal expansivity for enthalpy and heat capacity in the following equation used for MTDSC [3]:

$$dQ/dt = C_p dT/dt + f(t, T) \quad (1)$$

where Q is the amount of heat evolved, C_p the thermodynamic heat capacity, T the absolute temperature, t the time and $f(t, T)$ some function of time and temperature that governs the kinetic response of any chemical or physical transformation.

For MTTMA this becomes:

$$dL/dt = \alpha dT/dt + f'(t, T) \quad (2)$$

where L is the sample length, α is the thermal expansion coefficient and $f'(t, T)$ some function of time and temperature that describes dimensional changes due to deformation under the applied load or relaxation of stresses present in (for example) oriented materials. Over a broad temperature range $f'(t, T)$ — the “non-reversing” component of the length change — can be expected to follow an Arrhenius dependence with temperature reflecting the viscous properties of the sample. Providing the period of the temperature modulation covers a small temperature range then — to a first approximation — $f'(t, T)$ can be assumed constant and α found from the ratio of the amplitudes of the oscillating components of the rate of length change (dL/dt) and the heating rate (dT/dt) [8]. Alternatively, equation (2) can be expressed in its integrated form whereby:

$$\Delta L = \alpha \Delta T + g'(t, T) \quad (3)$$

where ΔL and ΔT are the changes in length and temperature respectively, $g'(t, T)$ is the integral of $f'(t, T)$. This form is particularly useful for quasi-isothermal measurements (where the underlying heating rate is zero). α is determined by the ratio of the amplitude of the oscillating part of the length change $\langle A_L \rangle$ divided by the amplitude of the oscillating part of the temperature change $\langle A_T \rangle$. The same technique can be used in MTDSC by exchanging enthalpy (the integral of heat capacity) for length. A pseudo-isothermal analysis (i.e., when the underlying heating rate is non-zero) according to equation (3) is carried out in the implementation of the online deconvolution procedure by TA Instruments using a discrete Fourier transform. Offline deconvolution has the advantage that a choice of models can be used to describe the sample response. This

requires that data are collected at short time intervals for highest resolution of the phase lag and can become computationally expensive for long experiments.

Practical Considerations

No system is capable of responding instantaneously to changes in temperature. For MTTMA there will be a time difference between the temperature modulation and the response of the specimen. This term (the phase lag, δ) arises from two effects: poor heat transfer from the furnace to the specimen (as occurs in MTDSC [9,10]) and any kinetically controlled events within the sample. Furthermore, again due to poor heat transfer, the sample may not be exposed to the same variation in temperature as that recorded by the temperature sensor (although the underlying change in temperature will be the same). This leads to an underestimate of α which must be corrected by appropriate calibration [11].

Thus, a typical MTTMA experiment yields the thermal expansivity (α) and phase lag (δ) during the course of the experiment in addition to the average rate of length change ($\langle dL/dT \rangle$) calculated as a sliding average over one modulation period. The non-reversing rate of length change may be calculated by difference between α and $\langle dL/dT \rangle$. The phase lag may also be used to divide α in to in-phase (α') and out-of-phase (α'') components as for MTDSC. For conventional TMA it is usual to normalize thermal expansivity for the initial sample length (L_0). Since MTTMA determines the thermal expansivity on a continuous basis it is more useful to normalise this signal using the average length over one modulation ($\langle L \rangle$) instead of L_0 . This is a similar procedure to using the instantaneous sample mass to normalize the DSC signal from a simultaneous DSC-thermobalance. The derivatives (α , $\langle dL/dT \rangle$, etc.) may be integrated with time or temperature to determine the reversible length change, total length change and non-reversible length change. Typical examples of this are presented in references 12 and 13. If the specimen is exposed to heating and cooling as a consequence of the temperature program then a technique known as "parsing" may be employed to break down the data into heat/cool/re-heat segments in order to study the effect of thermal history of the sample response [13].

Although low thermal mass samples (such as thin films and fibers examined under tension) make ideal specimens for MTTMA, since long, thin samples can be used to improve the signal-to-noise ratio without unduly compromising heat transfer, measurements may also be made under compression for the examination of bulk polymers. Any periodic modulation of temperature may be employed, as well as non-linear underlying temperature programs although, like MTDSC, sinusoidal, square or triangular heating profiles are the simplest to implement.

Experimental

Thermomechanical measurements were carried out on a TA Instruments 2940 TMA [14]. The instrument was fitted with a modified heater assembly which served to pre-heat the purge gas before circulation through the oven. All measurements were carried out under helium (flow rate: 100 ml/min) so as to ensure good thermal coupling between the oven, thermocouple and sample. Temperature calibration according to

ASTM Test Method for Temperature Calibration of Thermomechanical Analyzers (E 1263) was carried out using gallium, indium, tin, bismuth and lead. All measurements described here were made using a circular flat-ended "macro-expansion" probe (part number: 944123-901 from TA Instruments Inc. New Castle DE) of 6.07 mm contact diameter. Additional firmware was provided by the manufacturer to enable a sinusoidal modulation of the oven temperature over a range of operating conditions. In the absence of forced cooling of the oven, it was only practical to perform measurements above ambient temperature and under conditions where the maximum rate of cooling did not exceed 1°C/min. Addition of a cooling accessory (such as a refrigerated recirculator or liquid nitrogen cooling) would extend the operational range of the instrument.

Calibration

Temperature calibration in MTTMA may be carried out by reference to the melting temperatures of pure metal standards as for conventional TMA described above. Riesen and Schawe have discussed this with particular reference to fibers [15]. An additional calibration must also be made to take into account the effect of temperature modulation in calculating the thermal expansion coefficient by MTTMA from the length change data. This is illustrated for a series of aluminum cylinders examined under quasi-isothermal conditions using a $\pm 1^\circ\text{C}$ amplitude temperature modulation at a fixed isothermal temperature of 100°C . α (normalized for the average length of the specimen at 100°C) was calculated as described above. Results for three specimens of different dimensions are shown in Figure 1 along with the theoretical value calculated from data in ASTM Test Method for Linear Thermal Expansion of Solid Materials by Thermomechanical Analysis (E 831). It can be seen that at long modulation periods the thermal expansion coefficient measured by MTTMA coincides with the literature value. As the modulation period decreases, poor heat transfer to the specimen reduces the amplitude of the temperature modulation experienced by the sample below that recorded by the temperature sensor. This causes an apparent decrease in α . As the period is reduced from 900 to 150 s, the magnitude of this effect appears to follow the order of the specimen's size, indicating that low thermal mass samples and/or long modulation periods are to be preferred in this technique.

Practical considerations, however, mean that it is not always possible to use ideal conditions — therefore a correction must be applied depending on the thermal resistance of the system. In the absence of any non-reversible changes occurring in the sample (usually at the beginning of the experiment) the average rate of change in length ($\langle dL/dT \rangle$) should equal the reversing rate of length (determined from the ratio of the amplitudes of the modulated length ($\langle A_L \rangle$) and modulated temperature ($\langle A_T \rangle$)). Thus it is possible to derive a calibration factor (K) to correct for poor heat transfer:

$$K = \frac{\langle A_L \rangle / \langle A_T \rangle}{\langle dL / dT \rangle} \quad (4)$$

Although K will be a function of the thermal diffusivity of the specimen (and the efficiency of heat transfer from the furnace to the sample), once determined, K can

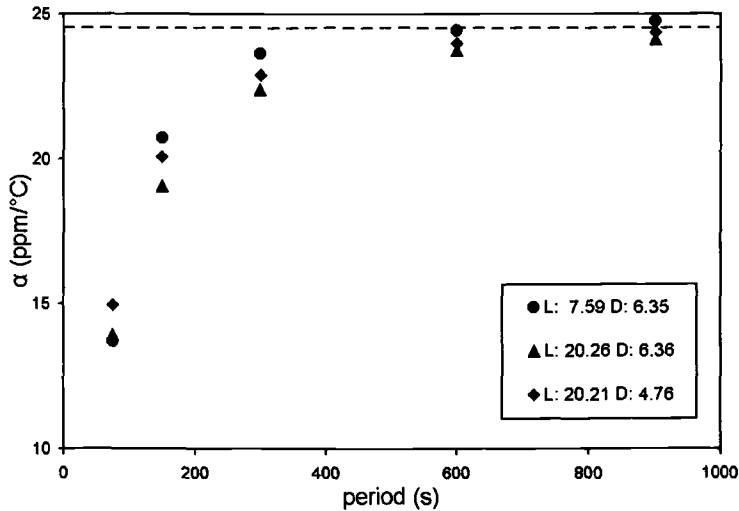


Figure 1 — Uncorrected thermal expansion coefficient (α) of different cylinders of aluminum of length (L/mm) and diameter (D/mm) indicated as a function of modulation period under quasi-isothermal conditions about a mean temperature of 100°C . Literature value indicated by a dashed line.

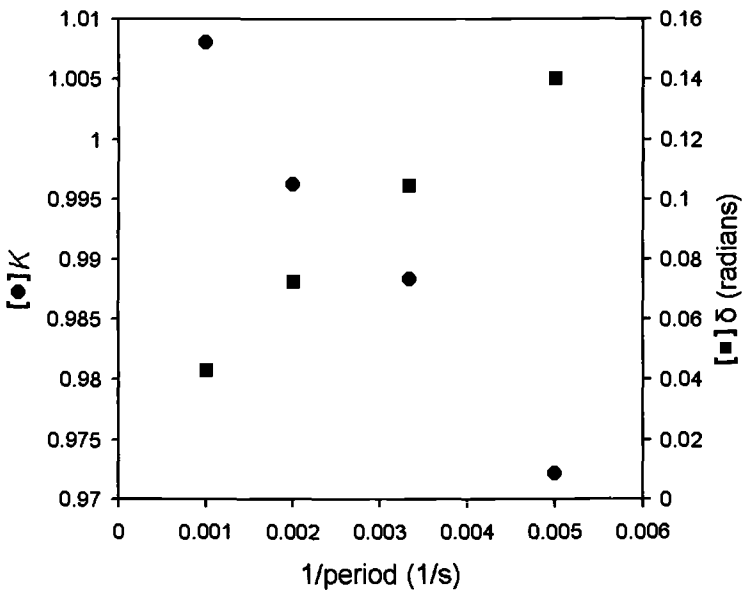


Figure 2 — Thermal expansion calibration factor (K) and initial phase lag (δ) versus the reciprocal of the modulation period for a sample of epoxy resin.

generally be assumed to be constant during the course of the experiment. The corrected value of α is then given by:

$$\alpha = \frac{\langle A_L \rangle / \langle A_T \rangle}{K \cdot \langle L \rangle} \quad (5)$$

In the absence of any irreversible length change occurring then K can be easily recalculated at any time during the experiment. If K is plotted as a function of frequency ($=1/\text{period}$) then an almost linear trend results (Figure 2). This observation suggests that use of a temperature modulation containing several frequencies (or simply scanning in frequency at a constant temperature) might afford an alternative means of calibration. Figure 2 also indicates that the phase lag also appears to be a simple function of modulation frequency. Correction of the phase lag for MTTMA is done by an analogous method to that described by Aubuchon and Gill for MTDSC [16]. Ancillary experiments demonstrate that if the amplitude of the modulation is increased (at the same period) K will decrease and that similar statements can be made concerning the dependence of the phase lag as a function of modulation conditions. Multi-frequency MTDSC experiments have been described by Reading et al. using a combination of two sinusoidal temperature modulations [17]. Recently, Androsch and Wunderlich have described the use of a triangular heating profile with a full Fourier transform to extract the heat capacity correction factor for MTDSC experiments [18]. Both approaches would appear to afford an alternative means of calibration in MTTMA.

MTTMA of the Glass Transition

Typical raw data from a MTTMA experiment on a block of cured epoxy resin (bisphenol-A-epichlorohydrin/triethylene tetramine, Struers "Epofix") are shown in Figure 3. It is possible to discern the modulation in length of the specimen brought about by the modulation in its temperature. Deconvolution of the signals into average length ($\langle L \rangle$), thermal expansion coefficient (α), $\langle dL/dT \rangle$ (ie. the derivative of the average length vs. temperature) and phase lag (δ) is shown in Figure 4. From the plot of the average length vs. temperature it is difficult to define the glass-rubber transition temperature of the material. The $\langle dL/dT \rangle$ plot does not aid interpretation either. The thermal expansion coefficient, however, clearly shows a step increase at the glass-rubber transition very much like the corresponding change in heat capacity observed for DSC. The glass transition temperature (T_g) may readily be assigned as the extrapolated onset of this process (or some other convenient point on this curve). The phase lag shows a characteristic peak similar to that seen in MTDSC during devitrification. The expansivity and phase lag curves above T_g appear to show a high temperature tail compared with the typical shapes that one would expect for a glass transition (a sigmoidal step in α and Gaussian peak in δ respectively) which might indicate that there is some other process occurring alongside devitrification.

A repeat run on the same sample was performed after allowing the instrument to cool slowly to room temperature. The data from both experiments are overlaid in Figure 5. The glass transition of the specimen has now increased by about 10°C suggesting that the initial material was incompletely cured. The distorted shapes of the plots of α and δ

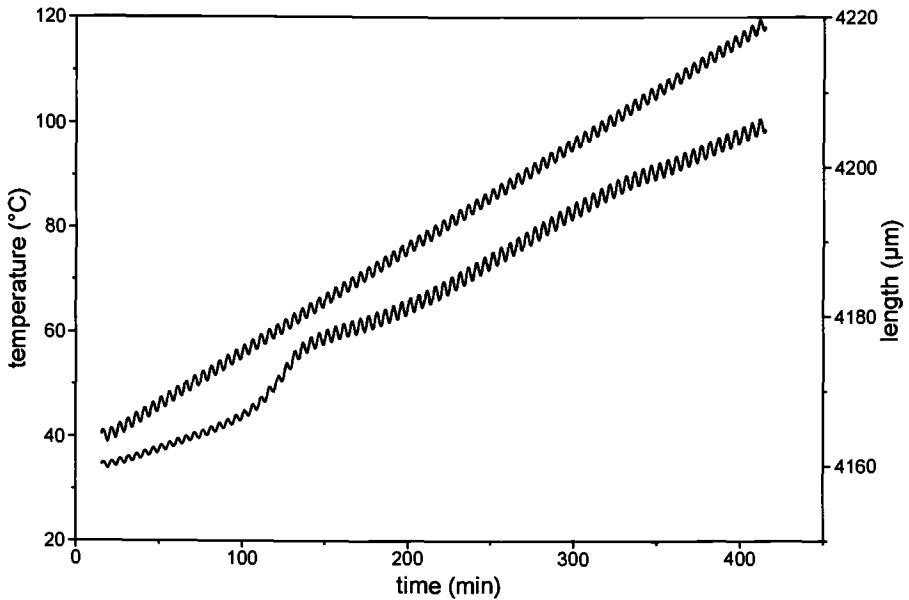


Figure 3 — Raw data for a sample of epoxy resin heated at $0.2^{\circ}\text{C}/\text{min}$ with a 1°C amplitude, 300 s temperature modulation (top: temperature, bottom: length).

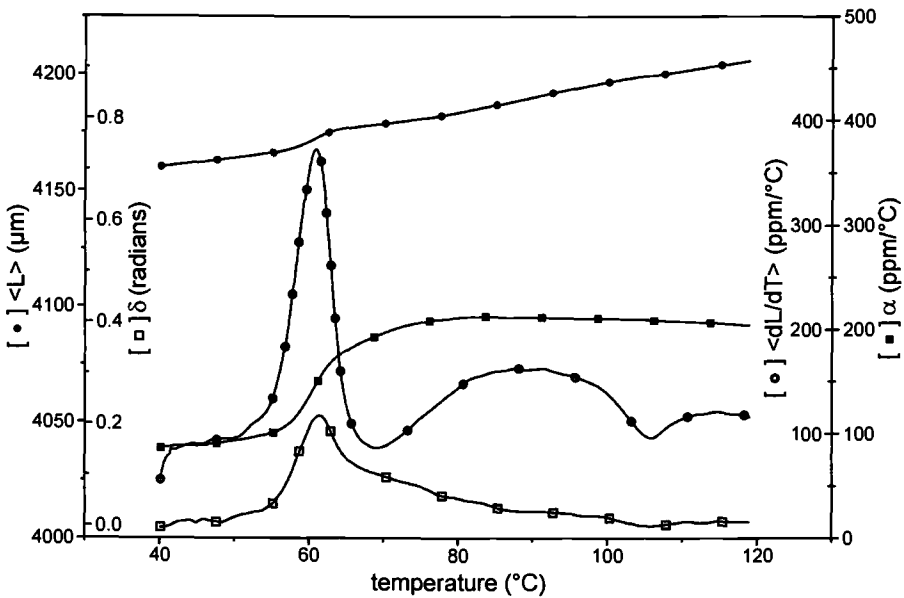


Figure 4 — Deconvoluted data from figure 3 (● : average length ($\langle L \rangle$), ■ : expansion coefficient (α), ○ : average rate of length change ($\langle dL/dT \rangle$), □ : phase lag (δ)).

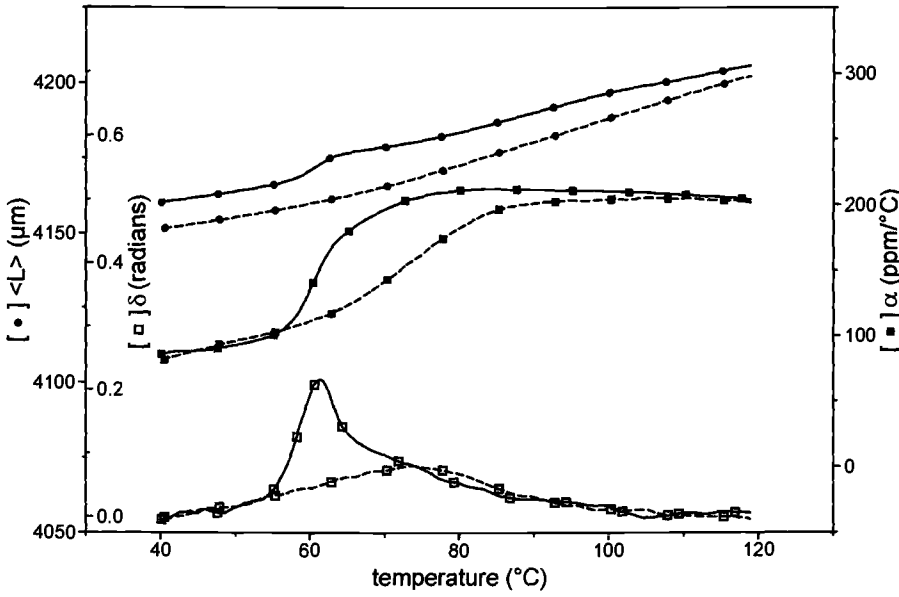


Figure 5 — Initial (solid lines) and repeat (broken lines) scans on epoxy resin (● : average length ($\langle L \rangle$), ■ : expansion coefficient (α), □ : phase lag (δ)).

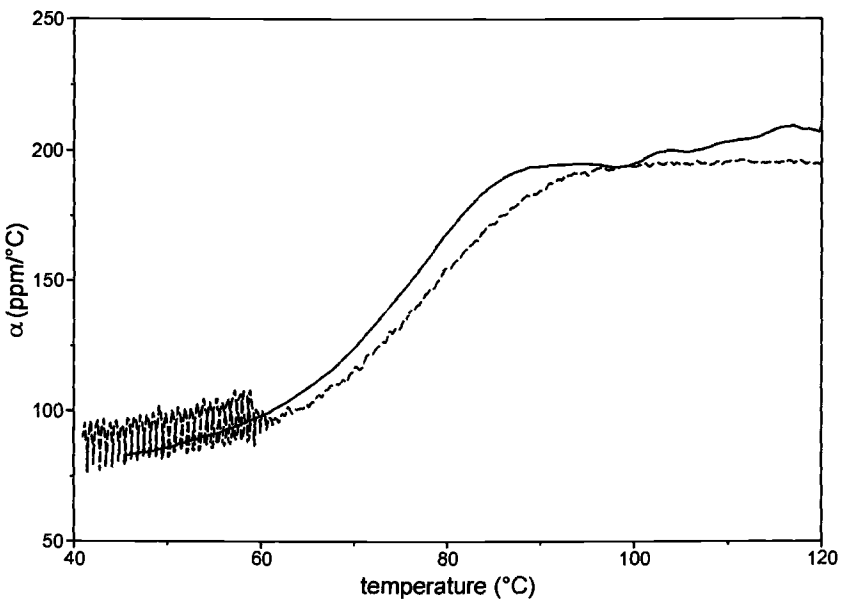


Figure 6 — Cooling scans at different modulation periods of 1000 s (solid line) and 100 s (broken line).

discussed above are presumably a consequence of further cross-linking taking place during the initial temperature scan. Further thermal cycling of the sample resulted in no change in properties.

The effect of modulation frequency on the measurement of the glass transition was investigated by performing cooling scans on the fully cured epoxy resin sample at the same underlying cooling rate but different modulation periods. Plots of thermal expansion coefficient vs. temperature for measurements at 100 s and 1000 s period are shown in Figure 6. The noise in the data obtained at 100 s period below 60°C is due to loss of proper modulation due to insufficient cooling capacity of the instrument. As would be expected by analogy with heat capacity measurements, there is a shift in the position of the T_g to higher temperatures with shorter modulation periods [19]. The apparent activation energy for the glass transition was found to be 459 ± 2 kJ/mol from an Arrhenius plot of the dependence of T_g on modulation period.

MTTMA of Melting

The reorganization of polymers as they are heated through their melting transition has been widely studied by MTDSC [20-23]. Although the melting of flexible macromolecules is an irreversible process, some of the overall melting may be reversible due to inherent annealing and crystal perfection. In order to investigate this phenomenon by MTTMA, identical experiments were conducted on a sample of poly(ethylene terephthalate) (PET) kindly supplied by ICI using the 2940 TMA and a TA Instruments 2920 MDSC operating in standard DSC mode. A temperature program consisting of twenty linear heat-cool ramps at 1°C/min over a temperature range of 5°C was applied in a step-wise isothermal fashion every 5°C. In effect this gives a triangular temperature modulation of $\pm 2.5^\circ\text{C}$ with a period of 600 s. It should be noted that such a waveform can be synthesized by a summation of a series of sine waves with a fundamental period (p) of 600 s and amplitude (A_T) 2.5°C plus odd harmonics ($p/3 = 200$ s, $p/5 = 120$ s, . . .) with decreasing amplitudes ($A_T/9$, $A_T/25$, . . .). The data from these experiments were analysed according to equation 3. For the DSC data it was necessary to integrate the heat flow with respect to time to obtain the cumulative enthalpy of the sample. By subtracting a moving average over one modulation the oscillating components of L and T are obtained (H and T for the DSC experiment). α (and C_p) are then obtained by a linear fitting procedure using the phase lag as an adjustable parameter to shift the data until the best fit is achieved [24].

Plots of α and C_p are shown in Figure 7 for both techniques. At each isotherm there is a characteristic decay in the parameter with time to reach a steady state value. The shape of the decay curves was fitted to a single exponential decay similar to that used by Schick et al. [25]:

$$y(t) = A + B \exp[-(t-t_0)/\tau] \quad (6)$$

where $y(t)$ is the value of α or C_p at time (t), t_0 is the start time of the isotherm, A and B are constants and τ is the relaxation time of the decay. It should be noted that Ozaki and Wunderlich have fitted similar C_p data to a double exponential decay and that recent work by Schick et al. use a Kohlrausch-Williams-Watts stretched exponential to describe

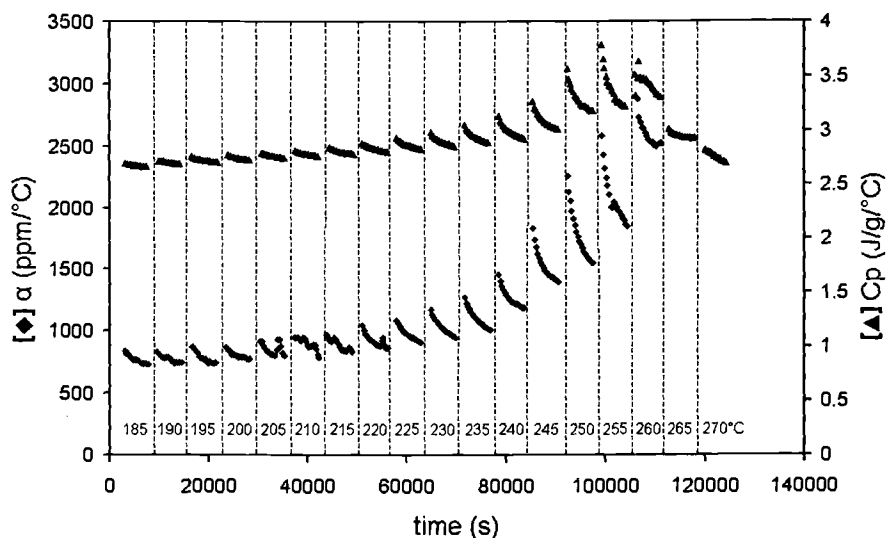


Figure 7 — Heat capacity (C_p (\blacktriangle)) and thermal expansion coefficient (α (\blacklozenge)) for PET during stepwise isothermal melting from 185 to 270°C in 5°C increments.

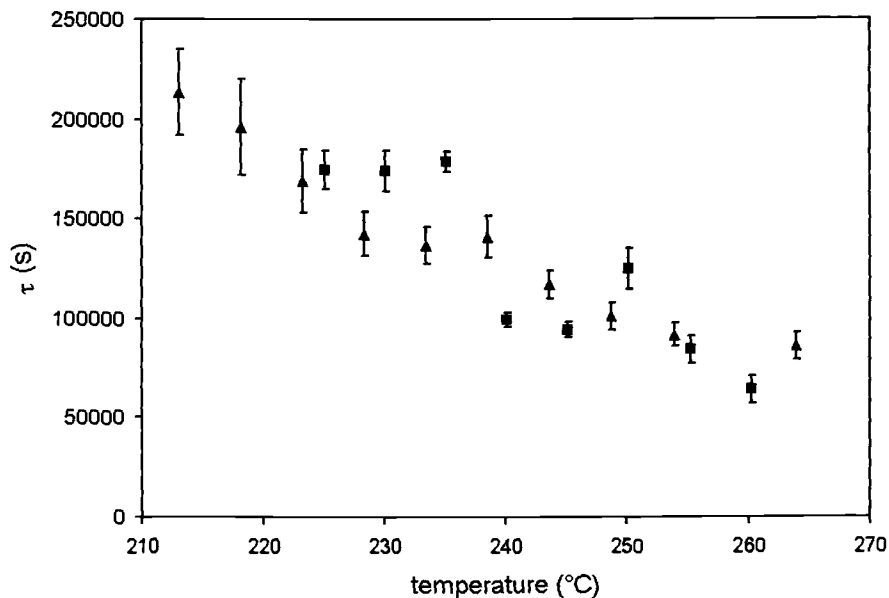


Figure 8 — Relaxation times from TMA (\blacksquare) and DSC (\blacktriangle) studies of PET melting.

the same process [20, 23]. In the present study, little improvement in fitting quality was achieved by using a more sophisticated expression. No attempt has been made to extract the frequency dependence of α and C_p through the melt although such information is contained in the raw data due to the use of a triangular waveform as discussed above.

A plot of the relaxation times to reach equilibrium is shown in Figure 8. There is reasonable agreement between both techniques given the crude nature of these measurements. Schick et al. have used modulated-temperature dynamic mechanical analysis (MTDMA) to follow reversible melting and crystallization in a number of polymers [25-28]. MTDMA would appear to be more sensitive to the final stages of these processes than MTDSC.

Conclusions

The benefits of applying a temperature modulation to the conventional linear change in temperature commonly employed in thermomechanical analysis have been illustrated by reference to the study of the glass-rubber transition of a thermosetting resin and the melting process of a semicrystalline thermoplastic polymer. Modulated-temperature TMA permits the measurement of coefficients of linear thermal expansion under quasi-isothermal conditions and allows the time dependence of relaxation phenomena to be studied. The irreversible effects of creep and stress relaxation may also be examined independently of reversible changes in dimensions that occur due to thermal expansion, thus simplifying the interpretation of such experiments.

References

- [1] Garn, L. E., and Sharp, E. J., *Journal of Applied Physics*, Vol. 53, 1982, p. 8974.
- [2] Sharp, E.J., and Garn, L. E., *Journal of Applied Physics*, Vol.53, 1982, p. 8980.
- [3] Reading, M., *Trends in Polymer Science*, Vol. 1, 1993, p. 248.
- [4] Golbrecht, H., Hammann, K, and Willers, G., *Journal of Physics E: Scientific Instruments*, Vol. 4, 1971, p. 21.
- [5] Neag, C. M., *Material Characterization by Thermomechanical Analysis*, STP 1136, A. Riga and C.M. Neag, Eds., American Society for Testing and Materials, Philadelphia, 1991 pp. 3-21.
- [6] Wetton, R.E., *Handbook of Thermal Analysis and Calorimetry. Vol. 1: Principles and Practice*, M. E. Brown, Ed., Elsevier Science B.V., Amsterdam, 1998 pp. 363-399.
- [7] Hedvig, P., *Applied Polymer Analysis and Characterization: Recent Developments in Techniques, Instrumentation, Problem Solving*, J. Mitchell Jr. (Ed.), Hanser, Munich, 1987 pp. 297-312.
- [8] Price, D. M., *Thermochimica Acta*, Vol. 315, 1998, p. 11.
- [9] Schawe, J. E. K., and Winter, W., *Thermochimica Acta*, Vol. 298, 1997, p. 9.
- [10] Cser, F., Rasoul, F., and Kosier, E., *Journal of Thermal Analysis*, Vol. 50, 1997, p. 727.
- [11] Price, D. M., US Patent 6,007,240, 28 Dec. 1999.
- [12] Price, D. M., *Journal of Thermal. Analysis*, Vol. 51, 1998, p. 231.

- [13] Price, D. M., and Foster, G. M., *Journal of Thermal Analysis and Calorimetry*, Vol. 56, 1999, p. 649.
- [14] Sauerbrunn, S. R., and Gill, P. S., *Material Characterization by Thermomechanical Analysis*, STP 1136, A. Riga and C.M. Neag, Eds., American Society for Testing and Materials, Philadelphia, 1991 pp. 120-125.
- [15] Riesen, R., and Schawe, J. E. K., *Journal of Thermal Analysis and Calorimetry*, Vol. 59, 2000, p. 337.
- [16] Aubuchon, S. R., and Gill, P.S., *Journal of Thermal Analysis*, Vol. 49, 1997, p. 1039.
- [17] Reading, M., Wilson, R., and Pollock, H. M., *Proceedings of the 23rd North American Thermal Analysis Society Conference*, Toronto (1994) pp. 2-11.
- [18] Androsch, R., and Wunderlich, B., *Thermochimica Acta*, Vol. 333, 1999, p. 27.
- [19] Birge, N. O., and Nagel, S. R., *Physical Review Letters*, Vol. 54, 1985, p. 2674.
- [20] Okazaki, I, and Wunderlich, B., *Macromolecular Rapid Communications*, Vol. 18, 1997, p. 313.
- [21] Schawe, J. E. K., and Bergmann, E., *Thermochimica Acta*, Vol. 304/305, 1997, p. 179.
- [22] Toda, A., Tomita, C., Hikosaka, M., and Saruyama, Y, *Polymer*, Vol. 39, 1998, p. 5093.
- [23] Schick, C., Merzlyakov, M., and Wunderlich, B., *Polymer Bulletin*, Vol. 40, 1998, p. 297.
- [24] Reading, M., US Patent 5,474,385, 12 Dec. 1995.
- [25] Schick, C., Merzlyakov, M., and Wurm, A., *Proceedings of the American Chemical Society Division of Polymeric Materials: Science and Engineering*, Vol. 78, 1998, p. 123.
- [26] Wurm, A., Merzlyakov, M., and Schick, C., *Colloid and Polymer Science*, Vol. 276, 1998, p. 289.
- [27] Wurm, A., Merzlyakov, M., and Schick, C., *Journal of Thermal Analysis and Calorimetry*, Vol. 56, 1999, p. 1155.
- [28] Wurm, A., Merzlyakov, M., and Schick, C., *Thermochimica Acta*, Vol. 330, 1999, p. 121.

Roger L. Blaine¹

Obtaining Kinetic Parameters Using Modulated Temperature

REFERENCE: Blaine, R. L., "Obtaining Kinetic Parameters Using Modulated Temperature," *Materials Characterization by Dynamic and Modulated Thermal Analytical Techniques*, ASTM STP 1402, A. T. Riga and L. Judovits, Eds., American Society for Testing and Materials, West Conshohocken, PA, 2001.

Abstract: Flynn and Dickens demonstrated in 1976 that continuous kinetic information may be derived from thermogravimetry profiles using a periodic temperature square wave signal. Blaine extended this approach to the sine wave. Extension of the sine wave approach to differential scanning calorimetry, however, requires consideration of the effects of the heat capacity heat flow, not present in thermogravimetry. The heat capacity term is always present and is theoretically 90° out of phase with the kinetic heat flow. Sine wave signals of the same period, however, add together to produce a sine wave of intermediate phase. To understand the effects of these mixed signals, a partial series of models is proposed for modeling pure crystalline and polymer melts on the way to a more complete understanding and measurement of kinetic parameters.

Keywords: differential scanning calorimetry, kinetics, melting, modulated temperature, thermogravimetry

Introduction

The dependent parameter generated in thermal analysis may be considered to be the summation of two terms, one of which is a function of the temperature rate of change and the other a function of temperature (and time) itself [1]. In modulated differential scanning calorimetry (MDSC®) the term proportional to temperature change is generally called the reversing term while that due to temperature is known as the nonreversing term. These reversing and nonreversing heat flows are also known as the heat capacity heat flow $((dq/dt)_C)$ and the kinetic heat flow $((dq/dt)_K)$, respectively. The total heat flow $((dq/dt)_T)$ is their sum.

$$\left(\frac{dq}{dt}\right)_T = \left(\frac{dq}{dt}\right)_C + \left(\frac{dq}{dt}\right)_K \quad (1)$$

¹ Applications manager, TA Instruments, Inc., 109 Lukens Drive, New Castle, DE 19720.

Furthermore, the reversing and nonreversing heat flow terms may themselves be the summation of a series of terms each deriving from a thermal event. Thus the heat capacity heat flow may be thought of as the sum of heat capacity, glass transition and other effects.

$$\left(\frac{dq}{dt}\right)_C = \left(\frac{dq}{dt}\right)_{Cp} + \left(\frac{dq}{dt}\right)_{Tg} + \dots \quad (2)$$

Similarly, the nonreversing heat flow is the summation of events such as melting, crystallization, reaction kinetics, etc..

$$\left(\frac{dq}{dt}\right)_K = \left(\frac{dq}{dt}\right)_{\text{melt}} + \left(\frac{dq}{dt}\right)_{\text{cryst}} + \left(\frac{dq}{dt}\right)_{\text{react}} + \dots \quad (3)$$

A few events, such as the glass transition, have both a temperature and a temperature rate of change dependence.

A similar series of equations may be developed for modulated temperature thermomechanical analysis [2, 3, 4] in which coefficient of expansion is derived from the rate of temperature change while creep and stress relaxation are functions of temperature and time.

In thermogravimetry, there is no property that is a function of the temperature rate of change $[I]$; only the weight loss term that is function of temperature and time. Thus thermogravimetry is a simplifying case for the study of modulated temperature effects.

Temperature Effects

In traditional thermal analysis, attention is usually focused on the temperature dependent term through the use of a constant heating rate (β). This approach forces the heat capacity term to be nearly constant permitting the use of linear interpolation of the "baseline" transitions such as melting.

The examination of kinetic effects, with temperature and time as independent parameters, involves the use of forcing functions. That is, a time dependent change in temperature is submitted to the test specimen and the dependent parameter is observed as a function of time. Commonly used forcing functions include the temperature step and ramp. These functions are easily achieved in thermal analysis and have been widely used for years.

In modulated temperature experiments, a more versatile forcing function is used, that of the temperature sine wave.

$$T_f = T_o + \beta t + A M \sin(2 \pi t / P) \quad (4)$$

where T_f is the furnace temperature, T_o is the initial temperature, A is the amplitude of the temperature modulation, M is a scaling factor to be explained later, t is time and P is the period. In this waveform, the temperature change rate is constantly varying providing a tool to study effects on the reversing parameter. Discrete Fourier transformation

deconvolutes the forcing functions and resultant waveforms into the reversing (heat capacity) heat flow and the nonreversing (kinetic) heat flow.

The temperature sine wave was first introduced by Reading in 1992 [5] and commercialized in 1993 by TA Instruments as modulated DSC®. The importance of the modulated temperature approach to thermal analysis is difficult to overestimate. In less than a decade, nearly half the papers presented at thermal analysis symposia deal with modulated temperature and every thermal analysis journal has devoted full volumes to the subject. No wonder that MSDC is considered to be “the greatest advance in DSC since its inception” [6].

Kinetics

Kinetics is the study of the relationship of a chemical reaction between time and temperature. Flynn first proposed the use of a periodic temperature program in thermogravimetry for the study of kinetics in 1969 [7] and Flynn and Dickens implemented their factor jump approach in 1976 [8]. In their approach, Flynn and Dickens used a temperature square wave to periodically move between two temperatures within the weight loss range. They then applied the Arrhenius and General Rate equations to the constant temperature peaks and valleys of square wave signal:

$$\begin{aligned} d\alpha_p/dt &= Z [f(\alpha_p)] \exp(-E / R T_p) \\ d\alpha_v/dt &= Z [f(\alpha_v)] \exp(-E / R T_v) \end{aligned} \quad (5)$$

where α is the reaction fraction, $d\alpha/dt$ is the rate of reaction, T is the absolute temperature, $f(\alpha)$ is the kinetic expression, Z is the pre-exponential factor, \exp is the natural logarithm base, E is the activation energy, and R is the gas constant. Casting equation 5 in its logarithmic form and solving for E yields:

$$E = R \left[\frac{T_p T_v}{T_p - T_v} \right] \left[\ln \left(\frac{d\alpha_p/dt}{d\alpha_v/dt} \right) - \ln \left(\frac{f(\alpha_p)}{f(\alpha_v)} \right) \right] \quad (6)$$

If there are sufficient steps across the transition, then there is little or no change in reaction fraction from the peak to the adjacent valley of the temperature step. In this case $f(\alpha_p) = f(\alpha_v)$, their ratio is unity, its logarithm is zero so the second logarithmic term may be ignored. Equation 6 then reduces to the form:

$$E = \frac{R T_p T_v \ln(d\alpha_p/d\alpha_v)}{T_p - T_v} \quad (7)$$

Building on its experience in MDSC, TA Instruments introduced modulate temperature thermogravimetry (MTGA™) in 1997[9]. As is the case with MDSC, real time discrete Fourier transformation is used to generate signals that may be substituted into equation 7. Specifically, the peak temperature is replaced with the Fourier transformed average temperature T and oscillation amplitude A (i.e., $T + A$), the valley temperature by $T - A$,

and $\ln(d\alpha_p/d\alpha_v)$ by L , the peak-to-peak amplitude of the oscillating $\ln(d\alpha)$ signal, producing the working equation:

$$E = \frac{R(T^2 - A^2)L}{2A} \quad (8)$$

There are several advantages of MTGA determination of kinetic parameters (and its factor jump antecedent). Since equation 8 contains no kinetic expression, it is "model free" with regard to activation energy, the most commercially important of the kinetic parameters. In "model free" kinetics, no knowledge of the form of the kinetic expression is required to answer this question. In order to obtain the pre-exponential factor, however, some reaction order model does need to be selected. The order is 1 for most decomposition and volatilization reactions of commercial interest. For many cases, then, a first order reaction model describes weight loss. With the selection of a model, the pre-exponential factor may also be calculated.

$$\ln(Z) = \ln[d\alpha / (1 - \alpha)] + E / R T \quad (9)$$

The second advantage is that as activation energy is generated as a real time signal, it may be plotted as a function of weight loss (conversion) directly without further data treatment. Such a data presentation aids the user in the interpretation of results. A constant value for E as a function of conversion indicates a simple decomposition.

The third advantage is the ability to use the calculated parameter for automatic control of the experiment. In dynamic rate (Hi-Res®) TGA the heating rate of the experiment is controlled by the rate of weight loss in a smooth, continuous fashion. The greater the weight loss, the slower (but not zero) the heating rate becomes. When the oscillatory temperature of MTGA is deconvoluted real time, the average rate of weight loss may be used in conjunction with the dynamic rate feature so that the heating rate is slowed in regions of interest. This reduces the overall experimental time.

In an attempt to further use these advantages, interest turns to MDSC. Here study of kinetics is more complicated because of the addition of a temperature rate of change term. In principle, the sinusoidally varying temperature function and the temperature rate of change function are out of phase with each other by 90°. By convention, the temperature rate of change parameter is taken to be in-phase, which causes the temperature signal to *lead* the temperature rate of change signal. Trigonometry tells us that the summation of two (or more) sinusoidally varying signals of the same phase is also a sinusoidally varying signal with a phase intermediate between the two signals. Thus a phase shift results when both a heat capacity heat flow and a kinetic heat flow are present. The presence of the phase shift, which in itself may be a function of experimental parameters, complicates the concept of deriving kinetic information from modulated temperature DSC.

In order to understand modulated DSC thermal curves in sufficient detail to extract kinetic information, we are building models that describe the heat flow signal. This work reports our initial activities dealing with the melt of pure crystalline materials and rapidly crystallizing polymers.

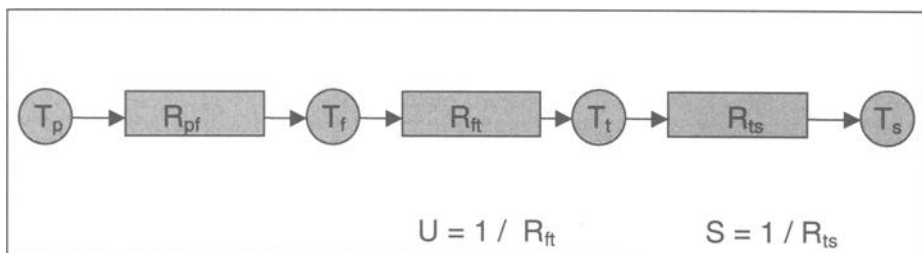


Figure 1 - *Thermal Resistor Model*

An individual kinetic expression (for whatever transition) may be thought of as the product of terms that are a function of the reaction fraction (i.e., $f(\alpha)$), temperature (i.e., $f(T)$) and time (i.e., $f(t)$). A suitable model for a transition requires understanding of each of these functions.

$$\left(\frac{dq}{dt} \right)_i = f(\alpha) f(T) f(t) \quad (10)$$

The study of the indium melt is a simple place to start since (during the melt of a pure crystalline material) the temperature of the sample becomes invariant. That is, during the melt of a pure crystalline material, there will be no contribution from the temperature rate of change dependent term in equation 1.

The response of the differential scanning calorimeter may be described by analogy to Ohm's law [10] known as the Newton equation. Figure 1 shows a thermal resistor network with the programmer (T_p) and furnace temperature (T_f) at one end, the actual sample temperature (T_s) at the other end and the indicated sensor temperature (T_t) in between. The thermal conductance (reciprocal of resistance) between T_f and T_t and T_t and T_s may be represented by terms U and S , respectively. In linear heating rate experiments, the resistance between T_t and T_s is small and is treated by temperature calibration. In some experiments, however, the value for S must be determined and used to obtain the precise sample temperature information. Such experiments include the temperature corrections used in the ASTM Method for Calorimetric Purity (E 628) and the Ozawa variable heating rate kinetic method of ASTM Method for Arrhenius Kinetic Parameters (E 698). The value for S is determined from the leading edge slope of an indium melt plotting heat flow on the Y-axis and sensor temperature on the X-axis as is shown in Figure 2. S is a negative number with units of $mW/^\circ C$.

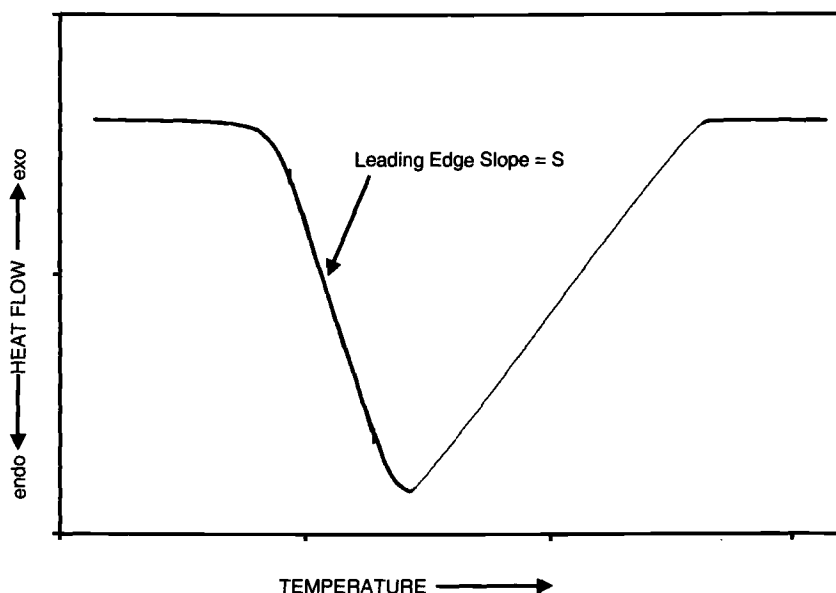


Figure 2 - Measurement of S

The value of U is obtained from a plot of sensor temperature as a function of time for the same indium melt as shown in Figure 3. The baseline before and after the transition is equal to β . During the melt, however, the sample temperature (T_s) becomes invariant leading to a change in slope of the T_t . U is derived from the ratio of the slopes of these two lines.

$$U = \Delta T_t / \Delta T_f \quad (11)$$

In MDSC, the feedback control algorithm operates not on the furnace temperature but on the sensor temperature so as to keep the oscillation temperature amplitude of the sensor (T_t) constant. This is accomplished by increasing the amplitude of the sine wave temperature at the furnace in the transition region where the sample temperature is constrained by the phase rule. This is accomplished through the value of M in equation 4. M has a value of $1/U$ in the region of the melt and a value of 1 outside the melt region. This may be modeled by the following equation:

$$M = 1 + ((1 - U) / U) [T_t > T_m] [\alpha < 1] \quad (12)$$

where T_m is the melting temperature and α is the fraction melted. The brackets indicate a logical expression that is 1 if the condition between the brackets is true and a value of 0 if the expression is false.

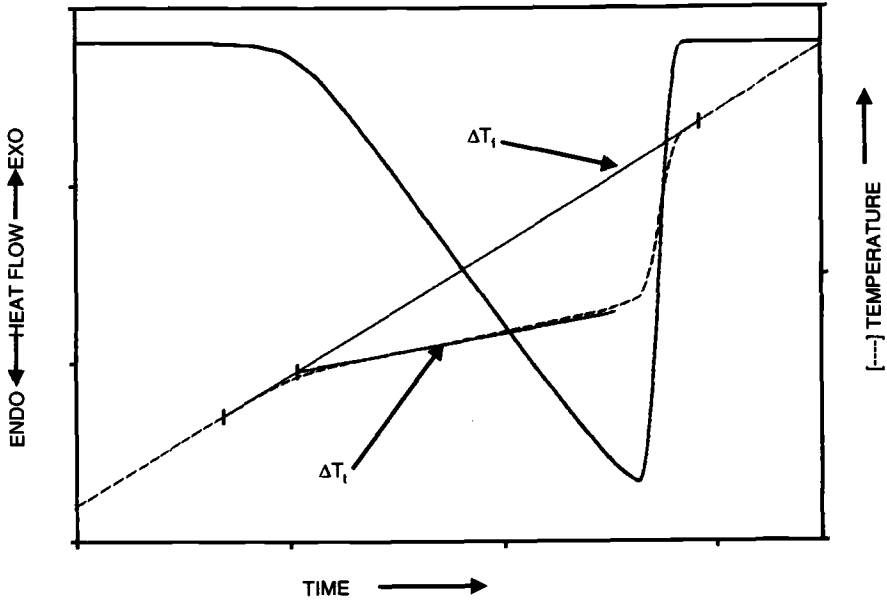


Figure 3 - Determination of U

Indium Melt

The heat flow profile for the melt of a pure crystalline material such as indium may be described as a zeroth order reaction [11]. In a zeroth order reaction, the reaction goes to completion at a constant rate without regard to the concentration or amount of the reactants (i.e., $f(\alpha) = (1 - \alpha)^0$):

$$\left(\frac{dq}{dt}\right)_{\text{melt}} = (1 - \alpha)^0 S (T_t - T_m) \text{ for } T_t > T_m \quad (13)$$

The zeroth order reaction term has a value of 1 for all case where α is less than 1; that is where the sample is incompletely melted. When $\alpha = 1$, the sample is completely melted and the $(1 - \alpha)^0$ goes to zero. In the modeling of the melt region, this may be addressed by the logical expression $[\alpha < 1]$. Thus equation 13 may be re-written in the form of:

$$\left(\frac{dq}{dt}\right)_{\text{melt}} = S (T_t - T_m) [T_t > T_m] [\alpha < 1] \quad (14)$$

In terms of the furnace temperature, equation 14 becomes:

$$\left(\frac{dq}{dt} \right)_{\text{melt}} = S U (T_f - T_m) [T_f > T_m] [\alpha < 1] \quad (15)$$

The fraction melted, α , is obtained by integrating the melting heat flow equation 13 as a function of time and comparing the results with the theoretical heat of fusion (H) for indium of 28.4 J/g taken from ASTM Method for DSC Heat Calibration (E 968) and the mass of the specific indium sample (G).

$$\alpha = \frac{1}{GH} \int \left(\frac{dq}{dt} \right)_{\text{melt}} dt \quad (16)$$

Substituting equation 15 into equation 16 and integrating using Simpson's rule and small time intervals Δt :

$$\alpha = \frac{S U \Delta t}{GH} \sum (T_f - T_m) [T_f > T_m] \quad (17)$$

Outside of the melting region, the thermal curve for indium is governed only by the specific heat capacity contribution. That is, since the indium temperature at the melt is fixed, there is no contribution in the model for heat capacity during the melting period.

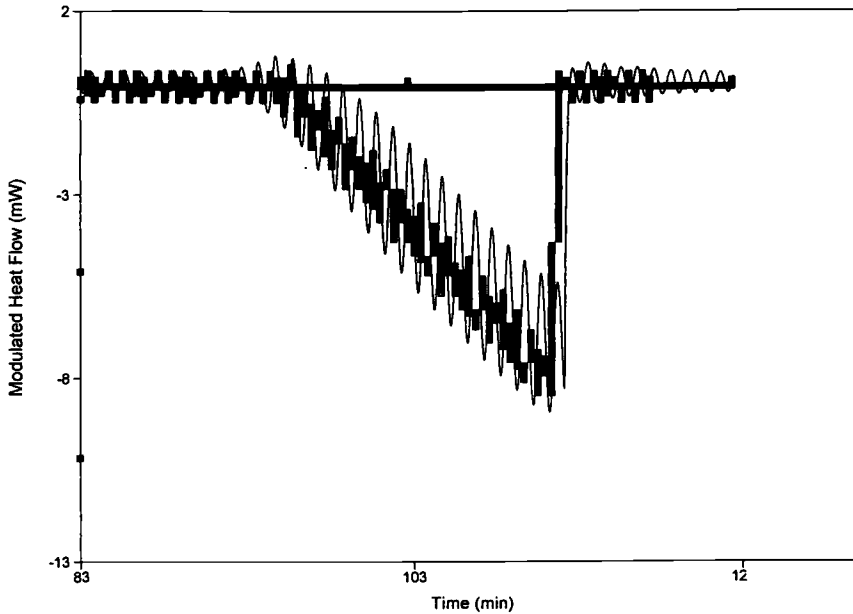


Figure 4 - Indium Melt

The value for C_p for indium changes very slowly in the temperature region near the melt and may be approximated by a single value of $0.25 \text{ J g}^{-1} \text{ }^\circ\text{C}^{-1}$ [12].

$$\left(\frac{dq}{dt}\right)_C = G C_p \left(\frac{dT_f}{dt}\right) \quad (18)$$

Using equations 4, 15, and 17 to describe the melt region and equations 4 and 18 to represent the region outside of the melt, the thermal curve for indium may be completely described.

A TI-83 Plus (Texas Instruments, Dallas, TX) programmable graphic calculator was used to profile these four equations. The heat flow curve is displayed on the Y-axis as a function of programmer temperature (or time) on the X-axis or as a function of the thermocouple temperature. These profiles may be compared with the actual thermal curves for an indium sample. To test the model, a very large ($G = 145 \text{ mg}$) indium sample was used at a very low heating rate ($\beta = 0.05 \text{ }^\circ\text{C/min}$) to ensure that a series of cycles was obtained. A heat/cool temperature oscillation amplitude ($A = 0.08 \text{ }^\circ\text{C}$) was used along with a commonly used period ($P = 1 \text{ min}$). The resultant synthetic and actual thermal curves are shown in Figure 4. The heavy line represents the TA-83 generated curve and the thin line the actual experimental results.

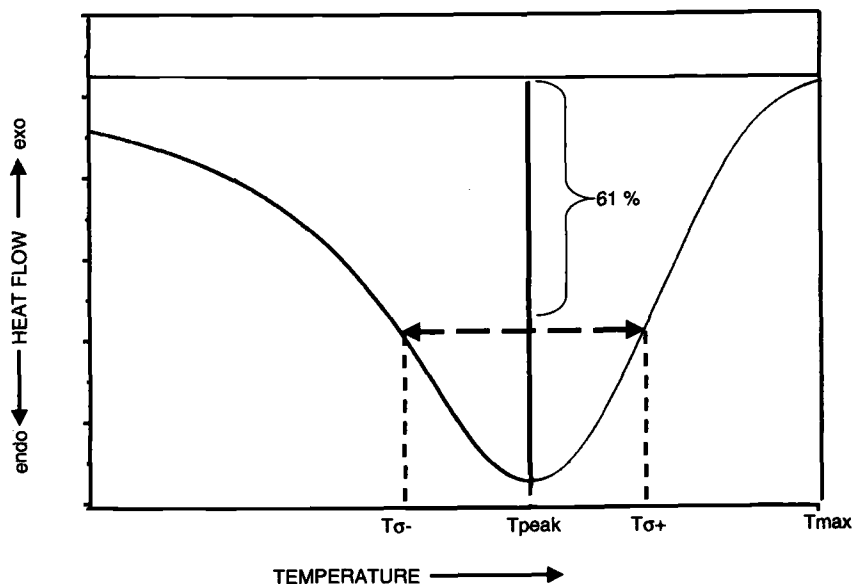


Figure 5 - Determination of Flory Equation Parameters

The overall shape of the synthetic profile is good, differing only in the comparative amplitude. The heat flow amplitude for the actual thermal curve is larger than that predicted by the simple model. Nonetheless, this simple model is surprisingly good.

Polymer Melt

The melting profile for a polymer is much different from the melting profile for a pure organic or inorganic material. It is reasonable, therefore, to anticipate that the model for a polymer melt will have a different basis than that for indium. This difference in shape is universally attributed to the molecular weight distribution observed in a polymer sample.

In polymer melting, the heat flow profile for a polymer at any given temperature corresponds to the number of molecules in the polymer sample with a given melting temperature. Some workers have used a gaussian distribution to describe polymer MDSC melting behavior [13]. The equation for a gaussian distribution is of the form:

$$Y = J \exp \{ -0.5 (X - b)^2 / \sigma^2 \} \quad (19)$$

where Y is the number of molecules at a given molecular weight, J is the number of molecules of the most probable molecular weight (i.e., at the peak of the curve), X is the molecular weight, b is the most probable molecular weight and σ is the standard deviation of the distribution. On a theoretical basis as well as a practical one [14], the

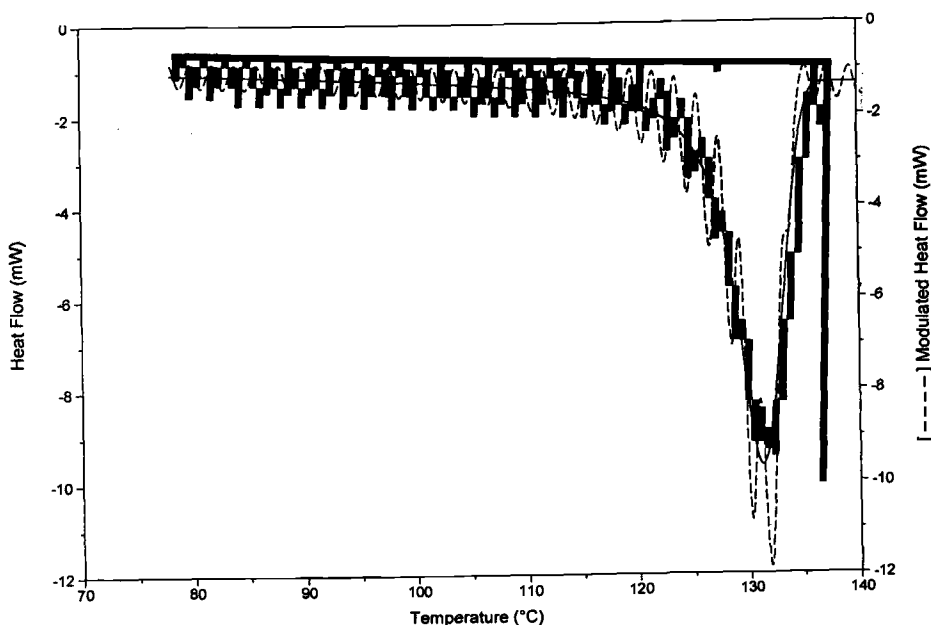


Figure 6 - Polyethylene Melt

molecular weight distribution for a polymer is logarithmic function of molecular weight rather than a linear one. Casting equation 19 in the form of the heat flow equation logarithmically related to molecular weight:

$$\left(\frac{dq}{dt}\right)_{\text{melt}} = J \exp \{-0.5 (\log DP - \log DP_{\text{peak}})^2 / \sigma^2\} \quad (20)$$

where molecular weight is expressed in terms of the degree of polymerization (DP), J is the heat flow at the peak maximum, and DP_{max} is the most probable degree of polymerization. The degree of polymerization corresponds to the (dimensionless) number of repeat units and is related to the molecular weight by the repeat unit molecular weight. For polyethylene, the molecular weight of the repeat unit is 14.0 g/mol of repeat units.

The relationship between degree of polymerization and the melting temperature of the crystals of a particular molecular weight is given by the Flory equation [14]:

$$DP = 2 R T T_{\text{max}} / H_{\infty} (T_{\text{max}} - T) \quad (21)$$

where T_{max} is the absolute melting temperature of the largest molecular weight fraction, H_∞ is the heat of fusion of 100 % crystalline polymer and R is the gas constant (= 8.314 J mol⁻¹ K⁻¹). The value for H_∞ for polyethylene is taken from the literature to be 290 J/g [15 - 20].

The values for J, T_{max} and σ may be evaluated from the thermal curve for the polymer. For example, Figure 5 shows the melting endotherm for polyethylene, in this case NIST Polyethylene SRM1475A. The value for J is the heat flow at the melting peak, here 8 mW. T_{max} is the temperature at the return to baseline after the complete melting of the sample, here 410 K (136.85 °C). The value for DP_{max} is obtained by substituting the melt endothermic peak temperature into equation 21. Similarly, the value for σ corresponds to the logarithm of the degree of polymerization corresponding to half-gaussian peak width at 61% of the peak height. The temperature values corresponding to these values are submitted to equation 21 to obtain the degree of polymerization at the upper and lower 1 σ positions (DPσ⁺ and DPσ⁻, respectively). The logarithmic values for these DP values are then compared to obtain the molecular weight distribution σ is estimated to be by σ = (log DPσ⁺ - Log DPσ⁻) / 2. For this polyethylene sample T_{max} = 131.2 °C, DP_{max} = 178, and σ = 0.20.

For polyethylene, specific heat capacity changes by 30% over the temperature 60 °C range of interest [21]. This change may be approximated by a linear equation derived from the specific heat capacity literature data:

$$C_p = \{1.800 + 0.013 (T - 350 \text{ K})\} \text{ J g}^{-1} \text{ K}^{-1} \quad (22)$$

Unlike the case with indium, where the sample temperature becomes invariant during the melt, heat capacity contributes to the heat flow throughout the polymer melt region. Equations 4, 20, 21 and 22 may be used to model the melting profile for polyethylene using the TI-83 Plus calculator. The resultant simulated thermal curve is plotted in Figure 6 in the heavy solid lines compared to the actual data in the lighter solid

lines. In this case heat only experimental conditions were used ($\beta = 2\text{ }^{\circ}\text{C/min}$, $A = 0.32\text{ }^{\circ}\text{C}$, $P = 1\text{ min}$) for an 8.41 mg sample size.

As was the case with the indium melt, the synthetic and actual thermal curves are qualitatively similar. The actual thermal curve has a higher heat flow oscillation amplitude than that predicted by the model. The source of this discrepancy is not known at this time.

Future Work

Work is underway to extend these models to a thermoset resin cure, an exothermic, kinetically controlled reaction with concurrent heat capacity effects. It is anticipated that this will be followed by high-energy reactions with their accompanying adiabatic temperature rise. And finally, we will turn our attention to the case of slowly crystallizing polymers, such as polyethylene terephthalate, which includes both cold crystallization and crystal perfection.

Summary

Preliminary models are proposed for the pure crystalline indium melt and rapidly crystallizing polyethylene crystalline melt under conditions of modulated temperature. The proposed models show good agreement between theoretical and actual thermal curves.

References

- [1] Gray, A. P., "A Simple Generalized Theory for the Analysis of Dynamic Thermal Measurement", *Analytical Calorimetry*, Vol. 1, R. S. Porter and J. F. Johnson (Eds.), Plenum Press, New York, 1968, pp. 209 - 219.
- [2] Price, D. M., "Modulated-Temperature Thermomechanical Analysis", *Journal of Thermal Analysis*, 1998, pp. 231 - 236.
- [3] Price, D. M., "Modulated-Temperature Thermomechanical Analysis", *Proceedings of the 26th North American Thermal Analysis Society*, K. Williams (Ed.), 1998, pp. 27 - 32.
- [4] Price, D. M., "Method and Apparatus for Modulated-Temperature Thermomechanical Analysis", U.S. Patent 6,007,240, 28 Dec. 1999.
- [5] Reading, M., Elliott, D., and Hill, V., "Some Aspects of the Theory and Practice of Modulated Differential Scanning Calorimetry", *Proceedings of the 21st North American Thermal Analysis Society*, W. Sichina (Ed.), 1992, p. 145.
- [6] Wunderlich, B., Jin, Y. and Bollar, A., "Mathematical Description of Differential Scanning Calorimetry Based on Periodic Temperature Modulation", *Thermochimica Acta*, 1994, 238, pp 277 - 293.

- [7] Flynn, J. H., "The Historical Development of Applied Nonisothermal Kinetics", *Thermal Analysis*, Vol. 2, R.F. Schwenker, Jr., and P.D. Garn (Eds.), Academic Press, New York, 1969, pp. 1111-1126.
- [8] Flynn, J. H., and Dickens, B., "Steady-State Parameter-Jump Methods and Relaxation Methods in Thermogravimetry", *Thermochimica Acta*, 1976, 15, pp. 1 - 16.
- [9] Blaine, R. L., "Modulated Thermogravimetry - A New Approach for Obtaining Kinetic Constants", *Proceedings of the 25th North American Thermal Analysis Society*, R. Morgan (Ed.), 1997, pp 485-492.
- [10] Baxter, R. A., "A Scanning Microcalorimetry Cell Based on a Thermoelectric Disc - Theory and Applications", *Thermal Analysis*, R. F. Schwenker, Jr., and P. D. Garn (Eds.), Academic Press, 1965, pp. 65 - 84.
- [11] Brennen, W. P., Miller, B. and Whitwell, J. C., "Thermal Resistance Factors in Differential Scanning Calorimetry", *Analytical Calorimetry*, Vol. 2, R. S. Porter and J. F. Johnson (Eds.), Plenum Press, New York, 1970, pp. 441 - 453.
- [12] *American Institute of Physics Handbook*, 3rd edition, D.E. Gray (Ed.), McGraw Hill, New York, 1972, pp 4-106 to 4-108.
- [13] Toda, A., Arita, T., Tomita, C., Hikosaka, M., "Computer Simulation of the Melting Kinetics of Polymer Crystals Under Condition of Modulated Temperature", *Thermochimica Acta*, 1999, 330, pp. 75 - 83.
- [14] Flory, P. J., "Thermodynamics of Crystallization in High Polymers. IV. A Theory of Crystalline States and Fusion in Polymers, Copolymers and Their Mixtures with Diluents", *Journal of Chemical Physics*, 1949, 17, pp. 223 - 240.
- [15] Dole, M., Hettinger, Jr., W. P., Larson, N. R., Wethington, Jr., J.A., "Specific Heat of Synthetic High Polymers. I. A Study of Polyethylene Including a Statistical Theory of Crystallite Length", *Journal of Chemical Physics*, 1952, 20, p. 781 - 790.
- [16] Wunderlich, B., Dole, M., "Specific Heat of Synthetic High Polymers. VIII. Low Pressure Polyethylene", *Journal of Polymer Science*, 1957, 24, pp. 201 - 213.
- [17] Quinn, Jr., F., L. Mandelkern, L., "Thermodynamics of Crystallization in High Polymers, Poly-(ethylene)", *Journal of the American Chemical Society*, 1958, 80, pp. 3178 - 3182.
- [18] Wunderlich, B., Cormier, C. M., "Heat of Fusion of Polyethylene", *Journal of Polymer Science, Part A*, 1967, 2, pp. 987 - 988.

[19] Atkinson, C. M. L., Richardson, M. J., "Thermodynamic Properties of Ideally Crystalline Polyethylene", *Transactions of the Faraday Society*, 1969, 65, pp. 1764 - 1773.

[20] Richardson, M. J., "Precision Differential Calorimetry and the Heat of Fusion of Polyethylene", *Journal of Polymer Science, Part C*, 1972, 38. pp. 251 - 259.

[21] Gaur, G., Wunderlich, B., "Heat Capacity and Other Thermodynamic Properties of Linear Macromolecules. II. Polyethylene", *Journal of Physical Chemistry Reference Data*, 1981, 10, pp. 119 - 152.

DYNAMIC TECHNIQUES—A

John H. Suwardie¹

Analysis of Curing Using Simultaneous Dynamic Mechanical and Dielectric Measurements

REFERENCE: Suwardie, J. H., “Analysis of Curing Using Simultaneous Dynamic Mechanical and Dielectric Measurements,” *Materials Characterization by Dynamic and Modulated Thermal Analytical Techniques*, ASTM STP 1402, A. T. Riga and L. Judovits, Eds., American Society for Testing and Materials, West Conshohocken, PA, 2001.

Abstract: Previously, curing reaction of a thermosetting system, with one of the components being a volatile material, was studied using Simultaneous Thermal Analyzer (STA). The actual heat of curing can be determined by subtracting the heat of volatilization from the heat of the curing process.

A new study of a similar thermosetting system using simultaneous dynamic mechanical and dielectric measurements will compare the onset and completion of the curing reaction between the two measurements. In addition, the new study will also compare between rheological properties such as dynamic loss modulus, G'' , and dynamic viscosity, ETA^* , and dielectric property such as dynamic loss parameter, ϵ'' .

Keywords: curing, thermosetting, rheological, dielectrical

Introduction

Dielectric analysis (DEA) is a material characterization technique that provides scientists with quantitative thermal, rheological and dielectrical information on a wide range of materials in their various forms: solids, liquids, pastes and films.

DEA can determine flow, degree and rate of cure, thermal transition and dielectric properties of thermoplastics, elastomers, composites, adhesives and coatings. It can also be used to characterize food products such as milk or chocolate [1] and pharmaceutical products [2].

¹ Rheometric Scientific, Inc. One Possumtown Road, Piscataway, NJ 08854, USA

As a thermal analysis (TA) tool, the DEA most closely relates to dynamic mechanical analysis (DMA) which measures mechanical properties, and differential scanning calorimeter (DSC), which measures heat and temperature transitions.

For the curing study, as presented on this paper, the DEA is more sensitive than DSC for analyzing the last stages of cure; its ability to evaluate liquids is an advantage over DMA. Combined with rheological analysis, the DEA is particularly effective to identify rheological changes during the curing, such as time and temperature that correspond to minimum viscosity, onset of cure, maximum rate of reaction and completion of cure [1].

The principle of DEA may be illustrated by the time-dependent electrical response of a sample placed between a pair of coplanar electrodes when sinusoidal voltage polarizes the sample, causing an oscillation of the molecules at the applied frequency but with a phase angle shift (θ). The measured induced current can be separated into two components, capacitance (C in farads) and conductance ($1/R$ in mhos) with the following relationships:

$$C = \frac{I_{\text{measured}}}{V_{\text{applied}}} \times \frac{\sin \theta}{2\pi f} \quad (1)$$

$$\frac{1}{R} = \frac{I_{\text{measured}}}{V_{\text{applied}}} \times \cos \theta \quad (2)$$

where V_{applied} is the applied voltage, I_{measured} is the measured current, f is the applied frequency in Hz, and R is the resistance in ohms.[2].

Frequency dependent measurements of the sensors impedance as characterized by its equivalent capacitance, C , and conductance, G , are used to calculate the complex permittivity, $\epsilon^* = \epsilon' - i\epsilon''$, where $\omega = 2\pi f$. f is the measurement frequency and C_0 is the air replaceable capacitance of the sensor.

$$\epsilon'(\omega) = \frac{C(\omega)_{\text{material}}}{C_0} \quad (3)$$

$$\epsilon''(\omega) = \frac{G(\omega)_{\text{material}}}{\omega C_0} \quad (4)$$

This calculation is possible when using a sensor whose geometry is invariant over all measurement conditions.

Both real and the imaginary parts of ϵ^* can have an ionic and dipolar component.

$$\epsilon' = \epsilon'_d + \epsilon'_i \quad (5)$$

$$\epsilon'' = \epsilon''_d + \epsilon''_i \quad (6)$$

The dipolar component ϵ_d arises from rotational diffusion of molecular dipole moments or bound charge [3].

The viscosity is frequently utilized as a measure of the extent of reaction since it can be directly related to those processing parameters. It is difficult to directly measure the viscosity of polymer parts during production but the viscosity may be estimated indirectly by monitoring the electrical properties of the material.

This is done on a general basis by comparing a known viscosity profile to the dissipation curve. The minimum in the dissipation curve usually correlates to a minimum viscosity, while the peak in the dissipation curve is associated with the gel point of the material. The kinetic modeling of the dielectric data is based on the six-parameter viscosity model, which has been converted to apply to the dielectric relaxation time [4].

Experimental

The epoxy system used in the experiment is Araldite F (diglycidyl ether of bisphenol A) cured with hardener HY905 (phthalic anhydride) and accelerator DY062 (tertiary amine) supplied by Ciba Specialty Chemicals (UK), Ltd. The ratio used for the curing is 60% Araldite F, 40% HY905 and 2% of the total resin for DY062. Previous study of the system in Simultaneous Thermal Analysis indicated that accelerator DY062 could prevent the devolatilization of the hardener during the curing [5].

The rheological and dielectric measurements are performed using Rheometric Scientific Advanced Rheometric Expansion Systems (ARES) coupled with HP4254A LCR meter. LCR meter is an instrument to measure inductance (L), capacitance (C) and resistance (R). The ARES is configured with a Force Convection Oven environmental system and dual transducers with range from 0.2 g.cm to 2000 g.cm torque. The 25mm upper and lower plate of the ARES is connected with electrode wires to the LCR-meter. The range of frequencies was from 20 Hz to 1.0 MHz.

The curing study at low frequencies is conducted with Multiwave Temperature Ramp Test. The temperature is increased from 25 °C to 100 °C at a 5°C/min ramp rate and kept at 100 °C for 30 minutes. The strain of 10% is maintained throughout the test. The sample is subjected to cyclic frequency sweep at frequencies of 0.25 Hz, 1 Hz, 5 Hz and 15 Hz.

The curing study at high frequencies is performed with Dynamic temperature Ramp Test. The frequencies of 20 Hz, 100 Hz, 1 KHz, 10 KHz, 100 KHz and 1 MHz are selected for the dielectric study. The capacitance (C) and Dissipation Factor (D) are continuously monitored during the experiment.

Results and Discussion

Figure 1 shows the complex viscosity, η^* , obtained from Multiwave Temperature Ramp for frequencies 0.25 Hz, 1 Hz, 5 Hz and 10 Hz. It displays the minimum viscosity of 0.44 Pa.s at 750 s followed by the increasing viscosity to mark the progress of the

curing reaction. The viscosity starts to level off after 1300 s and each frequency depicts the different value of maximum viscosity. The curing reaction at frequency 0.25 Hz shows the highest viscosity and frequency of 10 Hz as being the lowest.

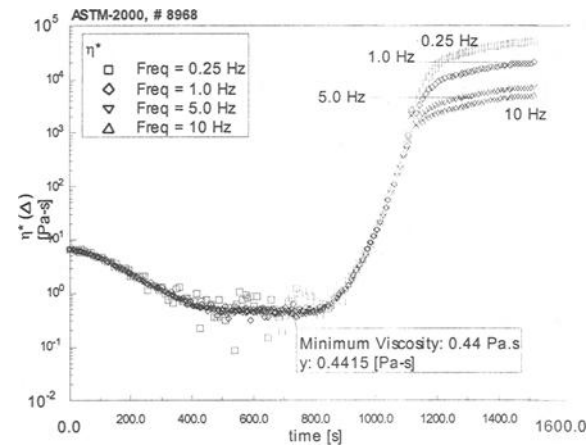


Figure 1: η^* , Low Frequencies

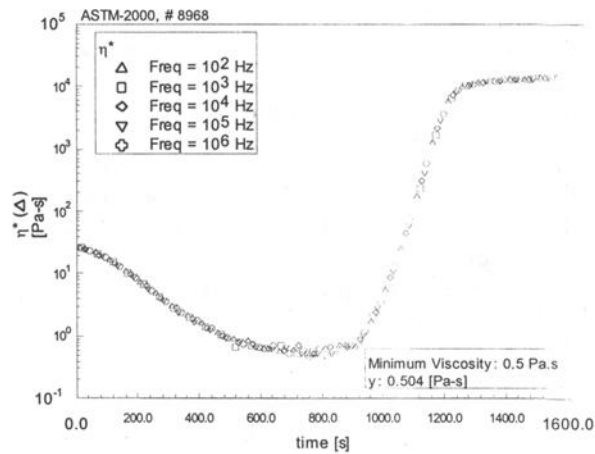


Figure 2: η^* , High Frequencies

Figure 2 displays the complex viscosity obtained at the higher frequencies associated with dielectric measurement. Six different frequencies from 100 Hz to 1 MHz are applied. It shows the minimum viscosity of 0.5 Pa.s at 760 s, similar with the one obtained at the lower frequencies. There is no difference in the maximum viscosity for all frequencies indicating the frequency independence at high frequencies.

Figure 3 depicts the damping function, $\tan \delta$ obtained from the Multiwave Temperature Ramp. In the curing study, the gel time can be defined by two different methods. The first method is defined as the G'/G'' cross over. The storage or elastic modulus, G' , is more dominant than loss or viscous modulus after the G'/G'' cross over. The second method determines the gel time as the time $\tan \delta$ at various frequencies cross each other [6]. The gel time calculated with this method is 1336 s.

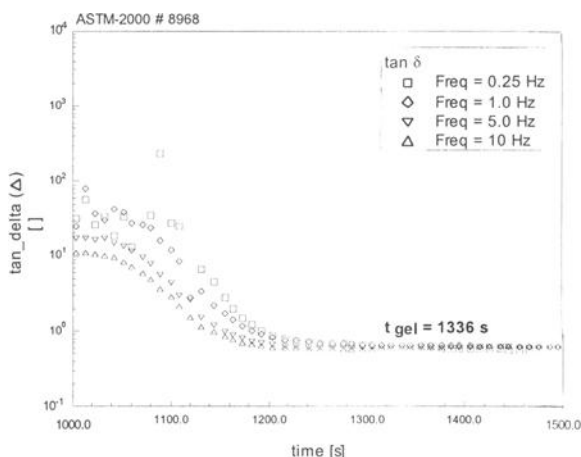


Figure 3: $\tan \delta$, Low Frequencies

Figure 4 displays the $\tan \delta$ obtained at higher frequencies. It does not show any differences at all frequencies. However, there are differences among the gel time determined using G'/G'' cross over as listed in Table 1. The second method is more preferred than the first one that shows the insensitivity of $\tan \delta$ at higher frequencies.

The insensitivity of η^* and $\tan \delta$ at higher frequencies as shown in Figure 2 and Figure 4 indicate that these properties are more suitably evaluated at lower frequencies. At higher frequencies, the evaluation of permittivity, as shown in Figure 5 and Figure 6, is more accurate and reliable.

Table 1: G'/G'' cross over as a function of frequency

Frequency, Hz	G'/G'' cross over, s	Instrument
1	1182.1	DMA
5	1156.5	DMA
10	1139.3	DMA
10^3	834.0	DEA
10^4	1089.0	DEA
10^5	1583.5	DEA

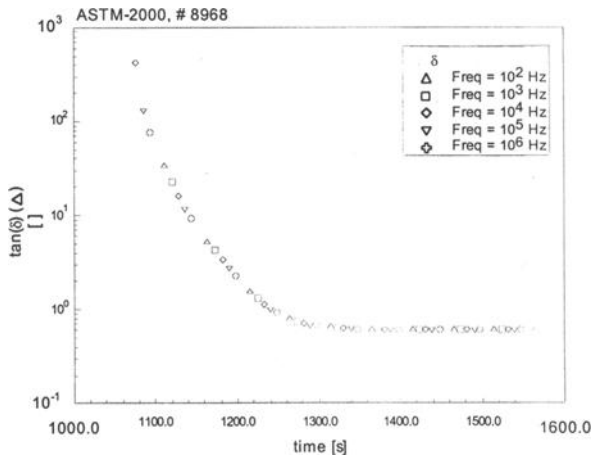


Figure 4: $\tan \delta$, High Frequencies

Figure 5 depicts the storage permittivity, ϵ' , obtained at different frequencies. All frequencies show the maximum value at approximately 800 s that is closely associated with the time of minimum viscosity shown in Figure 1 and Figure 2.

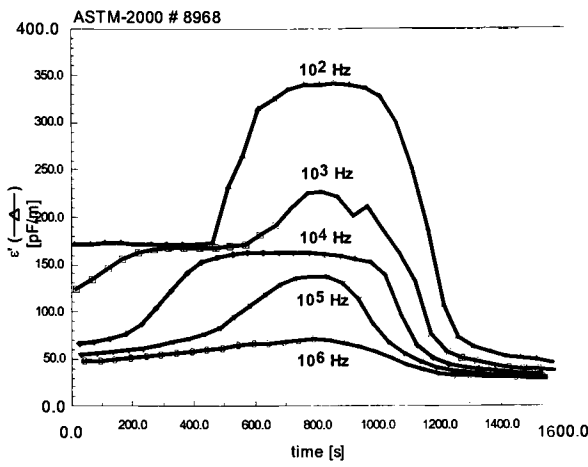


Figure 5: Storage Permittivity, ϵ'

Figure 6 shows the loss permittivity, $\epsilon'' \times \omega$, at different frequencies.

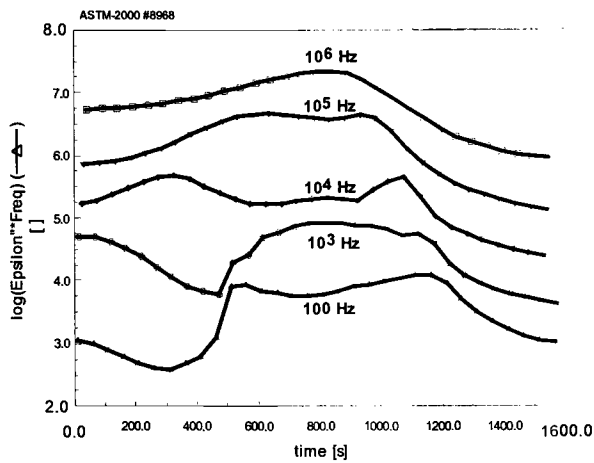


Figure 6: $\log(\epsilon'' \times \text{frequency})$

Conclusions

The curing reaction of DGEBA and phthalic anhydride was successfully studied using simultaneous rheological and dielectric measurements. The system shows the minimum and maximum viscosity for all frequencies. The minimum viscosity is closely related to the maximum value of the storage permittivity. The gel time of the curing reaction can be determined using $\tan \delta$ and G'/G'' cross-over.

Acknowledgments

The author is grateful to Dr. Kalidas Kale from Bristol-Myers Squibb Company in Hillside, NJ for his kindness in letting me use his DETA unit.

References

- [1] Sichina, W and Leckenby, J., "Dielectric Analysis Applications from Coatings to Chocolate," *American Laboratory*, October 1989, pp 72-80
- [2] Guma, N.C., Kale, K. and Morris, K.R., "Investigation of Film Curing Stages by Dielectric Analysis and Physical Characterization," *Journal of Pharmaceutical Sciences*, Vol.86, No.3, 1997, pp. 329-334.
- [3] Kranbuehl, D., Delos, S., Hoff, M., Haverty, P., Freeman, W., Hoffman, R., and Godfrey, J., "Use of the Frequency Dependence of the Impedance to Monitor Viscosity During Cure," *Polymer Engineering and Science*, Vol. 29, No.5, Mid March 1989, pp. 285-289.
- [4] Lane, J.W. and Seferis, J.C., "Dielectric Modeling of the Curing Process," *Polymer Engineering and Science*, Vol.26, No.5, Mid-March 1986, pp. 346-353.
- [5] Suwardie, J.H. and Artiaga, R., "A New Method to Determine the Kinetic Reaction by Simultaneous Thermal Analysis (STA)," *Proceedings of Ninth American Thermal Analysis Society*, September 1998, pp. 688-693.
- [6] Vlassopoulos, D., Chira, I., Loppinet, B., and McGrail, P.T., "Gelation Kinetics in Elastomer/Thermoset Polymer Blends," *Rheologica Acta*, Vol.37, No.6, 1998, pp. 614-623.

Alan T. Riga,¹ John M. Cahoon,² and Joseph W. Pialet³

Characterization of Electrorheological Processes By Dielectric Thermal Analysis

REFERENCE: Riga, A. T., Cahoon, J. M., and Pialet, J. W., "Characterization of Electrorheological Processes by Dielectric Thermal Analysis," *Materials Characterization by Dynamic and Modulated Thermal Analytical Techniques, ASTM STP 1402*, A. T. Riga and L. Judovits, Eds., American Society for Testing and Materials, West Conshohocken, PA, 2001.

Abstract:

An Electrorheological (ER) process occurs when the viscosity of fluids with dispersed particulates is modified by the application of an electric field. The ER fluids discussed in this study are dispersions of solid polymers in low dielectric base oil, an insulating fluid. When these special composite fluids are subjected to the electric field they exhibit increased shear stresses, static yield stresses and viscosity. A mechanism for ER behavior is based on the polarization of the dispersed polymer particulates. A crucial property of the ER event is the ability of the system to respond to the applied field. For example, in semi-passive shock absorbers, the response time is crucial to commercial development.

Dielectric Thermal Analysis (DETA) can measure a polarization response in an AC electric field at isothermal temperatures or by scanning temperature techniques. A Debye Plot of Tan Delta, a ratio of dielectric loss divided by the relative permittivity, versus frequency can fix the limits of a polarization or relaxation time. The critical peak frequency in the Debye Plot is inversely related to the polarization time. The ER response time in a commercial system is directly related to the polarization time. A series of polymer types have been studied in low dielectric oil and their DETA properties are reviewed.

Keywords: polyaniline, poly-N-methylaniline, Electrorheology, ER, response time, shear stress, static yield stress, dielectric thermal analysis, DETA, Debye Plot, dielectric loss, relative permittivity, polarization time, relaxation time

¹ Adjunct Professor of Chemistry, Cleveland State University, 2399 Euclid Avenue, Cleveland, OH 44115-2406

² Senior Corporate Scientist, TechCon Inc., 6325 Aldenham, Cleveland, OH 44143-3331

³ Project Manager, The Lubrizol Corporation, 29400 Lakeland Boulevard, Wickliffe, OH 44092

Electrorheological (ER) fluids are dispersions that undergo rapid and reversible changes in apparent viscosity when exposed to an electric field. Because of their potential uses as rapid, infinitely variable interfaces between electrical and mechanical components of intelligent systems, research on these systems has been going on in university and industrial laboratories since their discovery by Willis Winslow in the late 1930s [1]. A number of general reviews covering various aspects of ER fluids are available [2-10].

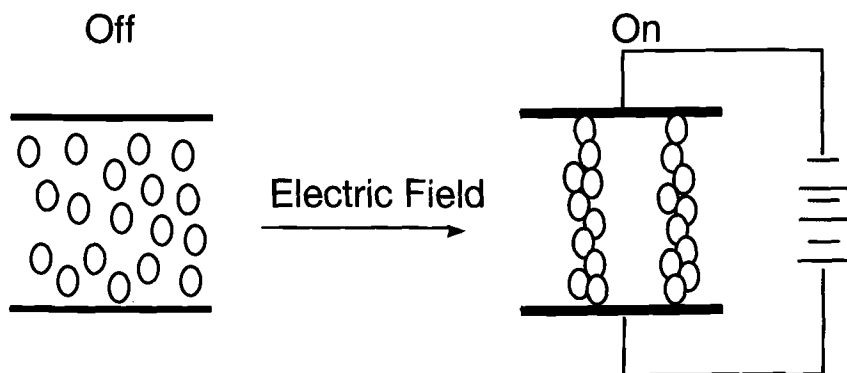


Figure 1. *Particle fibrillation*

ER fluids are typically dispersions of electrically polarizable particles in a low dielectric constant, low conductivity base fluid. When an electric field (typically a few kilovolts per millimeter) is applied, the particles are polarized (Figure 1). The field-induced dipoles on the particles cause them to align to form chains or fibrillated structures, which bridge the electrode gap. These chains have sufficient strength to interfere with the flow of the base fluid. Subjecting the chains to a strong shearing force will rupture the chains but the dipoles at the ends of the broken chains will attract replacement particles to reform the chains. Under constant shear, equilibrium between chain breaking and chain forming will be reached. This equilibrium results in the observation of a yield stress or an increase in apparent viscosity.

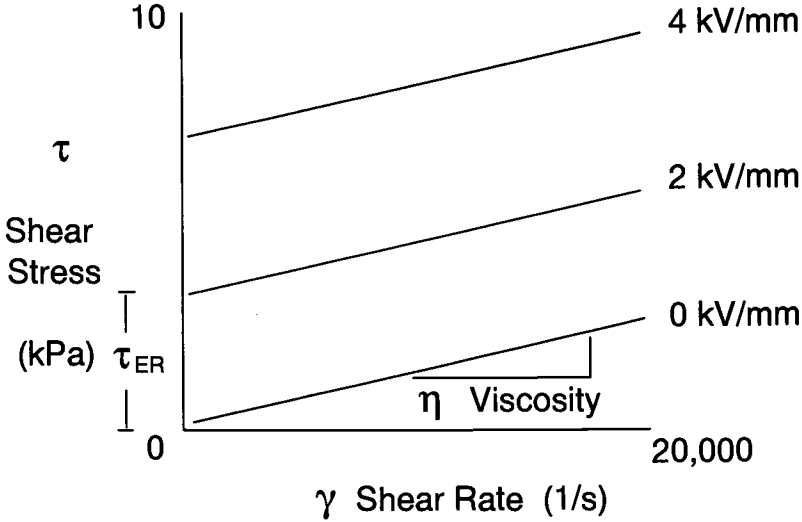


Figure 2. *Bingham plastic model*

The general properties of an ER fluid can be described using the Bingham plastic model (Figure 2)

$$\tau = \gamma\eta + \tau_{ER}$$

where τ is the shear stress, γ is the shear rate, η is the viscosity and τ_{ER} is the electric field induced dynamic yield stress.

The simplest model of the ER effect, which uses material properties to try to predict performance, is the Mason Number (Mn)

$$Mn = \frac{\eta_c \gamma}{2\epsilon_0 \epsilon_c \beta^2 E^2} \quad \text{where} \quad \beta = \frac{\epsilon_p - \epsilon_c}{\epsilon_p + 2\epsilon_c}$$

where η_c is the viscosity of the base fluid; ϵ_0 , ϵ_c , and ϵ_p are the permittivities of free space, the base fluid and the particles respectively; and E is the applied electric field. The Mason Number, which is the ratio of viscous forces to electrostatic forces, accurately predicts trends but does not predict actual yield stresses because it ignores limits on particle polarization and the effects of particle and base fluid conductivity. In the real world, the stress is limited by dielectric breakdown of the base fluid, conductivity of the base fluid and particle chains and saturation of the particle dipoles.

A number of ER fluid properties are important to designing equipment and selecting fluids for a commercial application. These properties include viscosity at zero field, yield stress under field, the electric field required, the current density observed and the response time. Generally, any attempt to optimize one of the properties will result in unacceptable values for another property. One measure of the overall merit of an ER fluid is the Winslow Number

$$Wn = \frac{\tau_{ER}^2}{\eta\phi}$$

where ϕ is the power density (electric current density x electric field) [11]. For any given application, it is possible to calculate the minimum Winslow Number required to have the required balance of field and zero field performance. Combining the minimum Winslow Number with equipment constraints allows specification of fluid requirements.

A wide variety of particles can be used to prepare ER fluids [3,6,8]. All of the particles are capable of being polarized but the polarization mechanisms vary. In general, the particles can be divided into extrinsically polarizable and intrinsically polarizable materials. The extrinsically polarizable particles require a strongly adsorbed high dielectric constant polar liquid, such as water or a glycol, to allow ion migration and formation of a strong induced dipole. The extrinsically polarizable particles include polar nonionics, such as cellulose and silica, and polar ionics such as zeolites and lithium salts of polyacrylic acid. A major weakness of the extrinsically polarizable particles is that, at high electric fields or temperatures, the adsorbed polar can be driven off of the particle, resulting in reduced polarization and increased conductivity. The intrinsically polarizable particles do not require an adsorbed polar because polarization occurs without ion flow. The intrinsically polarizable particles include inorganic and organic semiconductors, such as polyaniline, which polarize by electron flow and ferroelectrics, such as barium titanate, which can polarize by orientation of existing molecular dipoles.

Many potential applications have been proposed for ER fluids [7,9,12]. Most proposed applications involve static positioning, Poiseuille (duct) flow or Couette flow. Proposed uses include primary vehicle suspensions (shock absorbers), engine mounts, cab/body mounts, seat shocks, fan clutches, transmissions, bushings, brakes, tensioning clutches, torsion bars, journal bearings, beam stiffeners, positioning chucks, valves (such as ink jets), variable displacement pumps, peristaltic pumps, solenoids, heat transfer, shaft packing and dynamic balancing systems. Although prototypes for all of these applications have been developed, the commercial uses of the fluids have been limited to niche applications. An ER system will usually include the ER fluid, a power supply, electrodes, a body with fluid chambers and paths, sensors, control computers and algorithms [13] which determine when and how much the apparent viscosity should change. ER fluids cannot simply be "dropped" into existing systems. In order to take advantage of the capabilities of ER fluids, the fluids must be used as part of a system designed to take into account the strengths and limitations of ER fluids [12].

Most investigations of ER fluids concentrate on the yield stresses obtained and the current densities required obtaining the stress. For many applications the response time of the fluid is critical. Some academic investigators define the response time as the time required to obtain a detectable increase in stress after the electric field is applied. For commercial applications, a more useful definition for the response time is the time required for the ER stress to approach its steady state value. Although the time to approach steady state stress is important for a number of potential large volume ER applications, it is rarely addressed in the literature. The need for a short response time can be demonstrated by considering the use of an ER fluid in one of the most commonly suggested applications, an automobile shock absorber [14,15]. If a car travelling at 55 mph drives into a pothole with a diameter of one foot, the shock has only about 12 milliseconds to stiffen before hitting the other rim of the pothole.

Experimental Procedure

The response times, defined as the time for the shear stress to reach 80% of the steady state value, were measured in an oscillating duct (Poiseuille) flow device. In this device, the ER fluid was forced to flow between two chambers through an electrode gap of 1 mm at a shear rate of approximately $20,000 \text{ s}^{-1}$. After the zero field base line was determined, a series of 10 millisecond DC electrical pulse were applied to the electrodes, the shear stress versus time was recorded and an average shear stress versus time was determined for the field applied. The test was then repeated at other fields and temperatures.

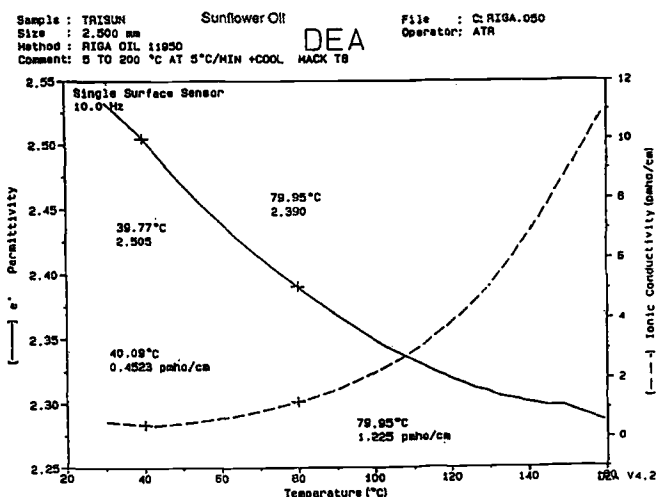


Figure 3. Dielectric Thermal Analysis of Sunflower Vegetable oil, Trisun®:
Permittivity and Ionic Conductivity

One material used in this study was a commercial starch and commercial sunflower oil (Figure 3). The starch with residual water in the vegetable oil comprised an Electrorheological (ER) fluid system. The starch content was varied from 1.0 to 40% by weight: 1, 5, 10, 20, 30 and 40%w. The composite fluids were shaken well before ER measurements.

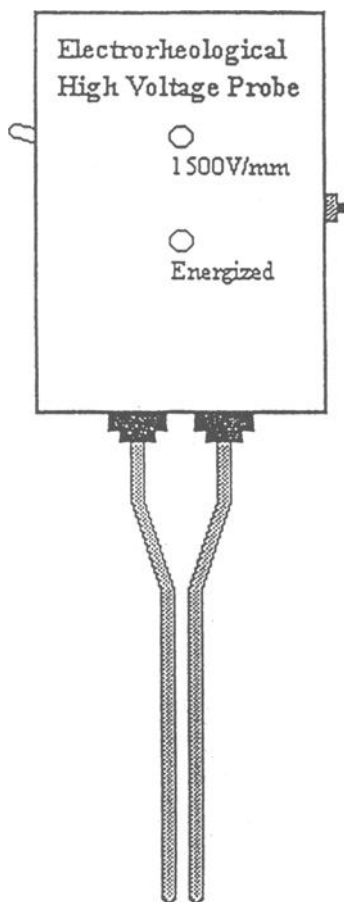


Figure 4. *Electrorheological High Voltage Probe.*

A high voltage source was built that delivered 1500 V/mm (Figure 4). The 3-mm parallel stainless steel probes were separated by 2 mm and were 125 mm in length. The various ER solutions were studied at 10°C intervals from 0 to 100°C.

The test probes were inserted into the ER fluids, the electric field was initiated and the fibrillated structures, which bridged the electrode gap, were measured along the probes, in mm. The strength of the ER structure in the applied electric field was determined by adding an increasing mass of an inert (elastomeric) material to the thickened fluid between the probes until the structure could no longer support the applied load. The maximum mass that sheared the ER bridged material is the apparent strength.

A 2970 Dielectric Analyser (DEA), TA Instruments, was used to measure the dielectric properties of the starch and vegetable oil systems. Various concentrations of starch in oil were examined with the gold ceramic interdigitated single surface sensor. The DEA applied voltage was 50V/mm. The samples were heated at 5°C/min to 120°C, with a 200 mL/min flow rate of nitrogen and scanned at the following frequencies: 0.05, 0.10, 1.0, 10, 100, 1000 and 10,000 Hz. Permittivity, including the high frequency dielectric constant, conductivity (PS/cm) and tan delta plots (dielectric loss factor, $\epsilon''/\text{permittivity}$, ϵ' versus frequency) were evaluated at 25 and 80°C.

Isothermal dielectric properties were determined with a Micromet AC Dielectrometer at 25 and 80°C. The aluminum interdigitated chip sensor was used for the isothermal studies.

Results and Discussion

The vegetable oil and starch models were selected as environmentally friendly materials for this part of the study. The fluid selection was based on sunflower oil's low permittivity, see Figure 3. The dielectric constant of this fluid was 2.39 at 80°C. Starch is slightly hygroscopic and was selected as the solid phase. The absorbed moisture on the starch particles has a dielectric constant of 79. The permittivity (dielectric constant) difference between the vegetable oil and the starch is necessary for the system to exhibit an ER event.

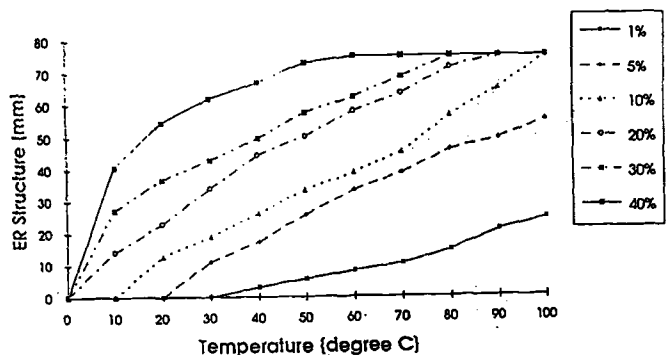


Figure 5. *Formation of ER Structures versus Temperature at Various Concentrations*

The ER structure observed between the probes (in mm) is plotted versus temperature at various concentrations (Figure 5). The ER event was also observed at higher temperatures and concentrations. The force (N) needed to shear the thickened ER fluid also depended on temperature and concentration. That is, the shear force on the ER system increased with concentration (Figure 6).

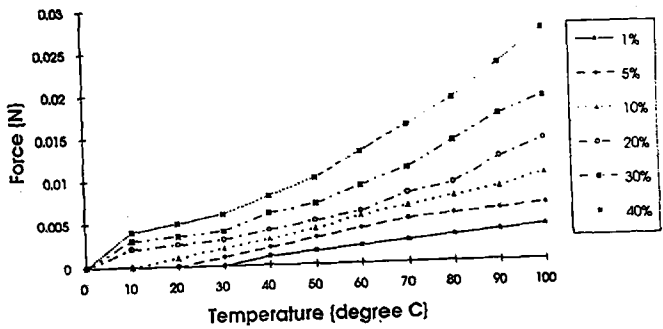


Figure 6. *Force versus Temperature at Various Concentrations*

The DETA study confirmed that the best model ER system was at higher temperatures and 40%w starch (Figure 7 and 8).

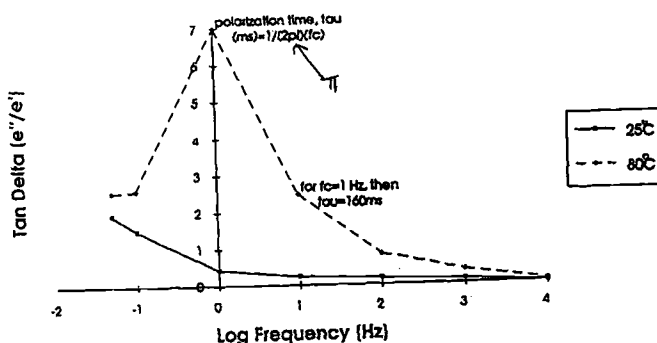


Figure 7. Tan Delta versus Logarithm of Frequency at 40% Starch ER System ($E = 50 \text{ V/mm}$)

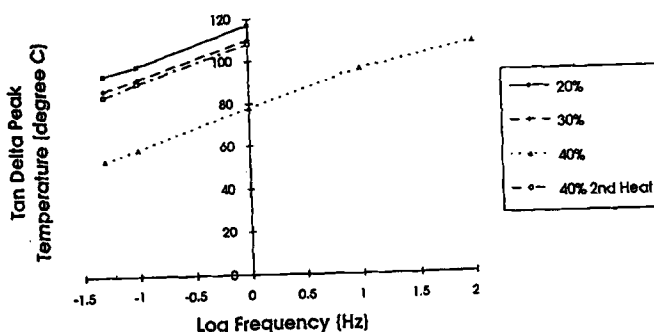


Figure 8. DETA of Starch/Sunflower Oil Composite ($E = 50 \text{ V/mm}$ at $T = 80^\circ\text{C}$)

The ER response at 40%w starch in oil was not observed at 25°C , but clearly seen at 80°C . The lower concentrations of starch, $<30\%w$, did not have a maximum in the tan delta versus log frequency curve. The latter is probably due to the low applied voltage at 50 V/mm . When the ER high voltage probe was used at 1500 V/mm the ER event was noted at temperatures $>30^\circ\text{C}$ for all concentrations of starch in oil. The tan delta versus log frequency plot, a Debye plot, graphically delineates the systems polarization time, that is, molecular mobility. The peak frequency, f_c , at a given temperature is inversely related

to molecular polarization. Fast polarization times (< 2 ms) is associated with the applied industrial ER systems, for example, polyaniline in a mineral oil.

The response times of ER fluids, containing polyaniline and poly-N-methylaniline, have been qualitatively ordered in a miniduct cell. These ER fluids were used as reference fluids to develop a relationship between the real world ER response time and the isothermal DETA properties.

Three polyaniline fluids ranked as a slow responding fluid (J105B), a moderately fast fluid (L105E) and a very fast fluid (L117A). Two poly-N-methylaniline ER fluids were ranked as somewhat slow (L095C) and fast (L023G). A numerical response time value was assigned to each of these fluids as follows: No activity = zero, L105E=2, L095C=4, L105E = 6, L023G=8 and L117A=10.

The Tan Delta versus log frequency curves (Debye Plots) clearly ranked these five fluids (Figure 9 and 10).

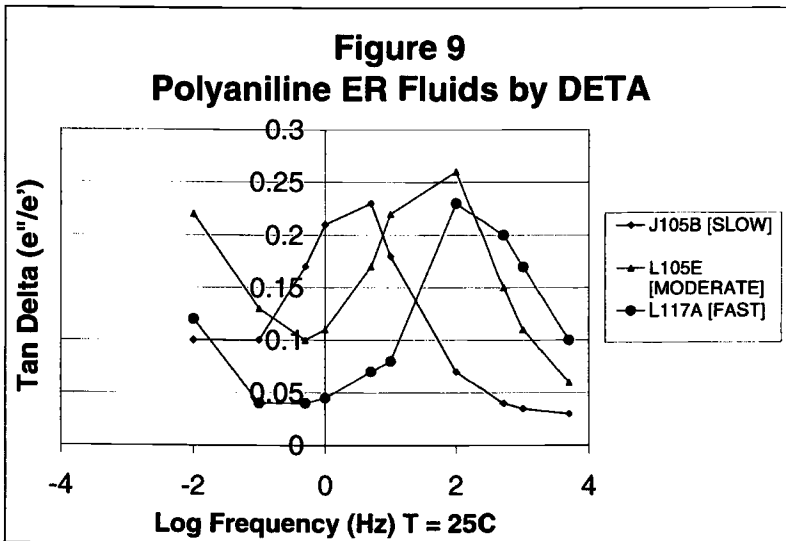


Figure 9. ER Fluids Containing Polyaniline
ER Response Time versus DETA properties at 25 °C

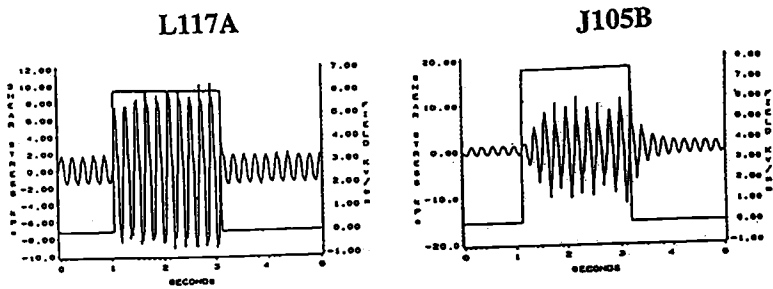


Figure 10a. Industrial ER Response Time Test in Seconds
Shear rate vs. Shear Stress: L117A, J105B

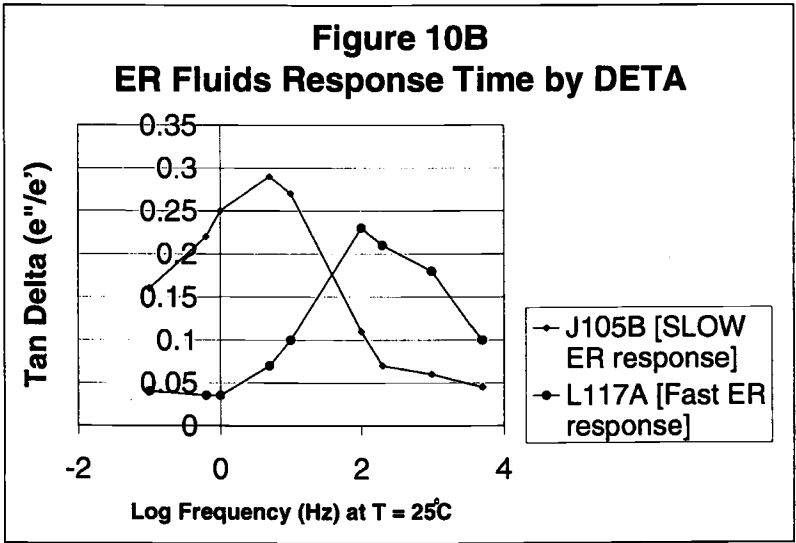


Figure 10B. ER Fluids Response Time by DETA: L117A, J105B & L063B

A plot of the polarization time, τ , based on the Debye Plot peak frequency, f_c , where

$$\tau = (1/2\pi f_c) (1000) \text{ ms}$$

at a given temperature was linearly related to the values assigned to these reference fluids (Figure 11).

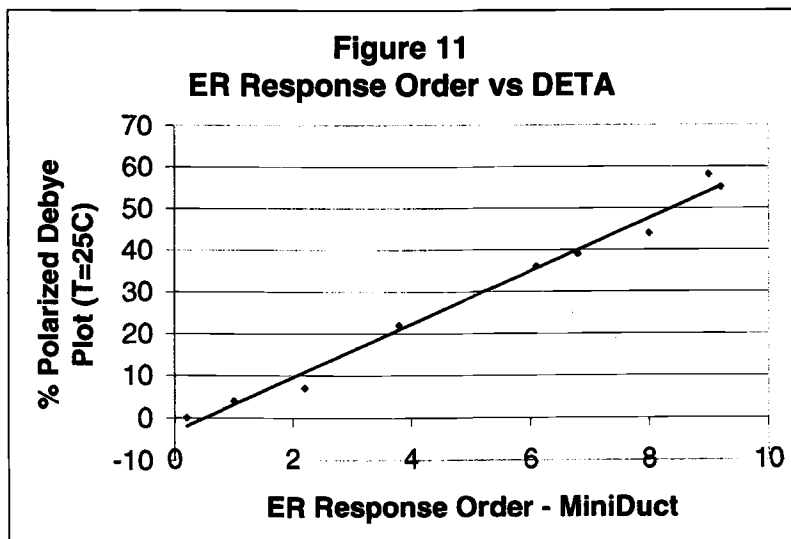
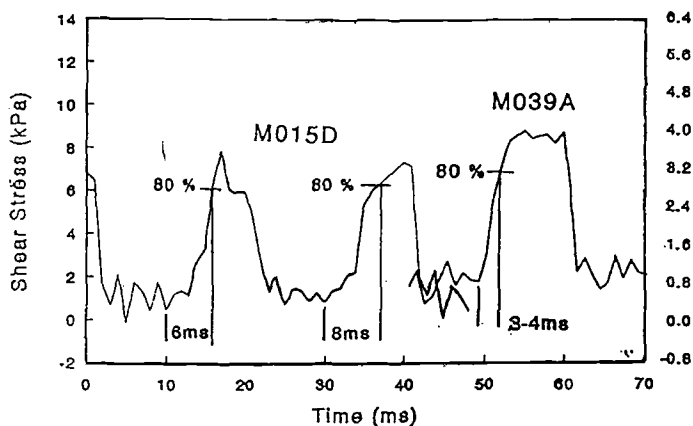
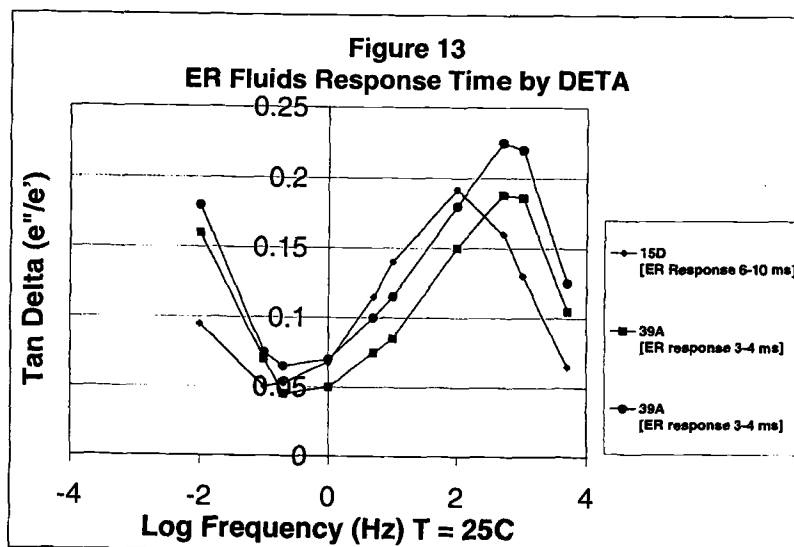


Figure 11. *ER Response Time vs. DETA % Polarized*
0 = no response; 2 = slow; 6 = moderate fast; and 10 = very fast

Two fluids containing copolymers with polyaniline were evaluated in a response time test. The observed response times were 3-4 ms and 6-8 ms (Figure 12).

Figure 12. *ER Response*

The Debye Plots for these fluids were significantly different, with the faster fluid having a higher peak frequency and lower polarization time (Figure 13). The isothermal DETA polarization time was directly related to the response time as measured by an acceptable industrial measuring device

Figure 13. *DETA of ER Fluids and the corresponding ER Response Time*

Multiple peaks have been observed in the Tan Delta versus log frequency curves. Analysis of the Debye Plots of the polyaniline ER reference fluids to determine the percentage polarized has been used to predict ER response time. It is assumed that the area under the Debye Plot curve is equal to complete polarization or 100% of the particles are polarized. The percentage polarized only in the "fast zone", that is, polarization over the range of 0.03 to 0.6 ms appears to be directly related to the real world ER response time, in the miniduct or an industrial millisecond test (Figure 14).

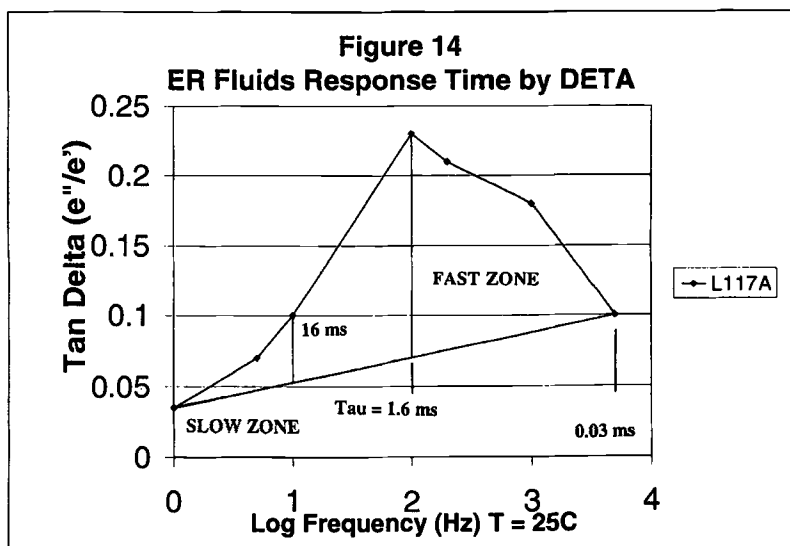


Figure 14. *ER Fluids Response Time by DETA at $T = 25^\circ\text{C}$*
Tan Delta (e''/e') vs. Log Frequency (Hz)

A plot of percentage polarized in the "fast zone" as a function of log polarization time, Tau, was linear (Figure 15).

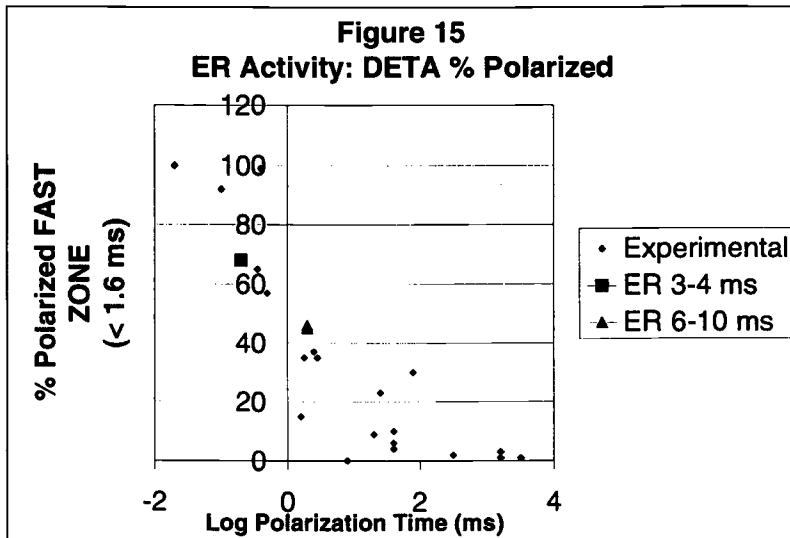


Figure 15. *ER Activity based on DETA at 25°C*
% Polarized in the Fast Zone = ER Response Time

The latter relationship includes four ER systems described by Block (3). The difference in the percentage polarized ($\tau = 0.03$ to 1.6 ms) between the 3-4 ms response time and the 6-8 ms response time fluid was 18% (Figure 16).

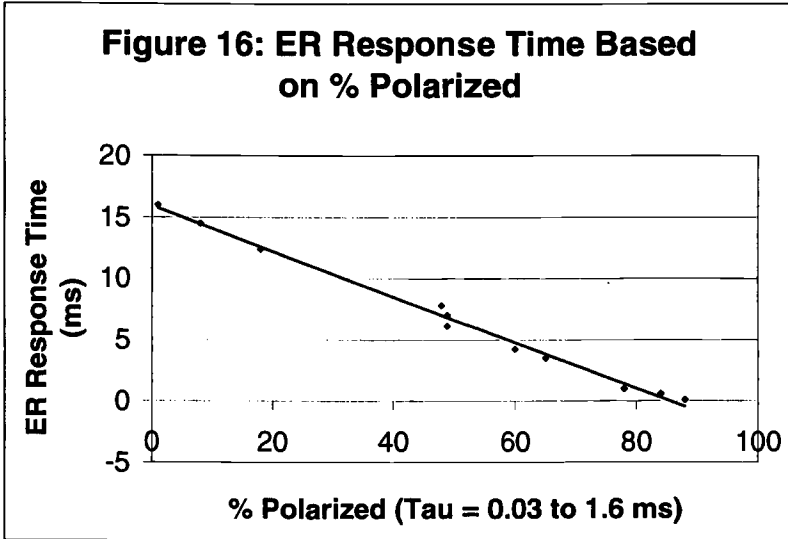


Figure 16. *ER Response Time based on DETA*

$$ER \text{ Response Time} =$$

% Polarized with a Polarization Time of 0.2 to 16 seconds

The repeatability of the percentage polarized in the fast zone was very good. Duplicate measurements were made for eight samples and the values had a maximum deviation of 5%.

DETA properties were determined for four polyaniline ER fluids where doping was studied. These samples are coded I095C, I095D, I097A and I097B. These four samples were examined at 25 and 80°C. The percentage polarized in the fast zone was determined for each fluid. The concentration of dopant directly affected the response time, that is, the higher the concentration of the dopant the faster the response time. The calculated response times and Tau polarization times for I095C, I095D, I097A and I097B are summarized in the Table 1. It is predicted, based on the DETA evaluation, that I097B was the fastest fluid. This conclusion is based on the fluids polarization time and percentage polarized in the fast zone. The ER response time used to evaluate industrial fluids versus the DETA “percentage polarized” gives a practical range of response times.

Table 1. DETA of Polyaniline containing ER Fluids
Correlation of DETA properties with ER Response Time

Sample Number	Polarization Time Tau (ms)			%Polarized in Fast Zone			ER Response Time		
Temp =	25	80	80°C	25	80	80	25	80	80°C
1097B	5.3	0.2	0.3	47	84	78	7	<1	1.0
1097A	16	0.3	0.3	19	87	79	12	<1	1.0
1095D	60	1.6	nv	6.2	60	62	15	4.5	nv
1095C	160	16	nv	0	0	nv	16	16	nv

ER response time (ms) = $[16 - 0.20 \times \% \text{Polarized}]$, where $r^2=0.8$

nv = no value

Conclusions

Dielectric Thermal Analysis yields practical electrical properties that are useful in rapidly evaluating commercial Electrorheological fluids. DETA, at a constant temperature, can predict electrorheology performance response times. An example of a weak ER system with *extrinsically polarizable* particles is the starch and oil model. However, optimum performance for this weak ER system was observed at a higher temperature (80°C) and starch loading (40%w). An example of a strong ER system with *intrinsically polarizable* particles is the polyaniline and vegetable oil system. Response times of these fluids containing polyaniline and poly-N-methylaniline ranked in a mini-duct flow industrial instrument were accurately predicted by the dielectric polarization time.

Acknowledgments

Funding from The Lubrizol Corporation and TechCon, Inc supported this work.

References

- [1] Winslow, W. M., "Induced Fibrillation of Suspensions," *J. Appl. Phys.*, Vol. 20, 1949, pp. 1137-1140.
- [2] Zukoski, C. F., "Material Properties and the Electrorheological Response," *Annu. Rev. Mater. Sci.*, Vol. 23, 1993, pp. 45-78.
- [3] Block, H., Kelly, J. P., "Electrorheology," *J. Phys D: Appl. Phys.*, Vol. 21, 1988, pp. 1661-1677.
- [4] Piolet, J. W. and Havelka, K. O., "Electrorheological Technology: The Future is Now," *Chemtech*, Vol. 26, 1996, pp. 3645.
- [5] Jordan, T. C. and Shaw, M. T., "Electrorheology," *IEEE Trans. Electr. Insul.* Vol. 24(5), 1989, pp. 849-878.
- [6] Piolet, J. W. and Havelka, K. O., "Electrorheological Materials," in *Polymeric Materials Encyclopedia*, Vol. 3, Salamone, J. C. Ed.; CRC, Boca Raton, 1966, pp. 2028-2038.

- [7] Coulter, J. P., Weiss, K. D. and Carlson, J. D., "Engineering Applications of Electrorheological Materials," *J. Intell. Mater. Sys. Struct.* Vol. 4, 1993, pp. 248-259.
- [8] Weiss, K. D., Carlson, J. D. and Coulter, J. P., "Material Aspects of Electrorheological Systems," *J. Intell. Mater. Sys. Struct.* Vol. 4, 1993, pp. 13-34.
- [9] Shulman, Z. P., Gorodkin, R., Korobko, E. and Gleb, V., "The Electrorheological Effect and Its Possible Uses," *J. Non-Newtonian Fluid Mech.*, Vol. 8, 1981, pp. 29-41.
- [10] Korobko, E. J., "Some Aspects of Electrorheology," *Intell. Mater. Sys. Struct.*, Vol. 3, 1992, pp. 268-295.
- [11] Boyle, F.P., "Performance Characterization of ER Fluids: Durability," in *Electrorheological Fluids – Mechanisms,, Properties, Structure, Technology, and Applications*, Tao, R. Ed.; World Scientific, Singapore, 1992, pp. 236-245.
- [12] Piolet, J. W. and Havelka, K. O., "Transportation and Industrial Applications of Electrorheological Technology: Design Considerations," *ASME ICE Spring Technical Conference*, Vol. 26(3), 1996, pp.9-18.
- [13] Boyle, F. P., Petek, N. K. and Smith, D. P., "Method for Controlling Motion Using an Adjustable Damper," US 5582385, 1996.
- [14] Petek, N. K., "Shock Absorber Using Electrorheological Fluid," *Automotive Engineering*, Vol. 100(6), 1992, pp. 27-30.
- [15] Petek, N. K., Romstadt, D. J., Lizell, M. B. and Weyenberg, T. R., "Demonstration of an Automotive Semi-Active Suspension Using Electrorheological Fluid," SAE Technical paper 950586, 1995.

Characterization of Organic Surfactants and Dispersants by Frequency-Dependent Dielectric Thermal Analysis and Electrochemistry

REFERENCE: John Cahoon, Alan Riga and Vadim Lvovich "Characterization of Organic Surfactants and Dispersants by Frequency-Dependent Dielectric Thermal Analysis and Electrochemistry," *Materials Characterization by Dynamic and Modulated Thermal Analytical Techniques*, ASTM STP 1402, A. T. Riga and L. Judovits, Eds., American Society for Testing and Materials, West Conshohocken, PA.

Abstract: Multi frequency electrochemical impedance spectroscopy (EIS), dielectric thermal analysis (DETA), and cyclic voltammetry (CV) were employed as a basis for evaluating organic detergents and dispersants in a hydrocarbon based lubricating oil. These dielectric and electrochemical techniques appear to be a powerful tool capable of detection and monitoring of oil additives, surfactants and dispersants, and investigation of general mechanisms of oil degradation in an operating engine. These techniques were applied to the identification and detection of various types of chemical additives.

Measurement of electrochemical impedance spectroscopy over a sufficiently wide range of frequencies, electrochemical potentials, and temperatures yielded detailed qualitative and quantitative information. EIS ceded the dynamics of charge transport and reduction or oxidation reactions of ionic species and individual chemical components across the bulk lubricant and at the electrode-lubricant interface. Highly selective studies of spatial distribution of charge-transfer processes taking place in bulk solution and at the interface were achieved. A combination of EIS and CV based electrochemical methods provided a complete chemical analysis of lubricant conditions. These included detection, quantification and differentiation of adsorption and lubricant film formation on an electrode surface, and investigating kinetics of reduction or oxidation reactions of major oil components (detergents, dispersants, etc.). DETA polarization plots clearly ranked the surface-active detergents and the less active dispersants. Frequency dependent EIS, and DETA, as well as CV can be easily used for characterizing chemical additives for engine oils.

Key Words: electrochemical impedance spectroscopy, dielectric thermal analysis, cyclic voltammetry, polymers, oils, detergents, dispersants.

¹ - Lubrizol Corp., Wickliffe, OH 44092

² - Cleveland State University and TechCon Inc., Cleveland, OH 44143

Introduction

For an accurate analysis of the detergent and dispersant chemicals of an engine oil a number of physical and chemical parameters need to be monitored. Most important parameters are operating temperature; viscosity; level of water, insoluble degradation products, wear metals, criterion of oil acidity and basicity - total acid number (TAN) and total base number (TBN); and concentration and type of the oil additives. Direct application of traditional analytical methods (spectroscopy, current/voltage electrochemistry) to monitoring of these parameters is complicated by high electrical resistance and low optical transparency of the oil media [1-3].

Application of electrochemical impedance spectroscopy (EIS) to oil analysis is devoid of problems associated with traditional analytical methods. Measurement of the impedance over a wide range of frequencies, electrochemical potentials, and temperatures can yield detailed qualitative and quantitative information on dynamics of charge transport and electron transfer reactions of individual chemical components across the bulk lubricant and electrode-lubricant interface. The impedance-frequency data can supply essentially all the information that can be obtained by a joint application of all other electrochemical techniques [4-11]. Moreover, the different charging components can be evaluated by this technique whereas other electrochemical methods can only yield a convoluted response. Mass- and charge-transfer processes in the vicinity of electrode/solution interface have different degrees of sensitivity to the perturbation frequency of an external electric field. Electrical properties of bulk solution are sensitive to high frequency perturbation. Charge- and mass-transfer processes taking place in the diffusion layer and double layer are sensitive to medium frequencies, while oxidation and reduction reactions and adsorption processes occurring at the electrode surface can be studied at very low frequencies. That allows for studies of spatial distribution of processes taking place in bulk solution and at the interface. A modified multi frequency / multi electrochemical potential EIS method was developed and applied to identification and detection of traditional oil contaminants monitoring acid-base changes in typical engine oil, and broader chemical characterization of lubricants. Additional studies of oil formulations by DETA and Cyclic Voltammetry (CV) were performed to compliment the EIS method.

Overview of analytical techniques

Cyclic voltammetry response in highly resistive media is limited by mass-transfer (migration) in the diffusion layer and high bulk solution resistance [12-14]. Migration limitations cause deformation of a sigmoid shape of voltammogram. High bulk solution resistance leads to a general shift of voltammetric peaks to higher overpotential values. Previous studies of fully formulated fresh and stressed oils with ultramicroelectrodes demonstrated a number of reduction and oxidation features (Figure 1).

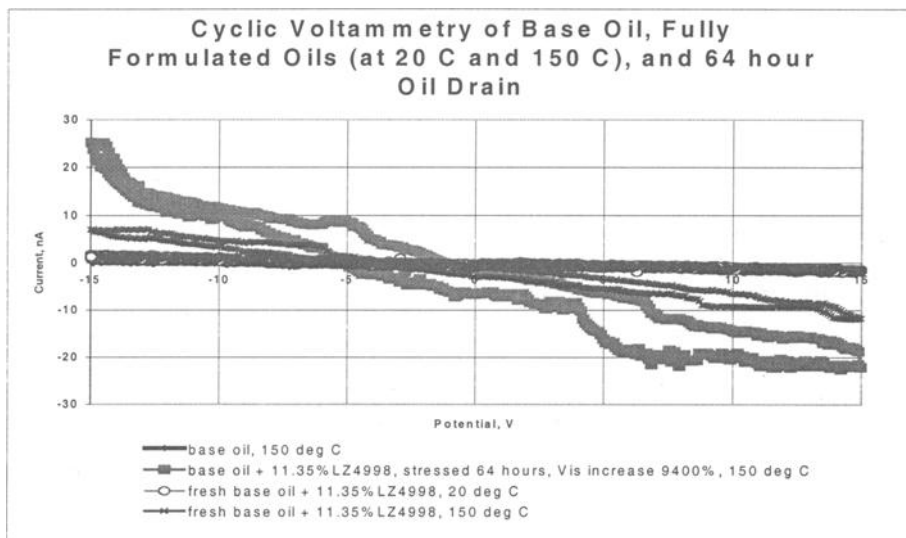


Figure 1 - Cyclic voltammograms of typical fresh and drain oils

Peaks identified as antioxidant oxidation, reduction of carbonyl compounds, and reversible reduction or oxidation chemistry of phenates and dispersants were detected [1]. Some relevant results on CV applications to chemical characterization of polymers and industrial lubricants appeared in the literature before [15-24].

Dielectric analysis measures two fundamental electrical characteristics of a material – capacitance and conductance – as functions of time, sampling frequency and temperature [25-26]. The capacitive nature of a material is its ability to store electrical charge, and the conductive nature is its ability to transfer electric charge. These electrical properties are related to molecular activity, allowing for probing the chemistry, rheology and molecular mobility of polymers, for example. The material to be analyzed is placed between two electrodes while an alternating (sinusoidal) electrical field is applied. This produces polarization within the sample, causing oscillation at the same frequency as the field but with a phase angle shift δ . The measured current is separated into capacitance and conductive components. Capacitance (induced dipoles and alignment of dipoles) can be determined by measurements of permittivity ϵ_1 , and conductance (dipole loss factor and ionic conductance) is proportional to loss factor ϵ_2 . The complex dielectric constant ϵ^* consists of both the “real” (permittivity) and the “imaginary” (loss factor) parts:

$$\epsilon^* = \epsilon_1 - i\epsilon_2,$$

with the loss tangent $\tan\delta$ being the ratio of ϵ_2 and ϵ_1 . Both loss factor and permittivity are frequency and temperature dependent. The dependence of ϵ_1 and ϵ_2 on sampling frequency results from the fact that a finite amount of time is required to align the dipole with changing electrical field. When dipoles are excited by moderate frequencies, they have enough time to become oriented, and their permittivity ϵ_1 is high while ϵ_2 is low. But when the frequency becomes so high that the dipoles can no longer follow the field, the dielectric constant falls precipitously and the material shows dispersion. This phenomenon is also followed by a sharp increase in dipole loss, resulting in a peak in ϵ_2 .

Chemicals and polymers with high permanent dipole moments (such as liquid crystals) show dispersion at significantly higher frequencies and have larger permittivity values than polymer molecules with weak or induced dipole moments. Increase in temperature of the media usually increases values of critical frequencies at which dispersion occurs.

Plot of ϵ_2 vs. ϵ_1 (known as Cole-Cole plot) is a semicircular arc with its highest point corresponding to a critical frequency where dispersion occurs. The dielectric behavior of complex chemicals or polymers quite often can be characterized by a distribution of relaxation times rather than by a single relaxation time, leading to departure from a perfect semicircular arc, or appearance of more than one arc if relaxation times of polymer components are very different. At very low frequencies, the Cole-Cole plot exhibits a straight line. This is due to conduction and interfacial (Maxwell-Wagner) polarization resulted from accumulation of charges at electrode interfaces. The higher the conductance of the conducting material, the higher is the frequency at which interfacial polarization occurs [26].

Electrochemical impedance spectroscopy is related to DETA, dielectric spectroscopy. It operates by analyzing contributions of real and imaginary parts of the impedance Z^* , with the imaginary part (Z_{im}) being determined by capacitance, and the real part (Z_{real}) by solution resistivity [27]:

$$Z^* = Z_{real} - iZ_{im}$$

After rearrangement of mathematical functions, a direct correlation between impedance and dielectric parameters can be established as:

$$Z^* = V/I = \frac{1}{i \omega \epsilon^* \epsilon_0 A/D} = \frac{D}{i \omega \epsilon_0 A (\epsilon_1 - i\epsilon_2)}$$

- where ϵ_0 – absolute permittivity of free space (constant);
 ω – sampling frequency ($2\pi f$);
 A – surface area of the electrode (plate);
 D – spacing (gap) between two parallel plates of the electrode.

After rearrangement, the correlation between real and imaginary components of impedance and dielectric will look like:

$$Z^* = \frac{D}{i \omega \epsilon_0 A (\epsilon_1 - i \epsilon_2)} \times \frac{(i \epsilon_1 - \epsilon_2)}{(i \epsilon_1 - \epsilon_2)} = \frac{D i \epsilon_1 - D \epsilon_2}{2\pi f \epsilon_0 A (\epsilon_1^2 + \epsilon_2^2)}$$

$$Z_{\text{real}} = \frac{-\epsilon_2 D}{2\pi f A \epsilon_0 (\epsilon_1^2 + \epsilon_2^2)}; \quad Z_{\text{im}} = \frac{-\epsilon_1 D}{2\pi f A \epsilon_0 (\epsilon_1^2 + \epsilon_2^2)}$$

A plot of Z_{im} vs. Z_{real} (Nyquist plot) usually yields a series of semicircular arcs and straight lines. For aqueous solutions and solutions of organic solvents with moderate-to-high conductivities, bulk solution resistance has low resistivity values with no capacitive contribution. This type of analysis is usually uncomplicated by bulk solution processes, and is limited primarily to analysis of charge-transfer kinetics at the electrode interface. Mass-transport and charge-transfer kinetics are two competing processes limiting the electrode reaction, with mass-transfer limitations being predominant at low frequencies (giving a straight line in the $Z_{\text{im}} = f(Z_{\text{real}})$ plot), and electrode kinetics at high frequencies where the reaction may not be facile enough to follow changing field. In this case, the Nyquist plot yields a semicircle.

Application of electrochemical impedance spectroscopy to polymer analysis gives somewhat more complicated plots. Typical parameters of a Nyquist plot of highly resistive polymers are presented in Figure 2. Mass transport through bulk polymer had both resistive and capacitive nature, and manifested itself in a high-frequency semicircle on Nyquist plot. Distribution of relaxation times for bulk solution species can be obtained from the analysis of high-frequency arc just like from Cole-Cole plots. Deformed arc with the center displaced below the real axis tells about multiple relaxations or multiple orientations of a suspended phase in the bulk polymeric solution. Bulk solution resistivity can be easily obtained at the point of intersection of the arc with Z_{real} axis. Second semicircle, which appeared at moderate frequencies, represents charge-transfer and double-layer capacitance, characteristic of mass- and electron-transfer processes ("exchange current") involving all ionic or charged species located in any given moment in the diffusion layer ($\sim \mu\text{m}$ thick layer in close proximity to the electrode surface). At a low-frequency domain this semicircle can be followed by vertical capacitive adsorption line, or by a series of semicircles (kinetic limitation) and 45° straight lines (mass transfer limitation for pure diffusion control), if electrochemical reduction or oxidation reactions of any particular solution component take place. In case of solid electrolytes (lubricants, polymers, etc.) migration limitations (absence of supporting electrolyte) often manifest itself in significant deviations from 45° angle.

Apparently, migration-limited charge-transfer case with slow movement of a few charged species also becomes complicated due to coupling between Faradaic current and double-layer charging current (interfacial polarization). The reduction or oxidation reactions occur at electrochemical potentials E_{redox} , characteristic of chemical nature of given solution component. Kinetics or reduction/oxidation processes can be determined through calculating charge-transfer (polarization) resistances and related rate constants of electron transfer. When discharge reduction or oxidation reaction happens, the medium-frequency charge-transfer semicircle usually decreases substantially. Both bulk solution and charge-transfer parameters are functions of electrochemical potential (i.e., of the mean electrode and solution charging levels). They may be affected by both interfacial polarization and rapid increase in charge-transfer within diffusion layer when facile discharge of individual chemical takes place for applied potential $E_{appl} > E_{redox}$. Current EIS work made it possible to detect oil contaminants and degradation, but also gave an opportunity to study possible adsorption and lubricant film formation on electrode surface, and determine kinetics of reduction or oxidation reactions of major oil components (detergents, dispersants, etc.). Adsorption processes manifest themselves in an additional capacitive 90° straight line at low frequencies in the Nyquist plot. Slight deviations from 90° (within $5-10^\circ$) are attributed to the dispersion of frequency due to the rough surface that is often associated with solid electrode. Adsorbed film resistivity and diffusion coefficients for transport of ion vacancies through the film may be established. Absence of vertical capacitive line at low frequencies indicates that a given electrode surface is immune to adsorption and film formation.

EIS has been applied to kinetic studies of polymer and chemical based solutions and polymer film electrodes. The power of EIS is easily established by the amount of information obtained in a single experiment:

- Resistance and relaxation frequency of bulk chemical or polymer;
- Relaxation distribution of active species in bulk chemical or polymer;
- Charge transfer resistance and relaxation frequency at electrode/solution interface;
- Rate of charge transfer in a chemical or polymer;
- Double layer capacitance and reduction or oxidation capacitance of a chemical or polymer;
- Electrochemical potential dependence of charge transfer and bulk resistances;
- Formation of polymeric film on an electrode surface;
- Electrochemical reduction or oxidation reactions of individual species in solution;
- Diffusion and mass-transport coefficients of ionic and electronic charge carriers.

The analyzed samples were differentiated on the basis of:

- Bulk solution resistance and relaxation frequency;
- Charge-transfer resistance and relaxation frequency;
- Number of reduction or oxidation reactions and their respective relaxation frequencies.

In order to investigate a complicated chemical system, the impedance should be measured over a wide range of frequencies, electrochemical potentials and temperatures. It should be noted that for a given window of frequencies available for a scan, an elevated temperature allows for determination of larger number of low-frequency phenomena, when effective frequency shift to higher values takes place for all bulk and interface processes (Figure 2). An effective alternative to temperature elevation would be expanding a scan to μHz frequency domain, which is not always possible with available equipment. Performing experiments at significant anodic or cathodic overpotentials forces oxidation or reduction of individual chemical components. These processes manifest themselves in additional low-frequency domain features at the impedance diagram (Figure 3).

Cyclic voltammetry and impedance spectroscopy can be viewed as somewhat related techniques in the same manner as impedance spectroscopy is related to dielectric spectroscopy. In cyclic voltammetry potential is applied in a cyclic fashion, and it is possible to present a traditional voltammetric experiment as sampling of solution at a frequency determined by potential sweep rate and potential scanning limits. In polymer analysis, where temperature and structure or individual polymers strongly affect impedance analysis, cyclic voltammetry – impedance spectroscopy correlation is also affected by temperature and chemical composition of analyzed polymer. In cyclic voltammetry, as in impedance spectroscopy, it is possible to determine sweep rates/scanning potential correlation corresponding to sampling charge-transfer kinetics, adsorption processes, or bulk solution impedance processes. From this analysis it becomes obvious, for example, that cyclic voltammetry-based bulk solution resistance measurements can be conducted only at very high sweep rates in relatively “short” potential window.

Impedance / dielectric thermal analysis, while providing a wealth of information about chemical-electrode interactions, electrode kinetics, and solution composition, is an instrumentally complicated technique requiring sophisticated instrumentation and competent operators. Cyclic voltammetry and dielectric spectroscopy have simpler instrumentation. Both methods provide information on the basis of relatively straightforward analysis of charge-transfer (cyclic voltammetry) kinetics by detection of various peaks or bulk properties of polymers by sampling permittivity or loss factor at selected frequencies.

Experimental conditions

The EIS/DETA and CV data for all oil samples was collected in laboratory between 40 °C and 120 °C. Electrochemical impedance spectroscopy was conducted on two parallel platinized titanium or platinum electrodes (one working and one reference/counter) with 1cm² surface area and 0.5 mm spacing between them. A cylindrical body of Teflon (22-cm

long, 2.5-cm diameter) enclosed both electrodes. The experiments in engine testing environment were performed on similarly designed "plug-type" sensor enclosed in stainless steel protective shell.

The EIS data for each oil sample was collected at 12 different electrochemical potentials within $\pm 14\text{V}$ potential window. For all experiments the analysis was conducted by measuring real and imaginary parts of electrochemical impedance at 20 discrete frequencies per decade from 100kHz to 1mHz. The electrochemical ac potential amplitude was fixed at 500mV. A separate 3-electrode electrochemical sensor was used for cyclic voltammetry studies. Cyclic voltammetry scans (5-50 mV/sec) between -15 and $+15$ V and between -10V and $+10\text{V}$ (vs. $\text{Ag}/\text{Ag}_2\text{O}$ reference electrode) on a platinum working ultramicroelectrode ($25\text{ }\mu\text{m}$ diameter) were employed to determine a basic chemical composition of the solutions. CHI-660A (CH Instruments, Austin, TX) and Voltalab 40 (Radiometer Inc., Westlake, OH) potentiostats were employed for CV and EIS data acquisition and analysis.

Dielectric analysis was conducted on single-surface ceramic electrodes with $\sim 4\text{cm}^2$ surface area and ~ 0.1 mm spacing between them. The equilibrium temperature for all experiments was fixed at 60°C for 30 minutes. A drop of solution (~ 50 mg) was placed on the sensor surface, with the sensor being replaced after each experiment. The measurements were conducted by applying frequency scan between 300KHz and 10 mHz with resulting permittivity, loss factor, and $\tan\delta$ values recorded by DEA 2970 Dielectric Analyzer (TA Instruments, Newcastle, DE). An alternate DETA scheme was to scan a candidate detergent or dispersant from 0.1 Hz to 10,000 Hz, from 25 to 160°C at $5^\circ\text{C}/\text{min}$ in a nitrogen atmosphere.

Results and Discussion

The EIS analysis was conducted by collecting values of resistance and relaxation frequency of bulk polymer (R_{bulk} , F_{bulk}), charge transfer resistance and relaxation frequency at electrode/solution interface (R_{ct} , F_{ct}), and parameters characteristic of electrochemical reduction or oxidation reactions of individual oil components (number of reactions, their critical frequencies, etc.).

The influence of temperature changes on EIS profile of typical diesel oil sample is demonstrated at Figure 2. Elevation in temperature increased general conductivity of oil samples, with the plot of conductivity vs. temperature generally following the Arrhenius type of dependency. Bulk resistance decreased while peak frequencies of bulk relaxations shifted to higher values. Charge transfer parameters (R_{ct} , F_{ct}) are functions of conduction in electrochemical diffusion layer (order of μm thick) and charging of capacitance associated with electrochemical double layer. Under normal circumstances (no preferential reduction or oxidation reaction) the conduction in this area of solution laying

in close proximity to electrode/solution interface is related to overall number and mobility of charged particles – ions, electrons and dipoles. Increase in solution temperature increased conductivity in diffusion layer, therefore decreasing R_{ct} and shifting frequencies of charge transfer relaxations to higher values. General increase of relaxation frequencies of bulk and charge-transfer processes at elevated temperatures makes possible to study low-frequency range where individual electrochemical reduction or oxidation reactions take place, provided that they can occur thermodynamically at a given electrode potential. Studies of these processes at room temperatures in oil solutions are complicated. Reduction or oxidation reactions of oil components are kinetically sluggish, and may be detected only at μHz frequency region, unavailable for all but most expensive pieces of EIS equipment.

The influence of electrochemical potential on EIS profile of typical diesel oil sample at fixed temperature is presented in Figure 3. With electrochemical potential becoming more anodic or cathodic mass transfer of charged species to electrode surface increased. That resulted in accumulation of charge carriers at the interface and within diffusion layer, causing interfacial polarization. In the present studies the potential shifted from 0V to $\pm 14\text{V}$. Some slight increase in R_{bulk} was observed. Increase in concentration of charge carriers in diffusion layer had much more pronounced effect on charge transfer resistance, which decreased very substantially (two-three orders of magnitude) with polarization shifted from 0V to $\pm 14\text{V}$. Decrease in R_{ct} was becoming most prominent when potential reached values of reduction or oxidation reactions involving individual components of diesel oil formulation – *detergents* at $E_{det} \sim +8\text{V}$ and *dispersants* at $E_{disp} \sim -7\text{V}$. The phenomenon of a significant decrease of charge transfer resistance when a system potential becomes sufficiently anodic or cathodic to allow for a specific reduction or oxidation reaction to occur is well known for both aqueous and non-aqueous systems. After potential equaled or exceeded values of E_{det} or E_{disp} , reduction or oxidation reactions involving detergents and dispersants were taking place, resulting in additional semicircle/45° straight-line combinations characteristic of kinetic or mass-transfer limited electrochemical reactions. Oil aging introduced significant changes in EIS plot, depicted in Figure 4. As oil ages it becomes more acidic with higher concentration of polar and ionic species followed by formation of highly conductive “associated structures” (Figure 5). Bulk resistance, R_{bulk} , decreased from average value of 85.3 MOhm ($\text{TAN} \sim 0.4$) to 64 MOhm ($\text{TAN} \sim 3.7$) at 60°C and from 9.94 MOhm to 6.99 MOhm at 120°C. It was accompanied by an increase of bulk peak relaxation frequency from 16.5 Hz to 20.1 Hz (60°C) and from 108.6 Hz to 179.9 Hz (120°C).

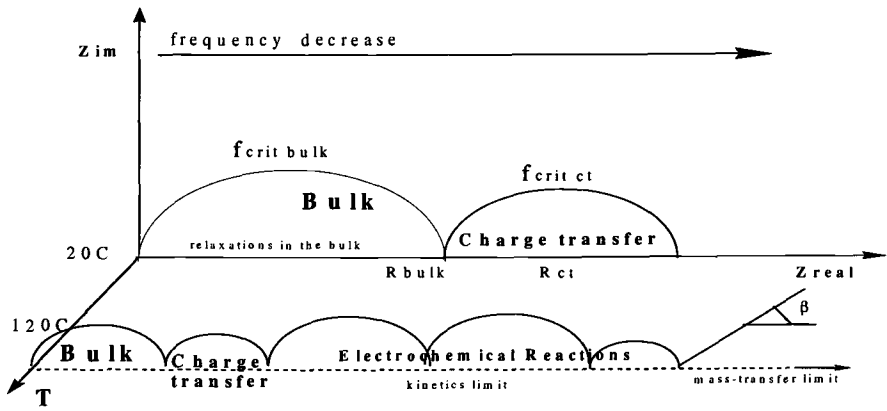


Figure 2 - Diagram illustrating the influence of temperature changes on EIS plot for a typical oil

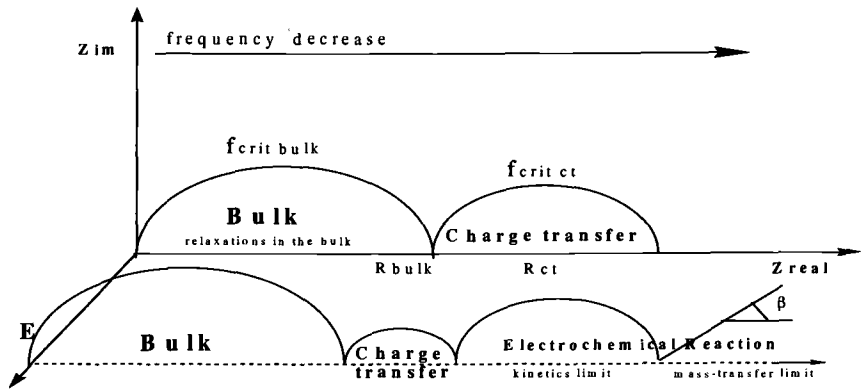


Figure 3- Diagram illustrating the influence of electrochemical potential on EIS plot for a typical oil at fixed temperature

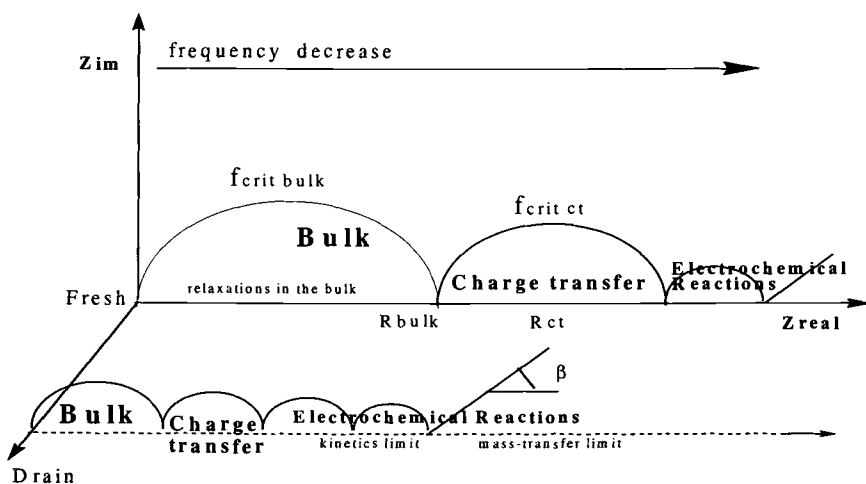


Figure 4 - Diagram illustrating the influence of oil aging on EIS plot for a typical oil

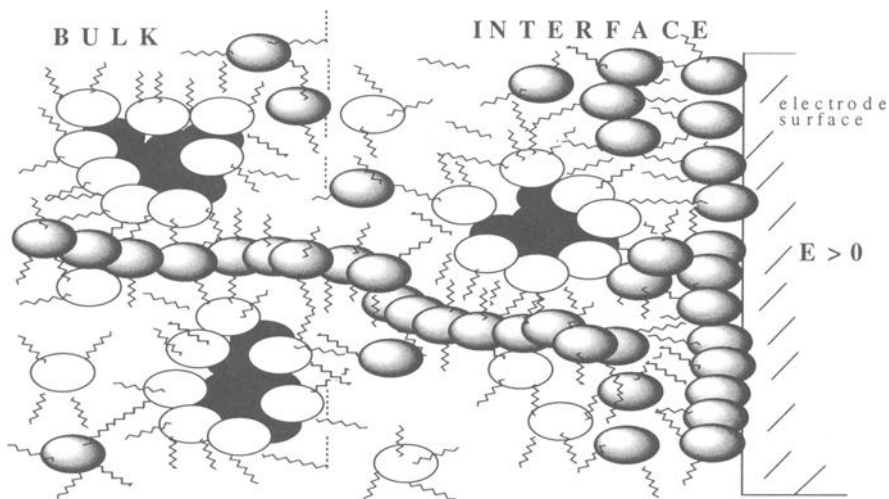


Figure 5 - Proposed mechanism of oil aging

When electrochemical potential reached typical values of discharge for detergents ($\sim +8V$) and dispersants ($\sim -7V$), additional combination of semicircular/45° straight-line profiles

were observed at mHz frequencies region of the Nyquist plot. The reduction or oxidation activity of detergents at high anodic potentials and dispersants at high cathodic potentials was observed. These features were much more pronounced for samples analyzed at 120°C, where all electrochemical processes are facilitated in higher conductive media. For dispersants samples reversible reduction at high cathodic region or detergents reversible oxidation at high anodic potentials were prominent. Reduction or oxidation activity of oil degradation products in more conductive media can be responsible for additional reactions. The processes of this type were also detected by the cyclic voltammetry studies. Additional reactions of oil degradation products were more prominent for samples analyzed at 120°C.

A typical detergent DETA Tan Delta (loss factor/ permittivity) versus temperature curve is seen in Figure 6. The $\tan \delta$ peak temperatures and their corresponding frequencies are: 17.82, 100 Hz, 53.3°C, 21.79, 500 Hz, 82.6°C and 22.25, 1000 Hz, 107.4°C. The peak frequency (F) is converted to polarization time (τ) with the following equation:

$$\tau = 1/2\pi F \times 1000 \text{ (ms)}$$

The DETA conductivity (PS/cm) of detergents, dispersants and base oils varied by several orders of magnitude, see Table 1. Detergent conductivity is $10^4 - 10^5$, dispersants $10^2 - 10^3$ and base oils 10^1 to 10^2 PS/cm. The structures displayed in Figure 5 represent molecular associations leading to enhanced conductivity relative to base oils.

For example, for F equal to 1000 Hz, τ is 0.16 ms. The $\tan \delta$ peak temperature is plotted versus the logarithm of the polarization time for a number of calcium detergents in Figure 6. The most surface active detergent in this series is D and the least active is E. The variation in surfactancy can be attributed to higher calcium to substrate ratio and molecular weight differences. In Figure 7 variations of metal and substrate of the detergents are clearly distinguished in the DETA plot. The most active is the sodium sulfonate and the least active is calcium carboxylate. It appears that both the substrate (sulfonate, phenate and carboxylate) and metals (sodium, lithium and calcium) are essential factors. Dispersants and detergents are differentiated in Figure 8. The dispersants are much less surface active than the detergents.

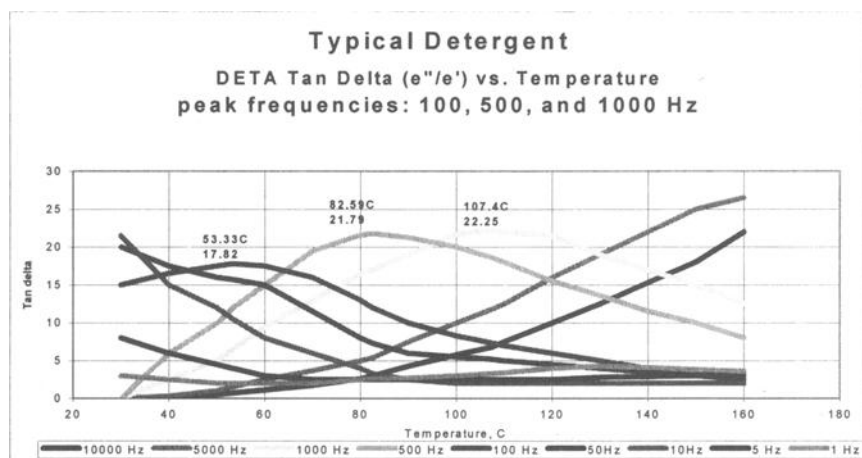


Figure 6 - Detergent DETA Tan Delta plot versus temperature

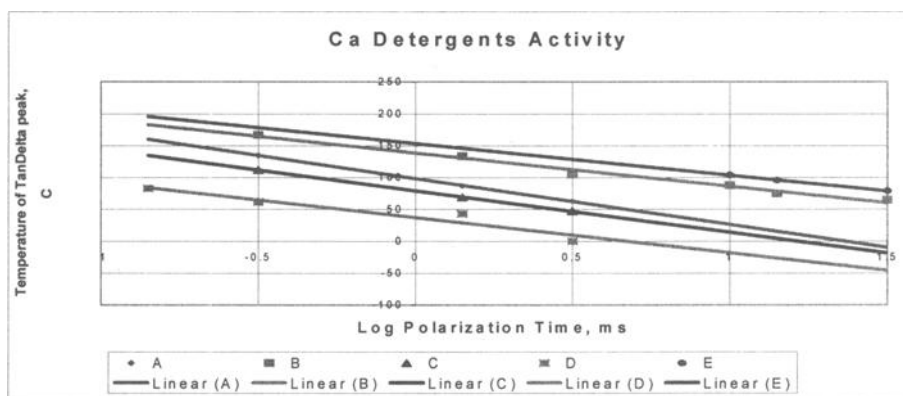


Figure 7 - DETA differentiation of activities of the Ca detergents

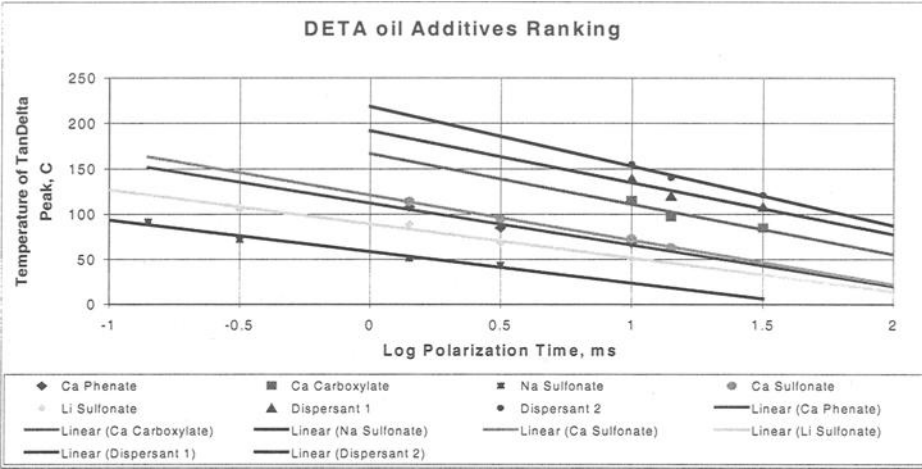


Figure 8 - DETA differentiation of activities of detergents and dispersants

Table 1

Detergent and Dispersant Conductivity (18Hz, 100C) by DETA

Sample (Typical 50% chemical in oil)	Conductivity (PS/cm)
Detergent 1	107,000
Detergent 2	84,000
Detergent 3	37,000
Detergent 4	22,000
Detergent 5	12,000
Dispersant 1	1080
Dispersant 2	910
Dispersant 3	770
Dispersant 4	620
Dispersant 5	540
Base Oil X	120
Base Oil Y	55
Base Oil Z	35

Conclusions

EIS, supported by cyclic voltammetry has been applied to detection of lubricant additives and studies of changes in oil electrochemical properties caused by oil degradation. Dependencies of polymer bulk resistance and relaxation frequency, charge transfer resistance and relaxation frequency, electrochemical reduction or oxidation reactions of individual species, and formation of polymeric film on electrode surface upon oil temperature, applied electric field, and TAN/TBN, were investigated.

EIS provides a wide range of opportunities for diversified analysis of polymer-based solutions. The developed EIS method was used for monitoring oil quality, and quantification of oil composition and specific chemistries in oil formulations. The scanning DETA technique clearly differentiates various detergents, dispersants and base oils.

6. References

- [1] Lvovich, V. "Electrochemical Sensors for Direct On-line Analysis of Chemical and Physical Properties of New and Used Oils," presented at *14 Annual Lubrizol Technical Symposium*, April 1999.
- [2] Morishita, S., Suzuki, K., Ashida, T., Tasaka, K., and Nakada, M. "Development of an On-Board Type Oil Deterioration Sensor," *SAE Technical Paper Series*, 1993, pp. 311-316.
- [3] Johnson, M. D., Korcek, S., and Schriewer, K. "In-service Engine Oil Condition Monitoring - Opportunities and Challenges," *SAE Technical Paper Series*, 1994, pp.183-190.
- [4] Ciureanu, M., and Wang, H. "Electrochemical Impedance Study of Electrode-Membrane Assemblies in PEM Fuel Cell. Electrooxidation of H₂ and H₂/CO Mixtures on Pt-based Gas-Diffusion Electrodes," *J. Electrochem. Soc.*, 146 (11), 1999, pp. 4031-4040.
- [5] Zen, J.-M., Ilangovan, G., and Jou, J.-J., "Square-Wave Voltammetric Determination and AC Impedance Study of Dopamine on Preanodized Perfluorosulfonated Ionomer-Coated Glassy Carbon Electrodes," *Anal. Chem.* 71, 1999, pp. 2797-2805.
- [6] Ion, A.C., Moutet, J.-C., Pailleret, A., Popescu, A., Saint-Aman, E., Siebert, E., and Ungureanu, E., "Electrochemical Recognition of Metal Cations by Polycrown Ether Ferrocene Films Investigated by Cyclic Voltammetry and

- Electrochemical Impedance Spectroscopy," *J. Electroanal. Chem.* 464, 1999, pp. 24-30.
- [7] Betova, I., Bojinov, M., Lankinen, E., and Sundholm, G., "Studies of the Reduction or Oxidation Behavior of some Polythiophene Derivatives by Impedance Spectroscopy in Symmetrical and Asymmetrical Configurations," *J. Electroanal. Chem.* 472, 1999, pp. 20-32.
- [8] Vorotyntsev, M., Badiali, J.-P., and Inzelt, G., "Electrochemical Impedance Spectroscopy of Thin Films with Two Mobile Charge Carriers: Effects of the Interfacial Charging," *J. Electroanal. Chem.* 472, 1999, pp. 7-19.
- [9] Bisquert, J., Garcia-Belmonte, G., Fabregat-Santiago, F., and Bueno, P. R., "Theoretical Model for AC Impedance of Finite Diffusion Layers Exhibiting Low Frequency Dispersion," *J. Electroanal. Chem.* 475, 1999, pp. 152-163.
- [10] Wang, S. S., and Lee, H. -S., "The Application of AC Impedance Technique for Detecting Glycol Contamination in Engine Oil," *Sensors and Actuators B40*, 1997, pp. 193-197.
- [11] Kaden, H., Fichtner, W., and Ahlborn, K., "On-Line System for Lubrication Diagnostics," *MTZ Worldwide* 61, 2000, pp. 8-11.
- [12] Bento, M. F., Thouin, L., Amatore, C., and Montenegro, M. I., "About Potential Measurements in Steady State Voltammetry at Low Electrolyte/Analyte Concentration Ratios," *J. Electroanal. Chem.* 443, 1998, pp. 137-148.
- [13] Bento, M. F., Thouin, L., and Amatore, C., "Potential Measurements in Steady State Voltammetry at Low Electrolyte/Analyte Concentration Ratios. Role of Convection on Ohmic Drop: A Simplified Model," *J. Electroanal. Chem.* 446, 1998, pp. 91-105.
- [14] Bento, M. F., Thouin, L., and Amatore, C., "Steady State Voltammetry at Low Electrolyte/Reactant Concentration Ratios: What it Means and What it Does not Mean," *J. Electroanal. Chem.* 463, 1999, pp. 45-52.
- [15] Sato, A., Oshika, T., "Electrical Conductivity Method for Evaluation of Oxidative Degradation of Oil Lubricants," *J. Soc. Tribol. and Lubrication Eng.* 48 (7), 1991, pp. 539-544.
- [16] Kauffman, R. E., "On-Line and Off-Line Techniques for Monitoring the Thermal and Oxidative Degradations of Aircraft Turbine Engine Oils - Part 1: Laboratory Evaluations," *Lubr. Eng.* 11, 1995, pp. 914-921.

- [17] Kauffman, R., "Development of a Remaining Useful Life of a Lubricant Evaluation Technique. Part III: Cyclic Voltammetric Methods," *J. Soc. Tribol. and Lubrication Eng.* 44 (6), 1988, pp. 709-716.
- [18] Kauffman, R., U.S. Patent 5,071,527, 10 Dec. 1991.
- [19] Lee, H-S., Wang, S. S., Smolenski, D. J., Viola, M. B., and Klusendorf, E. E., "In Situ Monitoring of High-Temperature Degraded Engine Oil Condition with Microsensors," *Sensors and Actuators B* 20, 1994, pp. 49-54.
- [20] Wang, S. S., Lee, H-S., and Smolenski, D. J., "The Development of In-Situ Electrochemical Oil Condition Sensors," *Sensors and Actuators B* 20, 1994, pp. 179-185.
- [21] Joseph, J., Kim, H-O. L., and Oh, S., "In-Situ Electrochemical Sensor for Measurement in Nonconductive Liquids," *J. Electrochem. Soc.* 140, 1993, pp. L33-34.
- [22] Price, R. J., and Clarke, L. J., "Chemical Sensing of Amine Antioxidants in Turbine Lubricants," *Analyst* 116, 1990, pp. 1121-1123.
- [23] Farrington, A. M., and Slater, J. M., "Monitoring of Engine Oil Degradation by Voltammetric Methods Utilizing Disposable Solid Wire Microelectrodes," *Analyst* 122, 1997, pp. 593-596.
- [24] Jacob, S. R., and Compton, R. G., "Electrochemical Studies of the Automotive Lubricant Additive Zinc N-Dibutylthiophosphate," *J. Electrochem. Soc.* 146 (7), 1999, pp. 2598-2605.
- [25] Seanor, D. A., "Electrical Conduction in Polymers," *Electrical Properties of Polymers*, D. A. Seanor, Ed., Academic Press, 1982, pp. 16.
- [26] Hedvig, P. *Dielectric Spectroscopy of Polymers*, John Wiley, New York, 1977.
- [27] MacDonald, J. R. *Impedance Spectroscopy*, John Wiley, New York, 1987.

DYNAMIC TECHNIQUES—B

Brian C. Sisk,¹ Kathy Chuang,² and Wei-Ping Pan¹

Development of Bismaleimide/Cyanate Ester Copolymers

REFERENCE: Sisk, B. C., Chuang, K., and Pan, W.-P., “Development of Bismaleimide/Cyanate Ester Copolymers,” *Materials Characterization by Dynamic and Modulated Thermal Analytical Techniques, ASTM STP 1402*, A. T. Riga and L. Judovits, Eds., American Society for Testing and Materials, West Conshohocken, PA, 2001.

Abstract: Since the beginning of the space age, the goal of materials development in the aerospace industry has been to replace metal alloys with much lighter polymer resins, while maintaining the strength over a wide temperature range characteristic of metals. Polymers such as polyimides and epoxies have been used to satisfy many needs, but strength, temperature resistance, and ease of processing are difficult to incorporate into a single polymer.

Because of this gap, bismaleimides and cyanate esters, and possibly combinations of the two, are seen as having potential in applications where ease of processing characteristic of epoxies is desired, but for which temperature resilience better than that of epoxies is desired. In this paper, bismaleimide and cyanate ester compositions based on commercially available monomers are created and evaluated to determine what monomers are favorable.

Keywords: cyanate ester, bismaleimide, thermoset, aerospace

¹Chemistry Department, Western Kentucky University, 1 Big Red Way, Bowling Green, KY 42101.

²NASA Glenn Research Center, MS 49-3, 21000 Brook Park Road, Cleveland, OH 44135.

Introduction

Historical

The aerospace industry, including commercial and cargo carriers as well as the National Aeronautics and Space Administration (NASA), is constantly in search of new materials that are lighter, tougher, more thermally stable, and/or cheaper than those that are currently used. The demands of NASA are most rigorous of all, as materials used in spacecraft must not only stand up to the rigors of conventional flight, including high mechanical stresses and temperatures, but must endure additional stresses. These include high g-forces and the cryogenic temperatures of space. Because of these added stresses, materials used in spacecraft must not only be tough and thermally stable, but must resist high strains and brittleness at extremely low temperatures. Additionally, materials used on spacecraft are designed to be as light as is practical, as the cost in fuel of getting extra weight into space is extremely high.

Finding a material that meets such specifications requires that properties be carefully tailored, and certain attributes must be compromised to maintain others. Currently there are a number of different groups of polymers used in aerospace applications. Chief among them are polyimides, epoxies, bismaleimides (BMI), and cyanate esters (CE). While polyimides have excellent thermal properties, they have poor processibility compared to other thermoset resins, particularly epoxies [1]. Epoxies are the opposite, being easily processible but much less stable thermally [2]. Therefore, there is a significant market for a polymer that has the processibility of an epoxy with the thermal stability of a polyamide.

Bismaleimides have also found wide use in the aerospace industry. Generally blended with tougheners, BMI has been used in such applications as aircraft "skin." With similar processing characteristics as epoxies and being much more easily processible than polyimides, BMI's have been tailored to applications where extreme temperatures that require polyimides aren't found, but for which temperature resistance is still desired. The major drawback of BMI, however, is that they are very brittle, and generally require toughening either by thermoplastics or through allyl-functionalized hardeners [2, 3].

Cyanate esters have also seen use in certain structural applications, as well as wide use in the electronics industry. Early in development, the first cyanate ester, Cyanate A in this study, was used as a laminate for circuit boards. They also possess a number of properties that make them suitable to many other applications. Among these properties are reasonable moisture absorption, low dielectric constant, high glass transition temperature (T_g), and a high toughness at a given T_g , especially compared to epoxies [4]. Low dielectric constant and moisture retention have made cyanate ester resins very attractive to the electronics industry, finding use in devices such as circuit boards, radomes, and antennae [5].

There seems to be no polymer, however, that is extremely tough, has a high T_g , is easily processible, and possesses exotic characteristics that make them applicable in diverse situations. The development of such a polymer (or copolymer) would prove beneficial. Potential applications would include structures in future relaunchable vehicles (RLV) for NASA, which are scheduled to replace the current generation of space shuttles.

To this end, there is currently renewed interest in using BMI and cyanate esters for copolymerization in structural applications. Both are easily processible and have a high degree of thermal stability that has resulted in their use in various applications such as electronics and aircraft. Glass transition temperatures (T_g) of homopolymers range from approximately 180°C to 380°C for CE and 180°C to 360°C for BMI. The most common BMI used, here referred to as BMI A, has a T_g of 342°C.

Many BMI and CE are also compatible with each other, as both react through pi-bonds. This allows them to polymerize with each other. BMI typically undergoes crosslinking through the double bond, while CE trimerizes, forming a six-membered polycyanurate (commonly referred to as triazine) ring [6]. Blends of CE and BMI have been successfully marketed, used frequently as insulators or for circuit board production in the early 1980s. Its use in such applications capitalizes on its temperature stability as well as its low dielectric constant [7].

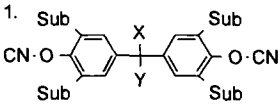
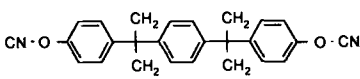
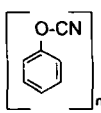
Cyanate Ester Monomers

Monomer properties of cyanate esters are much more diverse than those for BMI. Physical states vary from liquid to extremely viscous semisolid to crystalline solid among different monomers, even at room temperature. Color varies from white to amber to a deep red. Melting points also vary from well below room temperature for liquids up to 106°C for the crystalline solids. Cure conditions used are the same regardless of the melting point.

The structures of cyanate ester monomers vary greatly, more so than those of BMI. In addition to having a number of different groups possible between the aromatic rings, the aromatic rings themselves may be substituted. This allows for a much wider variety of properties among neat CE resins.

Some selected cyanate esters follow. Note the "base structures" below, one of which forms the basis for each monomer (Table 1) [8].

Table 1 – T_g Values for selected Cyanate Ester Monomers

<div style="display: flex; justify-content: space-around; align-items: flex-end;"> <div style="text-align: center;"> <p>1.</p>  </div> <div style="text-align: center;"> <p>2.</p>  </div> <div style="text-align: center;"> <p>3.</p>  </div> </div>					
Monomer	Base	X	Y	Sub	T_g (°C)
Cyanate A	1	CH ₃	CH ₃	H	289
Cyanate B	1	H	H	CH ₃	252
Cyanate C	1	CH ₃	H	H	258
Cyanate D	2	N/A	N/A	N/A	192
Cyanate E	3	N/A	N/A	N/A	~380

BMI Monomers

Two BMI monomers were used in this study. One, referred to here as BMI A, has a T_g of approximately 342°C. The other, referred to as BMI B, has a T_g near 177°C. Their structures are seen below in Figure 1.

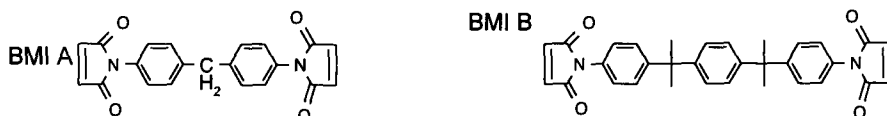


Figure 1 – Structures of the two BMI used

Selection of Monomers

As stated, there is a significant variety of monomers, particularly of cyanate esters. By varying nature and composition of these monomers, a wide variety of resins can be created. A list of the cyanate ester monomers used in this research follows (Table 2) [7].

Table 2 – T_g vs. Intralaminar Fracture Toughness (G_{IC})

Monomer	$T_g(^{\circ}\text{C})$	$G_{IC}(\text{J/M}^2)$
Cyanate A	289	140
Cyanate B	252	175
Cyanate C	258	190
Cyanate D	192	210
Cyanate E	350-380(est)	60
BMI A	342	...

Table 2 shows the glass transition temperature as well as the intralaminar fracture toughness value at room temperature. The glass transition is a measure of the point at which an amorphous polymer switches from a glassy to rubbery polymer, and the intralaminar fracture toughness is the amount of energy per cross-sectional area required to fracture the polymer. The former is a measure of thermal stability, the latter of physical stability. In general, as the glass transition temperature increases, a polymer becomes less tough (as measured by G_{IC}) because of the same factors that increase T_g : namely, increased crosslink density and stiffness. Table 2 largely mirrors that phenomenon.

Experimental

Monomers Used

The monomers used in this experiment are Cyanate A, Cyanate B, Cyanate C, Cyanate D, and Cyanate E cyanate esters, and BMI A and B. These names used to refer to the compositions are arbitrary. The compositions will vary, but with each employing a base concentration of a non-viscous monomer making up roughly 50% of the cyanate ester base mixture by mass. Other cyanate esters are added to change physical and thermal properties. One of the BMI may also be added from 0% to 20% by mass.

Cure Cycle

The cure cycle used is the one recommended by the manufacturer of the cyanate ester monomers for full cure. The cycle follows in Table 3.

Table 3 - *Curing Cycle*

Ramp (°C/min)	Temperature (°C)	Hold (min)
10	177	240
10	210	120
10	250	120

Thermal Analysis

Three main thermal techniques are applied to the cured samples. They include dynamic mechanical analysis (DMA), thermomechanical analysis (TMA), and differential scanning calorimetry (DSC).

DMA applies a physical stress to a sample, and measures changes in the sample as a function of temperature and time. The stress can be constant or oscillating, and the frequency can be controlled if the latter. In this study, a force with an amplitude of $\pm 0.500\text{N}$ was applied at a frequency of 1Hz. The parameters determined were storage modulus, a measure of the elastic nature of the sample, loss modulus, a measure of the viscous nature of the sample, and tan delta, a measure of the loss modulus divided by the storage modulus. This final value provides essentially a "viscoelastic index," and as such is an inherent property of the sample, and is sample geometry independent.

DSC measures calorimetric events by determining the difference in heat supplied to a sample and reference while keeping them at the same temperature. Additionally, the heating rate is modulated, which enables the instrument to determine what component of heat flow reverses, and which does not. These roughly correlate to reversible and irreversible transitions, the separation of which allows phenomena such as curing and glass transitions to be separated. DSC is used in this study primarily to monitor the cure.

TMA measures expansion as a function of temperature. Generally, the instrument is used to measure linear expansion, as in this study, although it is capable of performing volumetric expansion. Its utility is in providing coefficient of thermal expansion (CTE) values, and T_g values, as the CTE generally increases after the T_g .

Determination of Glass Transition Temperature

Three methods are traditionally used to monitor T_g values, DSC, TMA, and DMA. For these samples, it is assumed that DMA measures the most accurate (though not necessarily most precise) T_g values. This is because both TMA and DSC depend on a significant increase in molecular freedom of rotation in the amorphous phase, something that does not occur readily among thermosets. However, there is a distinct drop in DMA-measured storage modulus, and peaks in loss modulus and tan delta. All three methods were used early in the study, with DSC and TMA proving unable to provide distinct and repeatable T_g values.

Prediction of the Glass Transition Temperature

There are two formulas that are regarded as suitable for predicting T_g values. These are Fox's Rule, and the formula for weighted average. Since there does not seem to be universal consensus for either, both are used. The formulas are as follows.

$$\text{Fox's Rule:} \quad 1/T_g = \Sigma(X_i/T_{gi})$$

$$\text{Weighted Average:} \quad T_g = \Sigma(X_i T_{gi})$$

The values determined are similar, though not identical, for both. As will be seen, however, the trends are generally the same.

Results and Discussion

Predicted vs. Actual T_g

The monomer composition is likely the most difficult and important aspect of determining a method for creating a copolymer. Effectively choosing monomers as well as their relative amounts depends not only on their individual properties but also how they interact with each other. Therefore, it is important to calculate how a copolymer compares to what would be expected from it given the properties of its monomers.

The simplest way to do this is to divide the measured T_g by the expected T_g . The expected T_g is determined by predicting the T_g based on the monomers used, given homopolymer values determined using the same curing cycle. This is done for both the weighted average expected T_g as well as that predicted by Fox's rule, as both are used. The result is a dimensionless ratio that will be called " T_g ratio." Any copolymer with a T_g factor greater than one shows a favorable interaction among its constituent monomers; a T_g factor lower than one denotes an unfavorable interaction. A higher T_g ratio means that, when using a specific monomer to elevate the T_g , less of that monomer is required than would be predicted to achieve a specific T_g . Since monomer T_g values correlate well with stiffness and a lack of fracture toughness, less of such a T_g -elevating monomer could result in greater overall strength for the copolymer.

In the initial group of compositions, Cyanate B was used as a base CE, Cyanate D was used to add strength, and Cyanate E was used to elevate the T_g . In addition, BMI A was added for increased T_g and because it was hoped that the interactions between BMI and CE would be favorable.

Plots of T_g factor vs. actual T_g were made using both methods of T_g estimation, weighted average and Fox's rule (Figure 2). The purpose of this was to see if there were any temperature ranges that were better or worse than expected. Since it is known what monomers were used to raise and lower the T_g , it can be roughly determined which monomers are more or less responsible for the poor interaction. What is seen are two curves that appear parabolic in nature (Figure 3). From T_g values of 250 to 275°C the average T_g factor seems to decline, indicating that compositions with a T_g around 275°C seem to be disfavorable given the starting monomers. Until roughly 290°C, the T_g factor values seem to remain flat, but sharply increase after 300°C and do so for the remainder of the range.

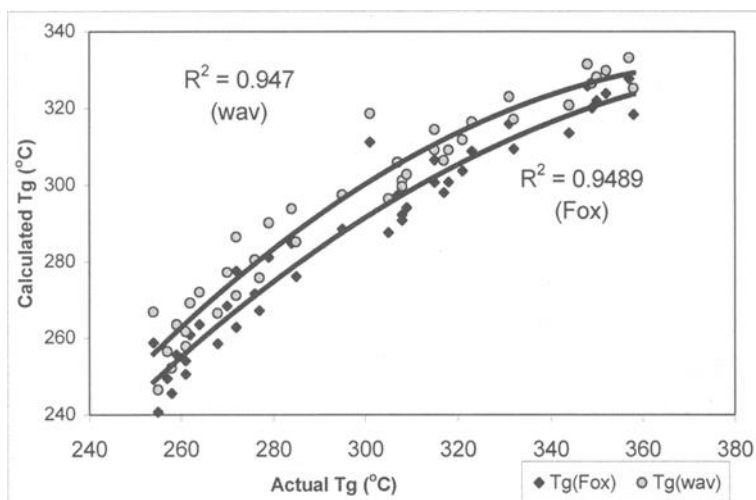


Figure 2-Calculated vs. Actual T_g

What must be realized is that these trends are not due to any nature of that particular temperature. Rather, the combinations of monomers that in this case would yield such a monomer vary in their favorability. The reason for this is likely explained by plotting T_g factor values against each monomer individually, except for Cyanate B, which was kept between 40 and 50% by weight of the total composition. Since it is used in all of the compositions in similar amounts, no trend can be determined.

This sort of plot is made for BMI A, using both Fox's Rule (Fox) and weighted average (wav) T_g values. Regression analysis of both Fox's Rule and weighted average data sets results in trendlines for each with a slightly positive slope and a correlation (R^2) just above zero. (Figure 4). This indicates that BMI A may have a slight favorable (or at least neutral) interaction with most of the other components. The fact that the correlation is low indicates that BMI A has a lesser effect upon T_g factor values than other components may.

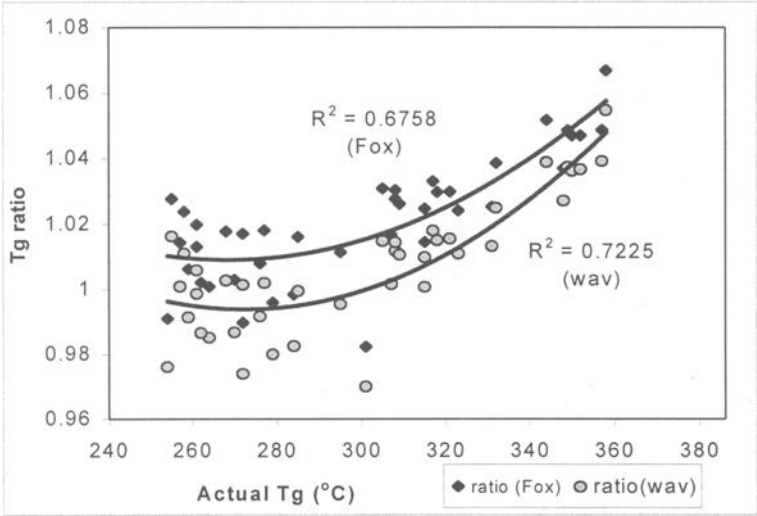


Figure 3 – *T_g Ratio vs. Actual T_g*

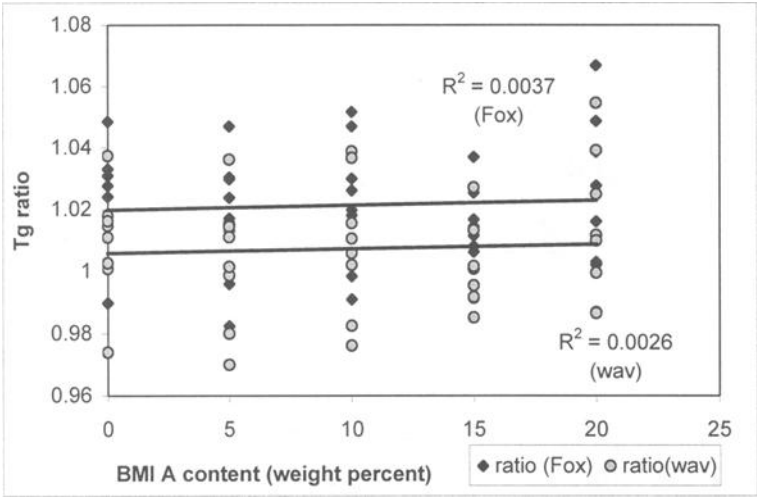


Figure 4 - *T_g Ratio vs. Concentration BMI A*

The relationship between T_g Ratio and Cyanate E is largely like the one seen between T_g Ratio and BMI A in Figure 4, with a slightly positive slope and positive but near-zero R² values. As the correlation is low, the effect isn't all that profound. The slope and correlation of the regression line indicate that the monomer should perform as well as predicted, though not likely significantly better. Regression analysis of the effects of

adding Cyanate E or BMI A show that their presence should not inherently result in significant deviations from calculated T_g values.

Finally, T_g factor vs. monomer weight percent is plotted for Cyanate D. What is seen is a parabolic curve, similar to that in the T_g factor vs. T_g plot (Figure 5). There is a comparably high positive correlation (with a negative slope) between Cyanate D content and T_g factor at low to medium Cyanate D concentrations, indicating that the interaction between Cyanate D and the other components used is an unfavorable one, at least for the amounts of Cyanate D that would be used. Note that the curve does rebound, but only above 30% Cyanate D content. Even then, there is no net advantage in T_g Ratio for Cyanate D, as the highest T_g Ratio values occur at or near 0% Cyanate D content. Importantly, the correlation coefficients are much higher for this component than for the others, which shows that it is the most important factor in determining T_g Ratio. Cyanate D shows a correlation of 0.5442, compared to 0.0026 for BMI, for example (both values reported for weighted average data).

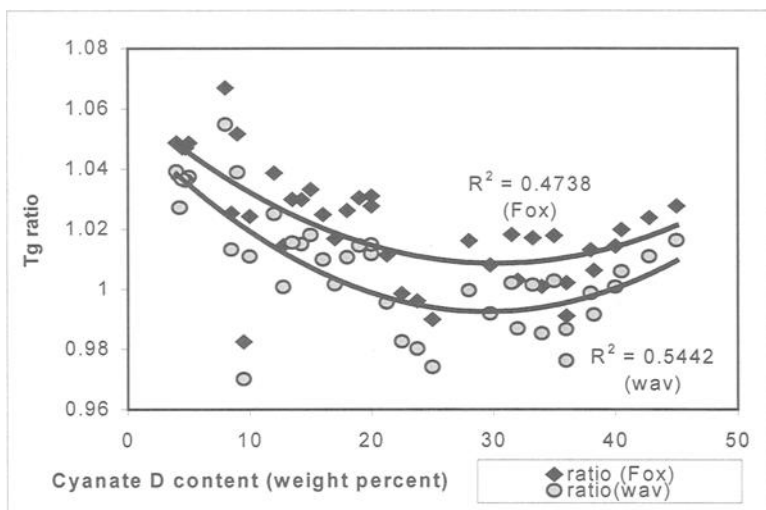


Figure 5 - T_g Ratio vs. Concentration Cyanate D

At higher concentrations, one can see that the slope of the curve levels out and then becomes positive. This occurs near 30% (by weight) Cyanate D. Remembering the negligible trends that existed with the other components, the question is why this clear trend exists with cyanate D. There can be a number of reasons for this trend. Possible explanations include compatibility, kinetics, and chemical structure of the monomers.

Compatibility could explain why Cyanate D seems to have a better relationship with itself than with any of the other components, including the upturn at higher concentrations of Cyanate D. Perhaps at 30% Cyanate D, there are enough homomolecular Cyanate D reactions to regain favorability. This trend could explain the curve in the T_g factor vs. T_g plot, because the increased T_g factor at lower temperatures (after the minimum) would be simply due to large Cyanate D content. Additionally, it may explain the positive correlation between concentration of T_g factor with both BMI A and Cyanate E. Increasing the amounts of these components decreases the amount of

Cyanate D for a given composition. These two components may have otherwise had slight positive correlations regardless, but they are in large part, if not entirely, due to the lessened influence of Cyanate D at high concentrations of BMI A and Cyanate E.

Cure Investigations

Cure kinetics is one choice for explaining the unsuitability of Cyanate D in compositions. FT-IR kinetic analysis showed that Cyanate D cures at a rate roughly half that of Cyanate C at 177°C, for example, when each is cured independently of one another. If Cyanate D is the slowest curing monomer in a batch, it is likely that the other, more reactive monomers will form a nearly complete network around pockets of Cyanate D, leaving gaps in the structure. If this were to occur, significant amount of the Cyanate D would cure by itself, after the matrix cured. Nearly all of the monomer will cure eventually, whatever its nature, but if it does so slowly a significant number of pockets with little adhesive area to the matrix may be formed.

If rate effects are significant, a number of other physical effects should be expected as well. Correlation of peak reaction rate vs. temperature follows, determined through DSC analysis, as seen in the Table 4.

Table 4 – *Peak Cure Temperature for Selected Monomers*

Monomer	Peak Cure (°C)
Cyanate B	323
Cyanate C	228
Cyanate D	278
Cyanate E	227
BMI A	190
BMI B	177

A greater exothermic/endothermic response at a given temperature implies a faster cure at that temperature (BMI cure shows an endotherm, cyanate ester cure an exotherm). Also, since the heat flow (exotherm/endotherm) increases slightly from room temperature, and then quickly at the curing onset, a relationship exists between rate of cure at 177°C and the temperature of the peak cure. In general, the greater difference between the peak temperature and 177°C, assuming the peak is higher, the more slowly the reaction proceeds. Note that while Cyanate D cures slowly, it is by no means the slowest. That distinction would go to Cyanate B, which experiences a peak exotherm nearly 50°C higher than any other monomer studied. The question then becomes, if Cyanate D performs poorly because of slow cure, why is there no problem with Cyanate B?

To determine whether any kinetic effect exists, multiple monomers can be combined and then subjected to DSC analysis as done on homomonomer compositions. There would be a few possible DSC profiles expected. One possibility would be two peaks, with maxima near those values found when scanning the individual monomers used. However, since the reactions are expected to be trimolecular, it is possible that there

would be four peaks - two corresponding to homomolecular reactions, and two corresponding to heteromolecular reactions, involving two molecules of one monomer and one of the other.

When this was done for Cyanates B and C, it was found that mixing those two monomers and curing them results in a single peak, somewhere between the maximum cure temperatures for the individual components. Incidentally, while the peak was broader than for a homomonomer cure, it wasn't markedly so, and there was little if any curing at the maximum cure temperature of the low-temperature-cure monomer. This indicates that the presence of different monomers greatly affects the ability of a monomer to even react with itself, indicating that the reactivity of these systems may be more complicated than previously believed. While the presence of only a single peak might be confusing, it is beneficial, as it shows that the components that cure at lower temperatures are prevented from curing before those that generally cure at higher temperatures, for whatever reason. This effect will have the effect of preventing large-scale heterogeneities that could, as mentioned, seriously compromise the stability of the resins.

This effect was also possible when curing BMI with CE, though it depended on the monomers used. When curing Cyanate B with BMI A, neither the BMI melting or curing peaks were seen. Evidently, when the cyanate melts, it dissolves the BMI to such a degree that its melting peak was not evident. Additionally, as it is able to readily co-cure with the cyanate component, no BMI curing endotherm is seen, only the cyanate curing exotherm. Additionally, it is not possible that the BMI endotherm was simply overwhelmed by the larger cyanate exotherm. The exotherm (in Joules/gram) for the mixture was actually larger than the pure cyanate exotherm, 615 J/g for the mixed sample, and 533 J/g for the pure Cyanate B sample. This would be impossible if the mixed sample represented the standard Cyanate B exotherm overlapping the BMI A endotherm. The fact that the mixed exotherm is larger implies fundamentally different chemistry than that seen in homomonomer interactions, which would be due to BMI/CE co-curing. Thus, Cyanate B and BMI A are able to react in a favorable manner, one in which they are able to thoroughly co-cure.

However, this was not the case for all monomers systems tested. Notably, when Cyanates B and D were combined, the result was a curing exotherm that looked more similar to an overlay of the two individual monomers, rather than a combination. This implies that Cyanate D retains its individuality when it is cured, something that is detrimental to the homogeneity (and hence the performance) of the system.

Even more distinct was the case of mixing Cyanate D and BMI A. The result was a curing endotherm for the BMI component, and a curing exotherm for the cyanate component. Clearly, there is very little if any cohesion between the two phases if they are self-curing, which must be the case if they retain their individuality to this degree.

Conclusions

A number of bismaleimide/cyanate ester compositions can be generated, with T_g temperatures that range from approximately 170°C to 350°C. This allows a great deal of "tunability," so that many different compositions can be created with a wide variety of physical properties, particularly T_g values. Given that an increase in strength follows a

decrease in T_g , a range of compositions can be created to maximize whichever property is desired while keeping the others within tolerances.

Bismaleimides, though they do have desirable properties, can be used only as a minor component in the resins, as they have limited solubility in liquid cyanate ester monomers. This limits bismaleimide concentration to approximately 15-20 wt%. Fortunately, Cyanate E can be substituted for BMI A, as its T_g is even higher. The limited solubility is more of a problem with BMI B, which has a lower T_g than any cyanate ester except Cyanate D, which is undesirable to use because of its demonstrated poor performance. Hence, BMI B has no ready replacement.

Cyanate D cannot be recommended unless it is a major component (over 30%), as it is detrimental to the T_g of the resulting composition when used as a minor component. Even then, it is not particularly beneficial, as its T_g Ratio is highest when none is used, as mentioned previously. Unless compositions with T_g 's near the lower range (below 245°C) are desired, it is recommended that Cyanate D not be used at all. This is particularly true for compositions that include BMI A, with which it experienced a strongly disfavorable reaction. Additionally, it is likely that the lower end of the temperature spectrum could be serviced by epoxy compositions, meaning that Cyanate D should experience limited use unless some of the more esoteric properties of cyanate esters are needed, such as low dielectric constant and radar transparency.

The most interest, at least for NASA, seems to be in a resin which has a T_g , defined as the onset of storage modulus by DMA, of roughly 250°C. As there is generally a 30°C lag between onset of storage modulus and tan delta for polymers such as these, a peak tan delta of 280°C is needed. To create this, the best composition from this study would be a base of Cyanate B, to which either Cyanate E or BMI A are added. A resin that was composed of 50% Cyanate B, 25% Cyanate E, and 25% BMI A would supply the desired properties.

Despite the disadvantages of bismaleimide/cyanate ester systems, they have significant potential for situations where ease of processibility is a priority, and some temperature resistance is desired. They may be able to fill a niche between epoxy resins and polyimides.

References

- [1] Lin, S.-C. and Pearce, E. M., *High-Performance Thermosets*, 1993, p13.
- [2] Barton, J. M., Hamerton, I., Jones, J. R., and Stedman, J. C., "Mechanical Properties of Tough, High-temperature Carbon Fibre Composites from Novel Functionalized Aryl Cyanate Ester Polymers," *Polymer*, 1996, 37(20), pp. 4519-4522.
- [3] Morgan, R. J., Jurek, R. J., Donnellan, T., and Yen, A., "Tough, Processible High Temperature Bismaleimide (BMI) Matrix Composites," *Proceedings of the American Chemical Society Division of Polymeric Materials: Science and Engineering*, 1994, pp. 426-427.
- [4] Shimp, D. A., and Chin, B., "Electrical properties of cyanate ester resins and their significance for applications," *The History and Technology of Cyanate Ester Resins*, Hamerton, I. Ed., 1994, pp. 230-247.
- [5] Hamerton, I., "Introduction to cyanate ester resins," *The History and Technology of Cyanate Ester Resins*, Hamerton, I. Ed., 1994, pp. 1-4.

- [6] Osei-Owusu, A., Martin, G. C., and Gotro, J. T., "Catalysis and Kinetics of Cyclotrimerization of Cyanate Ester Resin Systems," *Polymer Engineering and Science*, 1992, 32(8), pp. 535-542.
- [7] Motoori, S., Kinbara, H., Gaku, M., and Ayano, S., "BT Resin for Electrical Insulation Material," *IEEE*, 1981, p168.
- [8] Shimp, D., "Applications of Cyanate Ester (CE) Resins," *Proceedings of the American Chemical Society Division of Polymeric Materials: Science and Engineering*, 1994, pp. 561-562.

Anatoliy Ya. Goldman¹

Application of Theory to Prediction and Analysis of Dynamic Mechanical Properties of Polymer Composites

REFERENCE: Goldman, A. Ya., "Application of Theory to Prediction and Analysis of Dynamic Mechanical Properties of Polymer Composites," *Materials Characterization by Dynamic and Modulated Thermal Analytical Techniques, ASTM STP 1402*, A. T. Riga and L. Judovits, Eds., American Society for Testing and Materials, West Conshohocken, PA, 2001.

Abstract: A comparison was made between experimental and computed dependencies of the dynamic modulus, and the mechanical loss tangent of the composites with a glassy polymer matrix - styrene-acrylonitrile (SAN) or (SAN-P) acrylonitrile-methacrylate-styrene in ASA plastic (acrylonitrile-styrene-acrylic) copolymer with particles of a peroxidic butylacrylate rubber (BAR-P). The composite material was obtained by emulsion polymerization.

An algorithm was developed for determining, prediction and optimization of the viscoelastic properties of composite materials with spherically layered inclusions by varying microstructure parameters.

The dynamic mechanical characteristics of the grafted copolymer that form a part of the ASA plastic allow the viscoelastic properties of ASA plastic to be predicted with better precision than if the dispersed face were identified with the BAR-P itself.

Keywords: composites, prediction, dynamic modulus, mechanical loss tangent

Prediction of mechanical properties of composites usually begins with the determination of effective elastic and viscoelastic properties at small strains. This is the traditional method used for prediction of the properties of structural materials. Many important structural polymeric materials, such as impact-resistant polystyrene, ABS plastics, rubber-modified epoxy resins, various dispersion-filled polymers, and heterogeneous polymer blends, can be considered composites.

In connection with the variation in composition and structure of polymer composites, the problem of predicting mechanical properties in relation to the structure, composition, and properties of the components assumes particular importance. At small strain, impact - resistant and other plastics behave

¹Technical Specialist, Ph.D, Materials Engineering Department. Alcoa CSI, 1205 East Elmore Street, Crawfordsville, IN 47933

as viscoelastic composites. Their elasticity moduli, although chiefly determined by the properties of the rigid matrix, are affected by the presence of dispersed phase particles.

The lowering of rigidity (in impact-resistant plastics) or its increase (for certain other materials) is of immediate interest to users of plastic materials because the rigidity is often the determinant property for structural applications of polymeric materials. To compensate for lower rigidity, it is customary to increase the wall thickness of the pieces, which increases both the weight and the cost.

Thus the establishment of relations between structure and mechanical properties in the range of small strains is part of the investigation and prediction of effective elastic and viscoelastic properties of composite materials.

The study of viscoelasticity at small strains in polymeric blends produces necessary information on the temperature limits for the use of such materials, on their typical transitions, and on the role of the components.

One important theoretical problem is the determination of the temperature dependencies of the elasticity modulus E and the loss tangent $\tan \delta$ (the tangent of the mechanical loss angle) of polymeric and composite materials from the data on the initial components and the phase structure of the heterogeneous composites. In designing new composite materials, it is important to secure as much information as possible on their structure from dynamic mechanical tests. The solution of the problems requires a unified theoretical approach. In this context, the verification of some theoretical models of two-component microheterogeneous systems assumes considerable importance.

Theoretical Models

Many studies have been devoted to the determination of effective elasticity moduli of composite materials with a disperse filler of heterogeneous media in general. The composition of the viscoelastic properties of heterogeneous composite materials is explicitly or implicitly based on an analogy between elasticity and viscoelasticity; therefore, to write the equations for the latter it is appropriate to first consider the former. Several approaches to this problem differ in degree of generality. The hydrodynamic approach does not reflect the dependence of the effective properties on the elastic properties of the filler, the latter being assumed to be completely rigid. The most general approach is the use of the methods of elasticity theory and geometrical models of the composite medium. These are reviewed [1-4] and have been the most widely used.

In the well-known work of Hashin and Shtrikman [4], fundamental estimates were obtained for the elastic constants of heterogeneous materials using variational principles without consideration of the morphology of the composite medium. From the hypothesis of a segmentally homogenous (i.e., homogenous within the confines of each phase) stress-strain state, the theorem of minimum excess energy, and the theorem of minimum potential energy, the lower and upper bounds were established for the effective shear modulus G_* and the bulk modulus K_* of the composite.

As the estimates of G_* and K_* , one may choose the arithmetic or geometric means of the bounds or even the boundary values themselves. If the moduli of the matrix are lower than the inclusion moduli, then it is natural to employ the lower bounds; if the matrix is more rigid than the inclusion, it is natural to use the upper bounds.

The deficiency of Hashin-Shtrikman relations is their insensitivity to the structure of the composite. Moreover, if the moduli of the components differ widely, the usefulness for predictive purposes is limited.

On the other hand, the Hashin-Shtrikman bounds are a convenient method for verifying approximate theories, because an equation resulting in a value of modulus outside these bounds can be considered erroneous.

Methods permitting the computation of the effective moduli of the composite directly are of great interest. The simplest method is given in [5]; where spherical inclusions are assumed, the interaction between them is neglected, and the mean stresses in the matrix coincide with the applied stresses:

$$K_* = K_2 \left[1 + \frac{3\varphi(K_1 - K_2)a_1}{1 - \varphi + 3\varphi\alpha_1 K_2} \right] \quad (1)$$

$$G_* = G_2 \left[1 + \frac{\varphi(G_1 - G_2)a_2}{1 - \varphi + \varphi G_2 a_2} \right] \quad (2)$$

$$\alpha_1 = \frac{1 - \nu_2}{2K_2(1 - 2\nu_2) + K_1(1 + \nu_2)}$$

$$a_2 = \frac{15(1 - \nu_2)}{2G_2(7 - 5\nu_2) + 2G_1(4 + 5\nu_2)}$$

where

ν_1 and ν_2 = Poisson coefficients of the inclusion and matrix, respectively

G_1 and G_2 = shear moduli

K_1 and K_2 = bulk moduli of the inclusion and matrix respectively, and

φ = the volume fraction of the harder phase.

It is possible to show that taking the interaction between the inclusions into account, in the framework of a dipole approximation of the self-consistent method, does not alter equations (1) and (2). Thus, they apply at a considerably higher dispersed-phase volume fraction than was assumed in [5].

Simple transformation of equations (1) and (2) shows them to be coincident with the Hashin-Shtrikman lower bound if the dispersed phase is more rigid than the matrix, and with the upper bound in the reverse case.

Another somewhat artificial variant of the self-consistent method is proposed in [3], where the deformation of a spherical inclusion is considered. The inclusion is surrounded by a matrix layer in an infinite isotropic medium that has the properties of the composite; that is, the infinite isotropic medium has the effective properties being sought. Solving the resulting mechanical boundary value problem with subsequent application of the energy criterion for effective

homogeneity gives the following relationship for K_* and G_* of a filled composite material:

$$K_* = K_2 + \frac{(K_1 - K_2)\varphi}{1 + (1 - \varphi) \frac{(K_1 - K_2)}{(K_2 - 4G_2/3)}} \quad (3)$$

$$G_* = G_2 + \frac{(G_1 - G_2)\varphi}{1 + (1 - \varphi)(G_1 - G_2) \frac{[6(K_2 - 2G_2)]}{[5G_2(3K_2 - 4G_2)]}} \quad (4)$$

The solution for K_* of a polydisperse model [4] coincides with equation (3). Linearized relations of the form of equations (3) and (4) (at $\varphi \rightarrow 0$, $1 - \varphi \approx 0$) coincide with formulas obtained [5] for a model with a small volume fraction of spherical inclusions (a single inclusion in an infinite matrix) and also with the limiting relation for G_* of a polydisperse model. Thus for a composite with spherical inclusions randomly distributed in a matrix, all the known methods lead to the same end expressions. If G_* and K_* are known, the effective Young's modulus of the composite is

$$E_* = \frac{9K_*G_*}{3K_* + G_*} \quad (5)$$

In the limiting case when both components are incompressible ($K_{1,2} \rightarrow \infty$, $\nu_{1,2} = 0.5$), it follows from equations (1) and (2) that

$$E_* = E_2 + \frac{\varphi(E_1 - E_2)}{1 + \frac{2}{5}(1 - \varphi) \frac{(E_1 - E_2)}{E_2}} \quad (6)$$

where E_1 and E_2 are the Young's moduli of the dispersed and matrix phases respectively.

These solutions were obtained under the assumption of isolated, (noninteracting) filler inclusions. However, as studies of filled composites have shown, filler particles can form space-filling structures at volume fractions considerably below the maximum packing fraction φ_{\max} of typical "closepacking" arrangements. In a given range of volume fractions, the particles may form a "coagulation network" that can contribute to the effective mechanical properties of the composite and can accept external loads. The introduction of aerosol or soot particles into polyethylene leads to a structural network of the filler forming a self-generated reinforcing framework. In calcite-filled polyethylene the filler particles also form an aggregate structure.

A description of the effective elastic characteristics of a polymeric composite with a rigid aggregating filler has been proposed [6]. A peculiarity of such a medium is the varying cohesion of the inclusions depending on their volume fraction. This varying cohesion is accounted for by the introduction of an additional parameter. A method is discussed for the determination of the cohesiveness factor by statistical modeling of the medium geometry. The

marked influence of the aggregation on the relation between the elasticity modulus and the volume fraction of the filler is demonstrated by several examples.

Another characteristic of real composite materials is the complex structure of the particles of the dispersed phase and the appearance of transition layers on the boundary between the dispersed phase and the polymer matrix. Indeed, polymer systems in which one of the phases is continuous (polymer matrix) and the other disperse have found wide application as impact-resistant, damping, and film-forming materials. The structure of the dispersed-phase particles in such materials is quite complex. In many instances, it contains a copolymer formed as a result of grafting of the matrix polymers onto the dispersed-phase polymer. Then, on the boundary between the composite phases are layers that can be either very pliable or quite rigid (the so-called shell). Some polymer systems consist of a nucleus or core and several shells with differing properties. The properties of such systems are often different from those of analogous systems with homogeneous particles. To predict the viscoelastic behavior of such composites, one must account for the effects of particle shape, composition, geometry of the transition layers and properties.

Computed and Experimental Characteristic

A model has been proposed [7] for the prediction of the viscoelastic behavior of polymer composites with layered, quasispherical particles having multiple, differing layers. To compute the viscoelastic parameters of such composite materials the effective (self-consistent) field method was used. In this method the problem of the intersection of many particles in the composite is reduced to the problem of one isolated, spherically layered particle immersed in the matrix within a homogenous external field. For the solution of the problem, an effective algorithm was devised that is capable of considering particles with a practically unlimited number of layers with arbitrary viscoelastic properties. This algorithm, incorporated into a computer program, allows the determination of the effective elastic moduli of a composite with spherically layered particles and the calculation of the stress concentration on discrete inclusions. To calculate the loss tangent of the composite, the Volterra correspondence principle was used.

The experimental verification of the complex inclusion model was carried out for a composite material (ASA copolymer). Its matrix consists of the copolymer styrene-acrylonitrile (SAN) of a 75:25 mass composition, and the dispersed phase consists of 200 nm spherical particles of a peroxidic butylacrylate rubber (BAR-P). The composite material was obtained by consecutive emulsion polymerization. The experimental procedure and testing was described in [8]. Using Perkin-Elmer series 7e DMA, the dynamic mechanical test for ASA plastic and constituent components was performed.

For composites with inclusions having a core of radius $a_1 \sim 26.5$ nm and an external radius $a_2 \sim 100$ nm and having an inclusion volume fraction of 20%, $E.(T)$ and $\tan \delta.(T)$ are shown in Figures 1 and 2, and the dependencies of the

same parameters on the relative core and shell dimensions are shown in Figure 3.

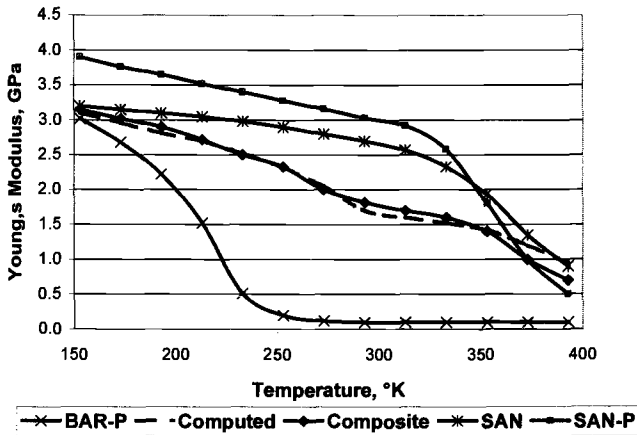


Figure 1 – Temperature dependencies of Young's modulus of ASA copolymer and constituent components

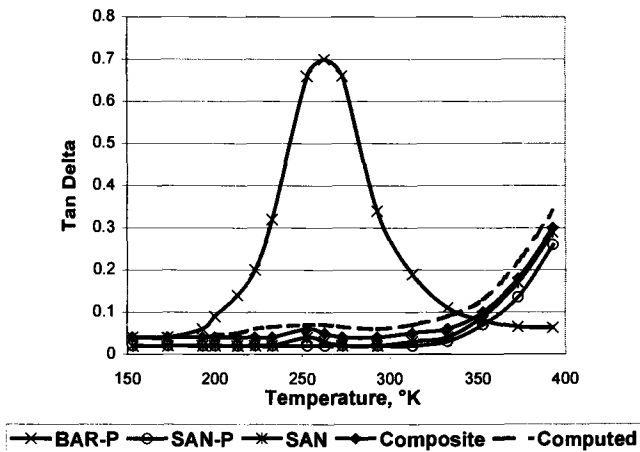


Figure 2 – Temperature dependencies of Tan Delta of ASA copolymer and constituent components

The test temperature (243 K) corresponds to the first maximum of the

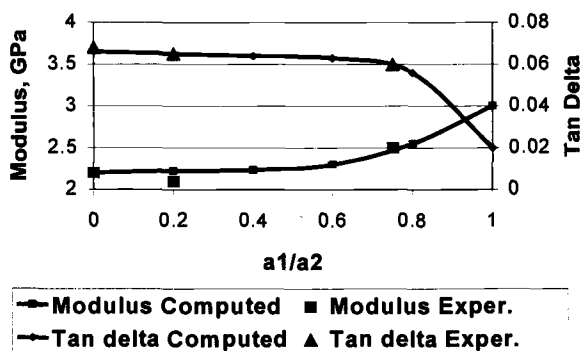


Figure 3 – *Dependence of the viscoelastic properties on the relative core size of the dispersed particle*

$\tan \delta(T)$ curve. Coincidence of the theoretical and experimental values of the effective parameters is attained when material of the spherical layer in the inclusions is not BAR but the copolymer of SAN and BAR with a mass ratio (grafting degree) of 1:8. Figures 4 and 5 show the relationship $E'(T)$ and $\tan \delta(T)$ for BAR, SAN, and the copolymer of SAN and BAR with the aforementioned grafting degree. As seen from the figures, one can assume to a first approximation, that the curves $E'(T)$ and $\tan \delta(T)$ of the copolymer are shifted along the abscissa with respect to the analogous curves for pure BAR. The shift interval is equal to the difference in the glass transition of SAN and BAR, multiplied by the ratio of these components in the copolymer.

A similar relationship holds for the statistical copolymer [9], but this fact is experimentally observed for the grafted copolymer considered here. Also, the relaxation peak of $\tan \delta$ of the grafted copolymer is analogous to the peak of BAR. This analogy is apparently due to the good solubility of SAN in BAR at low grafting degrees. Good agreement between the computed and experimental data was attained with SAN – grafted BAR.

Conclusion

The properties of ASA composite material can be predicted from the viscoelastic characteristic of the constituent components (SAN matrix and SAN – grafted BAR). The error does not exceed 10% at any ratio of the viscoelastic parameters of the separate layers at a moderate inclusion concentration.

This error level permits the use of integral Laplace transforms and generalization of the method to more complex viscoelasticity problems.

It also allows a theoretical solution to the problem of optimization of the properties of composite materials with spherically layered inclusions by varying the microstructure parameters.

Knowledge of the dynamic characteristics of the grafted copolymer that represent the material of the spherical layer in the inclusions allows the viscoelastic properties of the ASA copolymer to be predicted with better precision if the material of the layer is identified with the BAR itself.

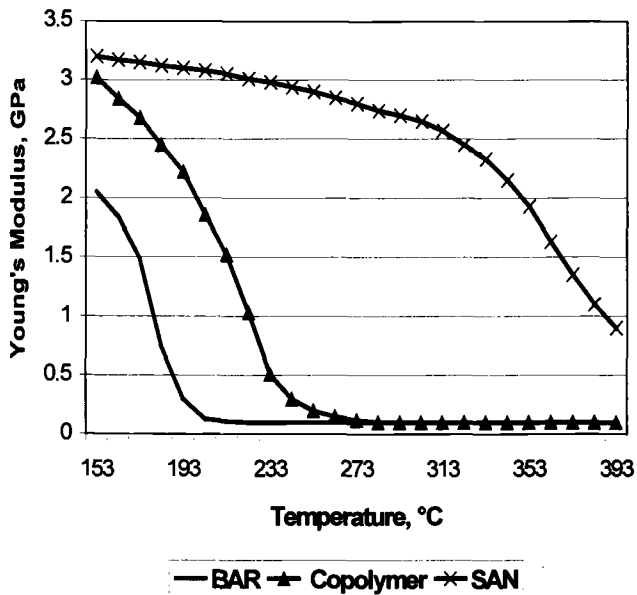


Figure 4 – Temperature dependencies of Young's modulus of BAR and Graft Copolymer SAN on BAR

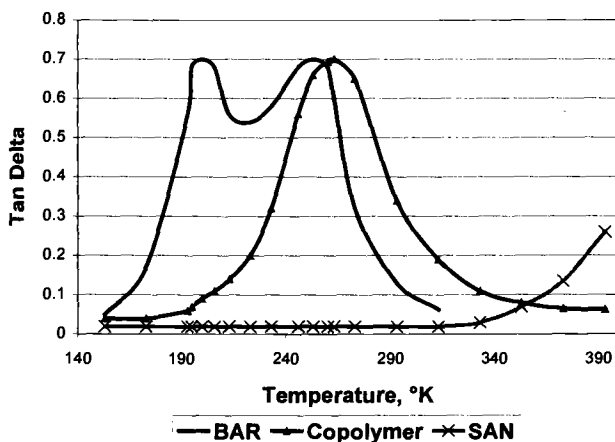


Figure 5 – Temperature dependencies of Tan Delta of BAR and Graft Copolymer SAN on BAR

References

- [1] Christensen, R. *Introduction to Mechanics of Composites*, John Wiley and Sons, New York, 1977.
- [2] Privalco, V. P. and Novikov, V. V., *The Science of Heterogeneous Polymers*, John Wiley and Sons, New York, 1995.
- [3] Kerner, E. N. "Elastic and Thermoelastic Properties of Composite Media," *Proceedings of the Physics Society*, Vol. 69, 1956, pp.808-813.
- [4] Hashin, Z. and Shtrikman, S. A. "A Variational Approach to the Theory of Elastic Behavior of Multiphase Materials," *Mechanics and Physics of Solids*, Vol. 11, 1963, pp. 127-132.
- [5] Krivoglaз, M. A. and Cherevco, A. S., "On the Elastic Moduli of Solid Mixtures," *Physical Mechanics of Materials*, Vol. 8, No. 2, 1959, pp. 161-166.
- [6] Dzenis, Yu. A. "Influence of the Aggregation of a Stiff Disperse Filler on Elastic Properties of the Polymer Composite," *Mechanics of Polymers*, No. 1, 1986, pp. 14-22.

- [7] Goldman, A. Ya., Ivanchev, S. S., Kanaun, S. K., Kudryavtseva, L. T., and Pavluchenco, V. N. "Viscoelastic Properties of Impact-Resistant Plastics with Spherical Inclusions", *Dokl. Academy of Science SSSR*, Vol. 291, No. 5, 1986, pp. 1142-1146.
- [8] Boiko, Yu. M., Brostow, W., Goldman, A. Ya., and Ramamurthy, A. C. "Tensile, Stress Relaxation and Dynamic Mechanical Behavior of Polyethylene Crystallized from Highly Deformed Melt," *Polymer*, Vol. 36, 1995, pp. 1383-1392.
- [9] Sperling, L. N. *Polymeric Multicomponent Materials*, John Wiley and Sons, 1997, p. 397.

Maria Cristina Righetti,¹ Maria Pizzoli,² and Giuseppina Ceccorulli²

Glass Transition Temperature of Selected Polymers by TMDSC, DMTA and DETA Analyses

REFERENCE: Righetti, M. C., Pizzoli, M., and Ceccorulli, G., "Glass Transition Temperature of Selected Polymers by TMDSC, DMTA and DETA Analyses," *Materials Characterization by Dynamic and Modulated Thermal Analytical Techniques, ASTM STP 1402*, A. T. Riga and L. Judovits, Eds., American Society for Testing and Materials, West Conshohocken, PA, 2001.

Abstract: Dynamic glass transition, related to the cooperative motions of amorphous polymeric segments, can be investigated by means of periodic techniques. Recently, temperature modulated differential scanning calorimetry (TMDSC) has offered the possibility to obtain α relaxation data at very low frequency (below 0.2 Hz). In this paper dynamic glass transition temperatures of an amorphous and two semicrystalline polymers, obtained by means of TMDSC, have been compared with dynamic mechanical (DMTA) and dielectric (DETA) results. The DMTA and DETA scans were performed at 3 Hz and in the frequency interval 10^2 - 10^4 Hz respectively. The frequency dependence of calorimetric, dynamic mechanical as well as dielectric data has been found successfully described by the Vogel-Fulcher-Tammann equation in the whole range of frequency investigated.

Keywords: temperature modulated DSC, dynamic mechanical spectroscopy, dielectric spectroscopy, α relaxation, nylon 6, ethylene-co-vinyl alcohol copolymer, cellulose acetate butyrate

Introduction

It is well known that the physical behavior exhibited by polymers in the solid state is governed by the molecular motions characteristic of the polymeric chains. The study of

¹ Researcher, Centro di Studio per la Fisica delle Macromolecole, Consiglio Nazionale delle Ricerche, Via Selmi 2, 40126 Bologna, Italy.

² Professor, Dipartimento di Chimica G.Ciamician, Università di Bologna, Via Selmi 2, 40126 Bologna, Italy.

the molecular origin of these motions is very interesting both from a theoretical and industrial point of view because the physical performance of polymeric materials basically depends on their relaxation behavior.

A typical relaxation spectrum of an amorphous polymer shows quite weak transitions in the glassy state, followed, at higher temperature, by a more intense absorption that is associated with the glass-to-rubber transition (α relaxation). Semicrystalline polymers may exhibit a further α_c relaxation connected with the presence of the crystalline phase [1].

All relaxation processes, observed as response to an external perturbation, occur when the frequency of the perturbation is equal to the characteristic frequency of the molecular motions, and move to higher temperatures as the perturbation frequency increases. As regards the glass transition, in order to distinguish the relaxation process from the vitrification event (the "thermal" glass transition) usually observed by conventional DSC, the concept of "dynamic" glass transition has been introduced [2, 3].

Dynamic mechanical (DMTA) and dielectric spectroscopy (DETA) represent powerful experimental tools in order to characterize the relaxation behavior of polymeric materials. The two techniques detect molecular motions by different means. It is normally assumed that all molecular relaxation processes are seen by DMTA, whereas the DETA method only reveals molecular motions involving dipolar species. The different relaxation responses, obtained by using various external oscillating perturbations, are useful in discriminating between different motional mechanisms and in developing molecular models able to explain and predict the experimental behaviors of polymeric materials.

The dynamic mechanical response of a viscoelastic material is usually given by the complex modulus E^* as a function of temperature and perturbation frequency. E^* is a complex quantity, $E^* = E' + iE''$, where E' is the storage modulus and E'' the loss modulus.

The complex permittivity ϵ^* ($\epsilon^* = \epsilon' - i\epsilon''$) is the experimental quantity obtained in the dielectric spectroscopy method, where ϵ' represents the real permittivity and ϵ'' is the dielectric loss factor.

The frequency range covered by the most common commercial dynamic mechanical and dielectric analyzers are 10^{-2} - 10^2 Hz and 10^2 - 10^5 Hz respectively. Recently a new technique, the Temperature Modulated Differential Scanning Calorimetry (TMDSC) has been developed, offering the possibility to study relaxation processes at very low frequency (10^{-3} - 10^{-1} Hz) [4].

TMDSC is characterized by a periodic temperature modulation which is superimposed to the conventional linear DSC temperature program [5-7]:

$$T(t) = T_o + \beta t + T_a \sin(\omega t) \quad (1)$$

where

T_o = starting temperature

β = underlying scanning rate

T_a = amplitude of the temperature modulation

ω = angular modulation frequency ($\omega = 2\pi\nu = 2\pi/t_p$, ν and t_p being the frequency and the period respectively).

The modulated heat flow rate Φ_m measured by TMDSC is averaged over the period of modulation, in order to obtain the so-called total heat flow rate (Φ_{total}) which is equivalent to the conventional DSC signal at the same heating rate β [8, 9]:

$$\Phi_{total} = m\beta c_{p,total} \quad (2)$$

where

m = mass of the sample

$c_{p,total}$ = specific heat capacity at the heating rate β .

The periodic heat flow rate (Φ_p), calculated by subtracting Φ_{total} from the measured heat flow rate Φ_m , is described by the following equation:

$$\Phi_p = \Phi_a \cos(\omega t - \delta_m) \quad (3)$$

where

Φ_a = amplitude of Φ_p

δ_m = phase angle between the heat flow rate and the heating rate.

The amplitude Φ_a and the phase angle δ_m are obtained by Fourier analysis. It is worth noting that both the phase angle due to the relaxation process occurring in the sample (δ_s) and the phase angle related to heat transfer effects (δ_{ht}) contribute to the measured δ_m . For this reason, in order to determine δ_s , the measured value of δ_m has to be suitably corrected [9].

In case of saw-tooth modulation, the temperature oscillation is given by a Fourier series:

$$T(t) = T_o + \beta t + \frac{8T_a}{\pi^2} \left[\sin(\omega t) - \frac{1}{9} \sin(3\omega t) + \frac{1}{25} \sin(5\omega t) - \dots \right] \quad (4)$$

where the higher harmonics have a progressively decreasing weight. For this reason the amplitude and the phase angle referring to only the first harmonic of the periodic component are usually taken into account.

The complex specific heat capacity, which is frequency dependent, is defined as:

$$c^* = c' - ic'' \quad (5)$$

The modulus of c^* identifies the thermal events which can be reversed in the temperature range covered by the modulation and can be obtained from:

$$|c^*| = \frac{\Phi_a}{m\omega T_a} \quad (6)$$

and the real and the imaginary components by:

$$c' = |c^*| \cos(\delta_s) \quad (7)$$

$$c'' = |c| \sin(\delta_s) \quad (8)$$

where δ_s is the phase angle due only to the relaxation processes occurring in the sample.

The aim of this work is to correlate α transition data obtained by means of TMDSC with dynamic mechanical and dielectric results. For this purpose, the relaxation maps of three polymers, two semicrystalline (nylon 6 and a statistical ethylene-co-vinyl alcohol copolymer) and one amorphous (cellulose acetate butyrate), have been investigated in a wide frequency interval, ranging from $6 \cdot 10^{-3}$ to $5 \cdot 10^4$ Hz. The frequency dependence of the dynamic glass transition temperature for these three polymers has been analyzed in terms of the Vogel-Fulcher-Tammann equation.

Experimental

Materials

Nylon 6 was a commercial sample (F34L) produced by SNIA Tecnopolimeri (Italy) ($\eta_{\text{rel}}=3.4$ in sulfuric acid at 20°C). Ethylene-co-vinyl alcohol copolymer (EVOH) was supplied by Nippon Gohsey (Soarnol D29) and contained 29 mol% of ethylene units. Cellulose acetate butyrate (CAB) was an Eastman Chemical product (CAB 531-1) with the following degree of substitution: $\text{DS}_{\text{Bu}}=2.6$ and $\text{DS}_{\text{Ac}}=0.2$. The number-average molar mass (M_n) and the mass-average molar mass (M_w) of CAB were 71600 and $161000 \text{ g} \cdot \text{mol}^{-1}$ respectively.

Experimental Methods

TMDSC measurements were carried out by means of a Perkin Elmer DDSC. The external block temperature control was set at -40°C . Dry nitrogen was used as purge gas at a rate of $35 \text{ mL} \cdot \text{min}^{-1}$. The instrument was calibrated in temperature and energy with high-purity standards (indium, cyclohexane, naphthalene) at a rate of $5^\circ\text{C} \cdot \text{min}^{-1}$, according to the procedures of conventional DSC. The heat flow rate was calibrated with sapphire [2]. In order to reduce temperature gradients and heat transfer effects, the samples were analyzed as films obtained by compression moulding. The sample weight was kept small and approximately equal to 5 mg. In order to erase previous thermal history and remove absorbed moisture as much as possible, the TMDSC scan was preceded by the following procedure. Nylon 6 and EVOH samples were heated to 150°C , kept at this temperature for 10 min, heated to complete fusion (240°C for nylon 6 and 210°C for EVOH) and subsequently cooled at $10^\circ\text{C} \cdot \text{min}^{-1}$ to 0°C . During the cooling step, crystallization of nylon 6 and EVOH occurred. Cellulose acetate butyrate samples were heated up to 170°C , i.e. above the melting temperature of the as-received material ($T_m = 151^\circ\text{C}$) and rapidly cooled to 40°C . By this thermal treatment totally amorphous

CAB samples were obtained. As far as the TMDSC scan is concerned, a saw-tooth temperature modulation was used. The underlying heating rate varied between 0.5 and $2^{\circ}\text{C}\cdot\text{min}^{-1}$, the temperature modulation amplitude was 1°C and the period ranged from 12 to 160 s (frequency from 0.0063 to 0.083 Hz). Nylon 6 and EVOH were analyzed from 0 to 100°C , CAB from 40 to 160°C . The glass transition temperature was taken as the maximum of the imaginary component of the complex specific heat capacity [3].

Dynamic mechanical measurements were performed with a Dynamic Mechanical Thermal Analyzer (DMTA Mark II - Polymer Laboratories) operating in the dual cantilever bending mode at a frequency of 3 Hz and a heating rate of $3^{\circ}\text{C}\cdot\text{min}^{-1}$. Samples in the form of small bars ($30\times 8\times 1.8$ mm), obtained by injection moulding at a temperature 30°C higher than the melting point, were investigated in a dry nitrogen atmosphere from -120°C up to 150°C . Measurements were performed both on room stored samples and on samples carefully dried in a vacuum oven at 150°C for 1 hour. The transition temperatures were taken as the peak values in the loss modulus curve.

The dielectric relaxation measurements were carried out with a Dielectric Thermal Analyzer (DETA - Polymer Laboratories) in the frequency interval from 10^2 to 10^4 Hz at a heating rate of $1^{\circ}\text{C}\cdot\text{min}^{-1}$. Films (about 0.1 mm thick) were prepared by compression moulding (2 min under a load of about 0.5 ton at 30°C above the melting temperature) with a Carver Laboratory Press. A first scan was carried out on samples previously maintained at room temperature. A successive scan was performed on the same sample after heating under vacuum up to 150°C directly in the DETA cell.

Experimental Results and Discussion

TMDSC Results

Figure 1 reports the real and the imaginary component of the specific heat capacity for nylon 6 at the indicated operative conditions. In correspondence with the glass transition, the real component (c') shows a step whereas the imaginary component (c'') is

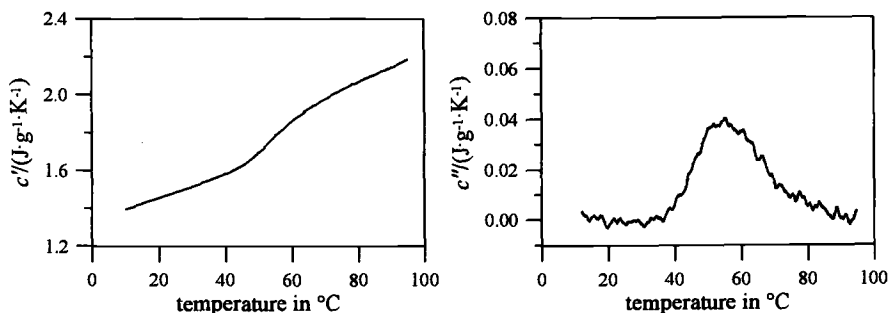


Figure 1 – Real (c') and imaginary part (c'') of complex specific heat capacity for nylon 6 in the glass transition region ($\beta=1.5^{\circ}\text{C}\cdot\text{min}^{-1}$, $T_a=1^{\circ}\text{C}$, $\nu=0.031$ Hz).

characterized by a peak. The physical meaning of c' and c'' has been recently clarified. According to ref. [10] the c' component is the reversing specific heat capacity in-phase with the temperature modulation and the imaginary c'' component is considered as a "kinetic" specific heat capacity. It identifies thermal events that, even if they do not occur instantaneously due to some kinetic hindrance, can be equally considered reversible because they are able to reverse during the temperature range covered by modulation.

The reversing c' and the "kinetic" c'' specific heat components have been calculated according to Equations (7) and (8), knowing the phase angle δ_s . In this connection, the measured phase angle δ_m has been corrected by subtracting the contribution due to heat transfer [9]. In Figure 2 an example of δ_m and δ_s curves is reported. It can be noted that δ_s is zero outside the temperature range relevant to the glass transition.

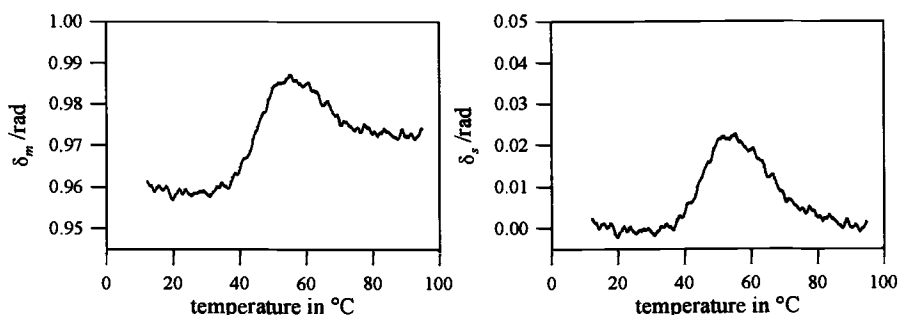


Figure 2 – Measured phase angle (δ_m) and corrected phase angle (δ_s) for nylon 6 in the glass transition region ($\beta=1.5^\circ\text{C}\cdot\text{min}^{-1}$, $T_a=1^\circ\text{C}$, $\nu=0.031\text{ Hz}$).

Since nylon 6 is a semicrystalline material, asymmetric broadening of the glass transition region is expected to occur, especially on the high temperature side of the transition [3], as actually revealed by Figure 1. As far as EVOH is concerned, very similar curves were observed, whereas the amorphous CAB showed a glass transition region more narrow and symmetric, as evidenced in Figure 3.

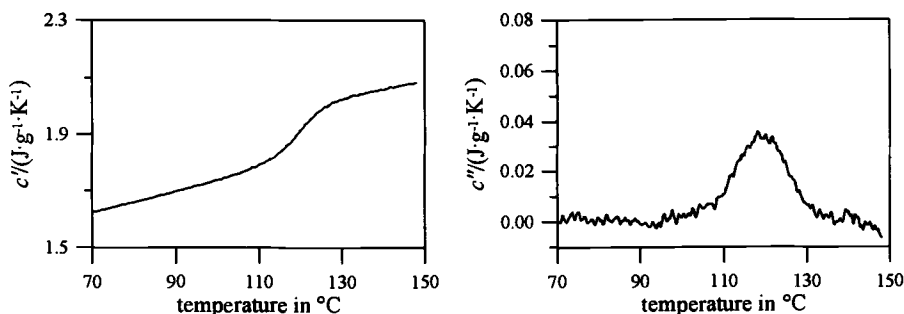


Figure 3 – Real (c') and imaginary part (c'') of complex specific heat capacity for CAB in the glass transition region ($\beta=1.5^\circ\text{C}\cdot\text{min}^{-1}$, $T_a=1^\circ\text{C}$, $\nu=0.063\text{ Hz}$).

DMTA Results

The dynamic mechanical behavior of room stored and dry nylon 6 is shown in Figure 4. The spectrum is characteristic of a semicrystalline polymer, with a small drop of the dynamic storage modulus E' in correspondence with the glass transition. Two relaxation processes are present in the temperature range investigated; for the dry sample the glass transition (α relaxation) is observed around 60°C and the low temperature secondary β relaxation appears at about -60°C . In agreement with the literature [1], the presence of water strongly affects both relaxations. The α process is seen to occur at lower temperature in the room stored sample, due to the plastification effect induced by water absorbed from the ambient. The β peak, which is commonly attributed to local motions of amide groups capable of interacting with polar low-molecular weight molecules [1, 11], also moves to lower temperature and magnifies in the presence of water.

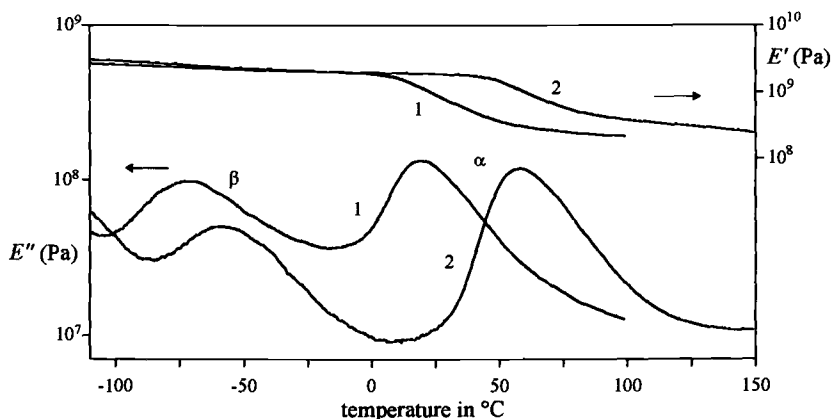


Figure 4 – *Dynamic mechanical spectrum of nylon 6: room stored sample (curve 1); after drying at 150°C for 1 hour under vacuum (curve 2).*

The relaxation spectrum of EVOH, reported in Figure 5, shows in the low temperature region two secondary absorptions (γ and β) influenced to a little extent by the presence of water molecules. The former is associated with local motions of methylene units pertaining to the ethylene sequences of the EVOH copolymer, the latter is related to local rearrangements of the $(-\text{CH}_2\text{-CHOH}-)$ sequences [12]. As found for nylon 6, absorbed water has a pronounced effect on the primary α relaxation, which is preceded by a shoulder at about 50°C in the room stored sample. The phenomenon is due to partial removal of absorbed water; after drying, the shoulder disappears and T_α moves to higher temperature. The relaxation spectrum of EVOH indicates the presence of a further (α_c) process, which is characteristic of both polyethylene and vinyl alcohol homopolymers [1] and whose molecular attribution is still an open question. Although it

appears only in the presence of a crystalline phase, a certain contribution from the amorphous phase seems to be required as well [13].

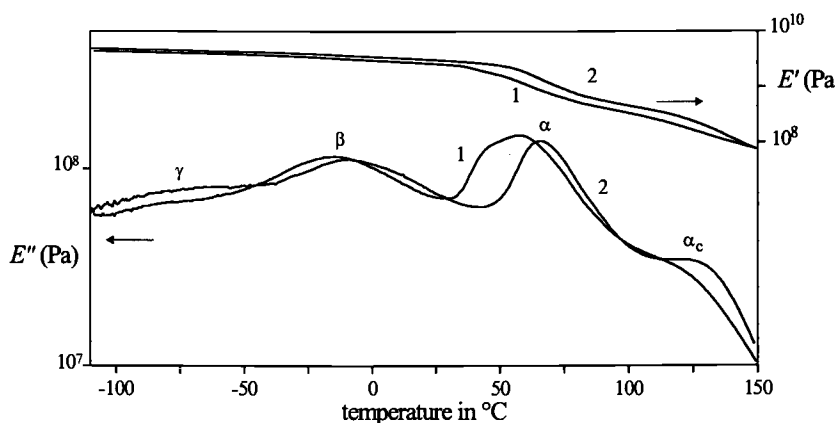


Figure 5 – *Dynamic mechanical spectrum of EVOH: room stored sample (curve 1); after drying at 150°C for 1 hour under vacuum (curve 2).*

The dynamic mechanical spectrum of CAB (Figure 6) confirms the totally amorphous state of the sample. The dynamic storage modulus E' shows a very steep drop in the α relaxation region, reaching values as low as 10^6 Pa in the rubbery state. A very broad loss region, typical of polysaccharides, is observed in the glassy state, whose origin is still controversial [14,15]. No substantial differences were found in the relaxation spectrum of room stored and dry CAB, apart from a weak shoulder at about 70°C in the E'' curve which has been correlated with the presence of absorbed moisture.

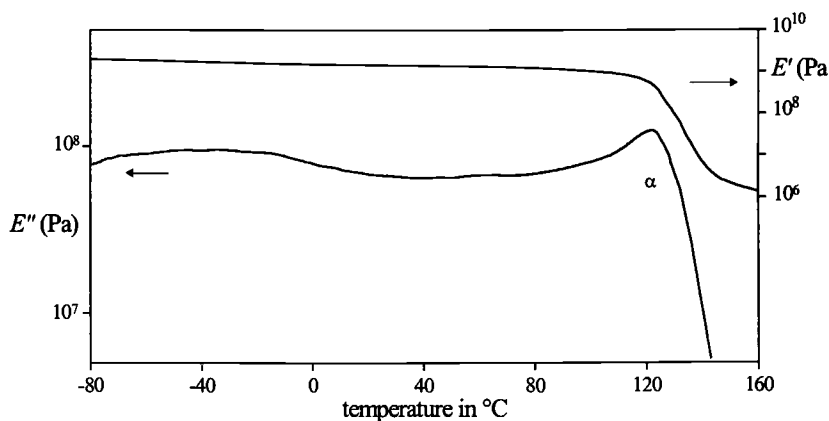


Figure 6 – *Dynamic mechanical spectrum of dry CAB.*

DETA Results

In Figure 7 the temperature dependence of ϵ' and ϵ'' for a room stored sample of nylon 6 is shown at several frequencies. After thermal treatment up to 150°C, the

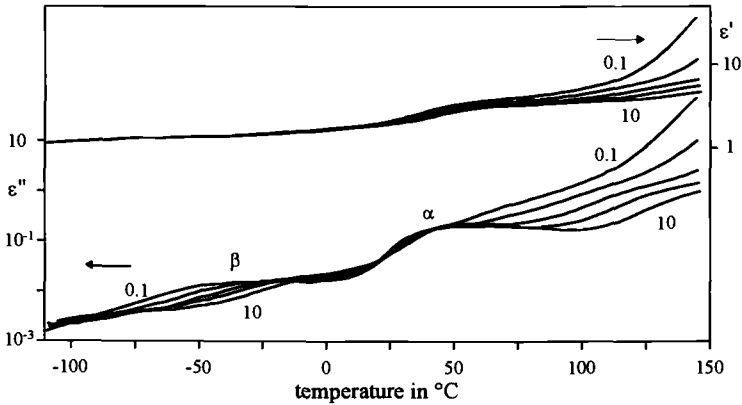


Figure 7 – Dielectric spectrum of room stored nylon 6 at different frequencies: 0.1, 0.3, 1, 3, 10 kHz

secondary β dissipation process is totally suppressed (Figure 8), indicating that the heating under vacuum in the DETA apparatus is very effective in removing water from the sample. In agreement with dynamic mechanical results, the α relaxation moves to

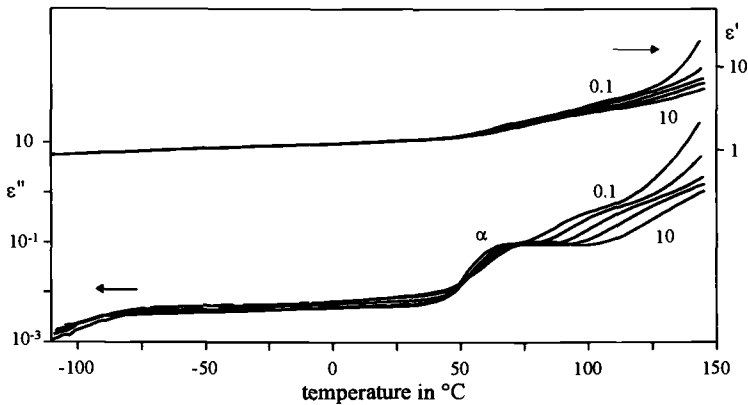


Figure 8 – Dielectric spectrum of dry nylon 6 at different frequencies: 0.1, 0.3, 1, 3, 10 kHz.

higher temperatures after the thermal treatment at 150°C. Unfortunately, a marked increase in the dielectric loss at high temperatures partially overlaps the dielectric α process, so precluding the possibility of determining the exact value of T_α at different frequencies. The phenomenon is the largest at the lowest frequency, as usually observed when interfacial polarization or conductive processes occur in the system under investigation [16].

In order to obtain the dipolar contribution to the dielectric loss, the measured ϵ' and ϵ'' have been converted to the complex electric modulus M^* by:

$$M^* = \frac{1}{\epsilon^*} = M' + iM'' \quad (9)$$

where

$$M' = \frac{\epsilon'}{\epsilon'^2 + \epsilon''^2} \quad (10)$$

$$M'' = \frac{\epsilon''}{\epsilon'^2 + \epsilon''^2} \quad (11)$$

The electric loss modulus M'' values so obtained are plotted as a function of temperature and frequency in Figure 9; it is clear that the α relaxation is now well resolved and separated from the dielectric dissipation occurring at $T > T_\alpha$.

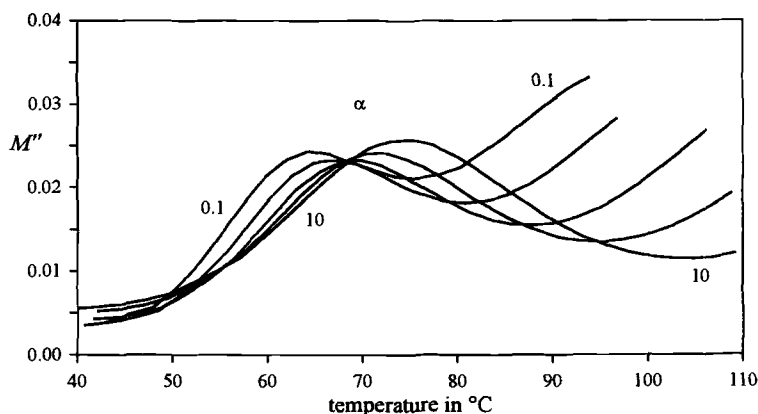


Figure 9 – Electric loss modulus of dry nylon 6 in the α relaxation region at different frequencies: 0.1, 0.3, 1, 3, 10 kHz.

Figure 10 reports the temperature dependence of the dielectric spectrum for a dry EVOH sample at different frequencies. Analogous curves were obtained for the room stored sample, apart from an increased dissipation factor in the glassy state and a shift to

lower temperatures of the α process due to absorbed moisture. As found for nylon 6, the dipolar relaxation associated with the cooperative motions of the amorphous polymer segments is partially obscured by a strong dielectric dissipation which increases with decreasing frequency. The experimental data have been analyzed in terms of M^* and the corresponding values of the electric loss modulus M'' are reported in Figure 11.

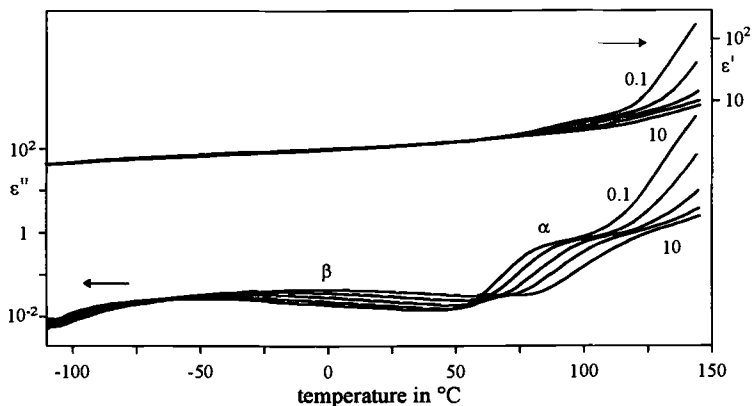


Figure 10 – Dielectric spectrum of dry EVOH at different frequencies: 0.1, 0.3, 1, 3, 10 kHz.

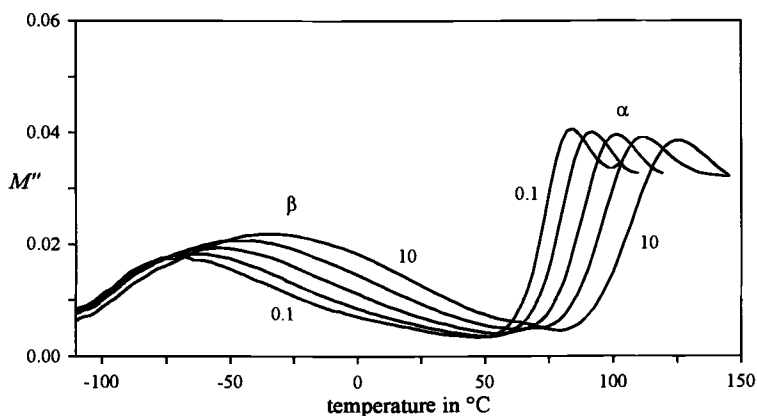


Figure 11 – Electric loss modulus of dry EVOH at different frequencies: 0.1, 0.3, 1, 3, 10 kHz.

The dielectric spectrum of CAB in the dry state (Figure 12) shows a secondary β relaxation more evident than in the dynamic mechanical curve of Figure 6. No extra

electric loss phenomena connected with conduction or interfacial polarization are observed at temperatures lower than 160°C. However, for the sake of comparison, values of T_α at different frequencies have been calculated from the peak temperatures of the electric loss modulus M'' data.

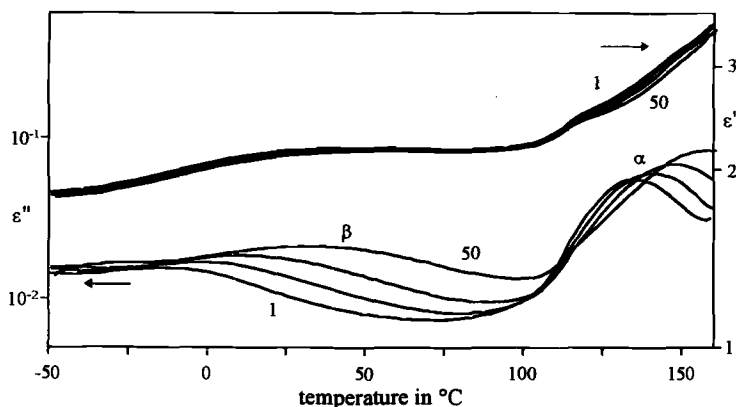


Figure 12 – Dielectric spectrum of dry CAB at different frequencies: 1, 3, 10, 50 kHz.

Conclusions

The experimental results obtained by means of TMDSC, DMTA and DETA techniques have been used to construct the α relaxation map of the polymers under investigation (see Figure 13). As usually observed for the relaxation associated with the glass transition, the plot of $\ln \nu$ vs. the reciprocal peak temperature shows a curved trace, the slope decreasing with increasing frequency. The data sets were well correlated for all the three polymers and satisfactorily described by the Vogel-Fulcher-Tammann (VFT) equation, which is commonly used to analyze the glass transition relaxation [17]:

$$\ln \nu(T) = A - \frac{B}{T - T_0} \quad (12)$$

where A , B and T_0 are fitting parameters, T_0 corresponding to the 'ideal' glass transition temperature, i.e. the temperature at which the relaxation time of the α process becomes infinite. The value of T_0 is usually found to be located approximately 20-70 K below T_g , the 'thermal' glass transition temperature, as confirmed by the data in Table 1, where the VFT fit parameters are listed together with the T_g values obtained by conventional DSC. As regards the different curvatures of the $\ln \nu - 1/T_\alpha$ plots shown in Figure 13, it is reasonable to suggest that they may reflect different chain flexibility as well as different intensity and type of intermolecular interactions in the polymers investigated.

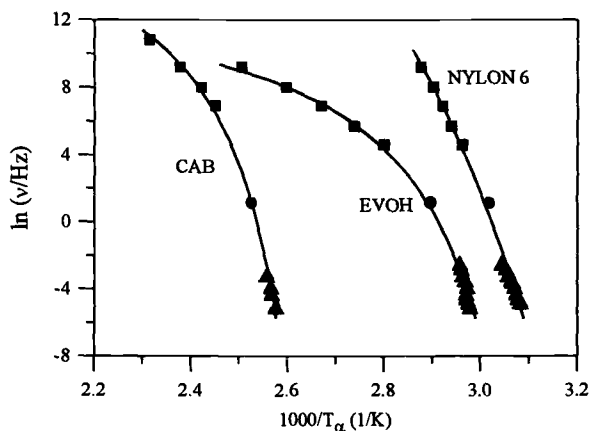


Figure 13 – Temperature-frequency dependence for the α relaxation process of CAB, EVOH and nylon 6: (\blacktriangle) TMDSC data: maximum of c'' curves; (\bullet) dynamic mechanical data: maximum of E'' curves; (\blacksquare) dielectric data: maximum of M'' curves. Solid curves are VFT fits.

Table 1 – VFT fit parameters

	A	B	T_o, K	T_g, K^1
Nylon 6	41.8	2453	272	325
EVOH	13.8	414	313	337
CAB	18.6	485	368	388

¹ experimental data by conventional DSC ($10^\circ\text{C}\cdot\text{min}^{-1}$)

Acknowledgements

The financial support of “Progetto Finalizzato Materiali Speciali per Tecnologie Avanzate II” is gratefully acknowledged.

References

- [1] McCrum, N. G., Read, B. E., and Williams, G. *Anelastic and Dielectric Effects in Polymeric Solids*, Dover, New York, 1991.
- [2] Boller, A., Schick, C., and Wunderlich, B., “Modulated Differential Scanning

- Calorimetry in the Glass Transition Region," *Thermochimica Acta*, Vol. 266, 1995, pp. 97-111.
- [3] Hensel, A., Dobbertin, J., Schawe, J. E. K., Boller, A., and Schick, C., "Temperature Modulated Calorimetry and Dielectric Spectroscopy in the Glass Transition Region of Polymers," *Journal of Thermal Analysis*, Vol. 46, 1996, pp. 935-954.
- [4] Reading, M., Elliott, D., and Hill, V. L., *Proceedings 21th NATAS Conference*, 1992, p. 145.
- [5] Reading, M., Elliot, D., and Hill, V. L., "A New Approach to the Calorimetric Investigation of Physical and Chemical Transitions," *Journal of Thermal Analysis*, Vol. 40, 1993, pp. 949-955.
- [6] Wunderlich, B., Jin, Y., and Boller, A., "Mathematical Description of Differential Scanning Calorimetry based on Periodic Temperature Modulation," *Thermochimica Acta*, Vol. 238, 1994, pp. 277-293.
- [7] Schawe, J. E. K., "A Comparison of Different Evaluation Methods in Modulated Temperature DSC," *Thermochimica Acta*, Vol. 260, 1995, pp. 1-16.
- [8] Wunderlich, B., "Modeling the Heat Flow and Heat Capacity of Modulated Differential Scanning Calorimetry," *Journal of Thermal Analysis*, Vol. 48, 1997, pp. 207-224.
- [9] Weyer, S., Hensel, A., and Schick, C., "Phase Angle Correction for TMDSC in the Glass-transition Region," *Thermochimica Acta*, Vol. 304/305, 1997, pp. 267-275.
- [10] Jones, K. J., Kinshott, I., Reading, M., Lacey, A. A., Nikolopoulos, C., and Pollock, H. M., "The origin and interpretation of the signals of MTDSC," *Thermochimica Acta*, Vol. 304/305, 1997, pp. 187-199.
- [11] Le Huy, H. M., and Rault, J., "Remarks on the α and β Transitions in Swollen Polyamides," *Polymer*, Vol. 35, 1994, pp. 136-139.
- [12] Kalfoglou, N. K., Samios, C. K., and Papadopoulou C., "Compatibilization of Poly(ethylene-co-vinyl alcohol) (EVOH) and EVOH-HDPE Blends: Structure and Properties," *Journal of Applied Polymer Science*, Vol. 68, 1998, p. 589-596.
- [13] Gedde, U. W., *Polymer Physics*, Chapman & Hall, London, 1995.
- [14] Ceccorulli, G., Pizzoli M., and Scandola M., "Influence of water on the secondary relaxations of cellulose acetate," *Polymer Communications*, Vol. 27, 1986, pp. 228-230.
- [15] Butler, M. F., and Cameron, R. E., "A Study of the Molecular Relaxations in Solid Starch Using Dielectric Spectroscopy," *Polymer*, Vol. 41, 2000, pp. 2249-2263.
- [16] Boyd, R. H., and Liu, F., "Dielectric Spectroscopy of Semicrystalline Polymers," *Dielectric Spectroscopy of Polymeric Materials*, J. P. Runt, and J. J. Fitzgerald, Eds., American Chemical Society, Washington DC, 1997, pp. 107-136.
- [17] Schönhal, A., "Dielectric Properties of Amorphous Polymers," *Dielectric Spectroscopy of Polymeric Materials*, J. P. Runt, and J. J. Fitzgerald, Eds., American Chemical Society, Washington DC, 1997, pp. 81-106.

Author Index

B

Bilyeu, B., 49
Blaine, R. L., 115
Brostow, W., 49
Burkholder, K. E., 67

C

Cahoon, J. M., 139, 157
Ceccorulli, G., 200
Chuang, K., 177

F

Fuller, L. C., 89

G

Goldman, A. Ya., 190

J

Judovits, L., 89

K

Kasap, S. O., 81

L

Ludwig, K. N., 67
Lvovich, V., 157

M

Menard, K. P., 49
Merzliakov, M., 32

O

Orliac, H., 17

P

Pan, W.-P., 177
Pialet, J. W., 139
Pizzoli, M., 200
Price, D. M., 17, 103

R

Reading, M., 17
Riga, A. T., 67, 139, 157
Righetti, M. C., 200

S

Schick, C., 32
Sisk, B. C., 177
Suwardie, J. H., 131

T

Tonchev, D., 81

W

Wiley, J. F., 67
Wunderlich, B., 3
Wurm, A., 32

Subject Index

A

Acrylonitrile-methacrylate-
styrene, 190
Acrylonitrile-styrene-acrylic
plastic, 190
Aerospace industry, 177
Amorphous fraction, rigid, 32
ATHAS database, 17

B

Bismaleimide, 177
Bisphenol-A polycarbonate, 32

C

Calibration, 103
Calorimetry, 32
Cellulose acetate butyrate, 200
Chalcogenide glass, 81
Chemical additive, engine oil,
157
Composite, fiber-reinforced
epoxy, 49
Composites, polymer, 190
Creep, 103
Crystalline melt model, 115
Crystallinity, 17
Crystallization, 32
Curing process, 49, 131
Cyanate ester, 177
Cyclic voltammetry, 157

D

Debye plot, 139
Detergents, 157
Dielectric analysis, 131
Dielectric loss, 139
Dielectric spectroscopy, 200
Dielectric thermal analysis,
139, 157
Differential scanning
calorimetry, 89, 115

dynamic, 89
modulated, 17, 89
temperature modulated, 3,
32, 89
glass transformation
studies, 81
glass transition, 67, 200
vitrification, 49
Dispersants, 157
Dynamic loss modulus, 131
Dynamic loss parameter, 131
Dynamic mechanical
spectroscopy, 200
Dynamic modulus, 190
Dynamic viscosity, 131

E

Ease of processing, polymer, 177
Elastomers, 67
Electrochemical impedance
spectroscopy, 157
Electrorheology, 139
Emulsion polymerization, 190
Epoxies, 177
Ethylene-co-vinyl alcohol
copolymer, 200

F

Fourier series, 3

G

Glass relaxation kinetics, 81
Glass-rubber transition, 103
Glass transformation, 81
Glass transition, 3, 200
chalcogenide glass system, 81
composites, 49
elastomers, 67
polymers, 103

H

Heat capacity, 3, 17, 32, 115
Heat, curing, 131

Heat flows, 81, 115
 Heat flux, 89
 Heat, volatilization, 131
 Heating rate, 67

I

Insulating fluid, 139
 Isothermal curing, 49

K

Kinetic parameters, 115

L

Latent heat, 3
 Least squares, 67

M

Mechanical loss tangent, 190
 Melting, 17, 103, 115
 reversible, 32
 reversing signal, 89
 Microstructure parameters, 190
 Modulation amplitude, 67
 Modulation frequency, 67
 Monomers, 177
 Multifrequency modulation, 3

N

Nylon, 200

O

Oils, 139, 157

P

Phase transition, 3
 Polarization plots, 157
 Polarization time, 139
 Polyaniline, 139
 Polybutadiene, 67
 Polymers (See also specific types), 103
 crystallization, 32
 dispersion, 139
 ease of processing, 177
 epoxy resins, 49

 glass transition, 200
 initial crystallinity, 17
 melting, 115
 metastable, 3
 resins, 177
 strength, 177
 Poly-N-methylaniline, 139
 Polystyrene, 67, 89
 Poly(styrene-co-butadiene), 67
 Polyvinylidene fluoride, 89
 Power compensation, 89

R

Relaxation time, 139
 Response time, 139
 Reversing signal, 17
 Rubber, peroxidic butylacrylate, 190
 Rubber-to-glass transition, 49

S

Sawtooth modulation, 3
 Sawtooth wave, 89
 Shear modulus, 32
 Shear stress, 139
 Shrinkage, 103
 Simultaneous thermal analyzer, 131
 Sine wave, 89, 115
 Spectroscopy
 dynamic mechanical, 200
 electrochemical impedance, 157
 Static yield stress, 139
 Strength, polymer, 177
 Styrene-acrylonitrile, 190
 Surfactants, organic, 157

T

Temperature resistance, polymer, 177
 Thermal expansion, 103
 Thermomechanical analysis,

modulated temperature,
103
Time response,
89
Time temperature transformation
diagram, 49
TMDMA, 32, 49
Transition parameters,
3

V

Vibrational heat capacity
contribution, 17
Viscoelastic properties, composite
materials, 190
Vitrification, 32, 49
Vogel-Fulcher-Tammann
equation, 200